Design, Synthesis and Evaluation of Iron(III) Selective Ligands for Biostatic Application

Michael Hunter

PhD

2013

Design, Synthesis and Evaluation of Iron(III) Selective Ligands for Biostatic Application

Michael Hunter MChem (Hons in Chemistry)

A thesis submitted in partial fulfilment
of the requirements of Northumbria
University for the degree of
Doctor of Philosophy

Research undertaken in the
Faculty of Health and Life Sciences

September 2013

Abstract

Bacterial pathogens, such as MRSA (methicillin-resistant *Staphylococcus aureus*) and VRE (vancomycin-resistant *Enterococcus*) give rise to nosocomial infections, especially to the immunodeficient. Disinfection of a surface is rarely 100% effective; microbes are almost always present on a surface, just in significantly reduced numbers. After disinfection, microbial repopulation to potentially dangerous levels on surfaces can be rapid if a nutrient source is made available e.g. soil or blood. With the exception of some lactic acid bacteria iron is ubiquitous among microbes as being necessary for growth and development within an environment. The implementation of a chelating agent, to restrict nutrient iron availability has been shown to reduce the rate of microbial repopulation post-disinfection.

The synthesis and characterisation of novel Fe(III) chelators is presented. Novel hexadentate chelators have been successfully synthesised utilising the previously assessed 1,3,5-tris(aminomethyl)-2,4,6-triethylbenzene core molecular scaffold; the 3,2-HOPO, 1,2-HOPO and 3,4-HOPO binding moieties have been explored in these ligands. In addition, two novel cyclotriguaiacylene (CTG) and two novel tris(piperazin-1-yl)-1,3,5-triazine based chelators have been produced; the 3,2-HOPO and 1,2-HOPO moieties have been explored for these cores. Furthermore, two novel tris(2-aminoethyl)amine (TREN) based chelators have been synthesised, which provide structural variation of literature compounds previously accessed. For comparison, literature compounds: EMECAM (pFe(III) = 32.6), CP130 (pFe(III) = 27.6) and TRENCAM (pFe(III) = 27.8) have been synthesised.

The MIC data shows three principal ligand candidates that display an inhibitory effect across the panel of microbes. The CTG-1,2-HOPO molecule, the TEB-1,2-HOPO molecule and TEB-R-3,2-HOPO molecule all inhibit growth at relatively low concentrations i.e. <500μM, with the exception of TEB-R-3,2-HOPO on *K. pneumoniae* which showed an MIC of 964μM. The kinetic assays performed have shown some of the ligands induce a desirable 'lag time' in the growth of organisms with respect to a control sample.

Contents

Acknowledgements

I would like to thank Dr. David Tetard and Dr. Lynn Dover for their valuable guidance, encouragement and advice throughout the project. Their insightful scientific discussions and their wealth of knowledge and expertise in chemistry and microbiology has been a great help throughout the project. In addition, I would extend my appreciations to Northumbria University and the Hospital Infection Society for the funding and resources for the project.

Special considerations go to all of the technical staff here at Northumbria University who have given an enormous amount of support. In particular, I would extend my gratitude to Dr. Steve Reed, Gordon Forrest and Jennifer Wright for all of their assistance through my time here. I hope they are always able to continue to encourage and support researchers here, who will all be as indebted to their patience and expertise as I am.

My thanks also go to my fellow researchers and friends at Northumbria University with particular appreciations to the members of 'team DT'; Adam Robinson-Miller, David Workman and Maryam Mousadoust for their friendship and help throughout. It would have been a far more gruelling journey without your support.

My appreciations go to my friends, both at home and far away, who have been supportive throughout the process. I would particularly like to extend my utmost gratitude towards Clare Mahon, Siobhan Telling, Stacey Culham and Terri Freedman for all of their support and friendship. As student life comes to an end I have to especially thank Shaun Robinson; a fellow researcher, friend, and for the last half of my PhD my flatmate, for making the last 18 months filled with laughter, good food and a family away from home.

Finally, I would express thanks to my family who have encouraged me every step of the way through the last 7 years. I don't know of any expression that can sum up the amount of support that my parents, Jeff and Lesley and sister Gemma have given me throughout my time at university. I can only think to say that without you by my side, none of this would have been possible, thank you.

Declaration

I declare that the work contained in this thesis has not been submitted for any other award and that it is all my own work. I also confirm that this work fully acknowledges opinions, ideas and contributions from the work of others. The work was done in collaboration with Northumbria University and The Healthcare Infection Society.

Name: Michael Hunter

Signature:

Date: 16/04/2014

"An investigator starts research in a new field with faith, a foggy idea, and a few wild experiments. Eventually the interplay of negative and positive results guides the work. By the time the research is completed, he or she knows how it should have been started and conducted." - Prof. Donald James Cram

Aims

The research presented here aims to expand the current hydroxypyridinone-based (HOPO) chelator technology with the thought to target Fe^{3+} binding.

This work will be focussed upon the design and synthesis of novel ligands that create restriction of nutrient Fe^{3+} in microbial systems, at low concentrations.

The ligands will be based upon new and previous core scaffolds and have incorporated a variety of HOPO moieties so as to provide a comparative study of the effect of these novel compounds on microbial systems. In addition, some literature based ligands will be synthesised so as to provide a basis for comparison of the efficacy of microbial growth inhibition of literature Fe^{3+} chelators with respect to the novel compounds.

The response of microbes which have current clinical relevance to these ligands will be assessed through microbiological MIC assays. In addition, an analysis of the growth profiles of these microbes will be provided, as a preliminary assessment of the longevity of any bacteriostatic effect produced.

Abbreviations

BnBr = benzyl bromide

BnCl = benzyl chloride

Boc = tert-butoxycarbonyl

CTG = cyclotriguaiacylene

CTV = cyclotriveratrylene

DCC = *N,N′*-Dicyclohexylcarbodiimide

DCM = dichloromethane

DIAD = diisopropyl azocarboxylate

DIPEA = *N,N*-diisoproylethylamine

DMAP = 4-(Dimethylamino)pyridine

DMF = dimethylformamide

DTPA = diethylenetriaminepentaacetic acid

EDCI = 1-ethyl-3-(3-dimethylaminopropyl)carbodiimide

EDTA = ethylenediaminetetraacetic acid

Ent = enterobactin

Et = ethyl

EtOH = ethanol

Me = methyl

MeOH = methanol

MRI = magnetic resonance imaging

NHS = *N*-hydroxysuccinimide

NMR = Nuclear Magnetic Resonance

Ph = phenyl

PTSA = *p*-toluenesulfonic acid

TBTU = *N,N,N′,N′*-Tetramethyl-*O*-(benzotriazol-1-yl)uronium tetrafluoroborate

THF = tetrahydrofuran

TsCl = tosyl chloride

1 Introduction

1.1 The Atmosphere, Early Life and Iron Availability

The composition of Earth's surface before 4 billion years ago is thought to have been dominated primarily by reductive species. The especially high concentrations of $H_{2(g)}$ and its compounds H_2O and H_2S were greatly significant and are thought to have controlled the chemical composition of the atmosphere and the planetary surface, particularly metallic species. Those metals whose sulfide compounds are largely insoluble, such as: Zn, Cu and Mo were scarcely available, especially within aqueous environments. By contrast elements such as: Na, K, Mg, Ca, Cl, P, S, C, H, N, O, Fe, Mn, V and W however, were readily available. The surface layers of the Earth were subject to thermal irradiation from the Earth's core and, in addition without an ozone layer (which developed sometime later), the surface was also subject to irradiation from the sun, both thermal and photonic.[1]

When exposed to high levels of this radiation liquid H_2O was subjected to photolysis, liberating molecular oxygen. In the still largely reductant-laden atmosphere the oxygen was highly reactive. As the oxygen generating process continued, over a period of around 4 billion years, the land, air and sea became deposited with oxidised species.[2] By this stage it is thought the atmosphere had altered dramatically and was now mostly comprised of $N_{2(g)}$, $CO_{2(g)}$ and $O_{2(g)}$.

With the elements available to early life, it is thought that C, H, N, O and S as well as, in small part P, were essential components of the earliest organic life. When primitive biosystems were developing, some 4 billion years ago, trace elements became important in various bioprocesses. Na, K, Cl, Fe, Ni and Cu were thought to be important in these bioprocesses due to their incorporation into essential biosynthetic pathways in life today. In addition, there are several biological pathways thought to be conserved throughout evolution, the vast majority of these containing a necessary Fe component to undoubtedly facilitate redox processes. Fe is also an

element thought to be conserved within organisms leading back to primitive anaerobic prokaryotes.[3]

Throughout the evolution of an oxidising atmosphere, it is thought chelating agents became necessary for metal solubilisation and the acquisition of nutrients. Accessible forms of: Mg, Fe, Co and Ni were available in such low abundance that those organisms that evolved primitive chelating systems would gain an advantage. Elaboration on these early systems is thought to have developed the complex systems now present in eukaryotic life, e.g. haem, ferritin, cobalamin.[1,3]

Microbes, plants and fungi have over time developed sophisticated Fe^{3+} regulatory systems to cope with the ever increasing $O_{2(g)}$ concentrations that limit Fe^{3+} availability. The release of molecules called siderophores (from the Greek meaning 'iron carrier') promotes solubilisation, uptake and the regulation of Fe^{3+} within these organisms.[4]

Within a biological system Fe^{2+} can react via the Fenton mechanism (initiation step shown below) to produce reactive oxygen species and so the biological Fe^{3+} concentration is kept at a constant level through regulatory proteins (homeostasis) such as ferritin, to avoid the potential damaging effects of such species within biological systems.[5]

$$Fe^{2+} + H_2O_2 \longrightarrow Fe^{3+} + HO^- + HO^{\cdot}$$

1.1.1 The Roles of Iron in the Bacterial Cell

Iron has several vital roles within bacterial cells. The metal is involved in metabolic and enzymatic processes which are required for cell proliferation. A summary of bacterial cell iron requirements is given in Table 1.1.[6]

Table 1.1 Summary of the role of iron within bacterial cells. Reproduced from: **Biochemical Education**, *1983*, **11**, 2, 54-63

Affected Area	Effects
Cell composition	Iron deficiency can cause: growth inhibition, decrease in RNA and DNA production, inhibition of sporulation, morphological alteration to cells
Intermediary metabolism	Processes requiring iron: tricarboxylic acid cycle, electron transport, oxidative phosphorylation, nitrogen fixation and aromatic biosynthesis.
Metabolic products	Products regulated by iron: porphyrins, toxins, vitamins, antibiotics, hydroxamates, cytochromes, pigments, siderophores, aromatic compounds, DNA and RNA
Proteins and enzymes requiring iron	Enzymes: Peroxidase, superoxide dismutase, nitrogenase, hydrogenase, glutamate synthase. Proteins: Cytochromes, ferridoxins, flavoproteins, ferritin.

Table 1.1 highlights the integral part iron plays within the processes required for bacterial cell proliferation and, those effects an iron deficiency would impart upon the cell. It is shown that a deficiency of iron would prevent the cells from functioning normally; a consequence of the detrimental impact such a deficiency would impose upon the enzymatic and protein-based processes.

1.1.2 Iron Bioavailability

The increase in oxidation state of metal centres such as iron from Fe(II) to Fe^{3+} generates a metal centre of higher Lewis acidity, due to increased electrophilicity. Fe^{3+} has an equilibrium concentration in water of around 10^{-18}M at pH 7, which even by diffusional processes is too low to sustain life at a microbial level.[7]

The insolubility of Fe^{3+} stems from the hard Lewis-acidic metal centre withdrawing electron density from solvating water molecules, causing the dissociation of protons from these complexes.[8] This generates insoluble $Fe(OH)_3$ or polymeric species, the process is shown in Figure 1.1.[9]

(1) $[Fe(H_2O)_6]^{3+} \rightleftharpoons [Fe(H_2O)_5(OH)]^{2+} + H^+ \quad K_a = 10^{-2.56}$

(2) $[Fe(H_2O)_5(OH)]^{2+} \rightleftharpoons [Fe(H_2O)_4(OH)_2]^{+} + H^+ \quad K_a = 10^{-3.76}$

(3) $[Fe(H_2O)_4(OH)_2]^{+} \rightleftharpoons [Fe(H_2O)_3(OH)_3] + H^+ \quad K_a = 10^{-6.33}$

Figure 1.1 Equations describing the dissociation of protons from solvated Fe^{3+} and the associated pKa values.

Siderophores are defined as low molecular weight chelating agents which have a very high specific affinity for Fe^{3+}. Their function is to mediate Fe^{3+} transport to cells. Approximately 500 known compounds fall under this definition of siderophore.[4]

The selectivity for ferric iron and the binding potency that these molecules display is dependent on a number of contributing factors. Firstly, the denticity of the ligand and the binding moiety have a large impact on the strength of chelation and on the metal selectivity. In addition, the arrangement of the binding moieties; attached to or included within a core backbone, impacts the selectivity of such ligands.[4] The factors effecting siderophore binding affinity will be addressed later within this chapter.

1.2 Siderophore Discovery

By the mid-1960s a range of molecules had been discovered and determined through experimentation to be important growth factors for microorganisms. These molecules were found to contain hydroxamic acid groups when the molecular structures were elucidated.

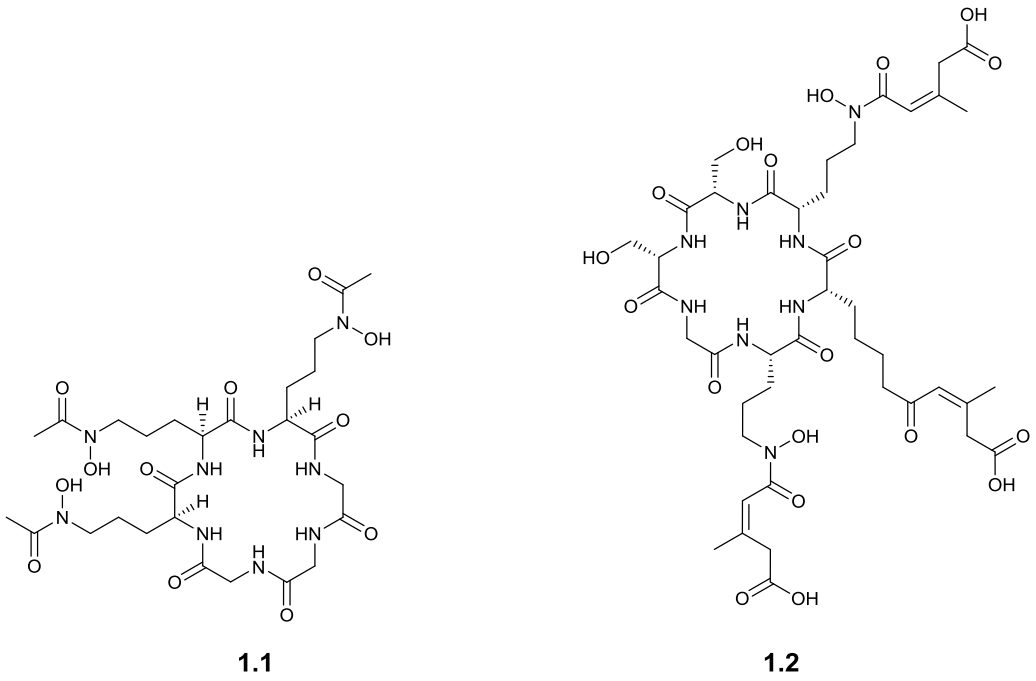

Figure 1.2 Molecular structures of ferrichrome (left) and of ferrichrome A (right)

This work began in 1952 where Neilands isolated an 'Organo-iron Pigment' from a rust fungus *Ustilago sphaerogena* and named the compound 'ferrichrome', Figure 1.2.[10] After further work in the area, a key observation was made in 1955 by Garibaldi and Neilands. It was shown that ferrichrome A production (Figure 1.2) by *Ustilago sphaerogena* was increased when the microbe was subject to iron limitation.[11] This led to the eventual eludication of the structure of ferrichrome and ferrichrome A, which were published in 1961 by Emery and Neilands.[12]

Around the same time in 1954, Snow *et al*., knowing the empirical formula of mycobactin, attempted to elucidate the structure through assessing the properties of products after performing degradation reactions, such as hydrolysis.[13] In addition, in 1954 Snow performed a set of experiments to define the coordinative groups of mycobactin, and did so correctly as the hydroxamic acid moiety. For mycobactin it was found that the addition of ferric chloride to

ethanolic solutions of the 'mycobactin acid' produced changes in the UV absorbance spectra which were consistent with Fe binding.[14]

It was in the late 1950s when catecholate-type moieties were beginning to be characterised and recognised as important structures in the regulation of iron in microbes. In 1958, Neilands and Ito isolated glycine and 2,3-dihydroxybenoic acid from an extract of *Bacillus subtilis* cultured under iron limiting conditions. These two products were the result of the hydrolysis of the parent compound, 2,3-dihydroxybenzoylglycine. Therefore, showing that under iron limitation *Bacillus subtilis* secretes this catecholate molecule.[15]

1.3 **1.4**

Figure 1.3 – Structures of 2,3-dihydroxybenzoylglycine (left) 2,3-dihydroxybenzoylserine (right)

Post discovery of the 2,3-dihydroxybenzoylglycine secretion, in 1966 Brot, Goodwin and Fales found that when cultures of *E. coli* were in their stationary growth phase the media in which they grew became red in colour. The attempted isolation of the compound responsible for the colour led to the identification of serine and iron, as well as the catechol moiety being present. When in an iron deficient media, a pale yellow compound could be isolated from the culture, which upon the addition of iron turned red. They concluded that *E. coli* was secreting compounds in response to iron limitation, capable of chelating iron. The group surmised that the compound was 2,3-dihydroxybenzoylserine (Figure 1.3), which mirrored the findings of the glycine conjugate by Neilands and Ito.[15,16]

Later, in 1970, O'Brien and Gibson correctly elucidated the structure of the tris-catecholate enterobactin (enterochelin) from the degradation products of molecules isolated from *E. coli*

cultures.[17] The compound was also independently isolated and characterised by Pollock and Neilands from *Salmonella typhimurium* in the same year.[18]

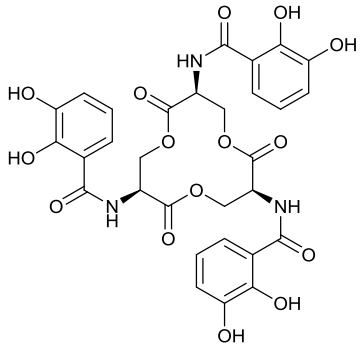

1.5

Figure 1.4 - Structure of enterobactin

Enterobactin was found to have an exocyclic structure (Figure 1.4, Figure 1.5), based on a triserine core scaffold bearing three arms. Coordination of iron occurs through three catecholate units to facilitate hexadentate binding.

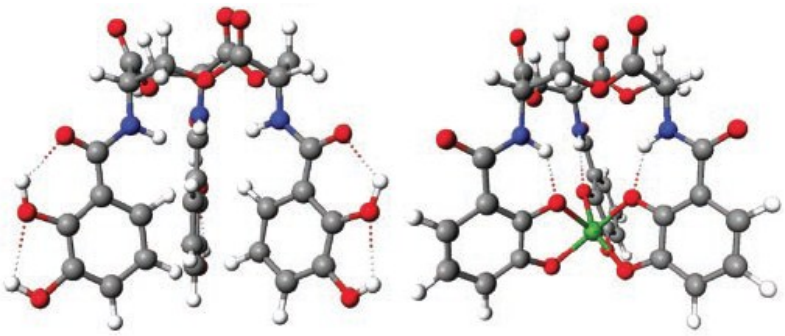

Figure 1.5 Representation of Fe^{3+} binding by enterobactin. *(Left)* Computer generated structure of uncomplexed enterobactin displaying H-binding network, *(Right)* structure of the V(IV)-enterobactin complex as a model for the Fe^{3+} complex. Reproduced from **PNAS**, *2003*, **100**, 7, 3584-3558.[19]

The core structure of enterobactin allows for the binding catecholate moieties to move minimally in order for iron complexation to take place (preorganised for iron binding), this reduces a disfavoured entropic contribution to the Gibb's Free Energy for the reaction and is the one reason for its remarkable affinity for Fe^{3+}, which will be discussed later in 1.5.1.

1.2.1 Ligand Denticity

Siderophores have been found to have a variety of denticities where; bidentate, tetradentate and hexadentate are the most common. However due to the thermodynamic considerations of metal-ligand complex formation, in general, siderophores which satisfy the octahedral arrangement i.e. hexadentate ligands, will form more stable Fe^{3+}-siderophore complexes. A general trend of ligand denticity and Fe^{3+}-ligand formation constant is displayed in Table 1.2.[20]

Table 1.2 Binding affinity for a range of ligands for Fe^{3+}, displayed in descending order of pFe^{3+} – data reproduced from **Nat. Prod. Rep**., *2010*, **27**, 637

Ligand	Denticity	Logβ (Fe^{3+})	pFe^{3+}
Enterobactin	6	49.0	35.5
MECAM	6	45.9	29.1
Ferrioxamine E	6	32.5	26.6
Amonabactin	4	34.5	26.0
Ferrichrome A	6	32.0	25.2
Ferrioxamine B	6	30.5	25.0
Ferrichrome	6	29.1	25.0
EDTA	6	25.1	23.4
Rhodotorulic acid	4	31.2	22.0
Rhizoferrin	6	25.3	20.0
N,N-Dimethyl-2,3-dihydroxybenzene	2	40.2	15.0
Acetohydroxamic acid	2	28.3	14.8
Hydroxide anion	1	11.7	14.6

It is shown that, with some exceptions, generally the higher the denticity of the ligand the stronger and more stable the Fe^{3+}-ligand complex, as denoted by the $\log\beta_{Fe^{3+}}$ and also the more efficient at scavenging Fe^{3+}, denoted by the pFe^{3+} value, discussed in 1.5.1.

A concentration effect is also apparent when we consider different denticities of ligands and those of higher denticity are favoured.

Bidentate	$Fe^{3+} + 3L^- \overset{\beta_3}{\rightleftharpoons} FeL_3$	$\beta_{310} = [FeL_3]/[Fe^{3+}][L^-]^3$
Tetradentate	$2Fe^{3+} + 3L^- \overset{\beta_2}{\rightleftharpoons} Fe_2L_3$	$\beta_{320} = [Fe_2L_3]/[Fe^{3+}]^2[L^-]^3$
Hexadentate	$Fe^{3+} + L^{3-} \overset{K_f}{\rightleftharpoons} FeL$	$\beta_{110} = [FeL]/[Fe^{3+}][L^{3-}]$

Figure 1.6 Equations displaying the equilibrium constants for bi-, tetra- and hexadentate Fe^{3+}-ligand complexation

The increased denticity of the hexadentate ligand, reduces the concentration requirement for that ligand to produce the fully saturated Fe^{3+} metal ion, in general this leads to a higher metal complex formation constant.[4,20]

In addition to a concentration effect we can also rationalise the trend displayed in Table 1.2 partially through the chelate effect. The chelate effect is the observed increase in complex stability for higher dentate ligands (polydentate) when compared to ligands of lower denticity with analogous binding sites (mono- or bidentate).[8]

There are a few apparent exceptions to the trend which links increased denticity and complex stability, both within natural and synthetic siderophores. An interesting illustration is provided by the synthetic molecules CP130 and its bidentate analogue 2-(3-hydroxy-2-oxo-1,2-dihydropyridin-1-yl)acetic acid. The compound named CP130 was first reported by Hider and coworkers in 1990 and was the first hexadentate 3,2-HOPO containing tripodal chelator.[21]

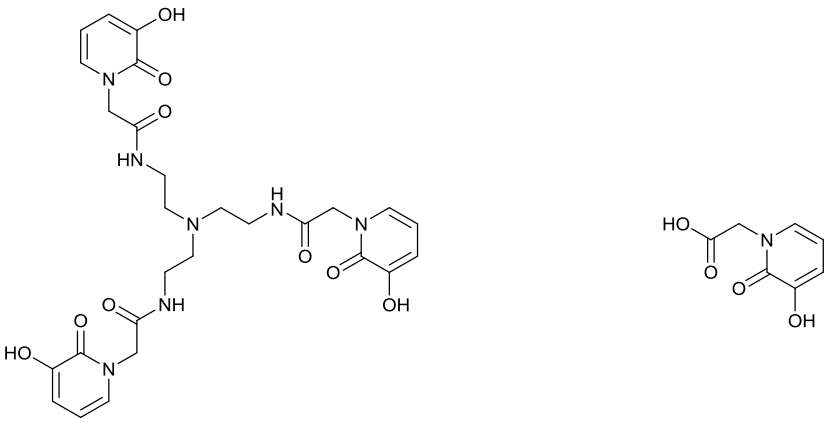

Figure 1.7 Structures of CP130 (left) and the bidentate unit (right)

The bidentate analogue has a reported $\log\beta_{310}$ of 32.3 whereas the subsequent incorporation of three bidentate units onto the TREN (tris(2-aminoethyl)amine) core produces the hexadentate chelator with a $\log\beta_{110}$ value of 28.8.[22] This drop in binding affinity has been attributed to disfavoured interactions when the hexadentate species forms a complex with Fe^{3+}, most likely the core scaffold influence. However, as the comparison is made between systems which vary in their stoichiometry, this conclusion is not strictly true. A better measure of binding affinity is the pFe^{3+} value which will be discussed in 1.5.1.

1.2.2 Arrangement of Binding Moieties

To achieve the hexadenticity required to saturate the coordination sphere of Fe^{3+} and hence produce strong Fe^{3+} chelation, the binding moieties of the most powerful siderophores can be incorporated within or around a core molecular scaffold.[23]

Siderophores have a diverse range of structures but the main families of architectural structures for hexadentate siderophores are displayed in Figure 1.8. The inclusion of; hydroxamate, catecholate or α-hydroxycarboxylic acid into the architectures displayed in Figure 1.8 is common in natural

siderophores. It is the incorporation of these groups into these arrangements, either mixed or the same type which has led to such a diverse library of natural siderophores.

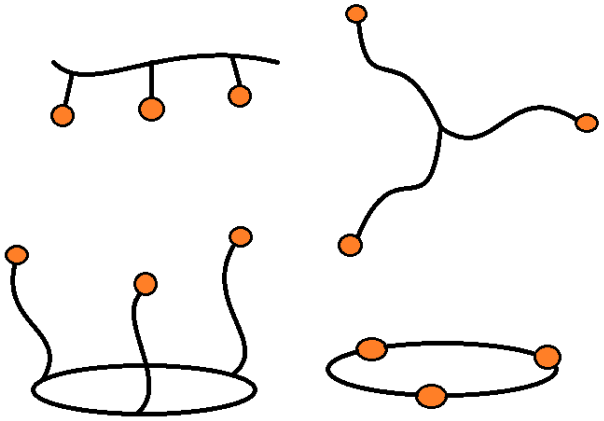

Figure 1.8 Common siderophore architectures. (i)top left, linear (ii) top right, tripodal (iii)bottom left, exocyclic (iv) bottom right, endocyclic. Orange denotes binding site, black lines are ligand scaffold.

Microbial siderophores adopt: linear, exocyclic and endocyclic architectures, examples to illustrate these are displayed in Figure 1.9.[4] Researchers designing synthetic analogues, such as CP130, have introduced the tripodal architecture.[24]

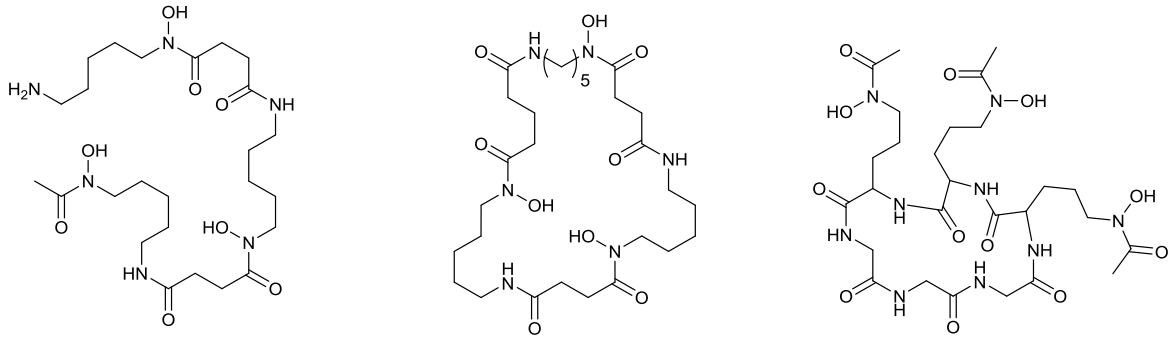

1.8 **1.9** **1.10**

Figure 1.9 Examples of natural siderophore architectures; desferrioxamine B (left, linear) desferrioxamine E (middle, endocyclic) and deferriferrichrome (right, exocyclic)

By way of example from natural siderophore molecules, as can be derived from Figure 1.9 that desferrioxamine E ($\log\beta_{110Fe}^{3+}$ = 32.5, pFe^{3+} = 29.7) has a higher affinity for Fe^{3+} than the linear desferrioxamine B ($\log\beta_{110Fe}^{3+}$ = 30.6, pFe^{3+} = 28.6). The marginally higher affinity may be attributed to the preorganisation towards binding Fe^{3+} achieved with desferrioxamine E, through having an endocyclic structure as opposed to the linear arrangement of the desferrioxamine B binding moieties.[20] Deferriferrichrome ($\log\beta_{110}$ = 29.1, pFe^{3+} = 25.2) has a lower affinity than both, this could be attributed to strain within the macrocycle core when Fe^{3+} binding occurs, or an insufficient organisation of the binding moieties towards the chelation of Fe^{3+}.[25]

The effect can also be noted when a comparison is made between the thermodynamic stability of the ferric complexes of enterobactin and the mono-hydrolysed linear enterobactin.

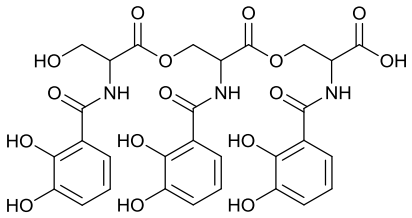

1.11

Figure 1.10 Structure of linear enterobactin

Enterobactin ($\log\beta_{310}$ = 10^{49}) displays a remarkably higher thermodynamic stability and therefore selectivity for Fe^{3+} over linear enterobactin ($\log\beta_{310}$ = 10^{43}). As the only difference between the two structures is the nature of the core scaffold (linear vs cyclic) the distortion in the stability constant is easily attributed to change in ligand architecture.[26]

1.2.3 Binding Moieties

Fe^{3+} has a high charge density and an ionic radius of around 0.64Å.[27] This creates a non-polarisable metal centre and therefore classifies ferric iron as a hard Lewis acid. With this realisation it is therefore not surprising that within natural siderophores, there is preferential incorporation of oxygen and nitrogen donor atoms into siderophore scaffolds. This can be seen as being the case with the natural siderophore examples shown in Figure 1.9. In addition, a five-membered chelate ring, producing a bite angle of approximately 69°, will be favoured over a six-membered ring because of the relatively large ionic radius of Fe^{3+}.[8] Despite the diversity of siderophore structures discovered in nature, there are a number of binding moieties that are conserved throughout the majority of siderophores. The catechol, hydroxamic acid and α-hydroxycarboxylic acid groups are the three groups found displayed most widely in natural siderophores, Figure 1.11.[28]

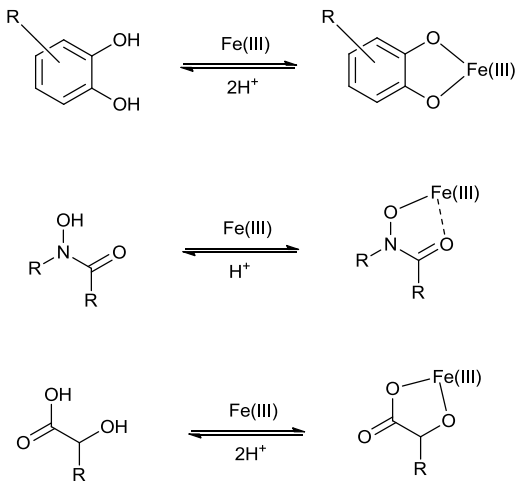

Figure 1.11 Examples of Fe^{3+} binding to common siderophore moieties (top) catechol (middle) hydroxamic acid and (bottom) α-hydroxycarboxylic acid

The catechol binding moiety is common throughout natural siderophores, most notably within the most powerful natural siderophore thus far discovered, enterobactin. There are also examples of

catecholic siderophores isolated from Gram-positive bacteria, such as bacillibactin (BB), isolated from *Bacillus subtilis* as well as related species *B. anthracis and B. cereus.*[29]

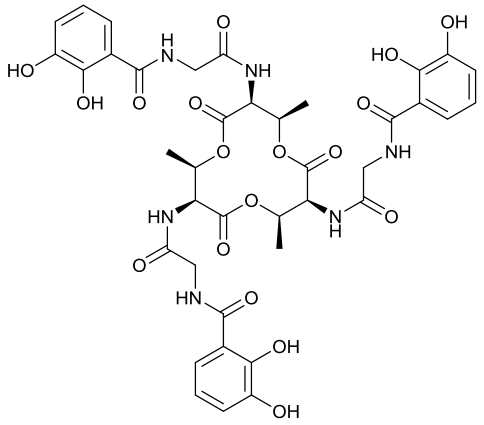

1.12

Figure 1.12 Structure of bacillibactin (BB)

There are many examples of the hydroxamic acid (Figure 1.11, middle) group within natural siderophores, the most well-known of which were displayed previously in Figure 1.9 within the desferrioxamine E and desferrioxamine B structures.[20,30] The α-hydroxycarboxylic acid group is most notably displayed within the marine siderophore families. Examples of which are displayed in Figure 1.13.

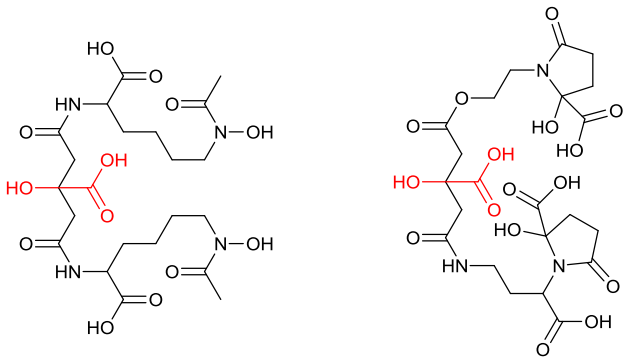

1.13 **1.14**

Figure 1.13 Structure of (left) aerobactin and (right) achromobactin displaying the α-hydroxycarboxylic acid binding group (red), structures reproduced from; **Coordination Chemistry Reviews**, *2010*, **254**, 288–296

Siderophores containing the α-hydroxycarboxylic acid moiety are susceptible to photolysis. UV photo-irradiation leads to the release of CO_2 and in turn reduction of the Fe^{3+} site to Fe^{2+}. This undoubtedly produces a less stable complex, as usually the Fe(II)-siderophore complexes have markedly lower formation constants and pFe(II) values, sometimes of up to 20 order of magnitude lower. This has been suggested as one of the possible iron release mechanisms utilised by marine bacteria.[31]

1.3 The hydroxypyridinone (HOPO) Moiety

In addition to the more common binding moieties discovered in the natural siderophore population i.e. hydroxamate, catecholate, there is another binding moiety found so far in only a few natural siderophores. The hydroxypyridinone (HOPO) moiety, one such example of this group isolated from nature is taken from the siderophore cepabactin (Figure 1.14) first isolated from *Burkholderia cepacia*.[32]

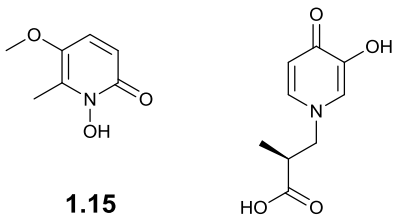

Figure 1.14 Structures of cepabactin (left) and mimosine (right), examples of the HOPO moiety found in nature

The HOPOs are very powerful Fe^{3+} ligands, stronger even than the catechol binding unit, Figure 1.15. They exist as three structural isomers, the 1,2-HOPO, 3,2-HOPO and the 3,4-HOPO (Figure 1.16).[28]

The HOPO groups are monoprotic acids and therefore form neutral complexes with trivalent metal cations,[33] the preferential affinity for the harder tribasic metal centres over the dibasic can be noted

through comparison of pFe^{3+} vs pFe^{2+} values. The limited abundance of the HOPO within the natural siderophore library could indicate that higher denticity ligands based upon these groups may be too powerful to be safely biosynthesised, stored or utilised by microorganisms. This maybe a mechanism by which recognition could be avoided by microbial uptake systems.

Ligand	Structure	pKa_1	pKa_2	$Log\,\beta_{310}$	pFe(III)
Acetohydroxamic acid		—	~9.5	~28	~13
Catechol		~8.5	~12	~40	~15
1-Hydroxypyridin-2-one		—	~6	~27	~16
3-Hydroxypyridin-2-one		—	~8.5	~32	~16
3-Hydroxypyridin-4-one		—	~10	~37	~20

pFe(III) = $-\log_{10}$ [Fe^{3+}] when pH = 7.4, [Ligand] = 10μM and [Fe^{3+}] = 1μM ; β = overall stability constant

Figure 1.15 Table displaying relative binding affinity for some bidentate units

As an example deferiprone, a 3,4-HOPO chelator has a logβ for Fe^{3+} of 37.2 where the corresponding Fe^{2+} logβ is 12.1, displaying the preference for hard cations.[34] Of the three isomers, the 3,4-HOPO displays the highest pFe^{3+} value.[35] In addition, the HOPO group is isoelectronic with catechol[33] and due to the zwitterionic nature of the HOPOs, they are bioisoteric with the catechol group, Figure 1.16.[36,37]

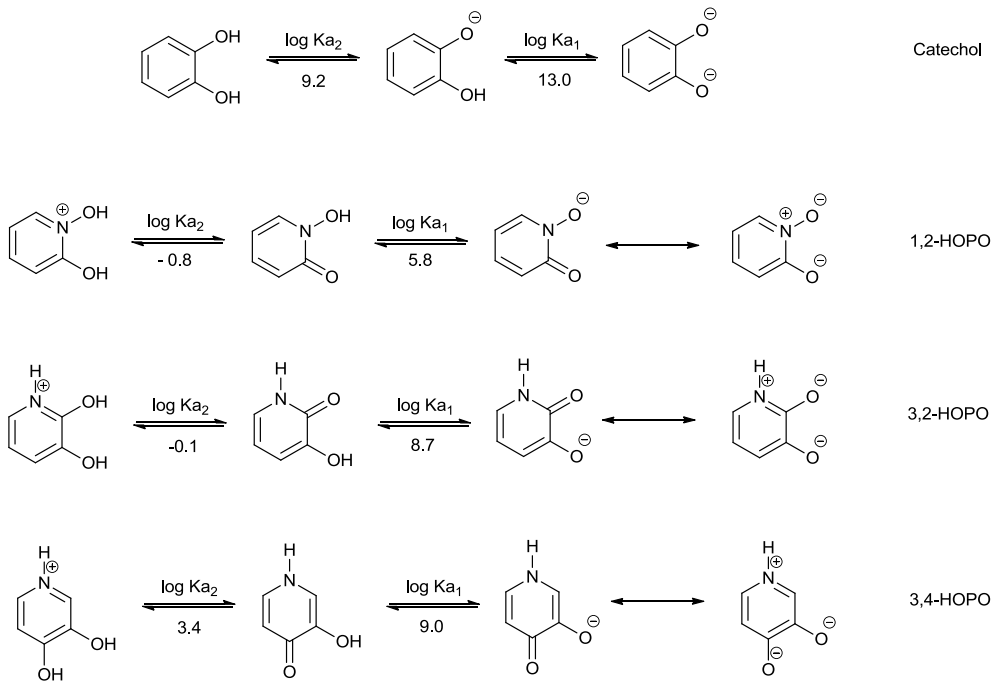

Figure 1.16 pKa values and structures of catechol and HOPO groups

1.3.1 Medicinal application of HOPOs

The HOPO moiety has current applications in medicine, deferiprone Figure 1.17 is an orally active 3,4-HOPO compound used in the treatment of iron overload. Deferiprone is an effective treatment for this condition, which can be brought on through iron supplementation following anaemia, as the properties of the 3,4-HOPO moiety lend well to the chelation of excess Fe^{3+} in vivo.[38]

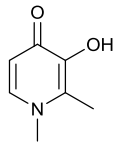

1.17

Figure 1.17 Structure of deferiprone

In particular, the affinity for the desired metal species i.e. Fe^{3+} over other metals within the biological system is highly desired when applying a chelator for this purpose in a biological system. Deferiprone is favoured amongst other treatments, such as DFO(B) due to its oral activity,

stability and low toxicity. However, some studies have shown links between deferiprone and patient hepatic fibrosis, which cast doubts on its continued usage in this area.[39]

1.3.2 Previous synthetic HOPO-based chelators

Hydroxypyridinone containing chelators have been accessed for a variety of: HOPO isomers, denticities and on several core molecular scaffolds. One of the earliest reported synthetic chelators containing the HOPO moiety (Figure 1.18), specifically the 1,2-HOPO moiety was reported in 1985 by Raymond *et al*.[40] The molecule presented contained features similar to that of rhodotorulic acid (section 1.8) and, as was discovered, both rhodotorulic acid and the HOPO compound were dianionic and tetradentate. Resulting from the tetradenticity, the ligand forms an Fe_2L_3 complex, as was shown for rhodotorulic acid.[41]

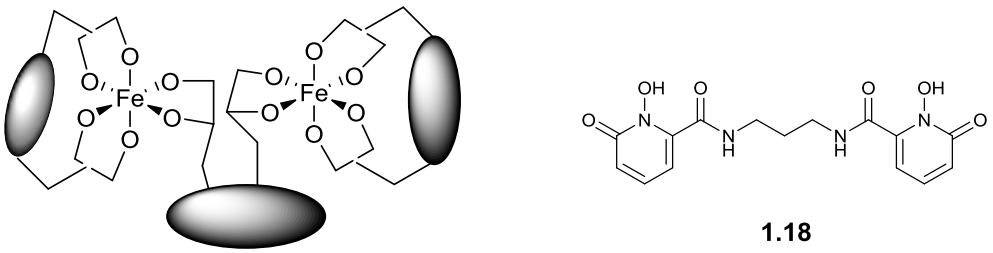

Figure 1.18 Complex structure for Fe_2L_3 (left) Structure of 1,2-HOPO tetradentate molecule reported in 1985 by Raymond *et al* (right)

The HOPO group has also been incorporated successfully into ligands designed for potential use as MRI contrasts agents, in particular targeting Gd(III) binding. The HOPO group, due to its affinity for trivalent metal cations was an obvious choice in this area of research. Examples in the literature include those of 1,2-HOPO and retro-3,2-HOPO containing ligands, Figure 1.19.[42-44]

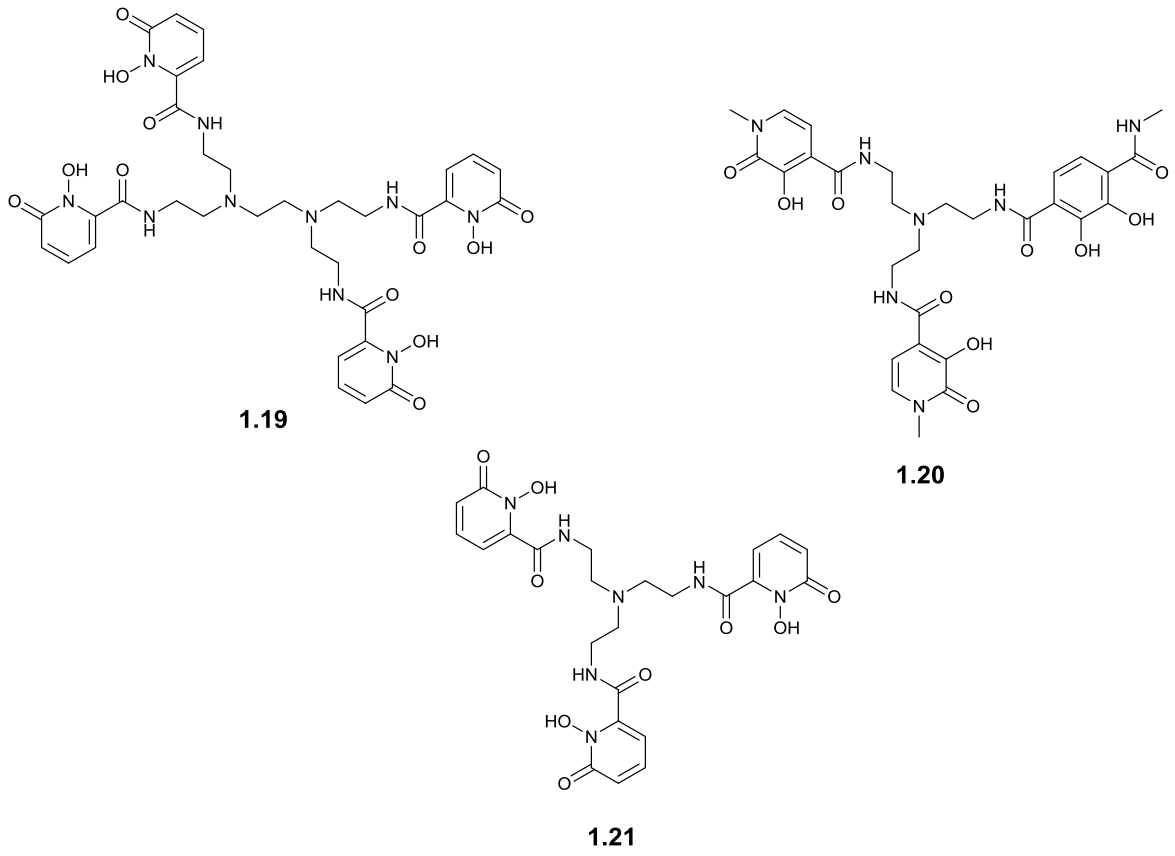

Figure 1.19 Structures of HOPO containing molecules designed for MRI contrast agents: H(2,2)-1,2-HOPO (top left), TREN-Me-3,2-HOPOTAM (top right) and TREN-1,2-HOPO (bottom)

In addition to MRI contrast agents, the HOPO moiety has been accommodated onto fluorescent probes for cell imaging purposes. The molecule in Figure 1.20 was published in 2010 by Hider *et al*.

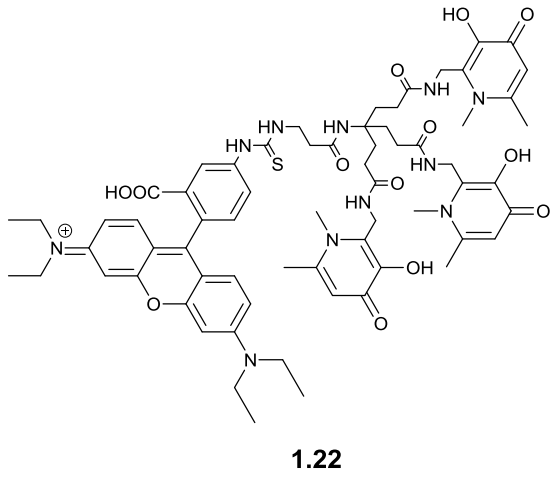

Figure 1.20 Fluorescent hexadentate Fe^{3+} chelator

The fluorescent probe was successful in allowing the intracellular compartments to which the chelator accumulated to be imaged. The fluorophore molecule was also shown to have an inhibitory effect on the growth of *Mycobacterium avium*.[45]

More recently, in 2011 Hider *et al*. published an article containing 3,4-HOPO containing chelators which were based upon tris(2-aminoethyl)amine and amine-triacid core scaffolds.

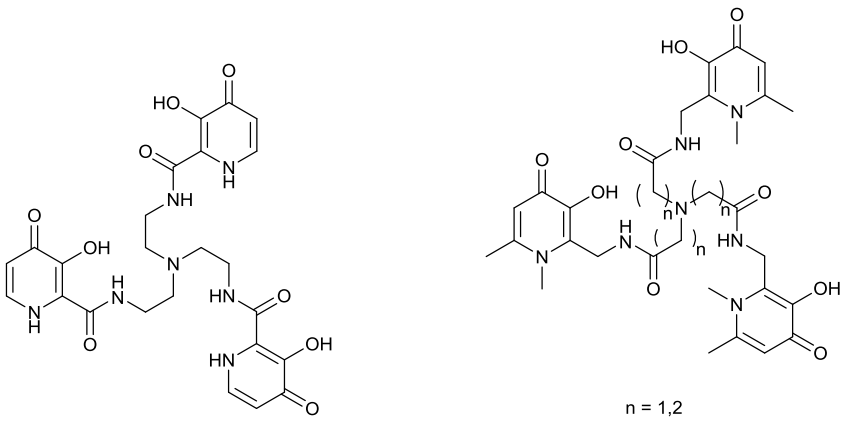

1.23 **1.24**

Figure 1.21 3,4-HOPO hexadentate chelators based upon amine-triacid core scaffolds

These compounds were tested for their antimicrobial properties with reference to DTPA (pFe^{3+} = 24.6). It was found that the compounds display antimicrobial activity against both Gram-positive and Gram-negative bacteria. The levels to which the antimicrobial activity was displayed are, with reference to molar concentration of the chelators, much lower than those of DTPA. Approximately 25/50% of the concentration of the HOPO containing chelators with respect to DTPA was required to induce inhibition. The inhibitory effect the molecules displayed was surmised to be attributed to their ability to disrupt bacterial iron absorption.[46]

There has been wide variety of tris-amide/amine based chelators which are tripodal in structure. However, HOPO containing chelators which are based upon more sophisticated core structures are less common throughout the literature, examples are given in Figure 1.22.

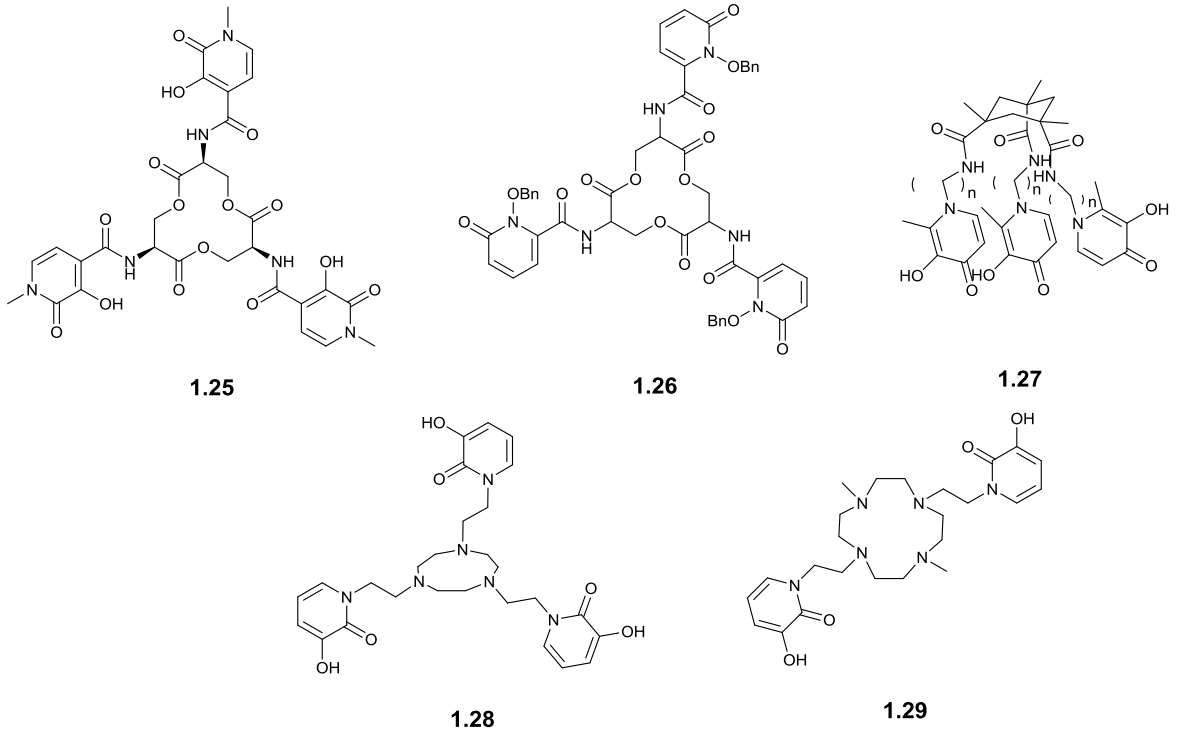

Figure 1.22 HOPO containing chelators based upon sophisticated core molecular scaffolds. Retro-3,2-HOPObactin (top left) 1,2-HOPObactin (top centre) KEMPPr(3,4-HP)3 (n = 3); KEMPBu(3,4-HP)3 (n = 4) (top right). N3(etLH)3 (bottom left), 4(N),10(N)-Bis[2-(3-hydroxy-2-oxo-2H-pyridin-1-yl)ethyl]-1,7-dimethyl-1,4,7,10-tetraazacyclododecane (bottom right).

Of those chelators displayed in Figure 1.22 the two HOPObactin analogues (top left and top centre) are those whose structures are the most similar to that of enterobactin.[39,47] The stability constant and pFe^{3+} have not been assessed for the 1,2-HOPObactin analogue as yet due to the inability to afford the deprotected ligand. However, for the retro-3,2-HOPObactin the results show that there is a significant loss of stability for this analogue with respect to enterobactin. Where we see enterobactin has a $pFe^{3+} = 34.3$ the HOPObactin analogue has a $pFe^{3+} = 27.4$[39,48] It is clear from these figures that the core scaffold, unlike in enterobactin, does not provide the increased stability for these pendant HOPO moieties which we see for the catecholate within the natural siderophore.

For the ligands KEMPPr(3,4-HP)$_3$ (n = 3); KEMPBu(3,4-HP)$_3$ (n = 4) (top right) the pFe^{3+} values are 28 and 26.8 respectively.[49] Despite the 3,4-HOPO moiety possessing the highest pFe^{3+} value in its bidentate state, this molecule does not reach some of the higher pFe^{3+} values we have seen for some other synthetic siderophores. This could be attributed to either inherent strain arising from an imperfect predisposition of the binding groups by the core scaffold, or that the para-situated

attachment (with respect to the carbonyl-functionality) of the binding groups to the scaffold interferes with stability, as an ortho-attachment has been shown to be important in some instances.[34]

There are but a few examples of macrocyclic core scaffolds bearing HOPO functionality. Those shown in Figure 1.22 (bottom left and right) were produced through similar synthetic methodology. The core scaffolds in these cases display an increased stability over a wide pH range, avoiding hydrolysis, unlike those based upon a hydrolysable core scaffold such as enterobactin and its analogues based upon the trilactone core. The introduction of secondary amine functionality into the core also improves the aqueous solubility of the chelators.[39]

1.4 Thermodynamic Considerations of Complex Formation

Complex stability can be considered as being the result of a series of contributing thermodynamic factors. Governing the thermodynamics of complex stability is the equation describing the Gibbs free energy of a reaction ΔG^o.

$$\Delta G^o = \Delta H^o - T\Delta S^o$$

Figure 1.23 Equation for the Gibbs free energy of reaction (kJ mol^{-1}), ΔH^o is the standard enthalpy of reaction ($Jmol^{-1}$), T is the temperature (K) and ΔS^o is the standard entropy of reaction ($JK^{-1}mol^{-1}$)

Highly charged ions in solution can be thought of as imposing order upon the molecules surrounding them e.g. solvent molecules, brought on by imposed dipole interactions. This imposition upon the surrounding molecules can be considered to be thermodynamically unfavourable in terms of the entropic contribution, $\Delta S°$. Therefore, the formation of complexes involving charged species would result in partial or complete cancellation of those charges in solution. This results in an increase in entropy for the system overall and provides a favourable contribution to the entropic considerations within the free energy of the system.

The total or partial cancellation of charges in solution has also a favourable enthalpic contribution, as the combination of oppositely charged species in solution and hence the partial or complete

cancellation of charges, in general, holds a significantly negative ΔH^{o}, favoured in terms of Gibbs free energy.

In addition, polydenticity in ligands has an impact on the thermodynamic favourability of complex formation. The chelate effect, as previously discussed will have enthalpic and entropic contributions to stability also. For example, a stabilising enthalpic contribution of the chelate effect would be the inductive contribution of electron density gained from atoms adjacent to the ligating sites. This will increase the donor strength of binding sites and increase the stability of the complex.

The overall entropic contribution stems from two major contributing factors. Firstly, the entropy surrounding metal-ligand complex formation is often more favoured for reactions in which the ligands are polydentate. This is because the polydentate ligands often displace several solvating molecules, leaving more free species on the product side of a reaction. This type of interaction leads to an increase in entropy of the system and thus increased thermodynamic favourability, Figure 1.24.

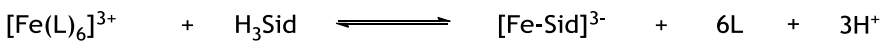

Figure 1.24 Reaction scheme for a hexadentate siderophore (H_3Sid) species displacing solvent molecules from ferric iron centre

Furthermore, polydentate ligands have an increased probability of complex formation due to the 'branches' of the complexed ligand directing the binding of the non-complexed 'branches'. The complexed binding sites hold the ligand in place making it more likely the other sites will bind.[8]

1.5 Expressing the Stability of Fe^{3+}-siderophore complexes

In order for many siderophores to bind Fe^{3+} the dissociation of protons from the ligand is necessary. This creates a competition between the Lewis acids Fe^{3+} and H^{+} for the ligands binding sites. This competition between the two has to therefore be accounted for when calculating equilibrium constants for Fe^{3+}-siderophore complex formation, Figure 1.25.[50,51]

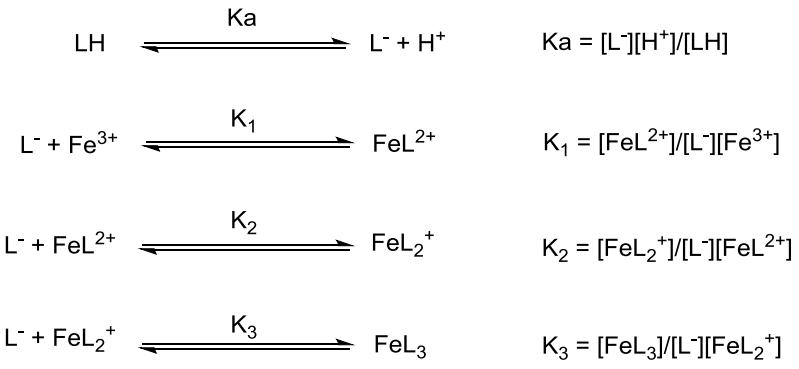

Figure 1.25 Equations displaying the stepwise addition of a monoprotic bidentate ligand (L) to Fe after proton dissociation

To simplify the expression of these stepwise stability constants it is often the case that these are often expressed as the product of the overall stability constant β, Figure 1.26.[51]

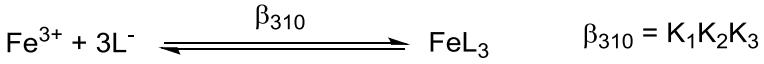

Figure 1.26 Reaction scheme for the overall stability constant defined for the addition of a bidentate monoprotic ligand L to Fe

With siderophore overall stability constants when the reaction involves multiple ligands of the same type (denticity and structure) the β values are displayed along with subscript notations in the form of β_{LMH} where, L = number of the same ligand involved, M = number of metal centres involved and H = number of protons involved in the stoichiometry of the equilibrium expression.

Figure 1.26 displays the case for monoprotic bidentate ligands, however the most powerful chelators are usually hexadentate. For these ligands the overall stability constant would take the form β_{110} for the fully deprotonated triprotic hexadentate ligand, .

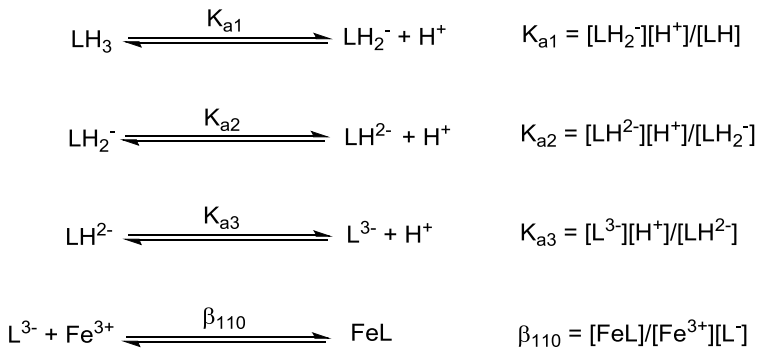

Figure 1.27 Equations displaying the stepwise deprotonation steps for a triprotic hexadentate ligand and the overall stability constant of such a ligand binding Fe

The presence of the competition between the Lewis acidic centres means that the equilibrium conditions for the reactions will be pH dependent. However, when we look at siderophore equilibrium constants it is often simpler to measure the conditions for the proton-free reaction, that is the β measured for the fully deprotonated ligand.

The overall stability constant does not account for the Lewis acid competition between H^+ and Fe^{3+} which would often be present in biological systems. For this reason it allows for the direct comparison only for ligands that are of the same denticity, which would give the same stoichiometry for the Fe^{3+}-ligand complex at equilibrium.[20]

1.5.1 pFe^{3+} as a measure of ligand binding efficiency

An alternative measurement of complex stability is to measure the equilibrium concentration of free Fe^{3+} in solution. This value is the pFe^{3+} and it is analogous to pH, in that it is defined as;

$$pFe^{3+} = -\log_{10}[Fe^{3+}]_{free}$$

The pFe^{3+} value is usually defined for pH = 7.4, $[Fe^{3+}]_{tot}$ = 1μM and [Chelator] = 10μM. The values obtained for the pFe^{3+} are dependent upon the pH, $[Fe]_{tot}$ and $[Che]_{tot}$ and as a result only those measurements taken using the same defined conditions are comparable. The Lewis acid competition of dissociated protons, ligand denticity and basicity as well as differences in metal-ligand stoichiometry is accounted for by the pFe^{3+} value and hence it is a more acceptable measure

of the ability of a ligand to bind Fe^{3+}. The $[Fe^{3+}]_{free}$ is understood as the non-complexed Fe^{3+} left in solution. The measurement was first realised by Raymond *et al*. in 1979 in order to characterise the Fe^{3+}-aerobactin complex. This value allows for the direct comparison of chelator strength as long as the conditions in which the measurements are taking are conserved in both cases, the one with the highest value of pFe^{3+} will be the stronger chelator.[52]

Enterobactin has an affinity for Fe3+ which is notable as being the strongest natural siderophore ever discovered with a $\log\beta_{110} = 49$ and pFe^{3+} of 34.3. [8,9]

Previous work has described the possibility of stronger iron chelators to be synthesised than enterobactin, as the core unit still holds some inherent strain, shown through molecular modelling. This study highlighted that the β_{110} has a connection with the inherent strain in the molecule and if this was brought to a minimum a theoretical maximum of β_{110} of $\sim 10^{57}$ +/- 5 which would equate to 10^{8} +/- 5 higher than that of enterobactin.[53]

1.5.2 Kinetic Considerations of ferri-siderophore Complexes

Generally, rate of ligand exchange for ferri-siderophore complexes is slow due to the overwhelming affinity of the siderophore for the Fe^{3+}. This ensures Fe^{3+} binding even at minute concentrations.[20] The dissociation of a siderophore from the complex has been investigated and found to be assisted by lowering the pH. For hydroxamate siderophores, the data suggests both multiple species and pathways are present in the dissociation of tris-chelated dihydroxamate complexes.[54]

The lability of ligands in general decreases with either increasing denticity or level of organisation towards the metal centre and so the bidentate and tetradentate siderophores show faster rates of dissociation and ligand exchange kinetics than the hexadentate analogues. This has been hypothesised to be associated with Fe^{3+} delivery to the cell in that, the bi- and tetradentate ligands would primarily bind the metal and then these would release the Fe^{3+} to the more powerful hexadentate siderophores, due to their lability.[34] As an example to illustrate, Raymond *et al*.

determined through $^{55}Fe^{3+}$ labelling studies that the exchange of the metal between ferrioxamine B and ferrichrome A is 50% complete after 220 hours at pH 7.4. The exchange is therefore quite slow but again this rate can be increased through lowering pH.[55]

1.5.3 Kinetic Vs Thermodynamic Considerations

In the design of novel synthetic chelators for bacteriostatic applications there will be consideration given to both the thermodynamic and kinetic factors which affect the binding of Fe^{3+} by a ligand.

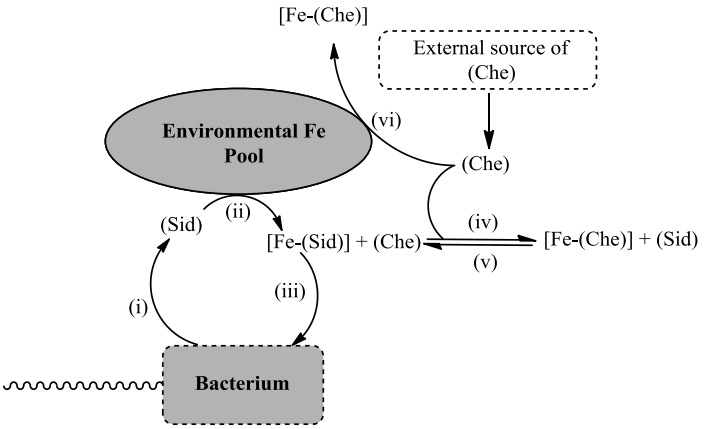

Figure 1.28 Diagram to represent effective routes to Fe^{3+} bacteriostasis by synthetic chelator (Che) with respect to natural siderophore Fe assimilation by bacteria (Sid). (i) Siderophore production and release (ii) ferri-siderophore complex formation and formation of equilibrium with (Che) (iii) diffusion of ferri-siderophore complex to bacterial cell (iv) competition of ferri-siderophore complex with synthetic chelator (Che) (v) Competition of ferri-(Che) complex with natural siderophore (Sid) (vi) depletion of the environmental Fe pool via (Che)

The design of new Fe^{3+} selective ligands will encompass those features which will produce thermodynamic complex stability as discussed in section 1.5. However, these will be in competition with the microbial systems (Figure 1.28). Depending on the rate of complex formation from the environmental Fe pool, different pathways to Fe^{3+} starvation must be addressed.

If complexation of the environmental Fe by the new ligands (Che) is achieved at a faster rate than that of the bacterium's own siderophore (Sid) released into the extracellular environment (i) then the competition for the metal should be thermodynamic between the (Sid) and the [Fe-Che] (v).

Alternatively, if the complexation of Fe by the (Che) occurs at a slower rate than that of the natural (Sid) (ii) then the thermodynamic competition will be between [Fe-Sid] and (Che), (iv). This competition is represented by the equilibrium in Figure 1.28. Though the competition for complex formation would not be mutually exclusive between the competing processes, one may dominate based on more favourable thermodynamic or kinetic properties.

As previously stated, the proposed high affinity Fe^{3+} ligands to be synthesised will incorporate design features to improve their likelihood in forming thermodynamically stable complexes however; little is known regarding the effect ligand structure has on creating kinetically favourable complex formation. Therefore, the thermodynamic factors which contribute to the design of high affinity Fe^{3+} chelators need to be addressed in the first instance to ensure that the ligands achieve the primary project aim. After these factors have been addressed the kinetic factors which contribute to Fe^{3+} binding can be studied further. Ideally, the rate of [Fe-Che] formation will be rapid to produce a kinetically viable ligand as well as the thermodynamic stability of the complex being favoured over the [Fe-Sid] complex.

The lability of the formed complex and rate of metal exchange between natural and synthetic competing ligands will become important if the bacterial response to Fe^{3+} starvation includes the secretion of large quantities of (Sid). It may be the case that there is a window in which the applied synthetic ligands function but are eventually overcome by far higher concentrations of (Sid) being introduced to the extracellular environment by the microbes. Literature suggests that the exchange kinetics between chelators of this nature are generally slow, therefore if the initial complexation of environmental iron by (Che) is rapid the exchange with (Sid) should be slow and the desired bacteriostasis should be observed. This effect may be measurable as a delayed response in bacterial growth over time with reference to cultures lacking (Che) i.e. a repopulation 'lag time' should be observable. However, if the opposing situation arises that of the [Fe-Sid] complex formation is more kinetically viable then this lag time may not be observed on a measurable timescale.[56]

1.6 Iron Uptake and Intracellular Release in Bacteria

1.6.1 Siderophore Mediated Fe^{3+} Acquisition in Bacteria

As described by Crumbliss *et al*. siderophore mediated Fe^{3+} acquisition in bacteria follows the general pathway displayed in Figure 1.29. Firstly the siderophore is biosynthesised and released by the cell into the surrounding environment. Then the siderophore forms a complex with iron, which is followed by diffusion of the complex to a cell's surface. Specific ferri-sideorphore receptor proteins on the surface of the cell recognise the Fe^{3+}-siderophore complex and facilitate transport of the complex into the cell's interior where finally the iron is released from the complex for use in microbial metabolic processes.[4]

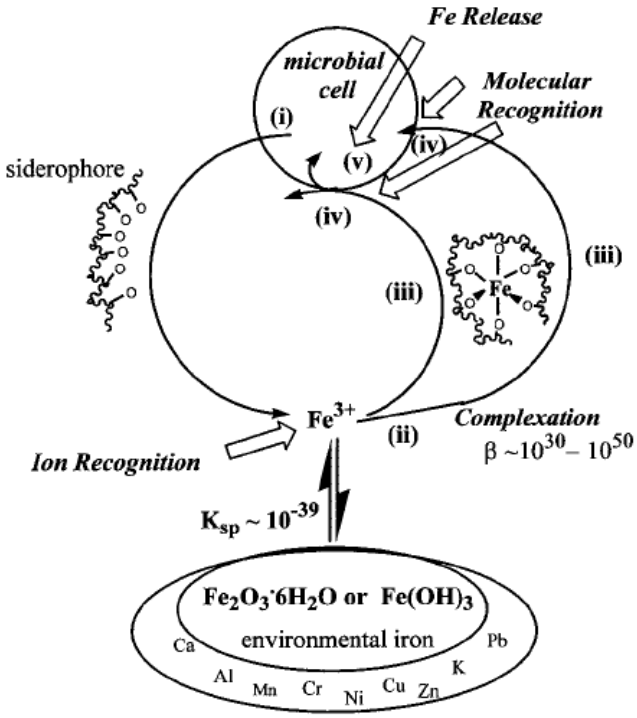

Figure 1.29 Diagram representing pathway for sideorphore mediated Fe^{3+} acquisition in bacteria; diagram from Hakim Boukhalfa & Alvin L. Crumbliss; **BioMetals**, *2002*, **15**,325–339

The generalised overview of siderophore-mediated iron acquisition is well established. It requires a high affinity receptor to capture and effectively concentrate the micronutrient at the cell surface. The ferri-siderophore complex is actively dissociated from the receptor and transported to the

interior of the cell where the iron is then downloaded from the complex by a reductive process to a less stable ferro-siderophore from which the metal can be readily exchanged.

The specific intricacies and differences between bacteria and their acquisition mechanisms have been studied. A simple classification of bacteria distinguishes Gram-positive and Gram-negative genera. The most conspicuous difference between these two groups is their distinctive cell envelope architecture; the variations herein have implications for the pathway for iron uptake. The following briefly relates these architectural differences and the structural biology solutions that have evolved to assure the efficient supply of iron.

1.6.2 Gram-negative Bacteria

The main structural difference seen in the cell envelope of the Gram-negative bacteria is their possession of an additional outer membrane that limits a secure periplasmic space in which a thinner layer of murein resides. The outer membrane affords the underlying bacterium some protection from toxins, degradative enzymes and detergents. Some passive diffusion of macronutrients across this membrane is facilitated through the relatively non-specific water-filled channels in porin proteins. This system is not adequate to support the uptake of scarce micronutrients such as ferri-siderophores and cobalamin. In these cases the necessary high-affinity receptor proteins are located within this outer membrane. The outer membrane has no ATP-binding cassette proteins to allow for an energy transfer to facilitate movement of the Fe^{3+}-siderophore complexes through the outer membrane, like we see in the cytoplasmic membrane. It has been suggested the energy to do this stems from interaction of the outer membrane receptor with the TonB system (TonB, ExbB and ExbD).[57,58]

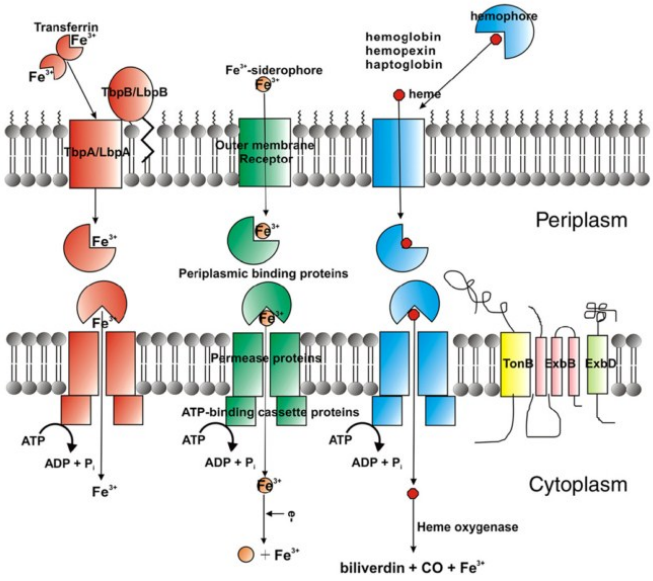

Figure 1.30 Diagram representing the biology of Fe^{3+}-siderophore complexes in Gram-negative bacteria – taken from **Biochimica et Biophysica Acta**, *2008*, **1778**, 1781–1804

The binding of the ferri-siderophore to the receptor must be strong and requires active dissociation in a structure that affords influx of the chelate to the periplasmic space. Crystal structures have been determined for the outer-membrane receptors FhuA (hydroxamate) FecA (citrate) and FepA (enterobactin) in *E. coli.* Also, FpvA (pyoverdine) and FptA (pyochelin) in *P. aeruginosa.*[59,60] These outer membrane receptors have a barrel and plug construction. The transmembrane channel is formed by a β-barrel protein domain that resembles the non-specific open channels of the porin diffusion channels. In this case the channel is blocked by a globular 'plug' or 'cork' domain that fills the channel and controls the movement of molecules through it. It is this domain that binds the ferri-siderophore complex. This binding event initiates a rearrangement of a part of the plug domain that faces the periplasmic space. The rearrangement allows the receptors' recognition by the periplasmic TonB protein which transduces energy to drive the translocation of the complex to that location via further rearrangement of the plug domain.[61]

The periplasmic binding proteins then interact with ATP-binding cassette proteins and permeases to facilitate movement of the complex through the plasma membrane. Not all bacteria have the three systems shown in Figure 1.30; haemoglobin, transferrin and lactoferrin and siderophore. Most have a combination of these systems.

1.6.3 Gram-positive Bacteria

Gram-positive bacteria present the least complex pathway for ferri-siderophore uptake. Their key outer structures are the cell wall and plasma membrane. The cell wall of Gram-positive bacteria is made up of primarily murein, polysaccharides, teichoic acid and cell wall-associated proteins. The murein is the major structural component forming a single macromolecular boundary to the cell. In order to support mass transfer of materials across the cell's margins, it has a well-hydrated and highly porous structure. Ferri-siderophores passively diffuse through the thick murein layer. Their active uptake commences when they encounter high-affinity cognate binding proteins that are anchored in the plasma membrane *via* a lipid modification. These receptor proteins intimately interact with permease and ATP-binding cassette proteins embedded in the plasma membrane to facilitate transport across the membrane, Figure 1.31. On sensing a ferri-siderophore loaded receptor, these ATP-binding cassette proteins transduce energy derived from the hydrolysis of ATP to affect the transport of the ferri-sidrophore complex through the integral transmembrane channel of the permease. One such example of this uptake system comes from *Bacillus anthracis* and related strains and is the uptake the ferri-siderophore complex ferribacillibactin.[29,62] Initial binding of the complex by the membrane protein receptor is followed by active uptake of the complex, mediated by the FeuA receptor protein.[57]

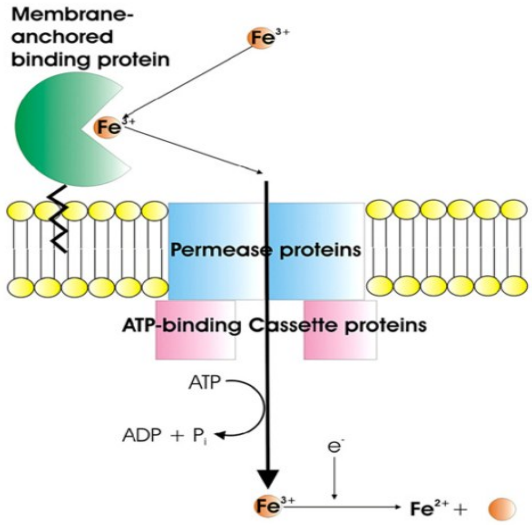

Figure 1.31 Diagram representing the Fe^{3+}-siderophore uptake in Gram-positive bacteria - taken from **Biochimica et Biophysica Acta**, *2008*, **1778**, 1781–1804

1.7 Siderophore Recognition

In terms of ferri-enterobactin uptake by *E. coli,* Raymond *et al*. discovered several important structural features, thought to be crucial in enterobactin to facilitate uptake and recognition of the ferri-siderophore complex.[63] The group synthesised enterobactin analogues to investigate which features of the natural molecules were necessary for molecular recognition and eventual uptake of the complex.

The amide functionality adjacent to the catechol rings appear to be necessary for recognition by the outer membrane receptor for Fe^{3+}-ent. However, the molecular structure of the nitrogen atom of the amide linkage is not significant for recognition. Both secondary and tertiary nitrogens in this position can be utilised as substrates for the receptor. Additionally, minor structural alterations to the binding unit were shown to reverse activity. No uptake was observed when substitution of the ring by methyl- or sulphate had occurred.

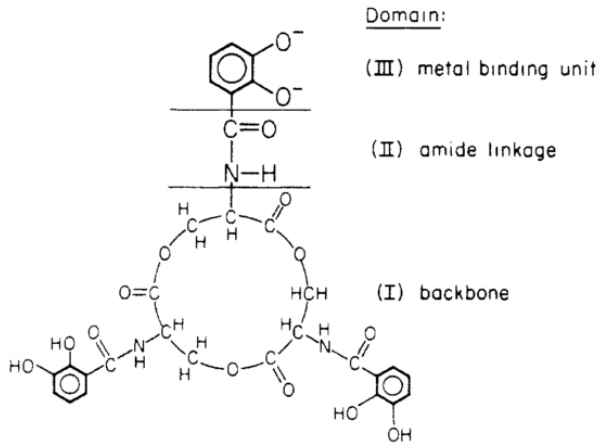

Figure 1.32 Highlighting the domains investigated by Raymond *et al*. from **J. Am. Chem. Soc**., *1988*, **110**, 2451-2464

In other examples, the configuration of the groups at the metal centre has been found to be important in siderophore recognition. Rhodoturulic acid is a tetradentate dihydroxamic acid siderophore. It accomplishes full saturation of the iron coordination sphere through forming the L_3M_2 ligand to metal stoichiometry.[26]

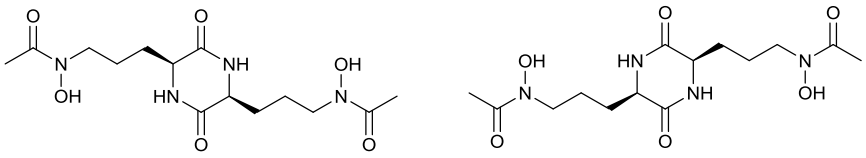

1.30 **1.31**

Figure 1.33 Structure of rhodotorulic acid (left) and enantiorhodotorulic acid (right)

The absolute configuration is Δ (right handed propeller) for ferri-rhodoturulic acid complex at the metal centre, opposite to that of ferrichrome. The enantiomeric derivative therefore has a Λ-configuration (enantiorhodotorulic acid) at the metal centre and it is this enantiomer which is successful in mediating iron transport to E. coli. It was concluded that this is a consequence of the receptor recognising the configuration at the metal centre, Figure 1.34.

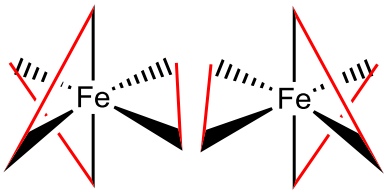

Figure 1.34 Diagram to show sterochemical configuration of enantiomers in octahedral Fe complexes (Λ-configuration right structure. Δ-configuration left structure)

In contrast, a recent study of the enzymatic hydrolysis of the ferric- enterobactin and bacillibactin trilactone backbones was performed by Albergel *et al*. in order to discover where particular chiral recognition occurs in the uptake of these complexes.[62] It was discovered that, in terms of enzymatic hydrolysis *in vivo* of these complexes, it is the trilactone backbone and not the configuration of the binding groups at the metal centre which is important for recognition. This was concluded from producing the enantiomeric forms of the complexes, which by definition have the alternate stereochemistry at the metal centre and seeing the effect this has on uptake. The enantiomeric complexes were able to be uptaken by the membrane receptors; however enzymatic

cleavage of the backbone within the periplasmic space could not be achieved, therefore leading to the conclusion that the chirality of this complex is recognised once uptake has occurred.

This suggests a different recognition pattern for chirality, contrasting with what has been observed for rhodotorulic acid and highlighting the differences in hydroxamate and catecholate uptake pathways.

1.8 Mechanisms of Fe^{3+} Release

1.8.1 Reductive Release

Several mechanisms for the release of Fe^{3+} from bacterial siderophore complexes have been proposed. For hydroxamate-containing siderophores, such as ferrioxamine B, the release mechanism is thought to be relatively simple and involves the reduction of the metal centre from Fe^{3+} to Fe^{2+}. This process significantly reduces the ligand's affinity for the metal centre and therefore the complex stability. The iron can now be more readily removed from the complex through exchange with other intracellular ligands. This general mechanism has been shown to be the case for several hydroxamate siderophore producing organisms.[64]

A reductive mechanism of iron release allows for the reutilisation of the siderophore,[65] and therefore poses a lesser metabolic penalty to the microbe. Biological reducing agents such as NADH hold reduction potentials of around -320mV and so are able to reduce ferri-siderophore complex which fall into this range such as the hydroxamate-based rhodotorulic acid, $E_{1/2}$ = -359mv.

However catecholate siderophores, in particular tris-catecholate siderophores such as enterobactin possess much lower reductive potentials, $E_{1/2}$ = -750mV for ferri-enterobactin.[4] Therefore these are out of the range of biological reductants and so other mechanisms for iron release are thought to be necessary. However the reduction potential can alter with respect to the $[H^+]$ and so an increase in acidity may lead to iron release via a reductive pathway.

1.8.2 Enzymatic Release

Although the ferri-enterobactin complex has been the most studied in terms of its iron release mechanism, there is no consensus on one mechanism for the release of the iron to the bacterial cell; several opposing theories have been put forward.

The Fes esterase enzyme that operates within the cytoplasm of the Gram-negative bacterium *E. coli* was found to be specific for the Fe^{3+}-enterobactin complex. A mechanism that involves the enzymatic hydrolysis of the enterobactin ligand by this enzyme leading to the eventual release of Fe^{3+} has been proposed.[62]

The enzyme can hydrolyse both the apo- and ferri- forms of the siderophore. Hydrolysis by Fes leads to the generation of dihydroxylbenzoylserine monomeric units binding Fe^{3+}.[26] The reduction potential of these monomeric units lies within the range of biological reducing agents and hence the process promotes Fe^{3+} release.

This hypothesis has some strong supporting evidence as mutant organisms lacking the Fes esterase enzyme turn pink due to an accumulation of Fe^{3+}-ent complex. The inability to release intracellular Fe^{3+} without the esterase would suggest that it is vital for the release of Fe^{3+}.[65] However, once hydrolysed the monomeric units can no longer be utilised as siderophores, this poses a significant metabolic cost to the organism and thus has become one of the main opposing opinions to the enzymatic release proposal.[66] However, it is worth considering that a lower concentration of enterobactin may be required to deliver sufficient iron to the cell in comparison to other, less potent siderophores.

Alternatively, protonation of the Fe^{3+}-ent complex leading to reduced stability of the complex or a conformation switch from the catecholate to salicylate binding mode has been suggested. The salicyclate mode requires the protonation of the Fe^{3+}-ent complex at the most basic catecholic site on each binding unit.[64,66]

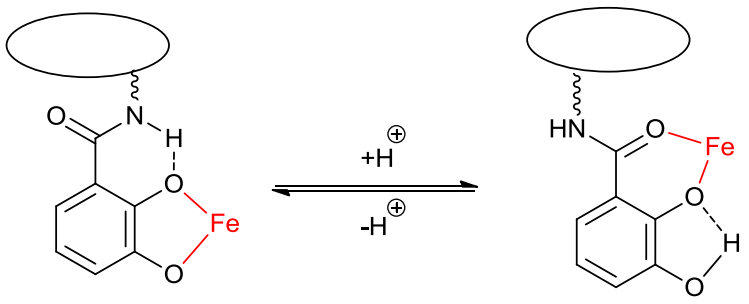

Figure 1.35 Diagram displaying the conformational shift due to protonation of a catecholate binding mode of iron to the salicylate mode

In addition, altering the lipophilicity of the complex environment or having a large concentration of Fe(II) chelant surrounding the Fe^{3+}-ent complex have both been proposed as possible mechanisms by which seemingly irreducible complexes by biological means may be reduced in vivo. These might promote a reductive, rather than enzymatic, release of iron to the bacterial cell.[64]

The primary function of the Fes esterase in this latter scenario would be the degradation of the apo-siderophore to limit the reformation of the of the ferri-siderophore complex. The subtle difference here is that the Fes esterase is not required for the removal of iron from the complex but it is required for effective utilisation of the enterobactin-delivered iron.

It is however still unclear as to which mechanism, or indeed combination of mechanisms under different conditions facilitates the release of Fe^{3+} from the Fe^{3+}-ent complex *in vivo*.

1.9 Synthetic Chelators

1.9.1 Fe^{3+} Affinity

There are now numerous examples of synthetic siderophores, some of which have stability constants and pFe^{3+} values approaching those of enterobactin, some well-studied examples are displayed in Figure 1.36.

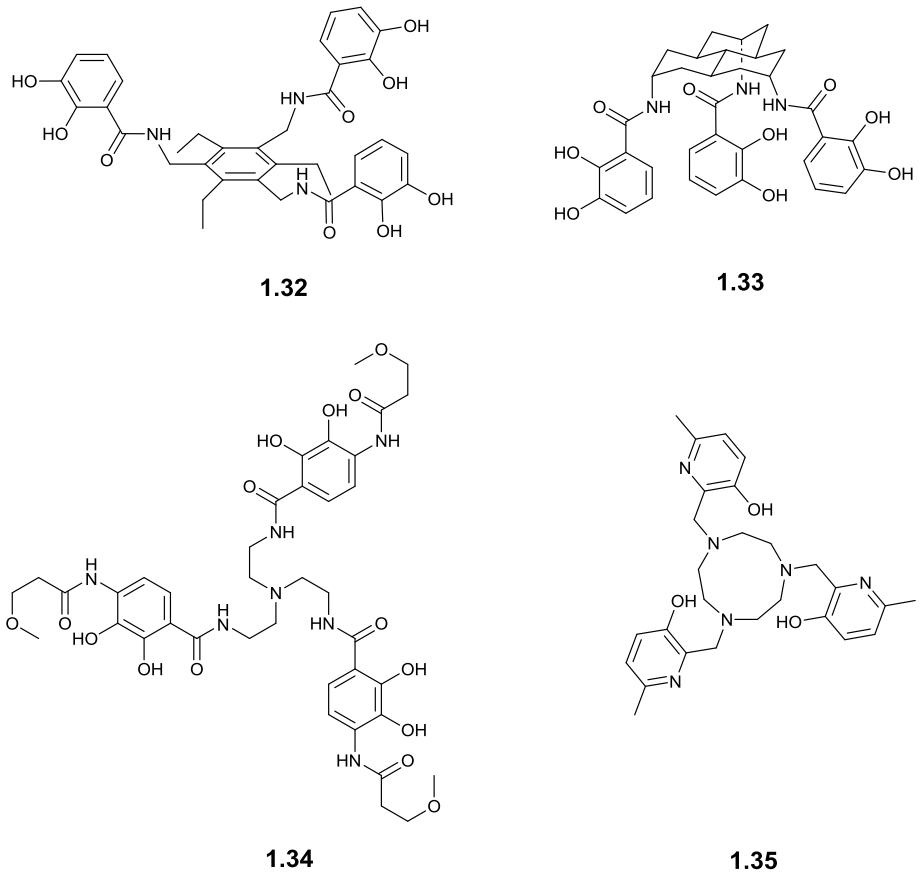

Figure 1.36 Examples of literature chelators. EMECAM (top left) carbocyclic triscatecholate (top right) TRENTAM (bottom left) TACN-MeHP (bottom right)

EMECAM (Figure 1.36) is a triscatecholate siderophore mimic; the ethyl- groups were included to probe the hypothesis that bulky groups would promote the preorganisation of the catecholate moieties towards Fe^{3+} binding.[67] When comparison is made between EMECAM, the methyl derivative MMECAM and MECAM (Table 1.3); we can see the larger the groups the more preorganisation towards chelation and in turn the higher the $\log K_{Fe}^{3+}$ and pFe^{3+} values.[53]

Table 1.3 Table displaying stability constants and pFe^{3+} values for synthetic chelators EMECAM, MMECAM and MECAM and natural siderophore enterobactin

Ligand	$\log\beta_{110}$ (FeL)	pFe^{3+}
Enterobactin	49	34.3
EMECAM	47.1(3)	32.6
MMECAM	45.8(5)	31.2
MECAM	43	29.4

The increase in the stability as larger groups are added has been attributed to an entropic contribution to the thermodynamic stability i.e. the binding moieties have to perturb less to bind Fe^{3+}. This allows for the increase of 10^4 in the $\log\beta_{110}$ and a 10^3 fold decrease in $[Fe^{3+}]_{free}$, almost approaching the pFe^{3+} for enterobactin itself.

The triscatecholate carbocyclic molecule (top right, Figure 1.36) is an example of an incredibly high $LogK_{Fe}^{3+}$ value of 48.8 which approaches that of enterobactin (10^{49}, Table 1.3).[68] The molecule was designed to probe the role of core rigidity with respect to Fe^{3+} binding. The carbocyclic structure displays some resemblance to the core scaffold of enterobactin in that it is in essence a 12 membered ring. However, the carbon bridges it features serve to enhance the rigidity in the molecule, causing some preorganisation of the binding motifs towards Fe^{3+} chelation.

TACN-MeHP (bottom right, Figure 1.36) is a hexadentate chelator comprised of a triazamacrocyclic core with bound functionalised pyridine rings. Fe^{3+} is bound through a combination of the core scaffold and the hydroxyl functionality of the pyridine moieties.[69,70] The pFe^{3+} of 40.3 exhibited by TACN-MeHP is the highest so far recorded for a chelator of synthetic or natural origin. However, this molecule is not as closely related to siderophore mimics as the other molecules due to its different binding mode and so does not serve as a viable comparison in this project. Although it displays an affinity for Fe^{3+} which is so far unrivalled its metal selectivity is significantly relaxed. Consequently issues relating to TACN-MeHP toxicity, thought to be due to its binding of other metal ions such as Zn(II) *in vivo* have already emerged. If applied to a bacterial culture, the bacteriostasis might arise through several contributing factors and a specific mechanism could be difficult to discern.[71]

TRENTAM (bottom left, Figure 1.36) was originally designed to probe whether the integration of more terephthalamide groups onto the TREN core would lead to an increase in Fe^{3+} affinity of the ligand.[72] TRENTAM possesses a pFe^{3+} of 34.2. Only enterobactin (pFe^{3+} = 34.3), a macrobicyclic compound and TACN-MeHP have ever been reported to surpass this value.

Analysis of the ligands discussed above have provided insights into design features that make an important contribution to powerful Fe^{3+} chelation. The ligands mostly contain: hard Lewis-base donor groups (with the exception of TACN-MeHP), are hexadentate and the core unit itself or the

groups attached to the core serve to preorganise the binding moieties towards iron chelation. It is these principles which therefore should be further explored in the design of new ligands in order to produce new synthetic chelators with improved Fe^{3+} binding properties compared to those described in the literature.

1.9.2 Antimicrobial activity

Inducing bacteriostasis through the application of a chelating agent has been a popular area of research for several years. It is known that the virulence of pathogenic bacteria has been linked to their ability to acquire Fe^{3+} from their environment. The application of a ligand which targets the binding of Fe^{3+} to bacterial populations should allow for restriction of nutrient iron and inhibit or distort the growth of the bacteria as a result.[73]

There are several examples in the literature of successful inhibition of bacterial growth through the application of chelators. These molecules tend to be high affinity Fe^{3+} ligands and are therefore said to be siderophore mimics. However, several mechanisms of bacterial iron acquisition have been targeted.

There are examples of siderophore mimics which restrict the extracellular Fe^{3+} availability and therefore reduce the growth rate of bacteria. By way of example in 1983 Bergeron *et al*. tested a series of catecholamide iron, Figure 1.37.[56]

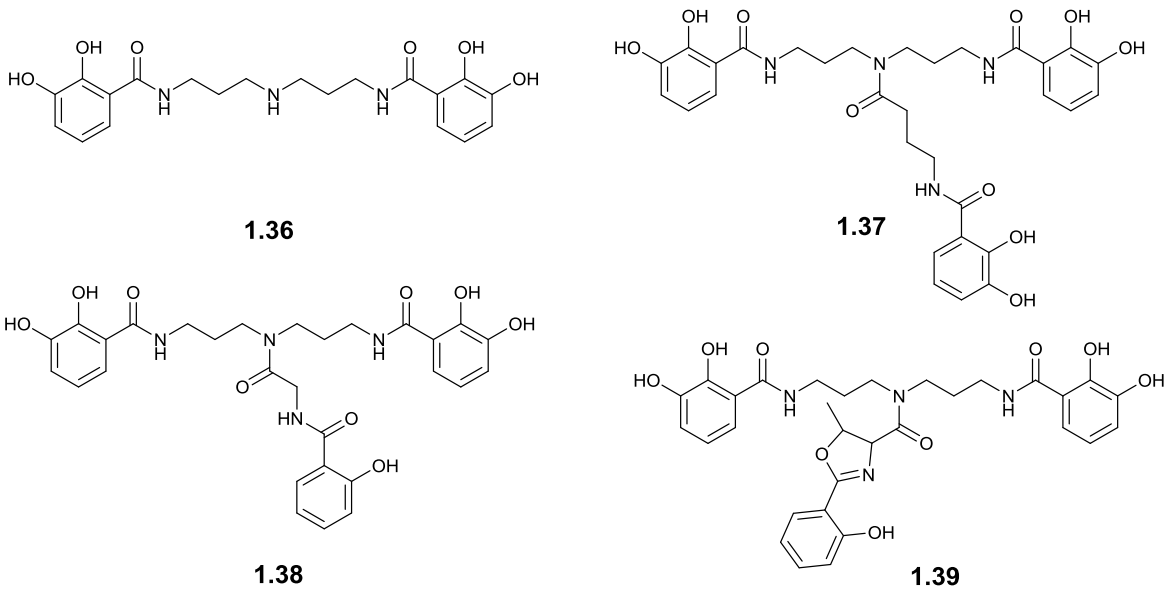

Figure 1.37 Structure of catecholamide chelators tested against organisms: *E. coli, P. aeruginosa, C. albicans* and *S. aureus*

These ligands (Figure 1.37) were capable of inhibiting the growth of the bacteria *E. coli, P. aeruginosa, S. aureus* as well as the dimorphic fungus *C. albicans*. In most cases the bacteria displayed an extended 'lag' period before growth was detected and they also failed to match the biomass yield achieved by untreated cultures. However, it was noted that in some cases after an extended lag period rapid growth ensued. This observation would be consistent with the bacteria secreting large quantities of their own siderophores competing for the available iron pool and overcoming the bacteriostasis imposed by the exogenous chelator treatment.

Furthermore, in 1985 compounds such as EDTA, DTPA and HBED (Figure 1.38) were tested on a range of mastitis causing bacteria for their antimicrobial/bacteriostatic properties. The research showed that the compounds were effective inhibitors of certain bacteria relating to this problematic infection. The effect seemed to be more marked against Gram-positive bacteria, especially in the case for EDTA which was much less effective against *E. coli* than *Staphylococcus aureus.*[73]

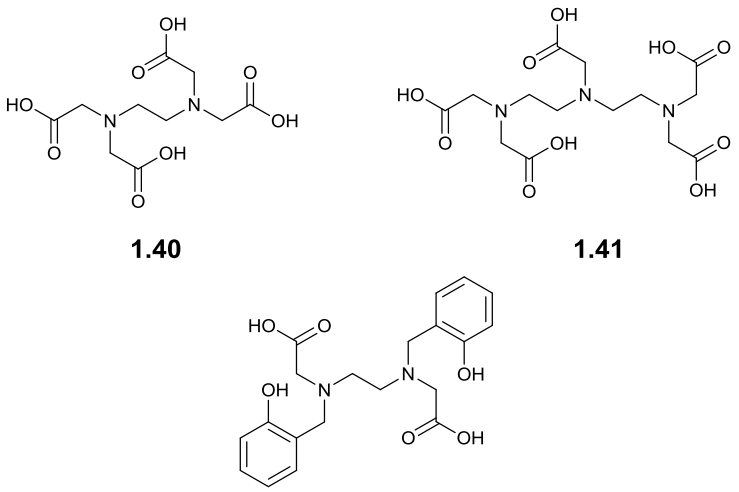

Figure 1.38 Structures of EDTA (top left) DTPA (top right) and HBED (bottom)

In addition, there are examples of synthetic siderophores, or toxic metal complexes of natural siderophores, which target the Fe^{3+} uptake systems of bacteria; through the blockage of the receptors necessary for ferri-siderophore uptake, growth inhibition can be induced. One example of such is that of the Sc(III)- enterobactin complex. In 1982 Rogers *et al*. described Sc(III) and In(III) enterobactin complexes as having a growth inhibitory effect on *E. coli* and *K. pneumoniae.*[74] They attributed this to competitive inhibition between the In(III)/Sc(III)-enterobactin complex and Fe^{3+}-enterobactin uptake systems. Evidence was presented that the Sc(III)-enterobactin complex even exerted a therapeutic effect on *E. coli* infected mice.

An alternative method to target bacterial growth has been the 'trojan horse' approach. The premise behind this method is the attachment of a molecule or antibiotic to a compound which is known to be taken up by the target organism. Once inside, the bioactivation of the compound results in the release of the active antibiotic and, in turn, produces the inhibition. This type of system has been shown to be effective against some mycobacteria and was reported in 2012 by Miller at al.[75] In this case mycobactins were synthetically altered to accommodate an antibiotic agent such as artemisinin. The mycobactin-artemisinin conjugate proved an effective inhibitor of *Mycobacterium tuberculosis* and also to four strains of *Plasmodium falciparum* (causative agent in malaria). The siderophore-drug conjugates were ineffective against a panel of bacteria, showing

mycobactin has limited potential as a broad host range delivery device but could prove useful against two of the three most prevalent infectious diseases of our age.

Of the three methods described (i) extracellular Fe^{3+} restriction (ii) Fe^{3+} receptor blocking and (iii) siderophore-drug conjugates; the extracellular Fe^{3+} restriction would seem to have the widest applications for use as a bacteriostatic approach. Reasoned by, assuming the Fe^{3+}-chelator complexes were not able to be metabolised or utilised by bacteria due to their 'alien' nature then the approach should target all bacteria which require Fe^{3+}. Whereas approach (ii) would be able to target certain uptake systems; however as previously discussed, bacteria have varied Fe^{3+} acquisition systems which cover a number of receptors, many of which are not characterised. It would be therefore difficult to target a wide range of bacteria with this approach. In addition, the use of metal complexes such as in the literature described, Sc(III) or In(III) would be unsuitable for widespread usage throughout areas which require disinfection due to their toxicity. The siderophore-drug conjugate approach would be an effective solution again to target specific organisms as the antibiotic agents required for the inhibitory effect are often specific to their target. This approach has the disadvantage to possibly promote resistance to the siderophore-drug conjugate and render the target immune to the compound. As antibiotic resistance is a universal issue facing the healthcare services, this approach could be problematic in this area.

An environment in which bacteriostasis induction would be of particular use is within hospitals. Over the past few decades the rise of cases of infection resulting from the hospital environment i.e. nosocomial and also involving those bacteria which are particularly virulent e.g. MRSA or VRE has been extensive. The application of a bacteriostatic agent to the hospital environment may serve to reduce the number, or the population recovery time after disinfection of a surface. This reduction in the growth of virulent organisms may serve to reduce the potential for the contraction of a nosocomial infection.

1.10 Scope of the Project

The project aims to develop novel chelators which are strong and selective for binding Fe^{3+}. The chelators will be designed to be applied to previously disinfected surfaces to prolong the period of microbiological disinfection though restriction of nutrient Fe^{3+}.

The literature data suggests that, as the HOPO moiety provides powerful Fe^{3+} binding with synthetically accessible derivatives that are able to be incorporated into a core molecular scaffold to produce hexadentate ligands, this group is ideal to attempt to achieve nutrient Fe^{3+} restriction.

The synthetic work within this project will involve the synthesis of novel hexadentate ligands based upon new and known core molecular scaffolds, which will be modified to include hydroxypyridinone binding moieties.

The strategy will incorporate molecules that will probe synthetic space in order to optimise: core size and rigidity, spacer length and rigidity and HOPO isomer to produce strong Fe^{3+} chelation i.e. *via* modulating entropic and thermodynamic contributions to complex formation. The core scaffolds and ligands themselves ideally should be resistant to biodegradative processes by, for example avoiding the incorporation of ester linkages within the core scaffold. Additionally, the core scaffolds utilised in these ligands should not be biomimetic of known siderophore core scaffolds in the hope to avoid recognition and possible uptake of the ferric-ligand complexes.

Once accessed synthetically the ligands will then be subject to microbiological testing. The efficacy of the chelators to create a bacteriostatic effect will be assessed through assay of minimum inhibitory concentration (MIC). The ligands will be tested on a diverse panel of clinically relavent microorganisms that differ in Gram-positive and Gram-negative species with differing iron acquisition systems.

Design and Synthesis of Novel Selective Fe^{3+} Chelators Based Upon Cyclotriguaiacylene Bearing hydroxypyridinone Moieties

2 Chapter Aims

This chapter aims to introduce cyclotriguaiacylene (CTG) as a viable choice for a core molecule, on which to base Fe^{3+} chelators. In addition, the chapter aims to provide the synthetic methodology required to produce the hexadentate chelators as shown in Figure 2.1.

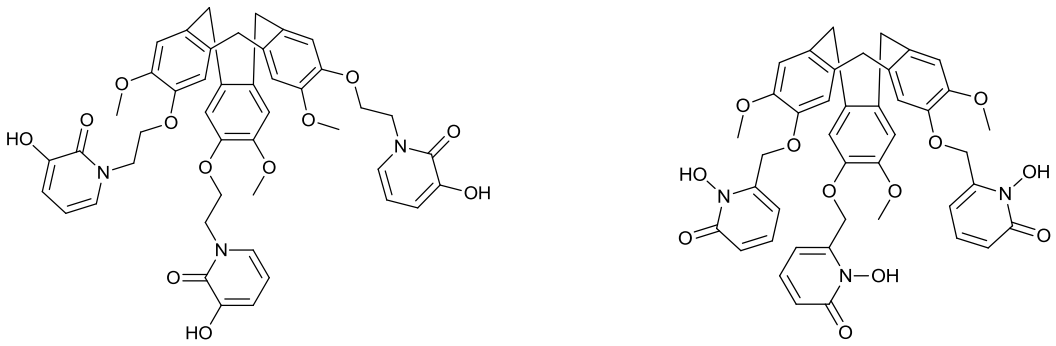

Figure 2.1 CTG based HOPO containing chelators

The synthetic methodology will be provided for the core molecule as based on literature procedures. The synthetic methodology for the HOPO units synthesised for attachment to the core will be given, based on literature procedures. The 3,2-HOPO and 1,2-HOPO bidentate molecules have been the focussed upon due to their accessible derivatives which allowing for attachment to the core scaffold.

The preparation of the protected hexadentate chelators and the subsequent deprotection methods are provided.

2.1 Introduction to CTG

Cyclotriveratrylene (CTV, Figure 2.2) is a cone shaped, rigid, lipophilic molecule. CTV is comprised of three substituted benzene rings, bridged by methylene groups, attributing the molecule with three-fold rotational symmetry. Primarily, chemistry surrounding the molecule has focussed upon complexation of small ionic molecules e.g. $MeNH_4^+$, within the 'bowl' molecular cavity. It has since become popular as a scaffold on which to build supramolecular arrays.[76] As a core scaffold unit itself, CTV cannot be directly functionalised to host the desired three bidentate ligands necessary to bind iron. Therefore, there is a need for a synthetically accessible derivative of CTV which can be functionalised in such a way as to incorporate three units on its structure.

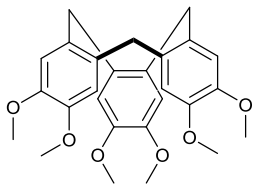

2.1

Figure 2.2 Structure of CTV

Such a molecule can be found in CTG (cyclotriguaiacylene, Figure 2.3); CTG retains its cone shaped structure but has three hydroxyl groups in replacement of three methoxy groups on the rings of CTV.[77] The rigidity and the three dimensional structure of CTG lend themselves favourably to the desired features previously discussed for strong chelation. That is, the molecule has the potential to be functionalised with three units, in our case the HOPO moiety, forming a hexadentate ligand. Also, the rigidity and the 'cone' or 'bowl' shape qualities of CTG may lend favourably to reducing the entropic penalty of metal complexation, by partially organising the binding moieties towards each other, as is observed for enterobactin (Figure 2.3). Additionally, as a core scaffold CTG would be resistant to enzymatic processes such as hydrolysis, which have been surmised to be integral in the release of iron to the bacterial cell. For example Fes enzyme in *E. coli* which breaks down the core unit of enterobactin to facilitate intracellular iron release, as discussed previously.

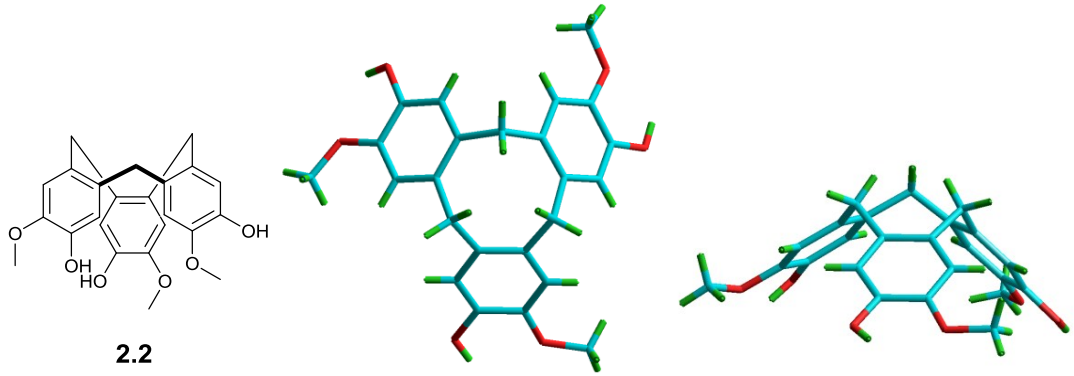

Figure 2.3 Structure of CTG (left). Tube rendered models of crystallographic data (middle and right) displaying C3v symmetry (middle) and bowl like character (right).[78]

Previously, CTG has been utilised as a scaffold on which to build Fe^{2+} and Fe^{3+} chelators.[79,80] These molecules contained: catecholate, hydroxamic acid and pyridine based binding moieties, tailoring their binding towards the Lewis acidity of the metal centre. Examples of these molecules which have previously been accessed for the binding of iron and based upon CTG are shown in Figure 2.4 (**2.3-2.5**).

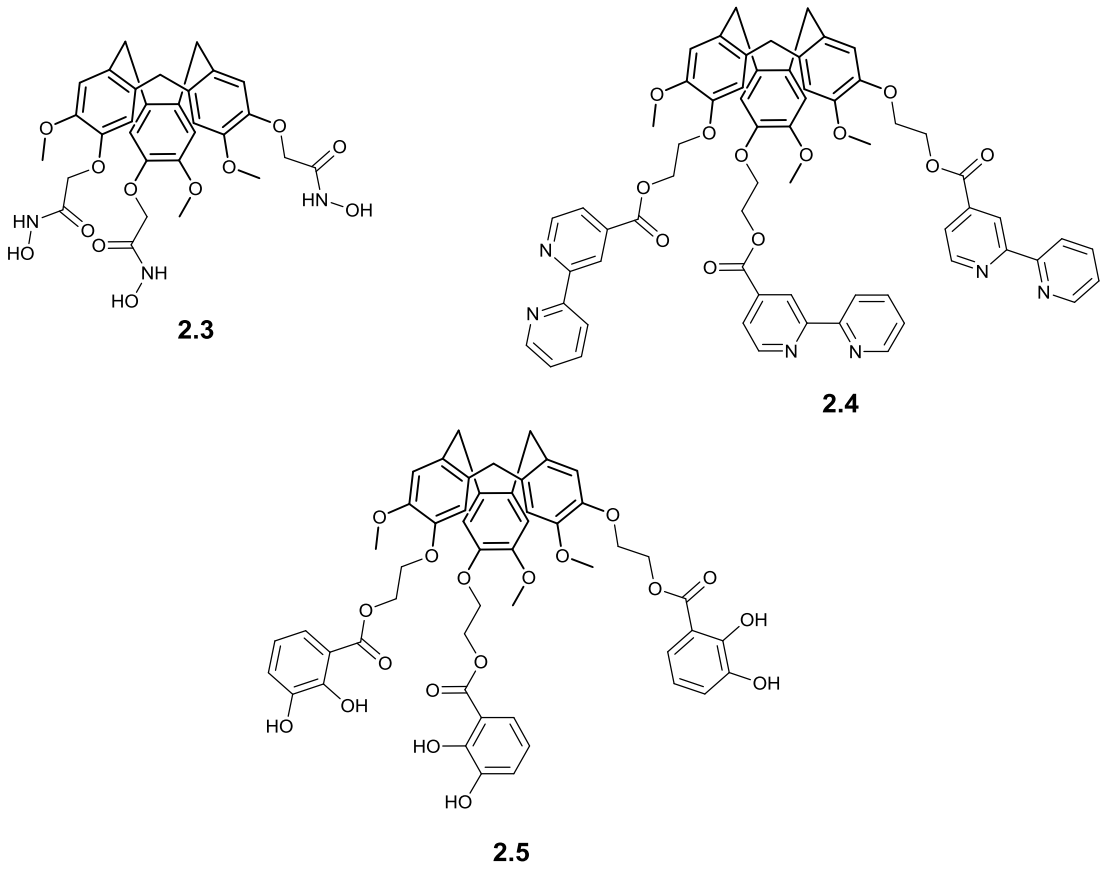

Figure 2.4 Examples of literature Fe^{2+}/Fe^{3+} chelators based on CTG scaffold

It can be noted that the positions of the phenolic -OH functionality and the –OMe are not randomly distributed but are in an alternating array around the molecule. This attributes the CTG scaffold with C_3 symmetry which should allow for functionalization to be concerted at all three positions.

The literature data suggests that the core unit is accessible in multigram quantities, from commercially available starting materials,[81] which is a desired quality for any synthetic undertaking. To date, no known Fe^{3+} chelators have been produced based upon the CTG core which contain HOPO moieties as the binding motif. In light of this and the qualities CTG possesses in relation to the core scaffold requirements, the molecule presents itself as a viable scaffold onto which HOPO groups can be coupled to facilitate Fe^{3+} binding.

2.2 Results and Discussion

2.3 Ligand Synthesis

2.3.1 Preparation of CTG (2.2)

From literature sources, the trimerization of 3,4-substituted benzyl alcohols is an effective route to the desired core scaffold CTG.[81] In particular the use of vanillyl alcohol (4-hydroxy-3-methoxybenzyl alcohol (**2.6**), (Figure 2.5) would allow for the production of the compound on multigram scale.[81,82]

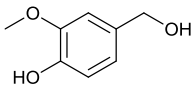

2.6

Figure 2.5 Structure of vanillyl alcohol

The synthesis of CTG by this route (Scheme 2.1) began with the allyl protection of vanillyl alcohol. The literature method was achieved successfully in yields of ~90%, using K_2CO_3 and allylbromide in acetone at reflux temperature. The oligomerization of the allyl-vanillyl alcohol was then attempted and it was found that as described a 2:1 methanol:70% $HClO_4$ would produce the tris-allyl-CTG (**2.8**) in yields 27-60%. A 10:1 ratio was attempted at first to limit the use of the acid however this failed to give the product. Subsequent deprotection of this allyl-CTG with Pd/C under acidic conditions in ethanol-dioxane (2:1) gave the desired CTG in yields up to around 60% (but as low as 20% in some instances).

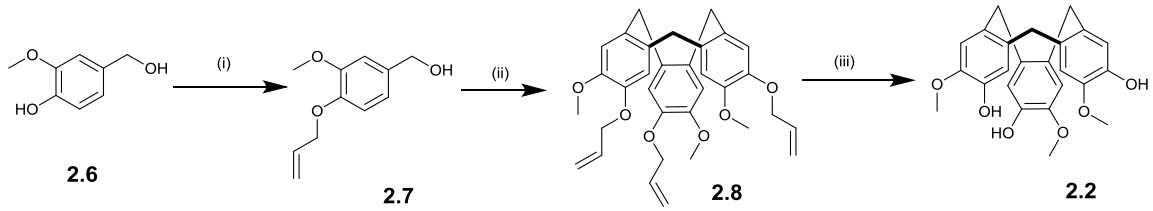

Scheme 2.1 Synthetic route for CTG. Reagents and Conditions: (i) allyl bromide, K_2CO_3, acetone (ii)70% $HClO_4$ in MeOH (iii) Pd/C, 70% $HClO_4$, EtOH, dioxane

As an aside, another method which promised a solvent free route to the allyl-protected CTG,[83] was also attempted, Scheme 2.2. It involved the grinding together of the allyl-vanillyl alcohol (**2.7**) with paratoluenesulfonic acid, without solvent and thus was attractive for its potential 'green' chemistry implications. However, unfortunately this did not produce the tris-allyl CTG as described and was subsequently abandoned in view of the less green but ultimately more effective method previously described.

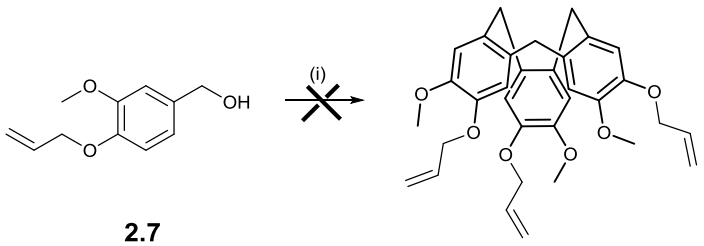

2.7 **2.8**

Scheme 2.2 Solvent free synthesis of **2.8**. Reagents and condition: (i) p-TsOH, pestle and mortar

2.3.2 Synthesis of 3-Benzyloxy-1-(2-chloroethyl)-1H-pyridin-2-one (2.13)

A diverse range of HOPOs are now synthetically achievable for all three positional isomers within the greater HOPO family (1,2-HOPO, 3,2-HOPO and 3,4-HOPO). Many of these HOPO moieties have the capabilities to be attached to the core molecules realised herein. However, the 3,2-HOPO has some of the most established chemistry. The 3,2-HOPO can be manipulated to incorporate various alkyl chains on the N-position of the ring, hence lending favourably to try and create molecules with various chain length as previously mentioned.

The 3,2-HOPO was therefore chosen as the isomer of HOPO to attempt and attach first to CTG. The synthetic route taken to reach 3-Benzyloxy-1-(2-chloroethyl)-1H-pyridin-2-one, a benzyl protected 3,2-HOPO with possible attachment point on the haloalkane chain, as has been previously shown, is depicted in Scheme 2.3.

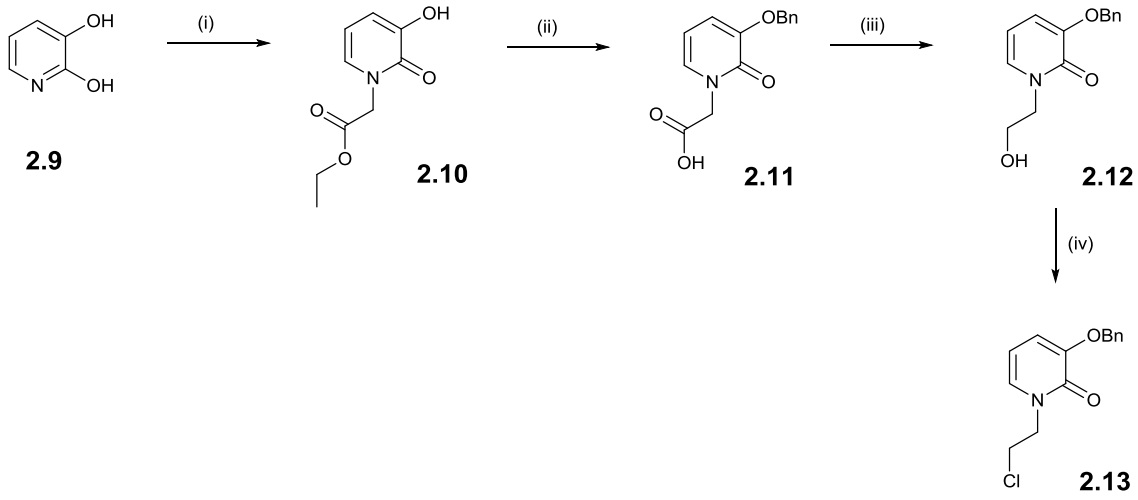

Scheme 2.3 Synthetic route to **2.13**. Reagents and conditions: (i) ethyl bromoacetate, 155°C, 48 hours (ii) 90% MeOH, NaOHaq (4M), BnBr/BnCl, reflux 8hours (iii) borane-THF, dry THF, rt (iv) TsCl, Et_3N, dry DCM/DCM, $SOCl_2$ reflux

The preparation of 3-benzyloxy-1-(2-chloroethyl)-1H-pyridin-2-one began with the synthesis of 1-[(ethoxycarbonyl)methyl]-3-hydroxy-2(1H)-pyridinone (**2.10**) from 2,3-dihydroxypyridine (**2.9**) and ethyl bromoacetate under reflux for 48 hours.[21] The reaction produces the pure compound in 25-50% yield (lit. 77%). Due to the large excess of ethyl bromoacetate required for this first step

(5 equiv.) it was briefly investigated whether this reaction could be made more economical, with respect to limiting the amount of this toxic reagent. The use of dyglyme as a high boiling point solvent with sodium iodide catalyst, in the presence of equimolar amounts of 2,3-dihydroxypyridine and ethyl bromoacetate was tried. The reaction was stirred at 140-150°C for 48 hours; unfortunately the only recovered product from the reaction was starting material. In light of this the literature methodology was returned to.

The following step in the reaction series is the benzyl protection of the 3-hydroxyl group on the pyridinone ring system and the parallel hydrolysis of the ester group to produce 3-(benzyloxy)-1-(carboxymethyl)-2-(1H)-pyridinone (**2.11**).[21] The reaction yields the desired product as a pure solid in yields around 60-70% (lit. 83%). The literature procedure facilitates the use of BnCl as the protecting reagent, however it was found this produced lower yields than using benzyl bromide and so this reagent was used in its place.

The reduction with borane-THF complex to produce 3-benzyloxy-1-(2-hydroxyethyl)-1H-pyridin-2-one (**2.12**) has been previously described and the procedure was followed as published, with the exception of the requirement of up to 5 equivalents of borane-THF complex to drive the reaction to completion.[84] Also, it was found that the product was not pure enough to be used without purification by column chromatography, however once this was performed the pure alcohol was isolated in yields typically around 30% (lit. 90%).

Finally the substitution reaction to produce the desired 3-benzyloxy-1-(2-chloroethyl)-1H-pyridin-2-one (**2.13**) was followed as described in the literature. With typical yields of ~80% after purification via column chromatography, the reaction proceeds as expected. To try and improve upon the yield of the reaction it was attempted with $SOCl_2$ in dry DCM under reflux. Although the product is realised from this reaction, with a yield before purification of 61%, it was found that the literature method was more effective. The reaction time utilising tosyl chloride is 4 days (see experimental), it is thought initially the tosylate is formed and then this then reacts with the chloride anion to produce the desired chloride.[84] The use of tosyl chloride over $SOCl_2$ for chlorination is not extensive in the literature and so one could hypothesise that the authors intended

to make the tosylate analogue of the 3,2-HOPO but found the chloride under these conditions dominated as the product.

2.3.3 Synthesis of 3-Benzyloxy-1-(2-chloropropyl)-1H-pyridin-2-one (2.17)

In an attempt to create a more diverse library of chelators containing the HOPO functionality, the chain length of attachment, or the spacer group, between the core and the HOPO was lengthened. The aim being that the viability of the attachment of the groups to the core would be similar, but produce molecules which could be compared with only one variable.

Therefore, the synthesis of 3-benzyloxy-1-(2-chloropropyl)-1H-pyridin-2-one (**2.17**) was of interest and was successfully achieved by initially following a procedure involving the CsF assisted 1,4-Michael addition of ethyl acrylate to 2,3-dihydroxypyridine to produce 1-[(ethoxycarbonyl)ethyl]-3-hydroxy-2(1H)-pyridinone (**2.14**), Scheme 2.4, in yields typically 60-70% (lit. 74%) as the pure product.[85]

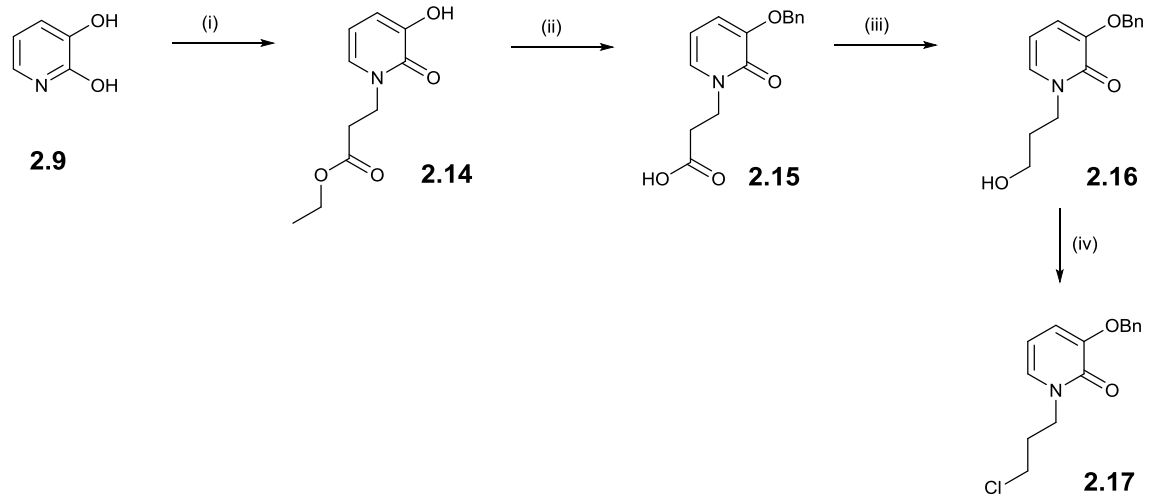

Scheme 2.4 Synthetic route to **2.17**. Reagents and conditions: (i) ethyl acrylate, CsF, MeCN, 90°C, 48 hours (ii) 90% MeOH, NaOHaq (4M), BnBr/BnCl, reflux 8 hours (iii) borane-THF, dry THF, rt (iv) TsCl, Et_3N, dry DCM/DCM, $SOCl_2$

The sequential steps in the synthetic scheme are analogous to those required for 3-benzyloxy-1-(2-chloroethyl)-1H-pyridin-2-one (**2.13**). The benzyl protection and in parallel ester hydrolysis occurs

as previously described for **2.10** to yield the pure 3-(benzyloxy)-1-(carboxyethyl)-2-(1H)-pyridinone (**2.15**) in yields typically 50-70%. Compound **2.15** is thought to be novel in that it has not previously been isolated in any known literature procedure to date, though molecules **2.16** and **2.17** have been previously accessed. The reduction with borane-THF yields the crude product and after purification the pure alcohol, compound **2.16** can be achieved in 30-40% yield. The chlorination of the alcohol with TsCl proceeds as described previously for 3-benzyloxy-1-(2-chloroethyl)-1H-pyridin-2-one (**2.17**) and yields the desired chloride in 52% yield after purification via column chromatography. As in the previous synthesis the use of $SOCl_2$ in the chlorination step has been explored for this molecule. The results were found to vary between repeats. In one experiment, the reaction has yielded the product as a crude solid in yield 36% after purification, but a further attempt produced near pure **2.17** in almost quantitative yield, requiring little to no purification. The reason for this is unclear, however both methods employed produced the desired compound which can be isolated in excellent purity after column chromatography.

2.3.4 Coupling of Prepared 3,2-HOPO Moieties with CTG

Functionalization of CTG with the 3,2-HOPO was firstly attempted via substitution chloride of **2.13** by CTG on the three sites (Scheme 2.5).

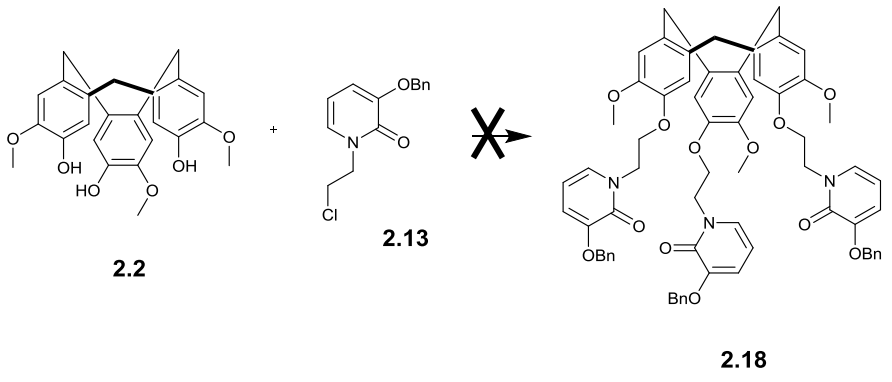

2.2 **2.13** **2.18**

Scheme 2.5 Addition of **2.13** to CTG. Reagents and conditions: (i) NaH, DMF, (ii) K_2CO_3, acetone

Firstly, the synthesis was attempted using a modified literature method, involving functionalization CTG through an alkyl halide.[28] The method employed the use of NaH in DMF. These conditions were explored but unfortunately the isolated product from the reaction was thought to be the result of elimination of HCl from the alkyl halide chain at the *N*-position of the 3,2-HOPO moiety (**2.19,** Figure 2.6). In light of this, the reaction conditions were altered to accommodate for the tendency of the N-alkyl group to degrade in the presence of strong nucleophiles.

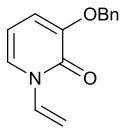

2.19

Figure 2.6 – Chemical structure of the product thought to be the result of using NaH as a base

Alternative conditions attempted included the use of K_2CO_3 with acetone as a solvent. Unfortunately, this reaction did not proceed as expected and a complex mixture of products was recovered after separation by column chromatography. It was noted that upon addition of K_2CO_3 to CTG the solid changed to a deep green from an off-white. This could have been due to the incorporation of the K^+ ion into the 'bowl' like cavity of deprotected CTG and is one hypothesis as to the failure of the reaction. This hypothesis could be tested via the addition of 18-crown-6 to the green solution to see if any colour change occurs, possibly the result of the competition for the K^+ ion, however this needs to be attempted to give evidence towards the hypothesis. Failing to produce the target molecule for the shorter chained 3,2-HOPO-chloride, analogous conditions were used to attempt the reaction with the longer chained 3,2-HOPO-chloride, Scheme 2.6.

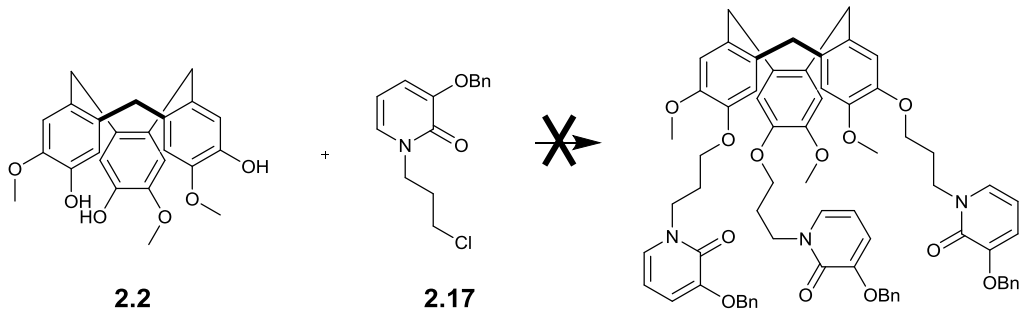

2.2 **2.17** **2.20**

Scheme 2.6 Addition of **2.17** to CTG. Reagents and conditions: (i) NaH, DMF, (ii) K_2CO_3, acetone (iii) K_2CO_3, acetone, NaI (iv) Cs_2CO_3, MeCN

Conditions attempted to produce the target molecule **2.20** **(**Scheme 2.6) were K_2CO_3 with acetone as the solvent with the addition of NaI as a catalyst. This reaction, as previously seen for the shorter chained 3,2-HOPO produced a complex mixture of products.

In addition, Cs_2CO_3 as a base in MeCN was tried; however this too failed to produce the target molecule. Here, Cs_2CO_3 was used to attempt to prevent the potential incorporation of the cation into the cavity of CTG, K^+ seemed to preferentially bind to the core scaffold however, the Cs^+ ion is larger and so it was hypothesised that incorporation of the cation would be somewhat decreased. Although the resulting product was not of compound **2.20** it was observed that the previously noted colour change did not occur when using Cs_2CO_3.

2.3.5 Preparation of Iminuim Salt (2.21)

In light of the failing of **2.13** and **2.17** to react with CTG via the expected route, a different synthetic methodology was required. Literature data provided an alternative bidentate unit which would allow the target compound to be accessed, the iminium salt (**2.21**), Scheme 6.[39]

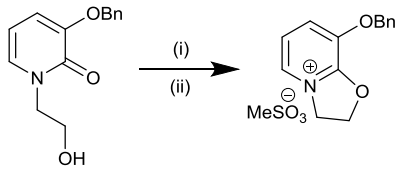

2.12 **2.21**

Scheme 2.7 Formation of iminium salt (**2.21**). Reagents and conditions: (i) $(MeSO_2)_2O$, Et_3N, dry DCM (ii) $CHCl_3$

2.21 was prepared in accordance with the literature procedure. **2.12** was stirred at room temperature in dry DCM under an inert atmosphere with Et_3N and mesyl anhydride. This produces the corresponding mesylated 3,2-HOPO which when stirred in chloroform, rearranges to produce **2.21** in high purity and good yields (72-85%). The 3,2-HOPO-hydroxyl intermediate was prepared as previously discussed. The compound was stored under an inert $N_{2(g)}$ atmosphere at 4°C prevent degradation by atmospheric moisture.

2.21 has been shown to be susceptible to ring opening reactions at two sites, Figure 2.7.[85,86] Path A is the desired route to the addition of the moiety to the core scaffold. Path B has been shown to be the product isolated in those reactions where the nucleophile (Nu^-) is a primary amine. The reaction of this group with more hindered amine nucleophiles and other functionality such as: phenols, thiols and hydroxyalkanes has been shown to favour the desired Path A, however; in the synthesis of the novel ligands utilising this group, though it would be unexpected, the possibility of the reaction occurring via Path B is always present.

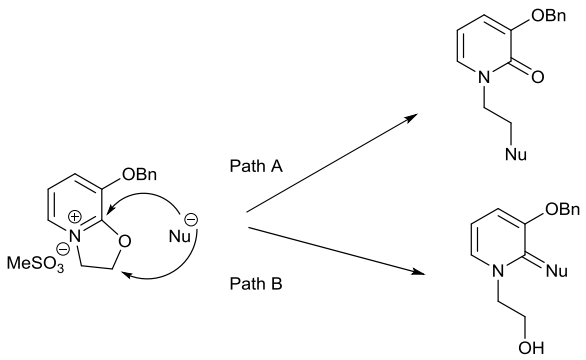

Figure 2.7 Demonstrating the possible ring opening pathways of **2.21** with a nucleophile (Nu^-)

2.3.6 Preparation of the novel CTG-3,2-HOPO (2.22) ligand

The reaction between CTG and **2.21** (Scheme 2.8) progressed well under conditions of Cs_2CO_3, dry MeCN, under reflux. The crude product was accessed in high yield; subsequent purification of the crude product via column chromatography gave the desired (**2.18**) in excellent yield (93%). As expected the reaction pathway for the ring opening of **2.21** by the CTG core scaffold progressed via the desired Path A and not Path B.

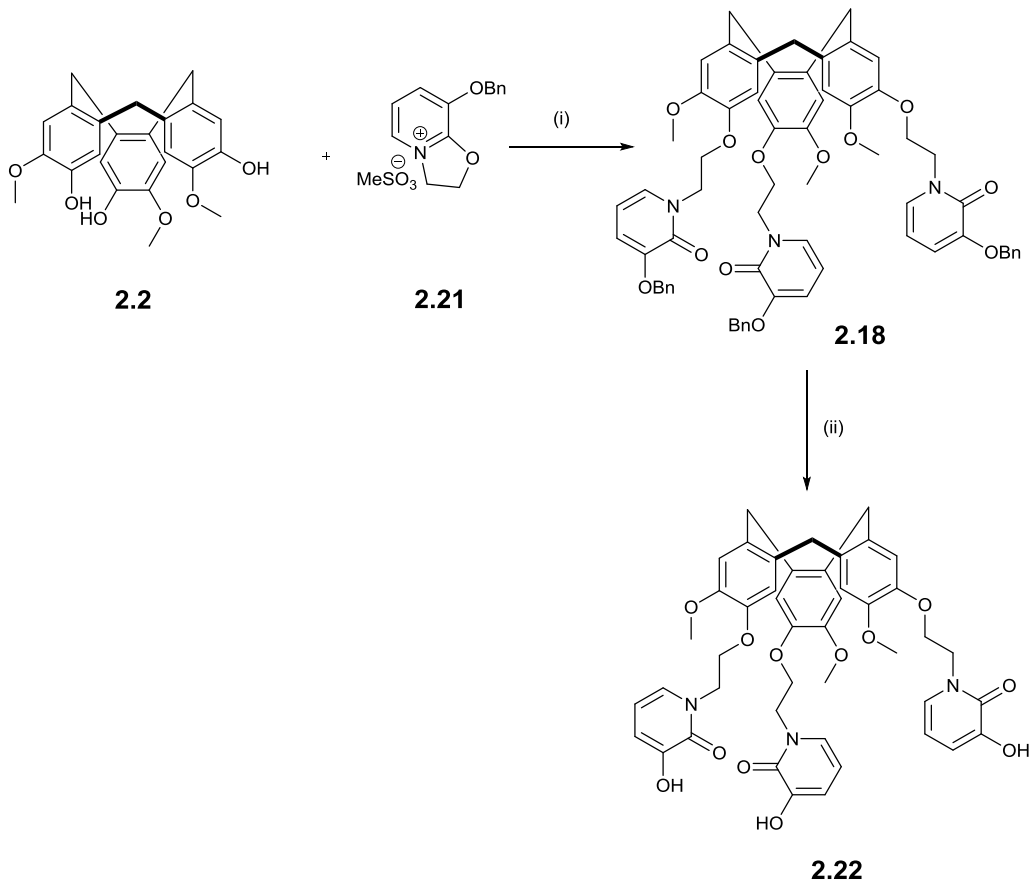

Scheme 2.8 Reaction of iminium salt (**2.21**) with CTG (**2.2**). Reagents and conditions (i) Cs_2CO_3, dry MeCN, reflux (ii) 1:1 37%HCl_{aq} and glacial acetic

The subsequent deprotection of molecule **20** was achieved through a standard debenzylation performed in 1:1 37%HCl_{aq} and glacial acetic acid over several days. The free ligand could be achieved in high purity through precipitation with ether from MeOH, after being stored at 4°C for 2 days. The yields for this deprotection were variable, from 12-28%. Undoubtedly, some of the compound did not precipitate out of solution when ether was applied and the reaction purification stage requires optimisation.

2.3.7 Preparation of novel 6-(chloromethyl)-1-(prop-2-en-1-yloxy)-1,2-dihydropyridin-2-one (2.28)

To achieve a variety of HOPO groups on the CTG scaffold a synthetically accessible derivative of the 1,2-HOPO was developed to allow for attachment to nucleophilic core scaffolds, such as CTG. The synthetic methodology for the preparation of **2.28** was developed in house and is yet to be published.[1]

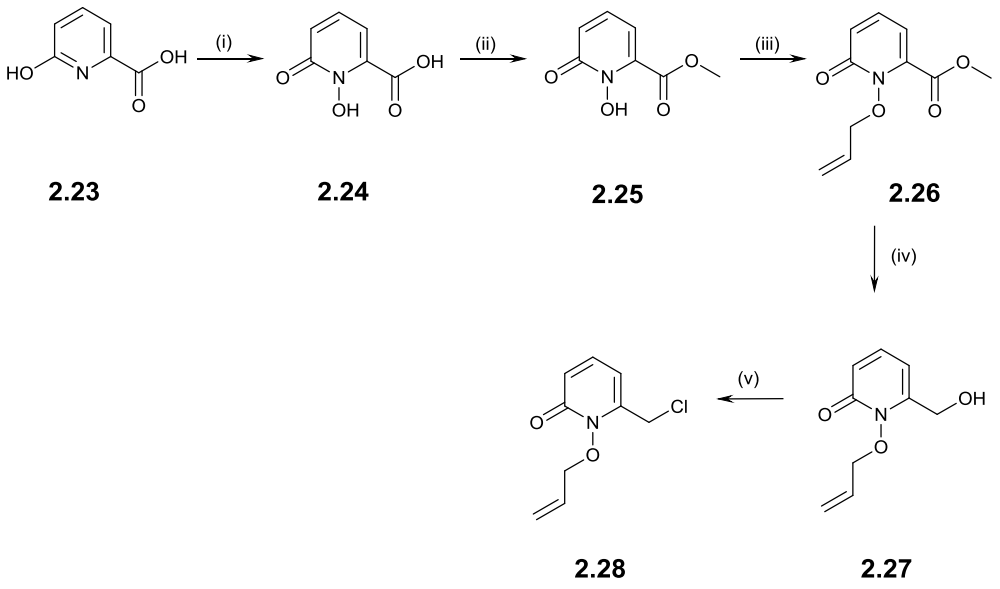

Scheme 2.9 Synthetic route for 1,2-HOPO molecules (**2.24-2.28**). Reagents and conditions; (i) peracetic acid, acetic acid (ii) $SOCl_2$, MeOH (iii) Allyl bromide, K_2CO_3 (iv) $NaBH_4$, MeOH, THF (v) $SOCl_2$, dry DCM

The preparation of **2.28** began with the *N*-oxidation of 6-hydroxy-picolinic acid (**2.23**), as has been previously shown in the literature.[87] However, it was found that the literature procedure requirement for TFA was unnecessary and the compound could be isolated in good purity and yield following through oxidation with peracetic acid in acetic acid. The reaction proceeds as expected to yield the desired N–oxide **(2.24)** in good yields (73-76%) and high purity, the crude isolate requiring no purification.[87] Step (ii) involves the methylation of the free acid (**2.24**) to ensure that

1 Synthetic methodology developed by David Workman, to be published.

over allylation does not occur in the following step. The methylation occurs as is reported in the literature to give **2.25** in excellent yields (up to 96%) and high purity, again requiring no purification.[88] Step (iii) yields the N-allyloxy protected HOPO (**2.26**) in yields of up to 98% without requiring purification. The subsequent reduction of **2.26** to the hydroxymethyl-1,2-HOPO (**2.27**) derivative was developed following a literature procedure and yields novel **2.27** in yields up to 41%, often requiring purification by column chromatography.[89] The chlorination of **2.27** occurs with good purity and yields of up to 81%, without the need for purification to give **2.28**.

2.3.8 Preparation of the novel CTG-1,2-HOPO (2.30) ligand

The formation of the protected tris-ally-CTG-1,2-HOPO molecule **2.29**, was successfully performed in dry MeCN with Cs_2CO_3 to yield the desired compound in yields up to 79% after purification.

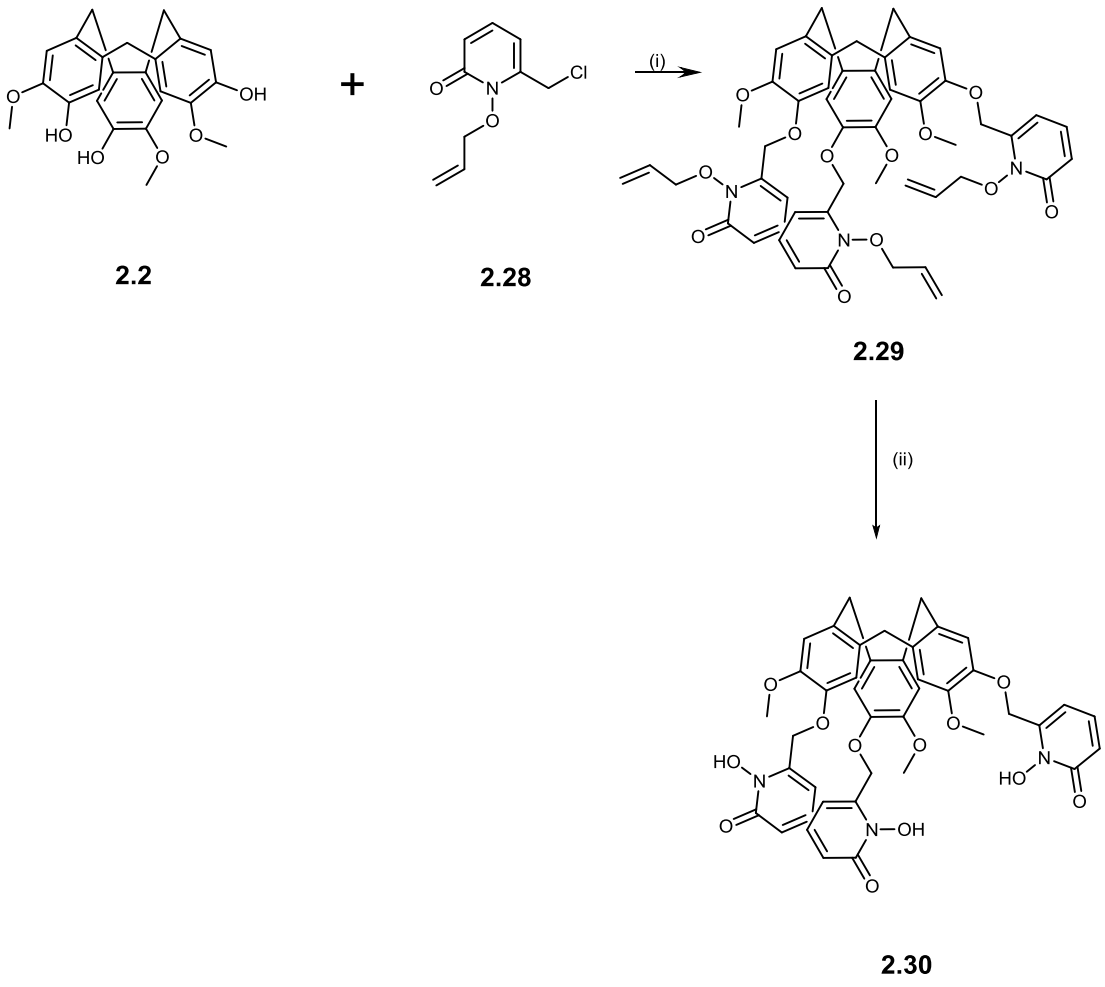

Scheme 2.10 Synthetic route for molecule (**2.30**). Reagents and conditions; (i) Cs_2CO_3, dry MeCN (ii) Pd/C, 0.15M TFA, dioxane:H_2O (4:1)

The subsequent deprotection of **2.29** to yield the free ligand was achieved utilising a literature method.[90] The method employs using Pd/C catalyst with H_2O:dioxane (1:4) as the solvent with 0.15M TFA. The reaction proceeds at reflux overnight to yield the desired **2.30** in yields up to 87%, the pure ligand could be isolated by precipitation from MeOH with diethyl ether.

2.4 L:Fe^{3+} Stoichiometry Determination

2.4.1 Modified Job's Plot Analyses for 2.22 and 2.30

L:Fe^{3+} stoichiometry was determined via a method described in the Experimental section, which is based on a literature procedure for L:M stoichiometry determination.[91]

The modified Job's plot analyses for **2.22** shows, in the first instance, after 2 days of equilibration a ligand: metal stoichiometry of 1:1. This would suggest efficient binding of the metal by the ligand as the desired stoichiometry was reached after a short time. To assess the stability of the complex in solution, and therefore the thermodynamic favourability, the measurements were repeated after 14 days equilibration. The results after 14 days showed the system was still displaying the same stoichiometry which would suggest that the binding of Fe^{3+} by this ligand was kinetically and thermodynamically favoured.

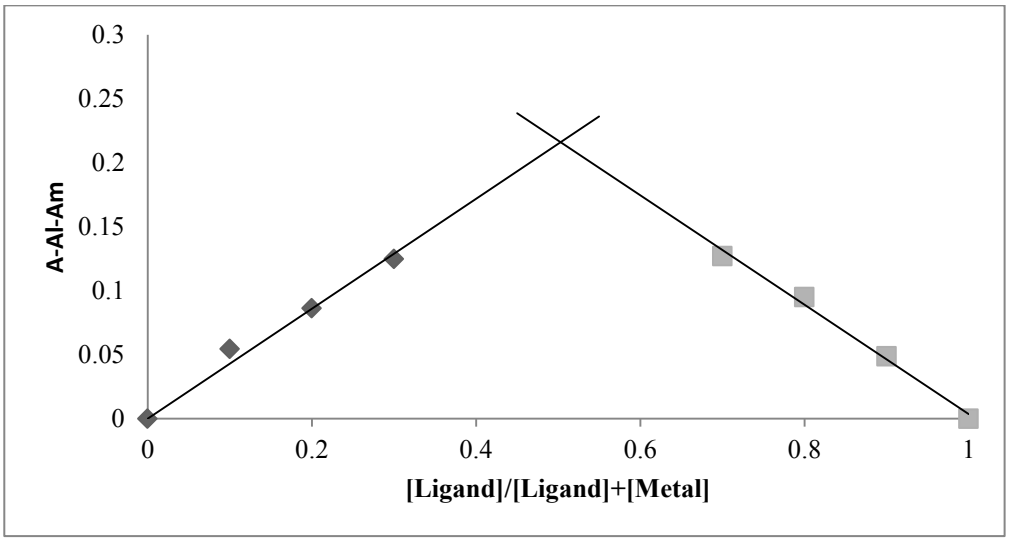

Figure 2.8 Modified Job's plot analysis for **2.22** binding Fe^{3+} after 2 days. Measurements taken at room temperature in DMSO/H_2O.

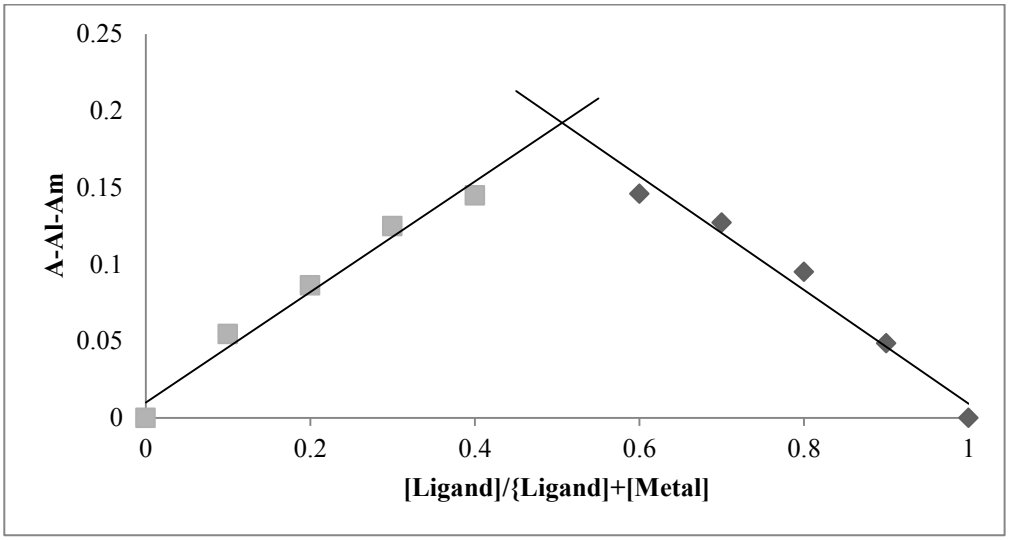

Figure 2.9 Modified Job's plot analysis for **2.22** after 14 days. Measurements taken at room temperature in DMSO/H_2O.

The modified Job's plot analysis for **2.30** showed in the first instance that after 2 days to equilibrate the system had reached a ligand:metal stoichiometry of 1.7L:1M. This ratio shows ineffective metal binding by the ligand, from the ideal 1:1 stoichiometric ratio. This could be result of the methylene bridges being insufficient to allow for thermodynamically stable metal binding. Alternatively, this could be the result of a slow rate of metal chelation by the ligand; the measurements were therefore repeated after 14 days of equilibration.

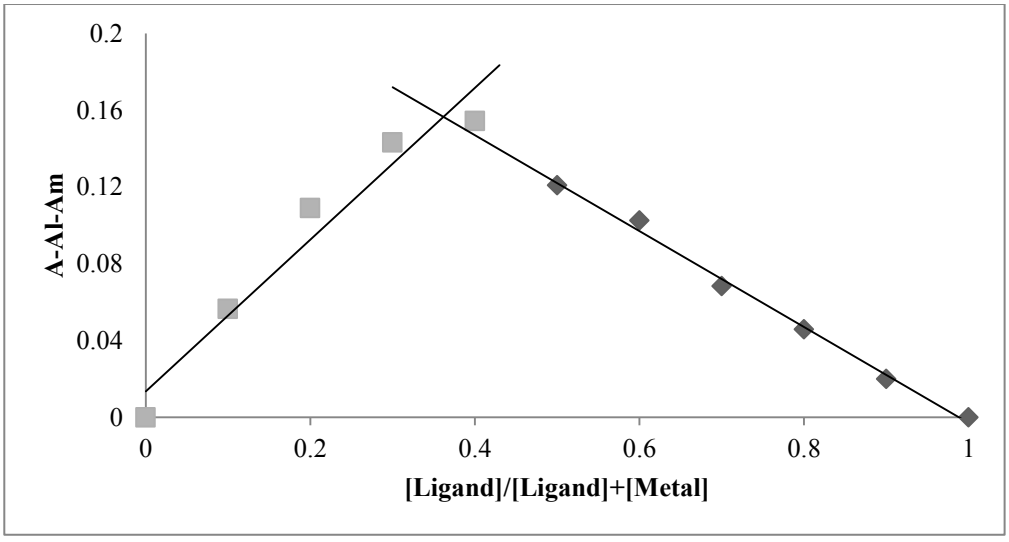

Figure 2.10 Modified Job's plot analysis for **2.30** after 2 days. Measurements taken at room temperature in DMSO/H_2O.

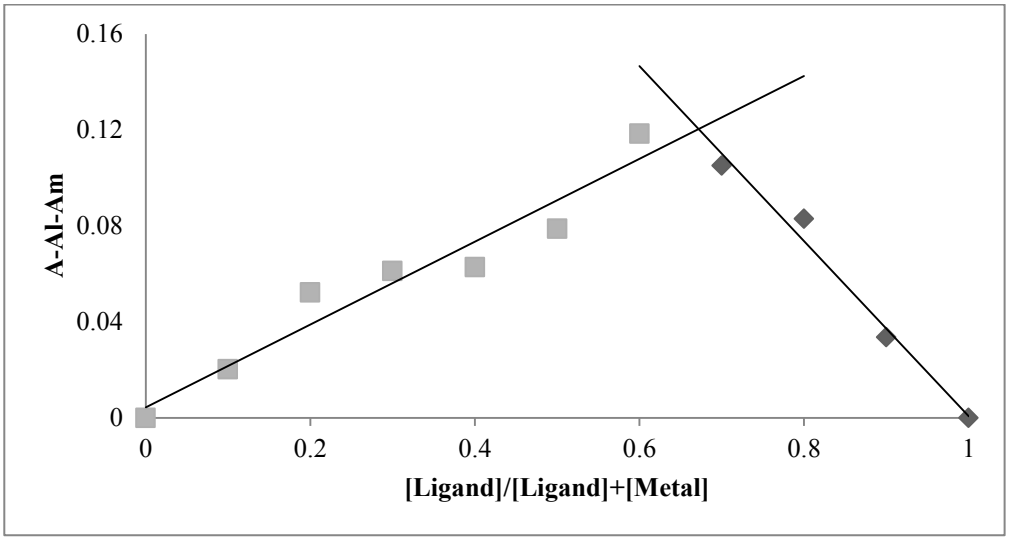

Figure 2.11 Modified Job's plot analysis for **2.30** after 14 days. Measurements taken at room temperature in DMSO/H_2O.

The data shown in Figure 2.11 for **2.30** displays a L:Fe^{3+} ratio of 1L:2M. The resulting re-equilibration of the system to incorporate more of the metal bound would suggest that the initial binding was slow. However, upon reaching an equilibrated state it appears the ideal 1:1 ratio has been exceeded. This could suggest the 'bowl' like character of CTG could be accommodating some of the Fe^{3+} cation, as has been shown for this core for a number of small ionic guest molecules.

2.5 Chapter Conclusions

This chapter has presented the successful design and synthesis of two novel hexadentate chelators, based upon the core molecular scaffold CTG. The chelators have design features which owe to the strong and selective binding of Fe^{3+} such as the inclusion of the HOPO moieties and the potential preorganisation the scaffold provides.

The synthetic methodologies for the ligands presented utilises readily available starting materials which are converted into the final ligands in several steps. The synthetic routes for the 3,2-HOPO moieties are from literature procedures and are all high yielding reactions, with little room for

improvement. In the 1,2-HOPO case, most of the reactions to obtain the 1,2-HOPO-chloride are high yielding except the reduction step, there is room here for improvement to the yield of the reaction, however the high purity which can be obtained from these methods is favourable.

The protected ligands are able to be accessed in good yields with high purity. The conditions required for their synthesis are mild and would lend well towards scale up to multi-gram quantities. The deprotection steps to access the free ligand **2.22** containing the 3,2-HOPO units, although provides the ligand with good purity does so in relatively low yields. This could be due to the purification via precipitation from methanol; some of the ligand may still be dissolved, lowering the accessible yield. However, the deprotection of **2.29** to access ligand **2.30** gives the pure product in 87% yield, which would lend itself well to scale up reactions. Although, alternative deprotection methods were not tested, one which does not require the use of a Pd/C catalyst would be more favourable in terms of 'green-ness' and more suited to scale up.

The UV-Vis analysis of the stoichiometry regarding the binding of Fe^{3+} yielded some interesting results. **2.22** showed efficient 1:1 L:Fe^{3+} binding after the initial reading and, in later readings also. This would suggest that the ligand does in fact bind Fe^{3+} with some degree of affinity and the resulting complex formed is both thermodynamically and kinetically stable over the time period. The analyses for (**2.30**) show that at the 2 day measurements the L:Fe^{3+} stoichiometry is measured at 1.7L:1M, however we see this re-equilibrate to 1:2 L:Fe^{3+} stoichiometry after 14 days. This result could be indicative of the incorporation of the Fe^{3+} into the molecular cavity of CTG as well as the binding of Fe^{3+} by the HOPO moieties. This hypothesis would also go towards confirmation that the K^{+} cation, as previously discussed, may also be incorporated into the molecular cavity of CTG preventing the nucleophilic attack of the 3,2-HOPO-chlorides (**2.13 and 2.17**). However, we do not see this behaviour for ligand (**2.22**). One possibility is that the longer chained HOPO ligands are more sterically hindering and therefore restrict the access to the 'bowl' cavity of CTG, preventing the binding of a secondary ion. This is yet to be established and is therefore only speculative at this point, further work is required to confirm.

2.6 Future Work

For the CTG scaffold, work which could extend what has been presented herein could take the form of improving the aqueous solubility of the ligand, possibly by functionalising the core scaffold with polar groups such as sulfonate.

In addition, though unsuccessful in this work, the achievement of the longer chained 3,2-HOPO on this scaffold would be a useful derivative for comparison and for determining how the chain length serves to effect the binding properties of ligands based on this core.

The data shows the possibility of **2.30** binding greater than one equivalent of Fe^{3+} after a 14 day period. This is an interesting property of this particular ligands and further study to confirm this or the achievement of a crystal structure of such a complex would be of particular interest. The addition of a longer-chained 1,2-HOPO derivative would also be of particular interest here so as to see if the greater than 1:1 stoichiometry for the complex still exists for this derivative. However, the bidentate longer chained 1,2-HOPO has not yet been accessed in a form which would allow for its attachment to the CTG scaffold.

The elucidation of the thermodynamic properties of the ligands i.e. pFe^{3+} and logβ values would be necessary to allow a comparison between the structural features of the ligands and the effect this has on binding strength. This data would also give an insight into differences noted between ligands when applied to a biological system.

Utilisation of the 1,3,5-tris(aminomethyl)-2,4,6-triethylbenzene Core Scaffold in the Synthesis of Novel Fe^{3+} Chelators Bearing hydroxypyridinone Binding Groups

3 Chapter Aims

The aims of this chapter are to introduce 1,3,5-tris(aminomethyl)-2,4,6-triethylbenzene (Figure 3.1) as a core molecule with potential to produce powerful Fe^{3+} chelators with the addition of HOPO binding groups. The core introduction includes previous work in this area and how this research is a logical expansion of that.

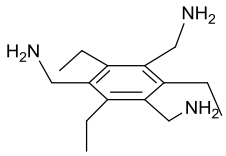

3.1

Figure 3.1 Structure of 1,3,5-tris(aminomethyl)-2,4,6-triethylbenzene (**3.1**)

The synthetic methodology for the core scaffold will be provided, based upon literature data. In addition the synthetic methods for the bidentate HOPO moieties which have not been previously discussed will also be provided herein.

The synthesis will be provided for the coupling of the bidentate units to the core scaffold and the subsequent deprotection of the hexadentate protected ligands. The 1,2-HOPO, 3,2-HOPO and 3,4-HOPO have all been accessed for this core molecule providing a range compounds for comparison. In addition, the synthesis of the previously accessed EMECAM will be described, following procedures based on previous literature.

Analysis of the compound's L:Fe^{3+} stoichiometric ratio, determined using UV-Vis spectroscopy and a modified Job's plot analysis is provided.

3.1 Introduction to 1,3,5-tris(aminomethyl)-2,4,6-triethylbenzene

3.2 Previous technology

Previously, the 1,3,5-tris(aminomethyl)-2,4,6-triethylbenzene core scaffold has been explored by Raymond *et al*. due to the ababab arrangement (groups arranged on alternating faces) of functional groups around the benzene core. This core has also been explored for Fe^{3+} chelation with catecholate binding groups. Molecules MECAM, MeMECAM and EMECAM were synthesised by Raymond *et al*. and reported in 1997.[67]

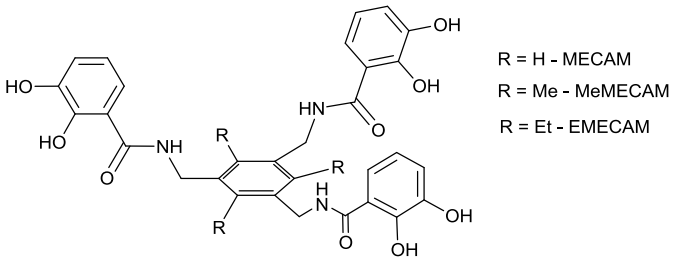

3.2

Figure 3.2 Structure of previous catecholate containing ligands MECAM, MeMECAM and EMECAM based upon the 1,3,5-tris(aminomethyl)-2,4,6-triethylbenzene core scaffold

As previously discussed (Chapter 1, Introduction) the EMECAM ligand, which bears ethyl functionality on the core scaffold which facilitates in the predisposition of the binding moieties towards Fe^{3+} chelation, has a high affinity for Fe^{3+}. As a result, the affinity for the metal centre has been reported as $\log\beta_{110} = 47.1$ and $pFe^{3+} = 32.6$[67] which is approaching that of enterobactin $\log\beta_{110} = 49$ and $pFe^{3+} = 34.3$.

The literature also provides information on the amide functionality of attachment and the effect that methylation at the 2° amide anchor has on the binding affinity of MECAM derivatives (**3.3**). This work reported in 1999 by Hider *et al*. was an investigation into the synthesis and properties of

ligands bearing 3,2-HOPO functionality. This article showed that employing TBTU (N,N,N′,N′-Tetramethyl-O-(benzotriazol-1-yl)uronium tetrafluoroborate) as a coupling reagent for acid-functionalised HOPO groups to the MECAM triamine core scaffold could be a viable synthetic methodology to produce ligands based on this core. The structures and binding affinities were provided for the ligands shown in Figure 3.3.

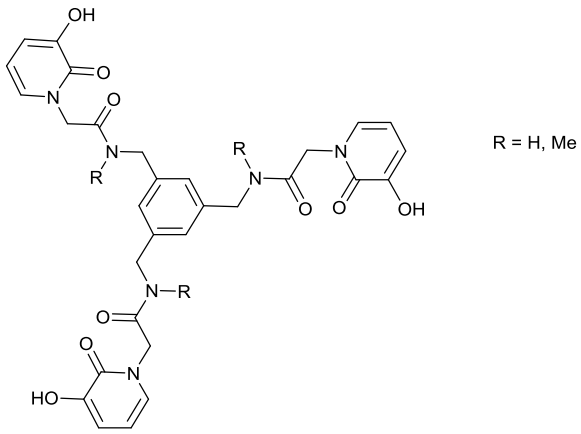

3.3

Figure 3.3 Structures of ligands presented in **Tetrahedron,** *1999*, **55**, 1129-1142 conatining 3,2-HOPO moiety as the binding mode

The ligand bearing 2° amide functionality (R=H) displayed a $\log\beta_{110}$ of 28.2±0.84 and pFe^{3+} of 24.8. Methylation of this position was shown to alter the affinity constants minimally as when R = Me, $\log\beta_{110}$ = 28.7±0.64 and a pFe^{3+} of 25.1.[92] The data showed that the disruption of the possible H-bonding network available to the 2° amide has little influence on the stability of complex formation.

In addition to being utilised for Fe^{3+} binding, the core scaffold has also been used to build sensors for citrate and monosaccharides. Examples of the structures of these molecules are displayed in Figure 3.4.[93,94]

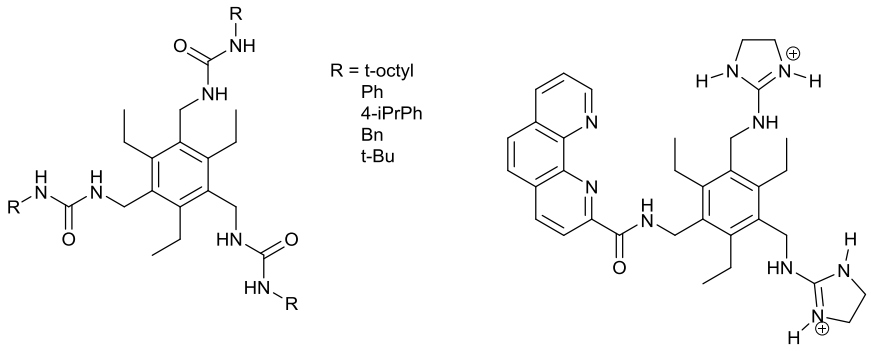

3.4 **3.5**

Figure 3.4 Molecules based upon the core 1,3,5-functionalised-2,4,6-triethylbenzene scaffold used for monosaccharide molecular recognition (left) and a citrate receptor (right)

Interestingly in 1998, Ward and Lutz published the synthesis of Fe^{2+} and Fe^{3+} chelators based upon the triethylbenzene core scaffold.[95] They reported the synthesis of a ligand with the potential property to switch binding mode depending on the oxidation state of the metal centre. The dodecadentate ligands which could host either Fe^{3+}/Fe^{2+} or a combination, Figure 3.5, were synthesised based upon the triethylbenzene and TREN core scaffolds. The harder metal centres preferring the inner coordinative atoms i.e. oxygen donors closer to the core scaffold where the softer metal centres would preferentially bind the bipyridine moieties

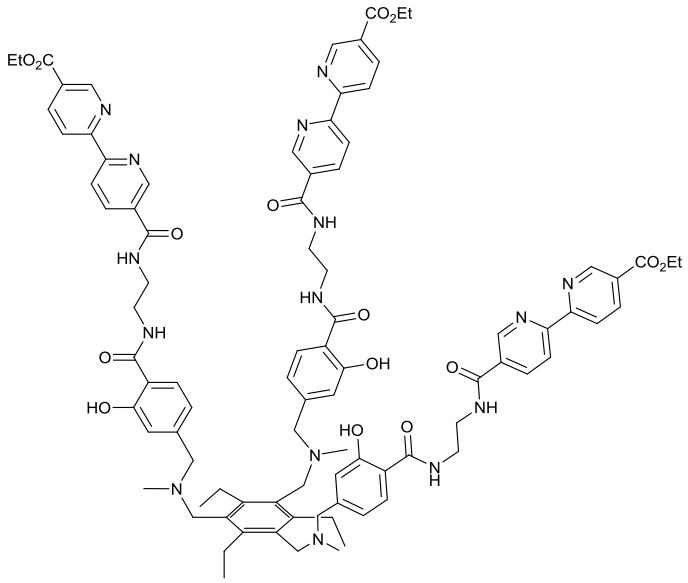

3.6

Figure 3.5 Example of a potential redox active Fe^{3+}/Fe^{2+} dodecadentate chelator reported in 1998 by Ward and Lutz

The molecule incorporates both hard and soft donor sites and so can accommodate either iron oxidative state. The ligands presented have the potential to sequester iron from the whole available pool which includes Fe(II) species, this could have attractive potential uses in the distortion of bacterial growth.

3.3 Bacterial testing

Molecules based upon the functionalised triethylbenzene scaffold have been shown to have effects on the growth of bacteria. In 1983 Raymond *et al*. published the effects of several enterobactin analogues on the growth profiles of *E. coli* strains.[96] It was discovered that both MECAM and MMECAM promoted the growth of several strains of *E. coli*, including those which were lacking the enterobactin receptor protein in the outer membrane. The results indicate that there is potential for the core scaffold to be utilised by bacteria and therefore have a promoting effect on the clinically relevant strains, rather than the desired bacteriostasis. Also, there is an increased risk of this occurring due to the analogues not appearing to be taken through specific membrane receptors, several uptake mechanisms seem to be operational.

However, the novel ligands to be presented herein contain HOPO moieties as the binding mode and, although these are bioisosteric with the catecholate moiety, the binding groups around the metal centre have been shown to be important in receptor recognition and so may help to reduce the potential of the ligands to be utilised by bacterial nutrient sequestration systems.

3.4 Results and Discussion

3.5 Ligand Synthesis

3.5.1 Synthesis of 1,3,5-tris(aminomethyl)-2,4,6-triethylbenzene (3.11)

The successful synthesis of the core scaffold has been previously reported via two synthetic routes. The first stage of the core synthesis is the same for both synthetic routes and involves the formation of the 1,3,5-tris(bromomethyl)-2,4,6-triethylbenzene molecule.

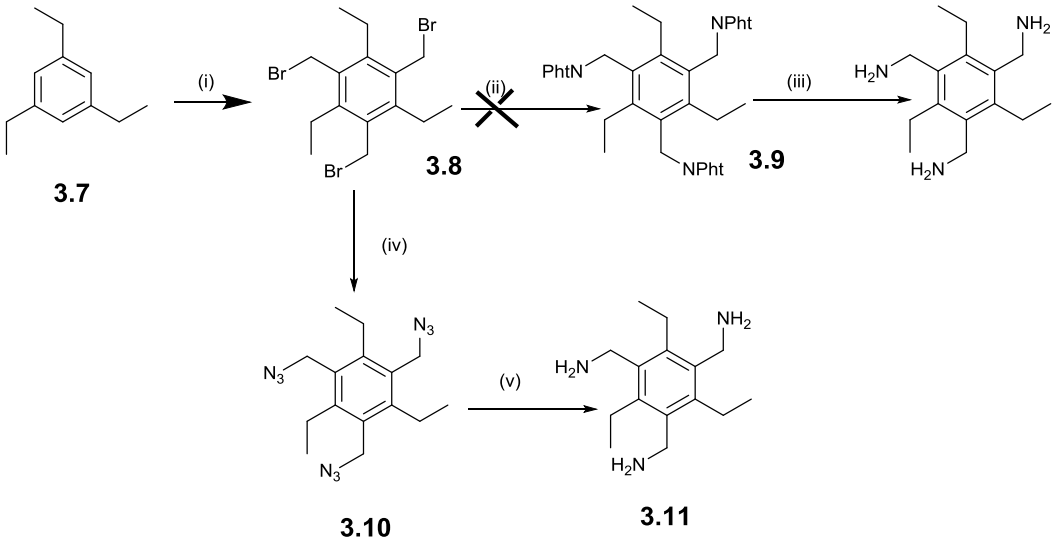

Scheme 3.1 Synthetic routes for the synthesis of core scaffold 1,3,5-tris(aminomethyl)-2,4,6-triethylbenzene (**3.11**). Reagents and conditions: (i) paraformaldehyde, 33% HBr in acetic acid, $ZnBr_2$, 90°C (ii) DMSO, potassium phthalimide, $N_2(g)$ (iii) $N_2H_2.H_2O$, EtOH/toluene, reflux (iv) NaN_3, DMF (v) PPh_3, THF, H_2O

The synthesis of **3.8** from 1,3,5-triethylbenzene proceeds as in the literature.[94] Paraformaldehyde is dissolved in 33% HBr solution in acetic acid, to which 1,3,5-triethylbenzene (**3.7**) is added with $ZnBr_2$ and the mixture heated to 90°C for 20 hours. The resulting precipitate is collected and after washing with H_2O and being dried in a desiccator yields the pure compound in yields 74-76% (lit. 97%).

The next synthetic stage had the option to synthesise the triphthalimide derivative or the triazide. To limit the potentially dangerous use of NaN_3, a potent toxin and also to avoid the synthesis of potentially dangerous relatively low molecular weight azide compounds the preparation of the triphthalimide (**3.9**) was attempted.[94] **3.8** was stirred with potassium phthalimide in DMSO and worked up as described in the literature. Unfortunately, a mixture of products was obtained and the pure compound was never isolated as described. The alternative synthetic route for this compound and the literature procedure for the synthesis of this compound described the use of a slurry of NaN_3 being poured down the condensing unit to the compound at 80°C.[93] However, it was discovered that simply stirring in DMF at room temperature was sufficient to provide the desired compound. The reaction was easily followed by TLC and after work up yielded the pure compound **3.10** in yields around 45% (lit.89%).[93] Following this synthetic route the triazide was reduced to the desired core molecule **3.11** via the Staudinger reaction with PPh_3, in THF and H_2O in 77% yield (lit. 99%).[93]

3.5.2 Preparation of 3-methoxy-1,6-dimethyl-2-oxo-1,2-dihydropyridine-4-carboxylic acid (3.14)

The retro-3,2-HOPO bidentate unit has previously been prepared in the literature. The methodology described the use of $NH_{3(g)}$ in the first stage of the HOPO formation. Instead of this $H_4N^+{}^-OAc$ was used as a source of NH_3 to avoid handling the gas.[97]

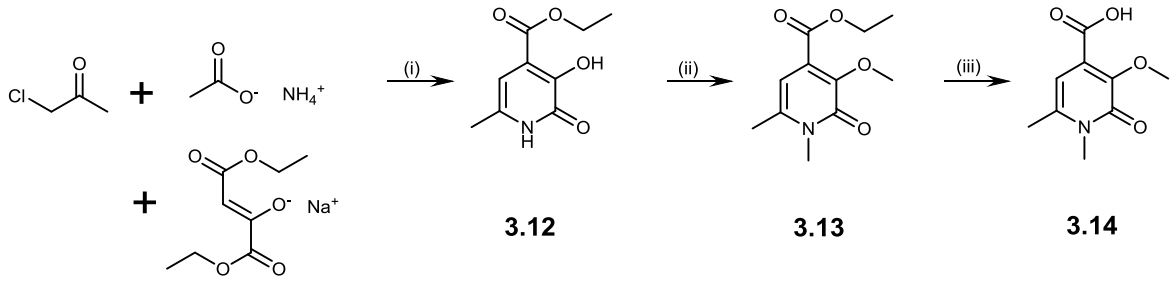

Scheme 3.2 Synthetic route for retro-3,2-HOPO. Reagents and conditions: (i) THF, $AlCl_3$ (ii) MeI, DMF, K_2CO_3 (iii) 1:1 MeOH:4M NaOH then 37% HCl

The preparation of **3.14** which includes carboxylic acid functionality, to allow attachment to the core scaffold is the reaction between chloroacetone, $H_4N^{+-}OAc$ and sodium diethyloxy acetate in the presence of $AlCl_3$ to produce the unprotected retro-3,2-HOPO-ester functionalised **3.12**, Scheme 3.2 in yields 35-43%. The next stage in the preparation is dimethylation/protection of the free hydroxyl and amine functional groups. This is done with MeI in DMF with K_2CO_3. The reaction proceeds to give the desired crude product **3.13** which is used in the next stage without purification.[98] The hydrolysis of the 4-ethyl ester groups takes place in MeOH with an equivolume of 4M $NaOH_{(aq)}$. The reaction is refluxed for 4 hours and, once the MeOH has been removed, acidification yields the crude product. This is recrystallised in EtOAc to yield the pure acid **3.14** in yields around 50% as a tan solid.[98]

3.5.3 Preparation of 1-(benzyloxy)-6-oxo-1,6-dihydropyridine-2-carboxylic acid (3.15)

The synthesis of 1-(benzyloxy)-6-oxo-1,6-dihydropyridine-2-carboxylic acid has been previously reported.[87] This compound allows for the incorporation of the 1,2-HOPO binding group onto this core scaffold via an amide linkage. The molecule was synthesised as per the literature procedure.

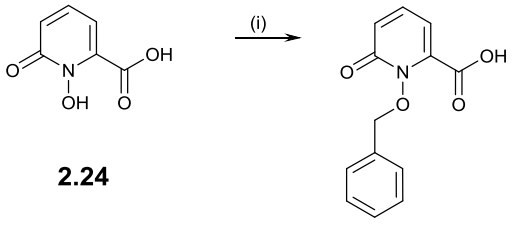

2.24 **3.15**

Scheme 3.3 Reaction scheme for the synthesis of the 1,2-HOPO-acid functionalised. Reagents and conditions: (i) K_2CO_3, BnBr, MeOH at reflux, 37% $HCl_{(aq)}$

The synthesis of **3.15** began with the previously synthesised 1,2-HOPO derivative (Chapter 2). **2.24** is subjected to benzylation at the N-hydroxyl position by benzyl bromide in MeOH under reflux. The acidification of the crude evaporated reaction mixture yields the pure product as a white solid in a good yield of 88%,.

3.5.4 Preparation of 2-[3-(benzyloxy)-4-oxo-1,4-dihydropyridin-1-yl]acetic acid (3.18)

The preparation of **3.18** was undertaken to allow for attachment of the 3,4-HOPO to the core scaffold, creating a series of ligands which incorporate a larger range of the possible HOPO isomers. The synthesis (Scheme 3.4) begins with the benzylation of maltol (**3.16**). This reaction is documented in the literature and occurs as is reported to give the desired benzyl protected maltol **3.17** in yields of approximately 86%.[99]

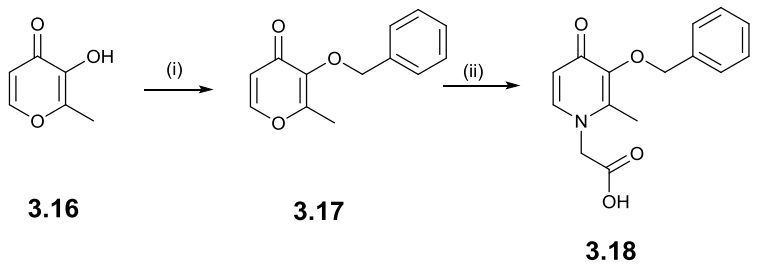

3.16 3.17 3.18

Scheme 3.4 Synthesis of 2-[3-(benzyloxy)-4-oxo-1,4-dihydropyridin-1-yl]acetic acid (**3.18**). Reagents and conditions: (i) 8M $NaOH_{(aq)}$, MeOH, BnBr, reflux (ii) Sodium glycinate, H_2O, reflux

The latter stage of the synthesis to yield the protected 3,4-HOPO occurs by reaction of benzyl maltol (**3.18**) with sodium glycinate in H_2O at reflux.[100] The reaction proceeds as in the literature procedure to yield the product in 65% yield, requiring no purification.

3.5.5 Preparation of protected ligands based on the 1,3,5-triethylbenzene-2,4,6-trisaminomethyl core scaffold (3.19-3.23)

As previously discussed (3.1 Introduction to 1,3,5-tris(aminomethyl)-2,4,6-triethylbenzene) the use of TBTU was already reported in the literature as being appropriate for the successful coupling of trisaminomethyl-aryl core scaffolds to acid functionalised HOPO groups.[53] The implementation of this method as described allowed for the preparation of the five ligands shown in Scheme 3.5.

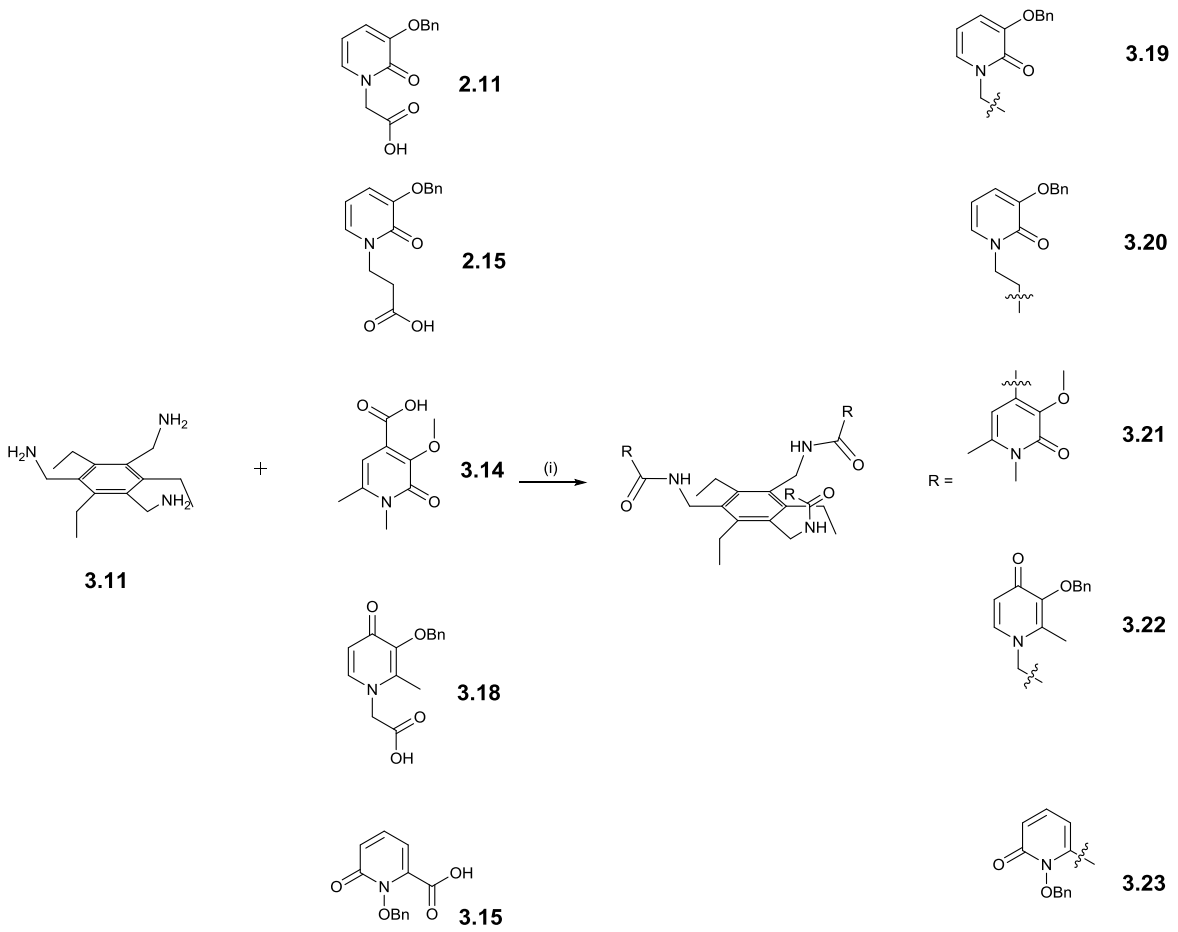

Scheme 3.5 Synthetic route for molecules **3.19-3.23**. Reagents and conditions (i) TBTU, N-Me-morpholine, dry DMF, 60°C

The molecules **3.19** and **3.20** were accessed using the previously described molecules **2.11** and **2.15**. For all the molecules **3.19-3.23** the coupling reaction proceeds to completion after 24 hours at 60°C. The DMF is then mostly removed and, following purification by column chromatography produces the protected ligands in yields: **3.19** 38-59% **3.20** 41-50% **3.21** 61-72% **3.22** 82% **3.23** 59-64%. This is an effective method to access **3.19-3.23**, however the obtained yields for some of the molecules after purification were less than for the others. When the same procedure is followed for each reaction it would be expected the yields to be approximately the same, especially between repeat reactions. In this respect the method can be somewhat unreliable and perhaps other coupling methods could aid in the optimisation of the lower yielding reactions, though this is yet to be explored.

3.5.6 Preparation of final ligands based on 1,3,5-tris(aminomethyl)-2,4,6-triethylbenzene scaffold (44-47)

The deprotection of the protected ligands **3.19**-**3.23** all occurred via the same method. A standard *O*-benzyl deprotection of 1:1 HCl:AcOH was performed for all these ligands, Scheme 3.6.

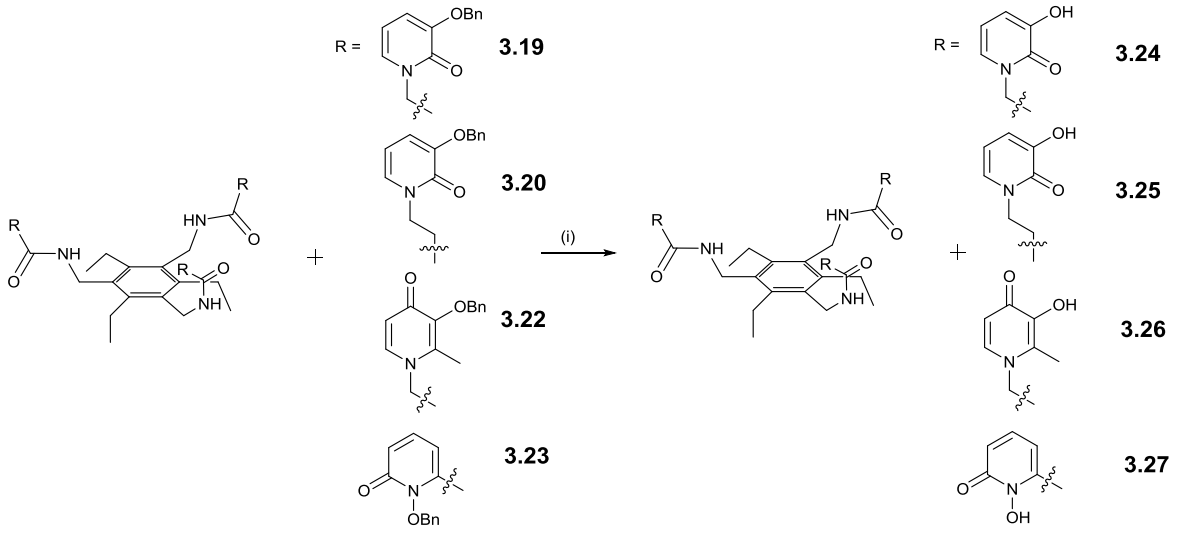

Scheme 3.6 Deprotection of ligands **3.19**, **3.20**, **3.22** and **3.23**. Reagents and conditions: (i) 37%HCl:glacial acetic acid 1:1, 60°C 5-7 days

The O-benzyl deprotection methods all produced the free ligands after several days at 60°C. Purification of the ligands was achieved through precipitation from MeOH with diethyl ether. The ligands were collected via suction filtration and stored in a desiccator as they appeared to be hygroscopic. Typical yields for the deprotection reactions were between 22-40% for the 3,2-HOPO and 1,2-HOPO containing ligands. The compounds were typically hygroscopic when isolated.

The deprotection method for the O-Me protected ligand **3.21** (Scheme 3.7) was performed using BCl_3 (1M in heptane) in dry DCM. The reaction was stirred for 2 days under an inert $N_{2(g)}$ atmosphere and the pure product could be isolated after quenching with MeOH, evaporating to dryness and precipitation of the pure product **3.28** was achieved with MeOH. The product could be isolated in typical yields of 55-60%.

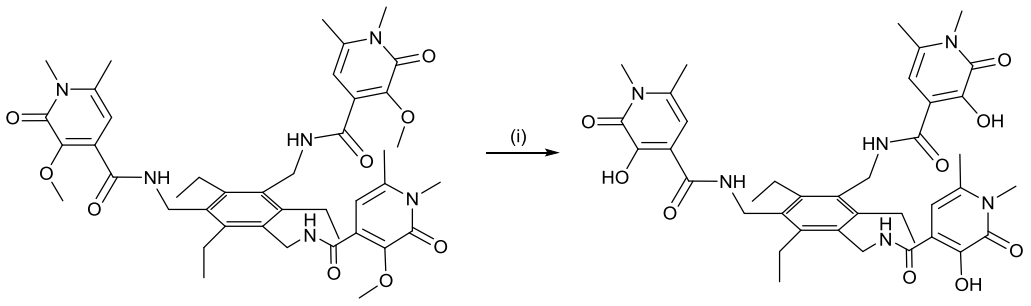

3.21 **3.28**

Scheme 3.7 Deprotection of ligand **3.21**. Reagents and conditions: (i) BCl_3 (1M in heptane), dry DCM, room temperature, $N_{2(g)}$, 2 days

3.5.7 Preparation of EMECAM (1.32)

The hexadentate, triscatecholate ligand EMECAM has been previously accessed in the first instance by Raymond *et al*. via the following synthetic route, Scheme 3.8.

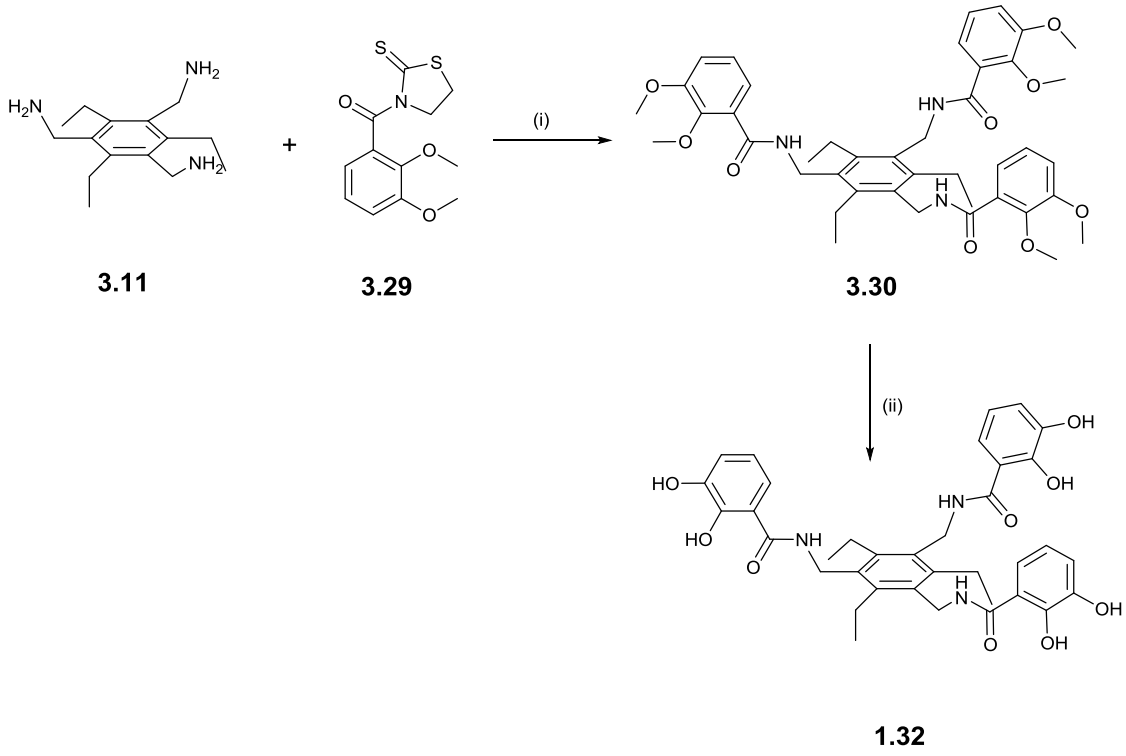

3.11 **3.29** **3.30** **1.32**

Scheme 3.8 Previous synthetic route for EMECAM. Reagents and conditions: (i) $CHCl_3$, room temperature-60°C (ii) BBr_3, DCM.

The synthetic methodology requires the protection of 1,2-dihydroxybenzoic acid and the subsequent activation with 2-mercaptothiazoline of this compound before coupling the activated ester with the 1,3,5-trisaminomethyl-2,4,6-triethylbenzene core scaffold. As has been previously noted the coupling reagent TBTU has successfully been utilised in the coupling of HOPO-acid derivatives with this core scaffold. This method was therefore employed in the synthesis of EMECAM to the advantage that it would allow the synthetic route to be one step shorter, through negating the requirement of an activation step.

The preparation of EMECAM began with the di-O-benzylation of the hydroxyl moieties on 2,3-dihydroxybenzoic acid (**3.31**) the procedure for which was based upon literature precedent.[101] This

reaction proceeded well with BnBr using K_2CO_3 as a base in a solvent of acetone. The O-benzyl protective group was utilised here instead of the O-methyl because of the previous success achieved with the protection group on this core scaffold for the HOPO ligands. The molecule **3.32** was achieved and used without further purification in the subsequent step.

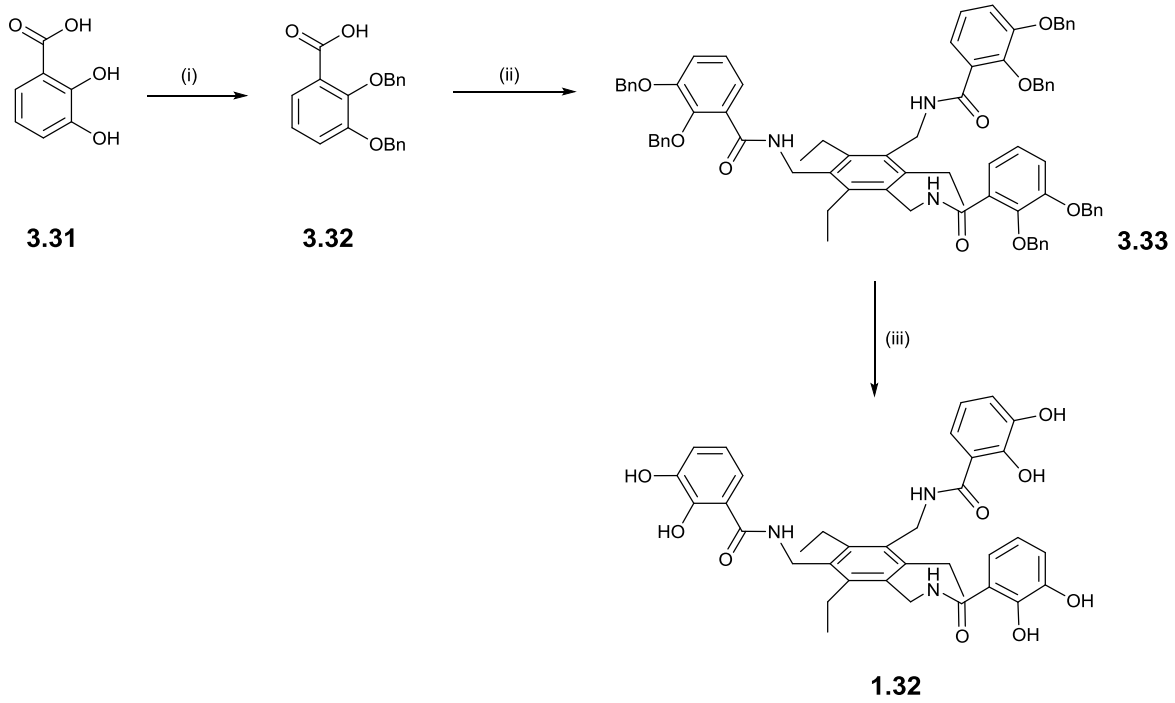

Scheme 3.9 Preparation of EMECAM. Reagents and conditions: (i) BnBr, K_2CO_3, acetone then 5M $NaOH_{(aq)}$, MeOH reflux (ii) **3.11**, TBTU, N-Me-morpholine, DMF, 60°C(iii) dry DCM, BCl_3 (1M in heptane), 18 hours, 0°C-room temperature

The coupling of **3.32** and the core scaffold **3.11** was performed under the same conditions as those that successfully produced the protected ligands **3.19**-3.**23**. The coupling reaction proceeded as per previously discussed and gave the protected ligand in 52-54% yield after purification via column chromatography.

The subsequent deprotection of **3.33** was attempted via the same method as per the other O-benzyl protected molecules. Concentrated acids 37% HCl:glacial acetic acid (1:1) were employed as the deprotection method. Unfortunately, the resulting product was not that of the expected deprotected molecule. The crude residue lacked the purity of free ligand which had previously been achieved for the other ligands.

Alternative deprotection methods were therefore sought. The deprotection via hydrogenation was attempted using Pd/C with a catalytic amount of H^+ in EtOH and H_2O. However, this reaction after 24 hours did not show complete removal of the benzyl protection by TLC. This could have been the result of the inability of the catalyst to access all of the groups to be removed due to steric hindrance. This method was therefore abandoned and as such a further method was sought. The use of BCl_3 in the removal of the O-benzyl groups proved to be an effective solution, Scheme 3.9.

The deprotection of the O-benzyl groups via this method produced the free EMECAM ligand in 85% yield as the pure compound after precipitation from MeOH with diethyl ether. The compound was found to be hygroscopic and so stored in a vacuum desiccator over P_2O_5.

3.6 UV-Vis Spectroscopic Determination of L:Fe^{3+} Stoichiometry

L:Fe^{3+} stoichiometry was determined via a method described in the Experimental section, which is based on a literature procedure for L:M stoichiometry determination.[91]

3.6.1 Modified Job's Plot Analyses for Ligands 3.24-3.28

The modified Job's plot analyses for the ligands **3.24-3.28** are presented. In these analyses an intercept of 0.5 at the x axis would indicate a ratio of 0.5:0.5 L:Fe^{3+} would be indicative of a 1:1 stoichiometric ratio. Some of the solutions were subject to precipitation; therefore some of the Job's plot analyses have been modified to omit spurious results for clarity.

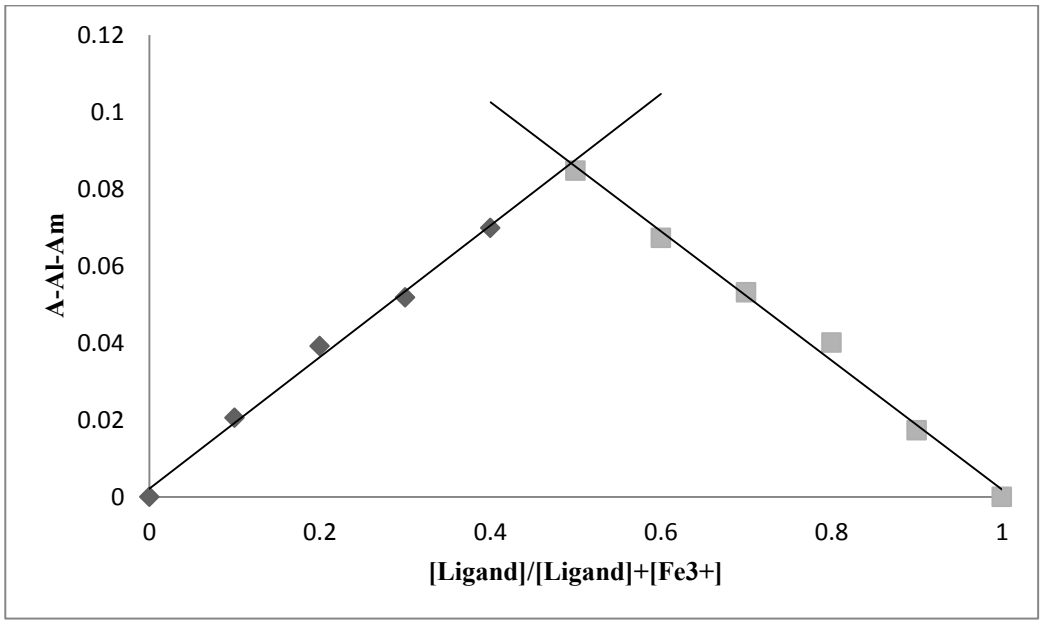

Figure 3.6 Modified Job's plot analysis for TEB-SC-3,2-HOPO **3.24** after 2 days. Measurements taken at room temperature in DMSO/H_2O.

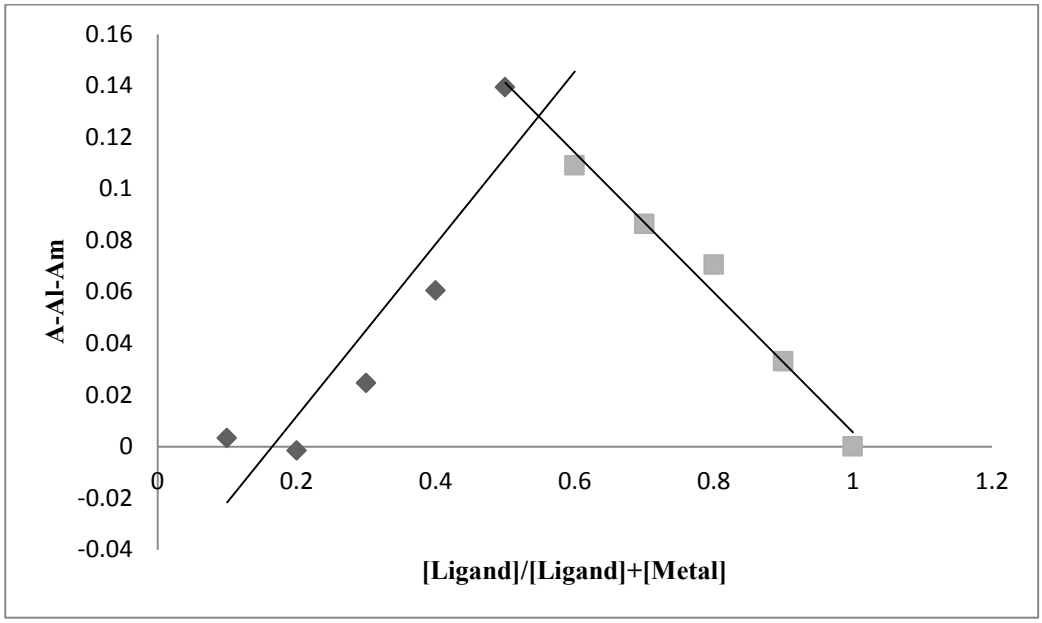

Figure 3.7 Modified Job's plot analysis for TEB-SC-3,2-HOPO **3.24** after 14 days. Measurements taken at room temperature in DMSO/H_2O.

The modified Job's plot analysis for ligand (**44**) showed that after a 2 day period of equilibration time the calculable L:Fe^{3+} stoichiometric ratio was 1:1. This indicates that the ligand binds the metal as expected and over a relatively short time period, owing to the kinetic viability of this ligand. The L:Fe^{3+} stoichiometry after 14 days for ligand **3.24** was shown to be 0.45:0.55, which is still close to the 1:1 L:Fe^{3+} which was described for the 2 day reading. This would suggest that the ligand complex is stable over this time period and so both thermodynamically and kinetically preferentially forms the 1:1 L:Fe^{3+} complex.

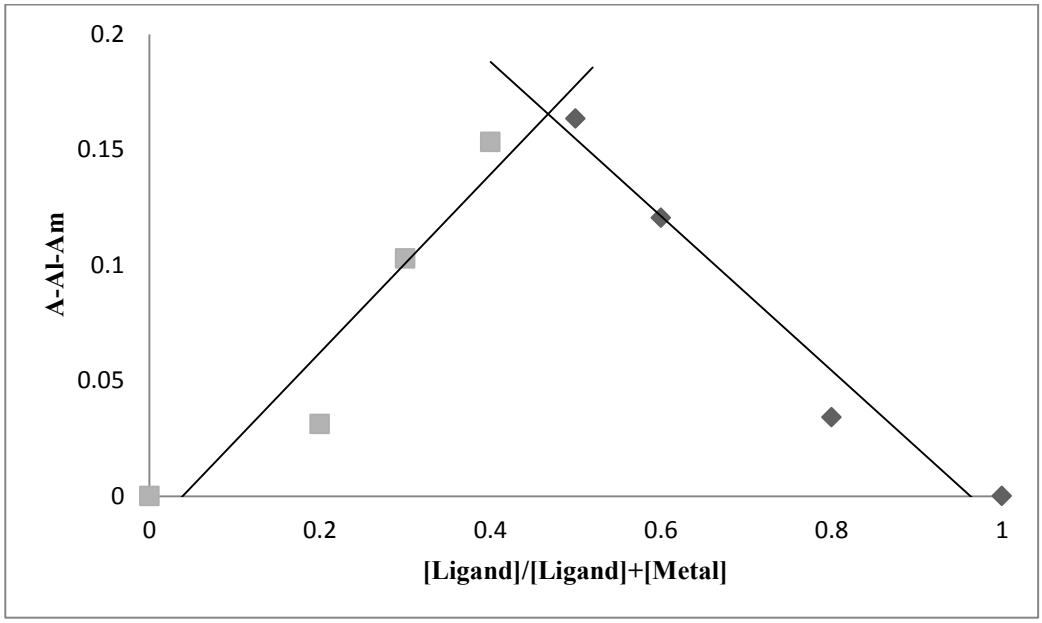

Figure 3.8 Modified Job's plot analysis for TEB-LC-3,2-HOPO **3.25** after 2 days. Measurements taken at room temperature in DMSO/H_2O.

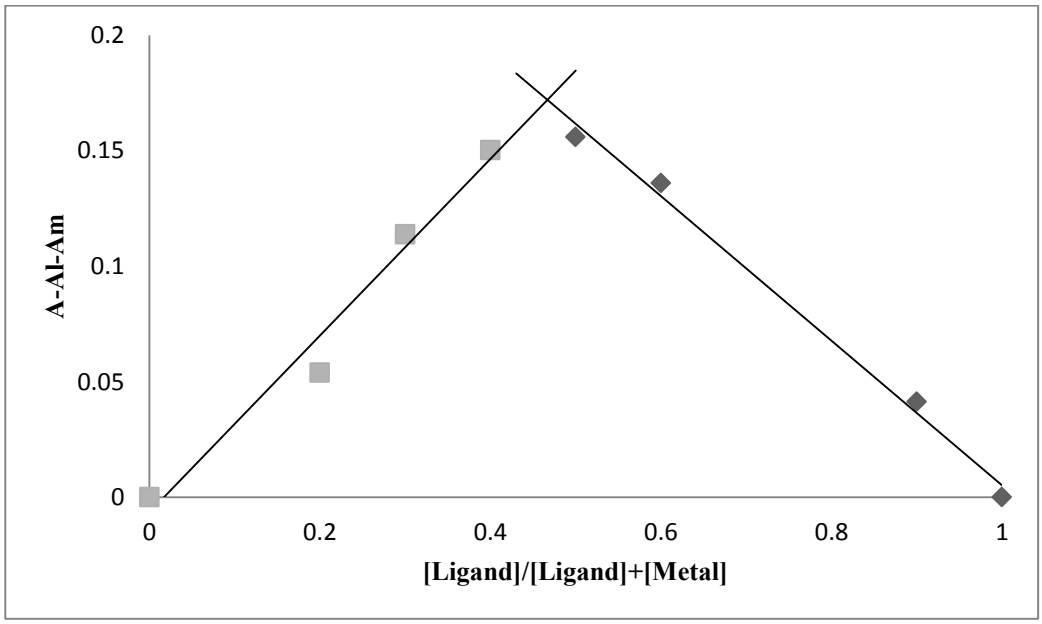

Figure 3.9 Modified Job's plot analysis for TEB-LC-3,2-HOPO **3.25** after 14 days. Measurements taken at room temperature in DMSO/H_2O.

For **3.25** the modified Job's analysis shows, in the first instance that after 2 days the L:Fe^{3+} stoichiometry is 1:1. This denotes efficient binding of the metal centre by the ligand, as designed. The measurements were repeated and after 14 days the L:Fe^{3+} stoichiometry was found to be the

same 1:1 as previously found. This would be indicative of thermodynamic stability of the complex as the formed ferric complex is stable over a long time period.

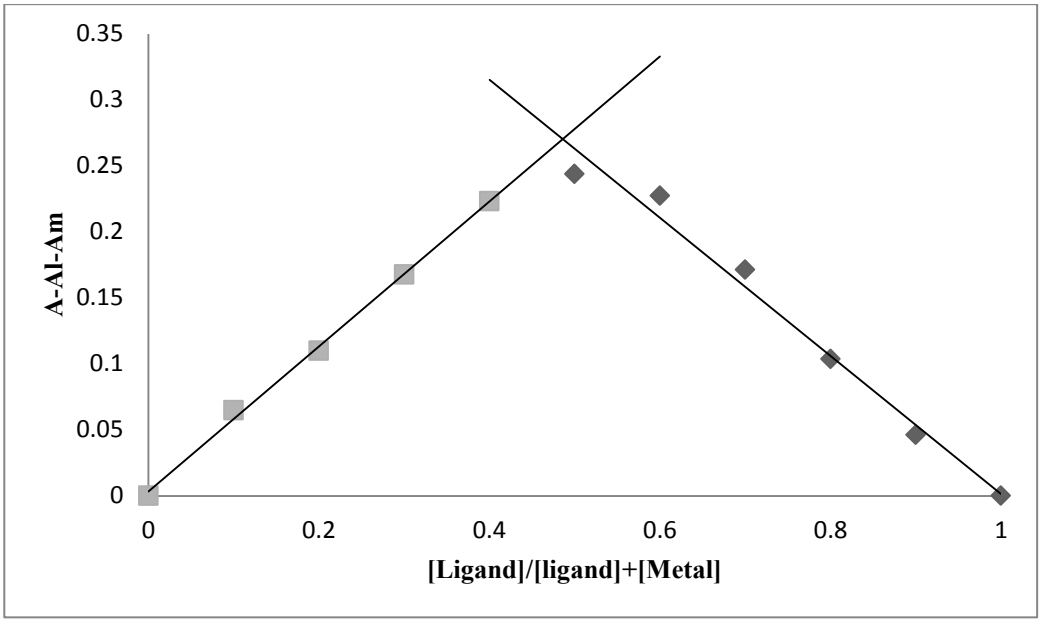

Figure 3.10 Modified Job's plot analysis for TEB-3,4-HOPO **3.26** after 2 days. Measurements taken at room temperature in DMSO/H_2O.

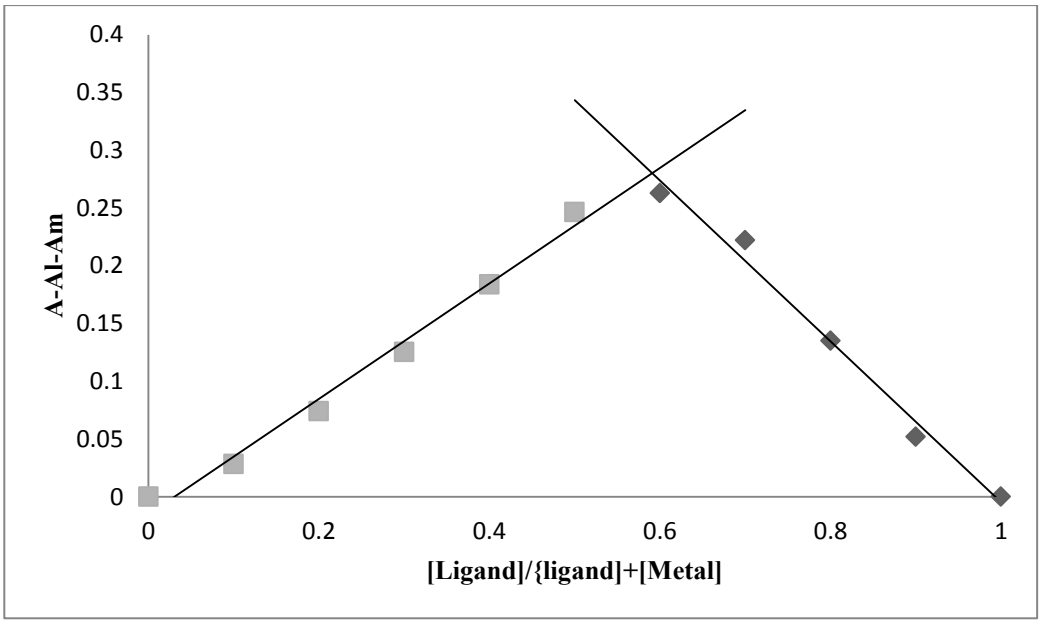

Figure 3.11 Modified Job's plot analysis for TEB-3,4-HOPO **3.26** after 14 days. Measurements taken at room temperature in DMSO/H_2O.

For **3.26** the modified Job's plot analysis showed in the first instance, after 2 days the L:Fe^{3+} stoichiometry to be 1:1. However, this ligand at the second reading, after 14 days, displayed a

L:Fe^{3+} ratio of 0.4:0.6, a result which indicates equilibration away from the ideal 1:1 ratio. This could be rationalised by the initial kinetically driven binding being thermodynamically unfavourable. If this is so it could be attributed to the meta-para attachment of the binding units with respect to the anchoring N-atom. It has been noted in the literature that an ortho-meta attachment is important for strong and favoured chelation and so where initially a 1:1 ratio is kinetically favoured it is not the most thermodynamically stable arrangement.

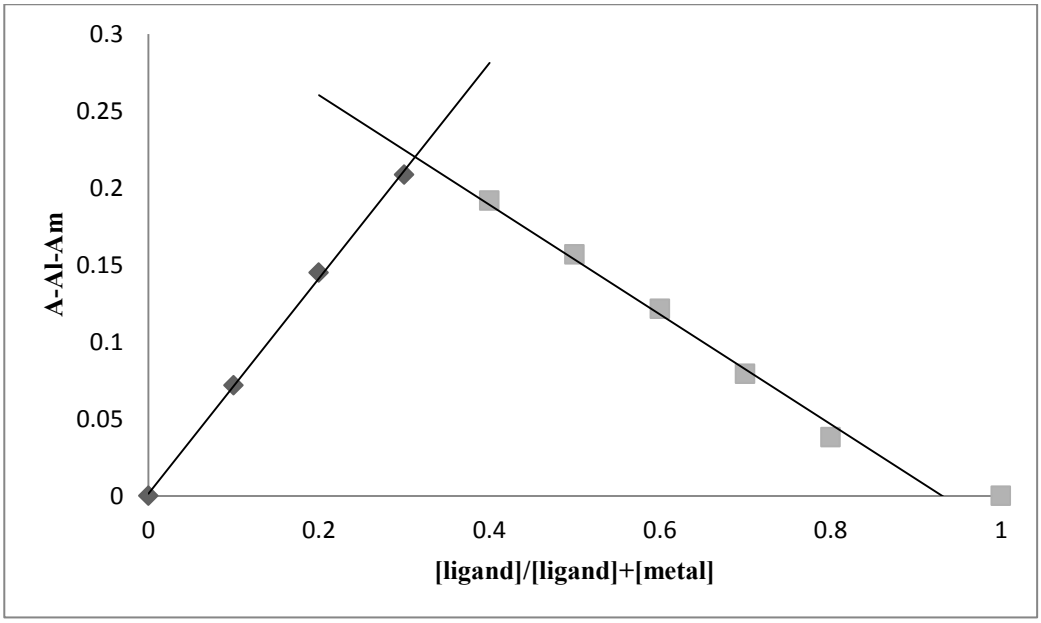

Figure 3.12 Modified Job's plot analysis for TEB-1,2-HOPO **3.27** after 2 days. Measurements taken at room temperature in DMSO/H_2O.

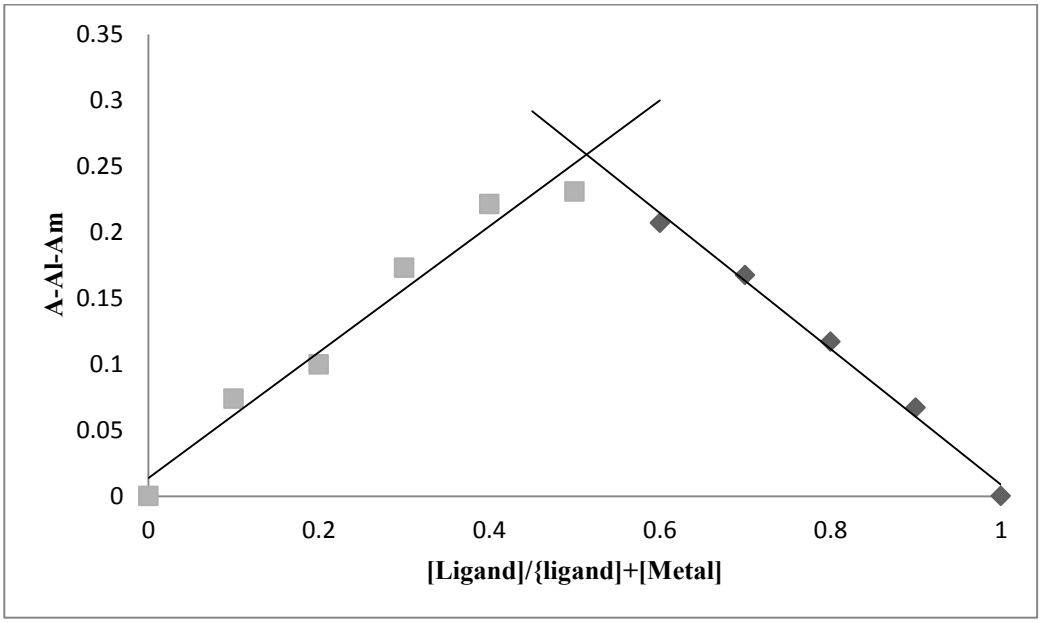

Figure 3.13 Modified Job's plot analysis for TEB-1,2-HOPO **3.27** after 14 days. Measurements taken at room temperature in DMSO/H_2O.

The modified Job's plot analysis for the initial reading taken after 2 days equilibration for **3.27** showed the molecule to have a L:Fe^{3+} stoichiometry of approximately 0.7L:0.3M. After 14 days this can be seen to re-equilibrate to a 1:1 ratio. This initial result could be due to the lower pKa of the 1,2-HOPO compared with the other HOPO moieties, in the first instance the binding of the metal centre maybe more favoured by the binding of more ligands per metal centre if the complex formation was under kinetic control. Then, as the equilibration time increases a re-equilibration to a 1:1 ratio is more thermodynamically favoured.

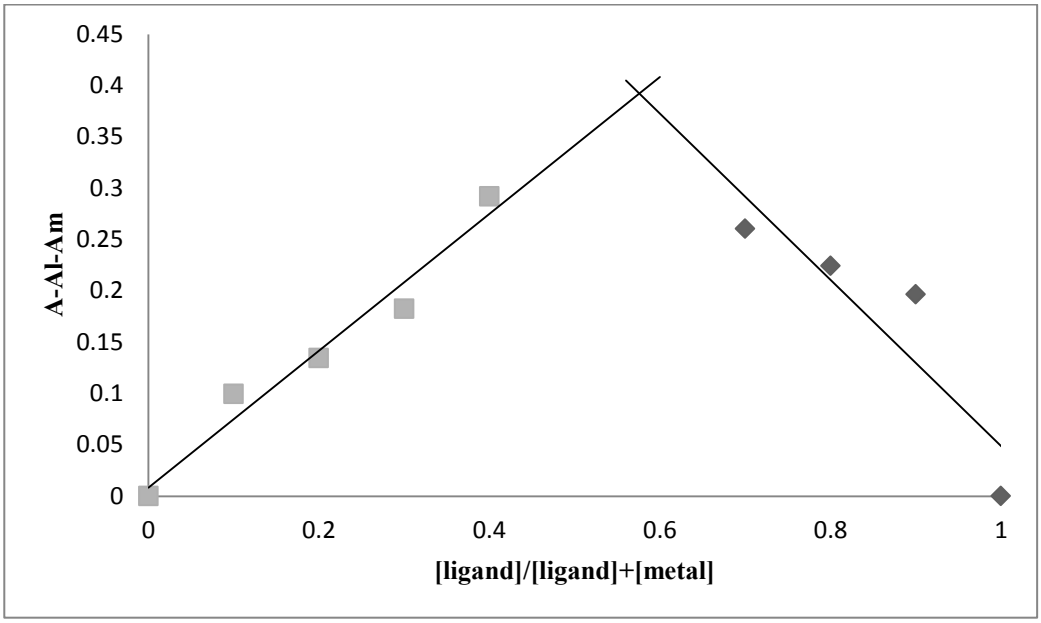

Figure 3.14 Modified Job's plot analysis for TEB-retro-3,2-HOPO **3.28** after 2 days. Measurements taken at room temperature in DMSO/H_2O.

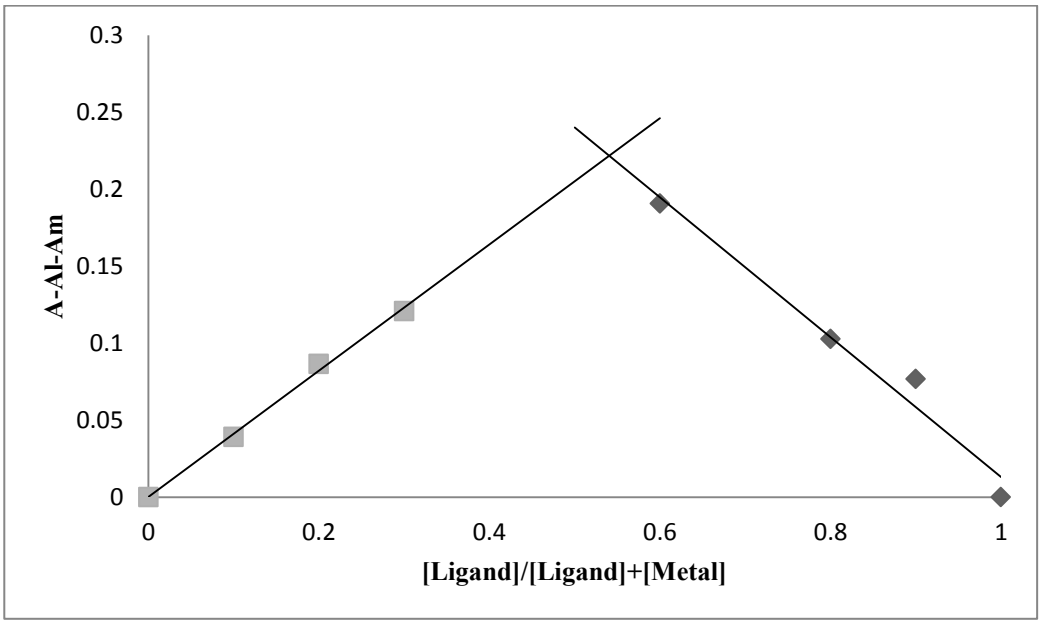

Figure 3.15 Modified Job's plot analysis for TEB-retro-3,2-HOPO **3.28** after 14 days. Measurements taken at room temperature in DMSO/H_2O.

The modified Job's plot analyses for the TEB-retro-3,2-HOPO ligand **3.28** reveal that at the initial reading taken after 2 days the stoichiometry is determined to be 0.44L:0.56M. This ratio is close to the ultimately desired 1:1 ratio. However, after the 14 day equilibration period it was noted that the

L:Fe^{3+} stoichiometry had changed only by a slight amount to 0.46:0.54. This ratio is closer still to the desired ratio and may indicate a re-equilibration to the more thermodynamically stable state over the time period. However the alteration is so small that further measurements are required to fully test this hypothesis. The non-ideal ratio we see in the first instance may be the result of the methylated N-atom which could serve to provide steric hindrance and hence slow the rate of formation of the metal complex. The results of all of the modified jobs plot analyses are displayed in Table 3.1.

Table 3.1 Table summary of the calculated L:Fe^{3+} ratios taken for the ligands **3.24-3.28**

Ligand	Initial Reading After 2 days /L:Fe^{3+}	Reading After 14 days/ L:Fe^{3+}
TEB-SC-3,2-HOPO 3.24	0.5:0.5	0.45:0.55
TEB-LC-3,2-HOPO 3.25	0.53:0.47	0.53:0.47
TEB-3,4-HOPO 3.26	0.51:0.49	0.40:0.59
TEB-1,2-HOPO 3.27	0.68:0.31	0.48:0.51
TEB-R-3,2-HOPO 3.28	0.44:0.56	0.46:0.54

3.7 Chapter Conclusions

In summary, five novel ligands based upon the 1,3,5-tris(aminomethyl)-2,4,6-triethylbenzene scaffold have been synthesised bearing a range of HOPO moieties. The ligands are based upon previously accessed molecules, however the coupling of these together on the triethylbenzene scaffold to produce powerful Fe^{3+} chelators remains novel. The ligands design include all of the necessary features to promote powerful Fe^{3+} binding and although the stability constants for the Fe^{3+} complexes have yet to be measured, the UV-Vis profiles and modified Job's plot analyses have shown the ligands to bind Fe^{3+} successfully.

The synthesis of the core molecule **3.11** occurs via a three step procedure, two of which are relatively high yielding. However, the second synthetic step to access the triazide derivative proved to yield the product in only 45% yield. It is possible that the loss of yield is due to the work up as it involves the addition of DCM to the reaction and then washing the excess NaN_3 and DMF out with H_2O. It is likely some of the compound is removed in these aqueous washings, as TLC indicated 100% conversion from the tribromide, and so an alternative work-up may prove to yield better. In addition, the alternative method from the literature which did not give the desired triphthalimide derivative may prove higher yielding if the reaction conditions were able to be optimised so as to produce the fully derivatised product.

The synthetic route for the retro-3,2-HOPO molecule **3.14** occurs via a 4 step reaction sequence. The first step is relatively low yielding at 35-43%. However, the starting materials for this reaction are relatively low cost, which would lend this reaction well to a scale up synthesis. Also, the product requires no extensive purification and so this would also be a desired attribute were the synthesis to be scaled. The subsequent step is the dimethylation of the ester-HOPO derivative, the reaction proceeds as expected and the product, after removal of the DMF and excess MeI was used without purification as the following step provided the necessary purification and the final acid-derivitised-retro-3,2-HOPO is isolated in around 50% yield. This yield could be indicative that the final compound is somewhat soluble when cool in EtOAc, the recrystallization solvent. Improved yields could be accessed by an alternative solvent.

The synthesis of **3.15** the 1,2-HOPO-acid derivative occurs via a modified literature procedure in good yield of 88%. The synthesis could be employed in scale up synthesis due to the compound being readily accessible in high yield and purity. In addition, the synthesis **3.18** via a two-step route, starting from maltol, also lends itself well to scale up reactions. The starting materials are accessible commercially for low cost and so the production of the compound is very economical.

The protected ligands were all able to be synthesised via the prescribed literature method published by Hider *et al*. The utilisation of the TBTU coupling reagent proved effective in that all of the coupling reactions were successful. However, the yields for these reactions were somewhat unreliable which could cause issues if the ligands were going to be applied to commercial

applications. However, the reactions were all able to be completed in a short time and only required purification by column chromatography to access the pure ligands.

The four O-benzyl protected ligands were all able to be easily deprotected in the presence of concentrated acids, precipitation of the free ligand afforded the pure product in all cases. The O-Me protected retro-3,2-HOPO derivative however required the use of BCl_3 (1M in heptane). This reaction does not lend well to potential scale up synthesis, due to the toxic nature of this reagent. Alternative methods were not attempted due to the small scale reaction being successful, however ideally a less toxic reagent should be sourced.

The UV-Vis spectroscopic determination of L:Fe^{3+} stoichiometry yielded some interesting results. In general, the ligands displayed L:Fe^{3+} of 1:1 or very close to this expected ratio. However ligand **3.26** appeared to equilibrate away from this 1:1 ratio. In the literature it has been shown that attachment point on the binding moiety to the ligand scaffold is important for the focus of the binding atoms towards the metal centre. The meta-para attachment this ligand has with respect to the N-atom in the ring system could create a disparate, unfocussed arrangement of the binding groups which overall could give a thermodynamically unstable complex and so could serve to drive the binding away from a 1:1 stoichiometry. **3.28** displayed slightly askew L:Fe^{3+} ratios from the desired 1:1 even after 14 days. This could be result of the steric hindrance the N-Me groups would contribute. However, if the metal were unable to sufficiently access the binding centre of the ligand the ratio would display a higher ligand contribution, in this case we see a more pronounced Fe^{3+} contribution. Further investigation is therefore required to elucidate the cause of this however, the 14 day reading indicated that the ratio was closer to a 1:1 complex and so the issue could simply be the rate of complex formation.

Design and Synthesis of Novel tris(piperazin-1-yl)-1,3,5-triazine based Fe^{3+} Selective Ligands Bearing hydroxypyridinone Binding Moieties

4 Chapter Aims

This chapter aims to explore the tris(piperazin-1-yl)-1,3,5-triazine core scaffold as a viable base on which to build strong and selective Fe^{3+} chelators. The chapter will provide the synthetic methodology to synthesise the molecules displayed in Figure 4.1.

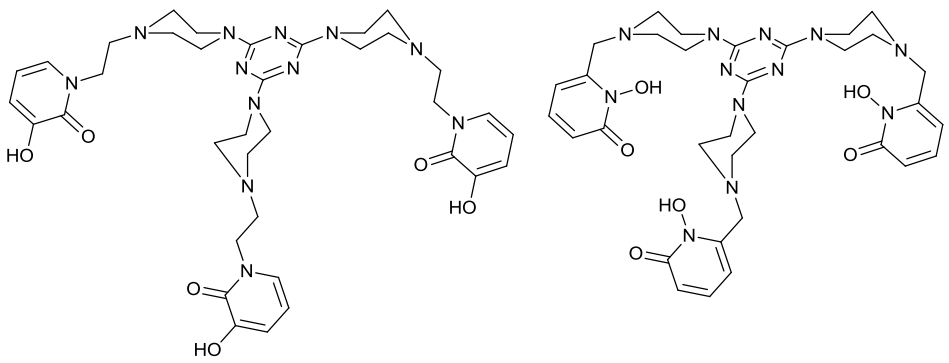

Figure 4.1 Structures of the tris(piperazin-1-yl)-1,3,5-triazine based chelators provided

The synthetic methodology will be provided for the core molecule as based on literature procedures. The synthetic methodology for the HOPO units synthesised for attachment to the core has been previously reported (Chapter 2). The 3,2-HOPO and 1,2-HOPO bidentate moieties have been the focussed upon due to their accessible derivatives which allow for attachment to the core scaffold.

The preparation of the protected hexadentate chelators and the subsequent deprotection methods are provided.

4.1 Introduction to tris(piperazin-1-yl)-1,3,5-triazine

The tris(piperazin-1-yl)-1,3,5-triazine core scaffold provides a favourable skeleton to allow for the incorporation of three HOPO binding units; due to the tri-piperazine scaffold which would be available to attach to appropriate electrophilic HOPO groups.

This core molecule has previously been synthesised to be the base of dendritic scaffolds which were made to function as drug-delivery vehicles, Figure 4.2 (**4.1**).

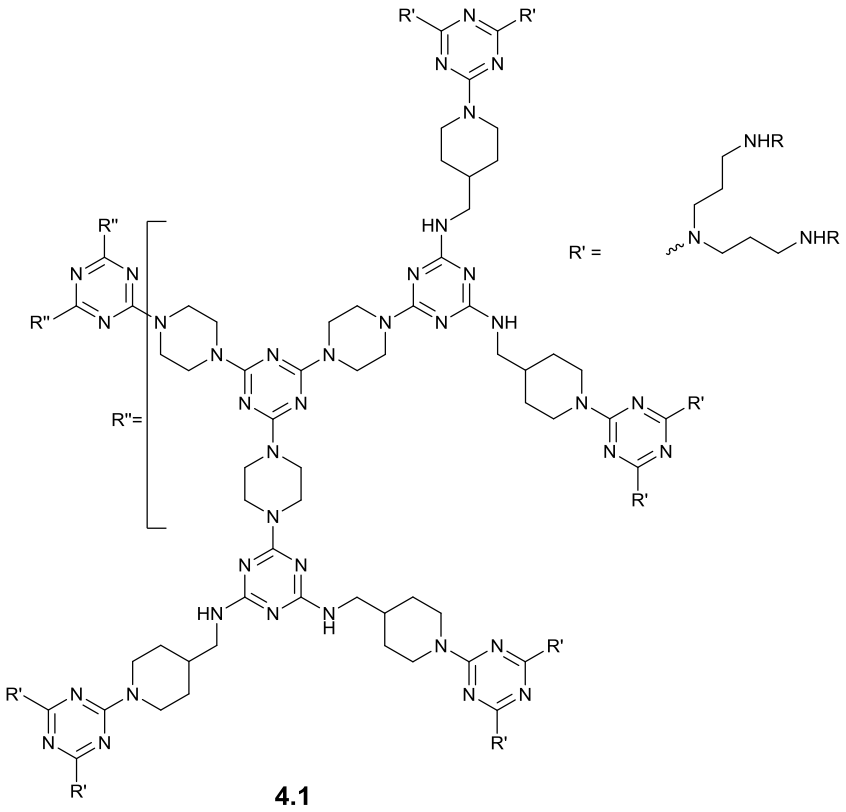

Figure 4.2 Structure of dendrimer containing tris(piperazin-1-yl)-1,3,5-triazine scaffold

The work was published by Simanek *et al*. in 2004.[102] The dendrimers were substituted with various surface groups such as phosphate, sulfonate and carboxylic acids. The research found that those groups containing cationic functionality were far more cytotoxic than those bearing anionic or neutral PEG groups, when tested on cell lines.

In addition in 2007 Simenak *et al*. synthesised more dendrimers based around this core scaffold. The aim of which was to allow for the protected amine scaffolds to provide molecular handles on which to create functionalise dendrimers, Figure 4.3.

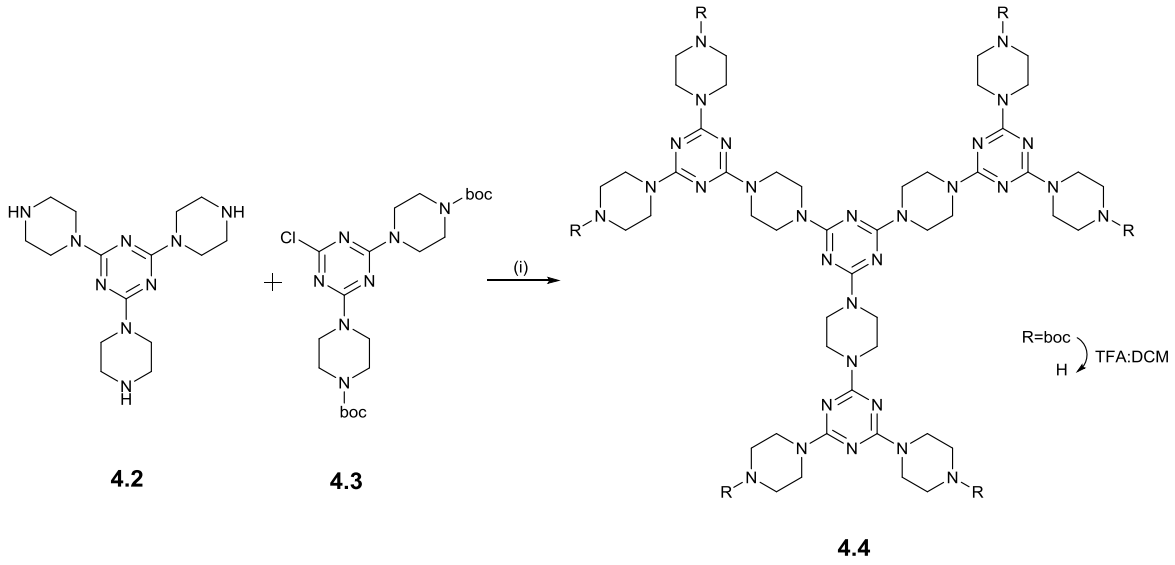

Figure 4.3 Structure of the dendrimer scaffold, based upon the tris(piperazin-1-y)-1,3,5-triazine molecule. Reagents and conditions: (i) K_2CO_3, $CHCl_3$, THF, rt, overnight

The synthetic routes to the molecules **4.1** and **4.4** displayed in Figure 4.2 and Figure 4.3 show that, not only is the tris(piperazin-1-y)-1,3,5-triazine core synthetically accessible from commercially available starting materials but the core scaffold is also able to be functionalised with electrophilic substrates, owed to the nucleophilic 2° amine systems.

As far as can be ascertained from literature searches, the core scaffold has never been utilised for the production of Fe^{3+} chelator technology. Due to these contributing factors, the core scaffold would seem an ideal choice from which to build Fe^{3+} ligands.

It is not immediately obvious for this core scaffold whether the hydroxypyridinone groups will have sufficiently long chains to allow successful binding of Fe^{3+}. The scaffold itself appears quite large. Due to the potential interconversion available to the piperazine ring systems between the chair conformers (Figure 4.4) it is unclear as to what conformation will be adopted by the ligands.

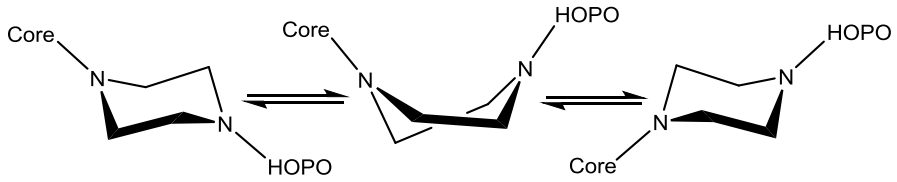

Figure 4.4 Figure displaying possible interconversion which may occur for the piperazine groups on the tris(piperazin-1-y)-1,3,5-triazine ligand. Showing two chair conformations (left and right) and the intermediary twist boat conformation (middle)

It is possible that once the HOPO groups bind Fe^{3+} this will create thermodynamic stability to prevent of this interconversion and affix the ligand so as to be organised towards the Fe^{3+} centre, it could be argued that the twist boat conformation, although perhaps not the most stable conformer before Fe^{3+} binding, may prove to be the conformation adopted because it angles the binding groups towards each other, Figure 4.5. However, the overall binding of Fe^{3+} will be dependent in the first instance on the chain length of the HOPO moiety.

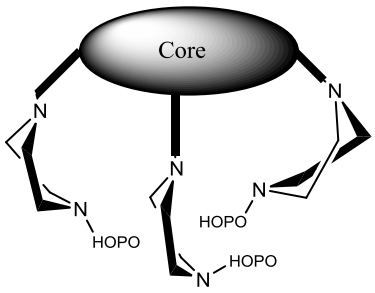

Figure 4.5 Possible conformation of the three piperazine units optimised for Fe^{3+} binding in the boat conformation

The interplay between the core scaffold conformations and the HOPO chain length may serve to create powerful Fe^{3+} binding if the correct parameters are found. It is therefore important to access a variety of chain length linkers for HOPO moieties for this core scaffold.

4.2 Results and Discussion

4.2.1 Preparation of tris(piperazin-1-yl)-1,3,5-triazine (4.2)

From literature precedents the synthetic route for the preparation of tris(piperazin-1-yl)-1,3,5-triazine **4.2** can be achieved by the route shown in Scheme 4.1.

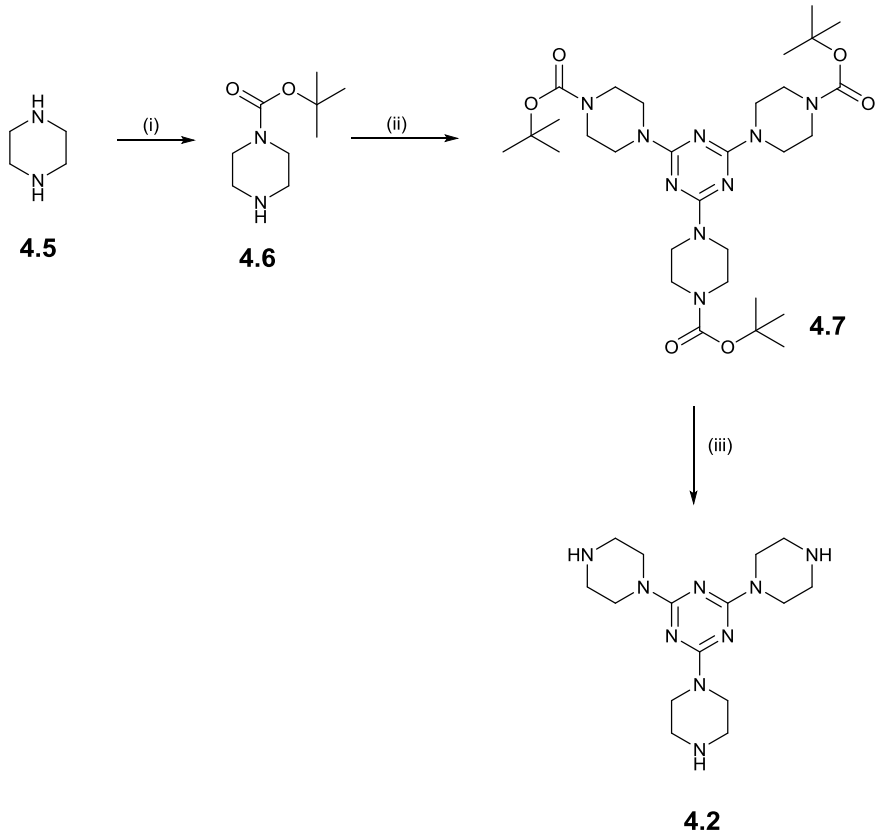

Scheme 4.1 Synthetic route for **4.2**. Reagents and conditions; (i) $(boc)_2O$, dry DCM, K_2CO_3 (ii) K_2CO_3, THF, 80°C, trichlorotriazine (iii) TFA:DCM (1:1)

The first step in the synthesis of **4.2** is the asymmetric mono-boc protection of piperazine. This reaction was performed in dry DCM with K_2CO_3 as a base. **4.6** was achieved in yield of 61% (lit. 88%) as the pure compound.[103] Step (ii) yields **4.7** as a result of a triple nucleophilic aromatic substitution at the three chloride sites situated around the trichlorotriazine ring system. The reaction was performed in THF at 80°C overnight, with K_2CO_3 as a base. The resulting product

achieved in 58% yield (lit. 86%) as the pure compound.[104] The deprotection of the protected core **4.7** was performed as a standard DCM:TFA (1:1) room temperature overnight reaction to yield the product **4.2** in 35% (lit. 95%) yield after workup.

4.2.2 Preparation of triazine-1,2-HOPO 4.9

As previously discussed (Chapter 2), the synthesis of 6-(chloromethyl)-1-(prop-2-en-1-yloxy)-1,2-dihydropyridin-2-one (**2.28**) was developed in house and has allowed for the attachment of the 1,2-HOPO moiety via nucleophilic substitution at the chloromethyl position. Therefore the triazine core molecule (**4.2**) was reacted with the 1,2-HOPO-chloride (**2.28**) to produce the allyl protected molecule (**4.8**), Scheme 4.2.

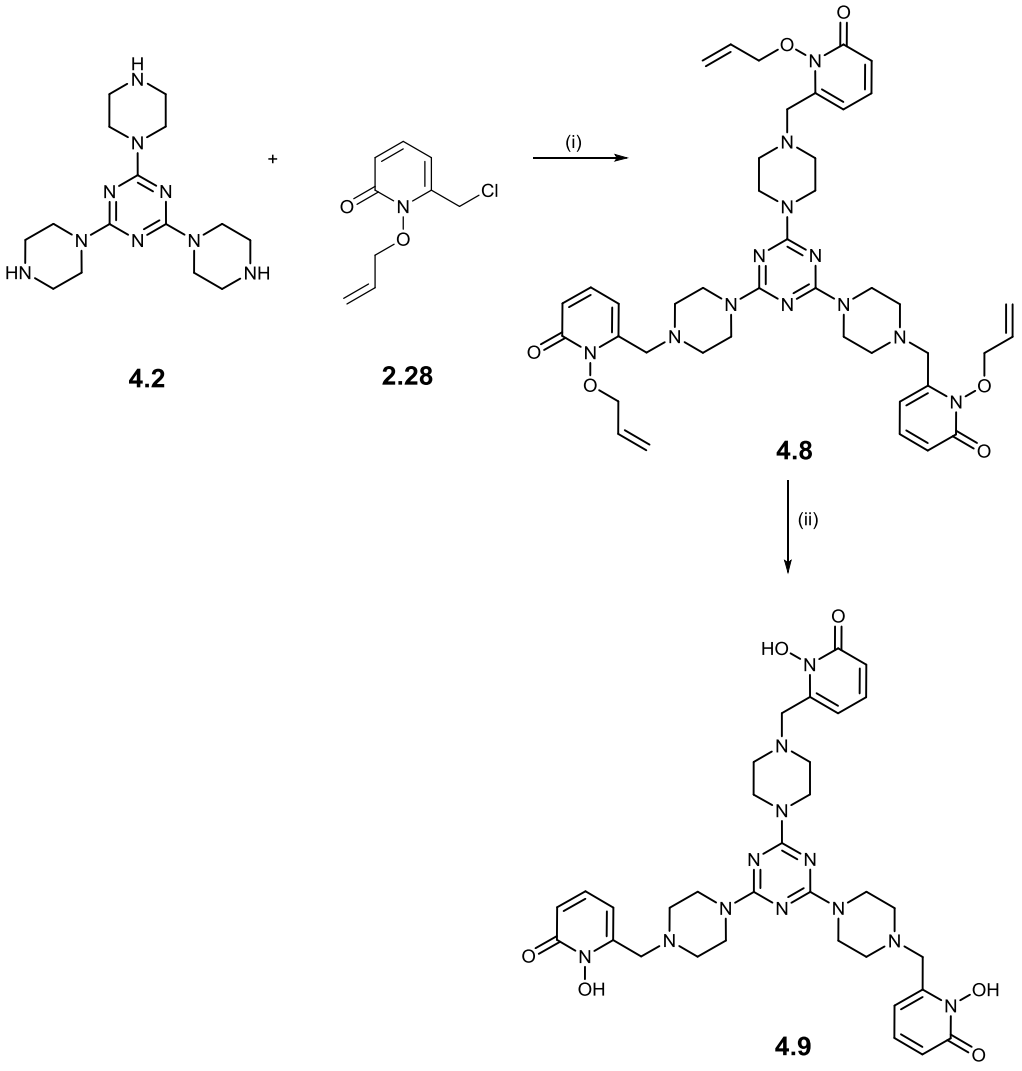

Scheme 4.2 Synthetic route to trazine-1,2-HOPO (**4.9**). Reagents and conditions: (i) dry MeCN, Et_3N, $N_{2(g)}$, reflux, 48 hours. (ii) Pd/C, dioxane:H_2O (4:1), TFA (0.15M), reflux

4.2 and **2.28** are reacted in dry MeCN in the presence of Et_3N for 48 hours at reflux to produce the desired protected ligand **4.8**. The crude ligand required purification via column chromatography, elution in DCM:MeOH 3-12% gave the desired product in 17% yield after purification. This method was devised from following a literature source for the addition of an electrophile to a piperazine core.[39]

The deprotection of the protected ligand **4.8** was achieved via the afore mentioned method for the allyl-deprotection of molecule (**2.29**).[90] This method employing the use of 0.15M TFA and Pd/C catalyst has been useful for allowing access to the free ligands containing the 1,2-HOPO moiety. The deprotection of **4.8** occurs to give the desired **4.9** in 79% yield, requiring no purification except the precipitation of the pure ligand from MeOH with diethyl ether.

The first step of the synthesis of **4.9** i.e. the synthesis of the triamine core occurs with a 27% loss of yield when compared to the literature value provided. This is possibly due to the amine being partially soluble in the aqueous phase during the work up, some may be left behind if sufficient repeated extractions with ether are not performed. Step (i) is the nucleophilic substitution reaction which occurs via the displacement of the three chloride ions by the mono-boc piperazine. This reaction again occurs with some loss of yield from literature precedent which may be due to insufficient reaction time, although the synthetic method was followed as was described. The final stage in the core molecule synthesis is the deprotection of the three boc groups to yield the free amine. There is here significant loss of yield with respect to the literature. This is most likely due to the deprotected core molecule being soluble in the highly basic aqueous solution which the crude residue is dissolved in. The extractions of this solution with DCM were therefore insufficient to allow effective transfer of the product to the organic phase. In future, the synthesis of this molecule could be improved upon by using a solvent which allows more favourable transfer of the product into the organic phase. Alternatively, if one cannot be found which surpasses DCM in this way simply more extractions of the aqueous phase are necessary. Despite this the synthesis of the core can be scaled up to produce multi-gram quantities of the desired amine. The starting materials are cheap and the reactions occur with little need to purify.

The substitution reaction (i) which occurs via nucleophilic attack of the electrophilic chloromethyl position of the bidentate HOPO unit produced the compound in only 17% yield. However, the purification method was suitably tailored to provide the desired compound in excellent purity. Future synthetic attempts to produce this compound would require optimisation of the reaction parameters if scale up is to be desired. The deprotection produced the desired ligand in 22% yield. Again, if scale up of this molecule is required then these conditions would require optimising.

4.2.3 Preparation of triazine-3,2-HOPO (4.11)

As previously discussed (Chapter 2), the synthesis of the literature compound iminium salt **2.21** allowed for the attachment of the 3,2-HOPO moiety to CTG via a two carbon chain. **2.21** has previously been shown to react with hindered nucleophiles, such as secondary amines to allow for the attachment of the moiety to a scaffold. The triazine core molecule **4.2** was reacted with the iminium salt to produce the protected molecule **4.10**, Scheme 4.3.

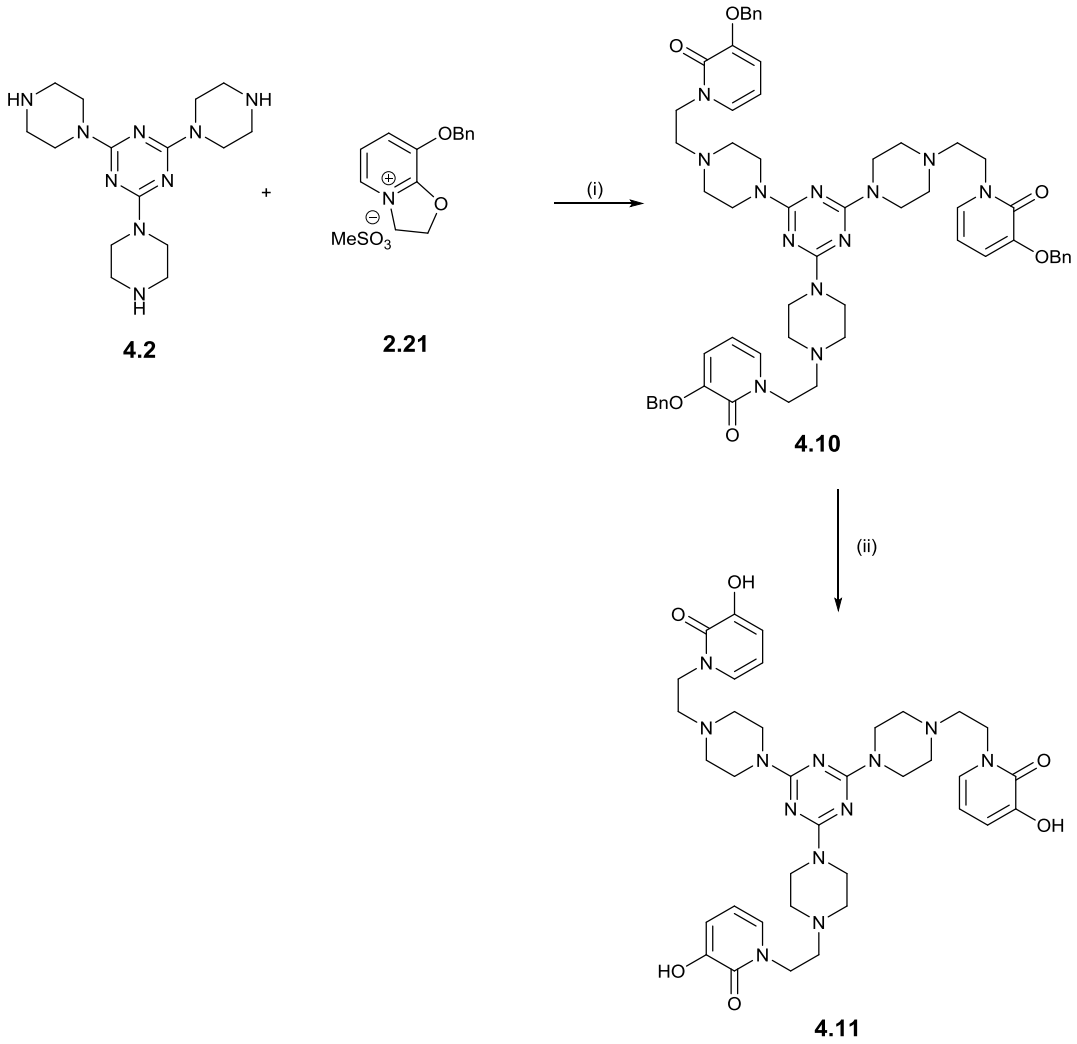

4.2 **2.21** **4.10** **4.11**

Scheme 4.3 Synthetic route to the triazine-3,2-HOPO ligand (**4.11**) Reagents and conditions: (i) dry MeCN, Et_3N, $N_{2(g)}$, 3 days room temperature then 24 hours reflux: (ii) 37% HCl:glacial acetic acid (1:1), room temperature to 60°C, 5 days

The synthesis of **4.10** was performed in dry MeCN with Et_3N as a base. The reaction was in the first instance stirred at room temperature; however TLC showed that after 3 days the reaction was incomplete. After a further 24 hours at reflux, TLC showed the consumption of the starting materials had taken place. After workup, the product was purified with column chromatography and yielded the desired protected ligand in 26-29% yields after purification.

The subsequent deprotection of **4.10** was performed as a standard O-benzyl deprotection using concentrated acids 37%HCl:glacial acetic acid (1:1). The deprotection conditions afford the desired molecule **4.11** after precipitation from MeOH with diethyl ether in yields around 22%.

The synthesis of the triazine-3,2-HOPO protected ligand begins with the nucleophilic addition of the triamine-triazine core scaffold to the iminium salt. The addition reaction occurs in yields up to 29%. This is a relatively low yield and does not reflect the yield achievable when the CTG core is subjected to the same bidentate unit. This could be due to the use of Et_3N as a base in the reaction. **2.21** has been shown to produce alternative products to the desired ring opening through multiple competing pathways of addition, when small molecule nucleophiles are present, such as primary amines. However, because a tertiary amine was used, this degradation should not have occurred. The loss of yield would suggest that multiple pathways were present producing side products which were not isolated. The desired protected ligand is however achieved in good purity after chromatographic purification. If this reaction were to be scaled up, the reaction conditions should be optimised so as to improve upon the yield, possibly through discounting the use of triethylamine as a base. The deprotection to produce the free ligand occurs in yield around 22%. This low yield is undoubtedly due to some of the ligand being soluble in the MeOH-ether solution and not fully precipitating out. This method did provide the product in sufficient quantity to take through to the bacterial testing phase.

4.3 UV-Vis Determination of L:Fe^{3+} Stoichiometry

L:Fe^{3+} stoichiometry was determined via a method described in the Experimental section, which is based on a literature procedure for L:M stoichiometry determination.[91]

The modified Job's plot analyses for the triazine-1,2-HOPO chelator **4.2** is displayed in Figure 4.6. The data shows that in the first instance, the L:Fe^{3+} stoichiometry is calculated as being 8.4L:1.6M. This would suggest that the binding of Fe^{3+} by this ligand is inefficient.

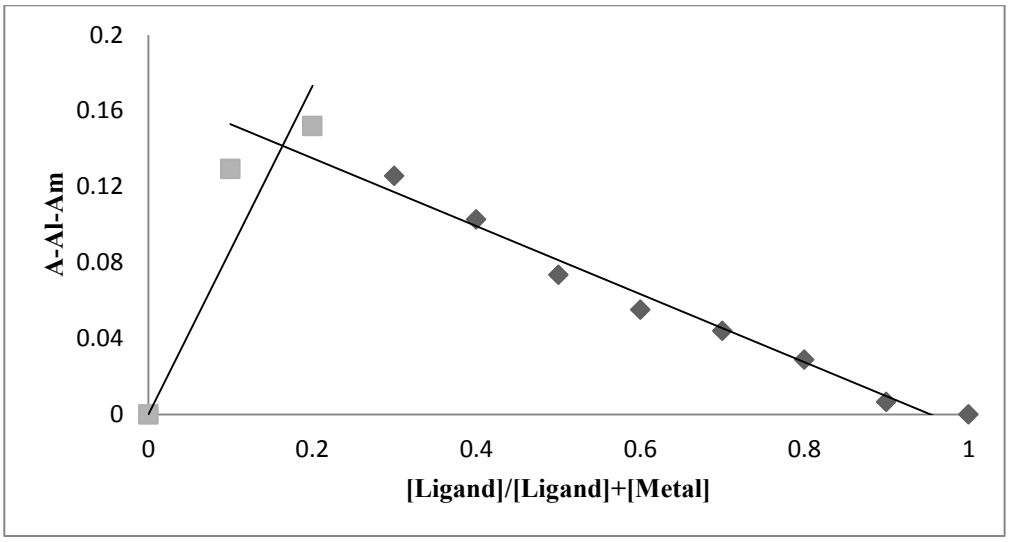

Figure 4.6 Modified Job's plot analysis for triazine-1,2-HOPO ligand **4.2** after 2 days. Measurements taken at room temperature in DMSO/H_2O.

The poor binding of Fe^{3+} by this chelator could be due to the core molecule providing ineffective preorganisation of the binding moieties towards the metal centre. If this is the case a more rigid group than the piperazine functionality could produce a better ligand for this particular binding group on this core. Alternatively, the core scaffold could be too large for the methylene bridges to effectively bind the metal centre. This would provide a large entropic barrier to chelation as the HOPO moieties would have to move a great deal to bind the metal centre and, if they are able to chelate the metal, the affinity would be somewhat reduced.

The modified Job's plot for the same ligand after 14 days of equilibration shows the ratio L:Fe^{3+} to have changed to 1.5L:1M. This stoichiometric ratio is somewhat more favourable to the initial readings as it is closer to the ideal 1:1 L:Fe^{3+}.

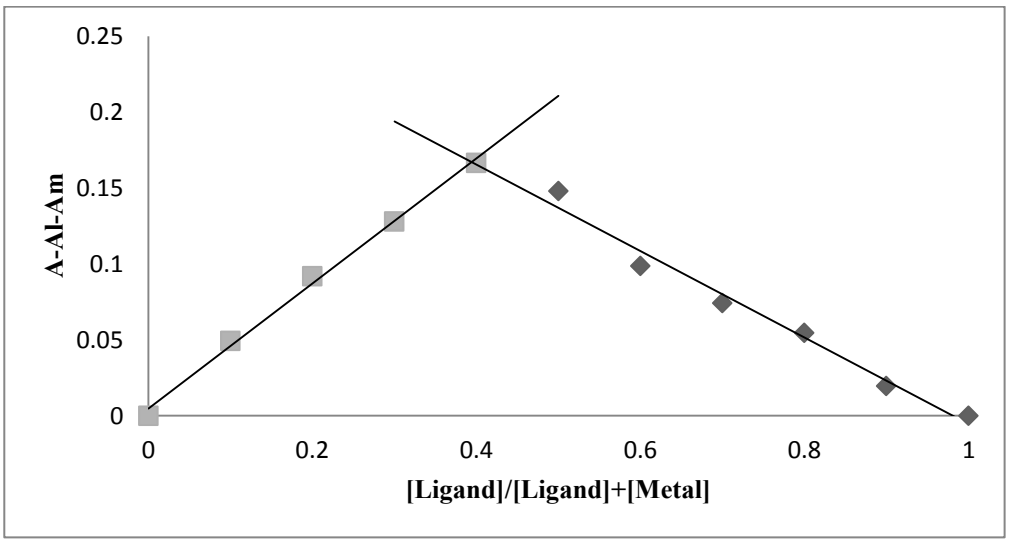

Figure 4.7 Modified Job's plot analysis for triazine-1,2-HOPO ligand **4.2** after 14 days. Measurements taken at room temperature in DMSO/H_2O.

The re-equilibration to this ratio could suggest that kinetically the binding of Fe^{3+} is slow, but overall is not as thermodynamically unflavoured as the original data suggests. It is possible that this ratio could be interpreted as 3L:2M which could give rise to the arrangement displayed in Figure 4.8. In this way, one chelating group is dissociated from a metal centre for each ligand. This sort of arrangement could be due to the protonation of one binding group per ligand, the cause of which could possibly be the lower pKa of the 1,2-HOPO ligand. The proton concentration in solution would be higher for this ligand due to the low pKa of the proton at the N-OH of the 1,2-HOPO; protonation therefore of one binding group per ligand would cause its dissociation and give arrangements such as have been noted for tetradentate chelators.[26]

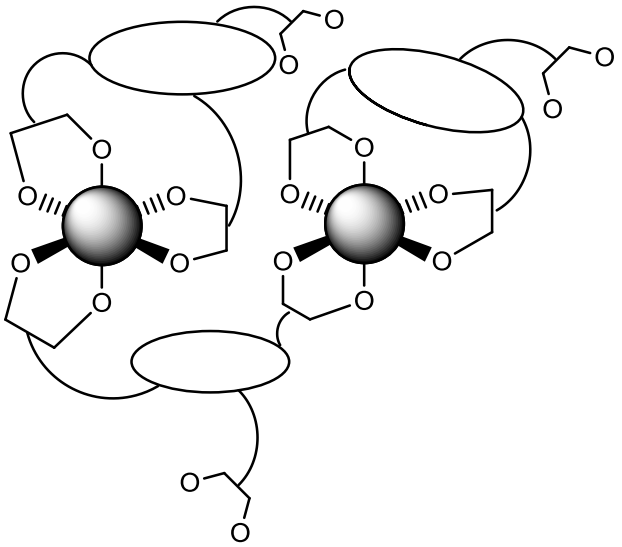

Figure 4.8 Representative diagram to display the possible 3L:2M stoichiometric arrangement of species in solution for ligand **4.2** at 14 days

Alternatively, the 3L:2M stoichiometry could be simply due to the chain linkage attaching the HOPO moieties to the core scaffold being too short, preventing a 1:1 L:Fe^{3+} stoichiometry due to the three binding units being unfavourably arranged to facilitate the saturation of the coordination sphere of Fe^{3+} by one ligand.

The modified Job's analyses for ligand **4.11** show that at the first point of measurement the L:Fe^{3+} stoichiometry could be calculated as 4L:1M, Figure 4.9. When compared to **4.2** this ratio is somewhat the same and undoubtedly the reasons for the inefficient binding of the metal centre are similar. The rate of chelation of the metal centre could be reduced if the core fails to properly organise the ligands toward the binding of Fe^{3+}.

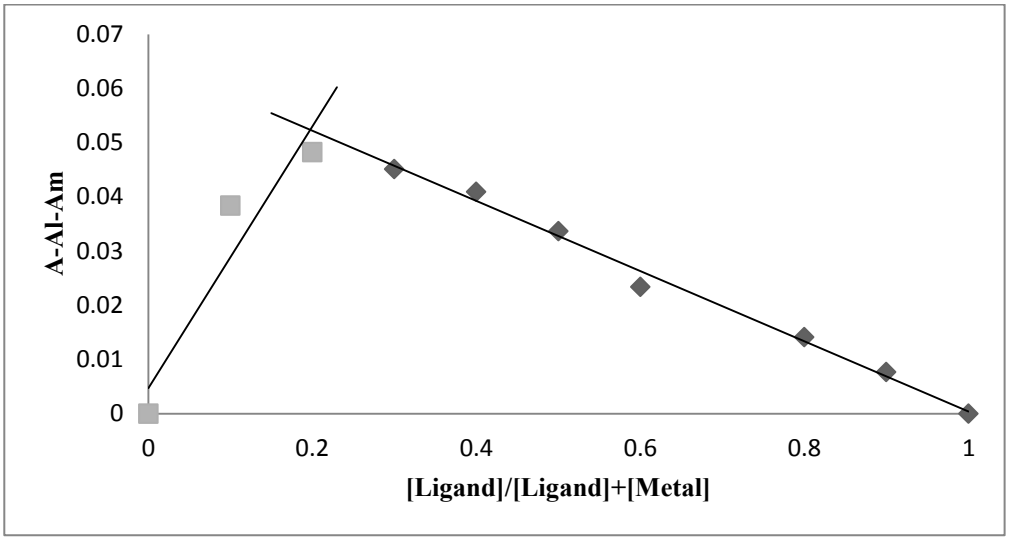

Figure 4.9 Modified Job's plot analysis for triazine-3,2-HOPO ligand (58) after 2 days

However, if we consider the measurements taken at a later time we can see that the L:Fe^{3+} stoichiometry has changed to now be 0.52L:0.48M, Figure 4.10. This result shows that the binding of Fe^{3+} is now almost in the desired 1:1 ratio. The realisation that this ligand, now containing a two carbon chain linker to the core scaffold can equilibrate, given time, to a 1:1 stoichiometry would suggest that the core scaffold is able to organise the binding moieties towards chelation and the chain length of **4.2** was not sufficient to facilitate chelation.

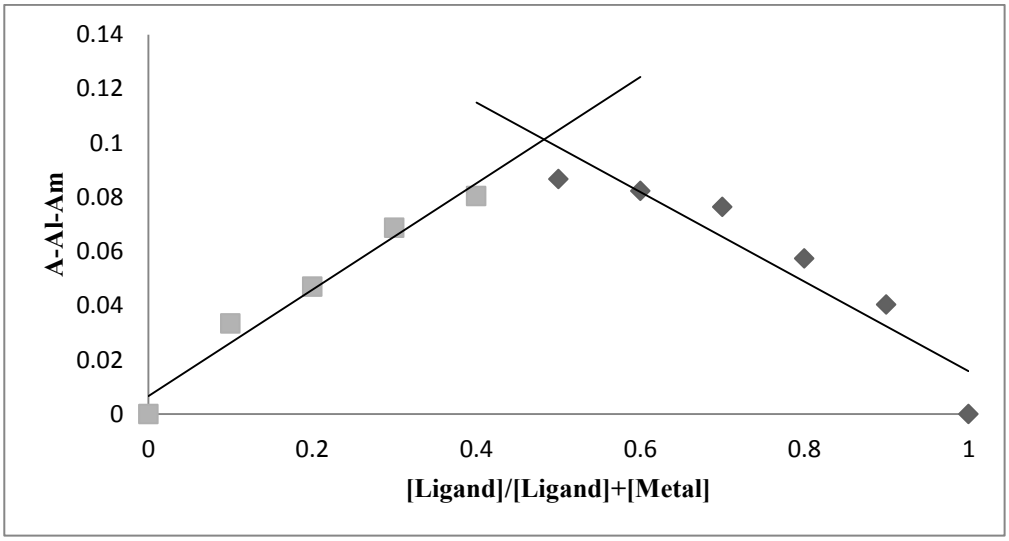

Figure 4.10 Modified Job's plot analysis for triazine-3,2-HOPO ligand (58) after 8 days. Measurements taken at room temperature in DMSO/H_2O.

4.4 Chapter Conclusions

This chapter has presented the successful design and synthesis of two novel hexadentate chelators, based upon the core molecular scaffold tris(piperazin-1-yl)-1,3,5-triazine. The chelators have design features which owe to the strong and selective binding of Fe^{3+} such as the inclusion of the HOPO moieties as the binding mode and the potential preorganisation the scaffold provides.

The analysis of the UV-Vis spectral data revealed some interesting results. The 1,2-HOPO unit attached via a methylene linker appears to either show signs that the linker is too short to allow efficient binding of the metal centre. The data collected for the 3,2-HOPO analogue, which is supported by a two carbon linker, showed more favourable stoichiometric ratios were achievable after several days. This would suggest at least a two carbon linker chain is possibly required to allow binding of an Fe^{3+} centre on the core scaffold. Unfortunately the 1,2-HOPO analogue with a two carbon linker is not currently accessible in a derivative to allow attachment to the core scaffold.

4.5 Future work

The synthesis of the long chained 1,2-HOPO derivative is currently underway but has yet to be derivative in such a way as to allow attachment to the triazine core scaffold. This work would allow a better comparative between the 1,2-HOPO and 3,2-HOPO binding units on the same core and how this effects their respective biological activities and Fe^{3+} binding properties.

Attempted synthesis of the longer 3,2-HOPO derivative for this core scaffold was not pursued due to the previous failures on the CTG scaffold. Once this chemistry has been improved and a viable coupling method/optimised reaction conditions have been discovered for this LC-3,2-HOPO coupling, the synthesis of the triazine derivative would be particularly sought after as it would provide a more flexible attachment of the HOPO to the core. This would allow a comparison, as per the chapter introduction, of the chain length properties with respect to the binding mode and strength, once the thermodynamic properties of the ligands have been determined i.e. pFe^{3+}, $\log\beta$.

The Use of Cholic Acid as a Core Scaffold in the Design and Synthesis of Novel Strong and Selective Fe^{3+} Chelators Bearing HOPO Binding groups.

5 Chapter Aims

This chapter aims to introduce cholic acid as a feasible choice of core molecular scaffold on which to attempt to build powerful Fe^{3+} ligands. Within is presented the methodology behind the attempted functionalization of cholic acid to facilitate Fe^{3+} binding.

5.1 Introduction to Cholic acid

Bile acids have previously been noted as being versatile building blocks for several supramolecular arrays. They are considered important precursors for pharmaceutical industries due to their rigid, curved defined structures, Figure 5.1. In cholic acid, Figure 5.1 the three hydroxyl functionalities have chemically different properties and the molecule is available commercially at low cost. All of these features make them an attractive core scaffold.[105]

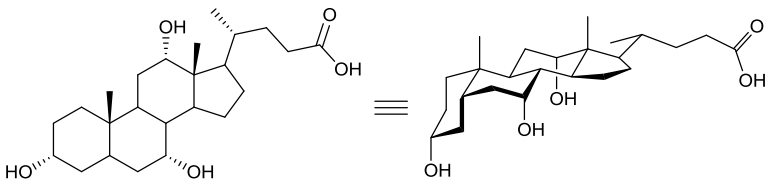

5.1

Figure 5.1 Representative chemical structures for cholic acid 2D (left) and 3D (right)

The 3D stucture of cholic acid lends itself well to being a viable molecular scaffold on which to build strong and selective Fe^{3+} chelators. The hydroxyl functionalities, as can be seen in Figure 5.1, are all presented on the same face of the molecule. It is this feature which could contribute to the preorganisation of pendant binding moieties and allow for the production of strong Fe^{3+} ligands. In addition, the three hydroxyl groups which, if three bidentate units could be attached would allow for the full saturation of the Fe^{3+} coordination sphere.

5.2 Results and Discussion

5.2.1 Preparation of methyl cholate (5.2)

The carboxylate group has been shown to bind Fe^{3+} and so in order to functionalise cholic acid with HOPO moieties and ensure the binding mode of the ligand will be through the HOPO units the methylation of the acid moiety was necessary.

The methylation of cholic acid was performed in MeOH with H_2SO_4 at reflux, Scheme 5.1. The reaction proceeds as described in the literature, the product achievable in good purity after recrystallization in toluene as a white solid in yields 66-88%.

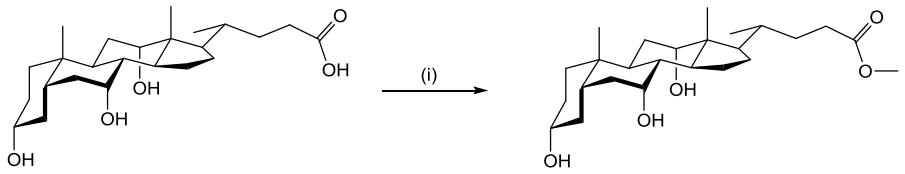

5.1 **5.2**

Scheme 5.1 Synthesis of methyl cholate (**5.2**). Reagents and conditions: (i) MeOH, H_2SO_4, reflux

5.2.2 Functionalising methyl cholate with the HOPO moiety

The 3,2-HOPO-chloride (**2.13**), the synthesis of which was previously discussed (Chapter 2) provided a possible way to allow the attachment of the HOPO units to the core scaffold. The nucleophilic attack of the alkyl halide chain would allow for the functionalization of the core scaffold. The reaction conditions which were employed in the attempted synthesis of the target molecule are displayed in Scheme 5.2.

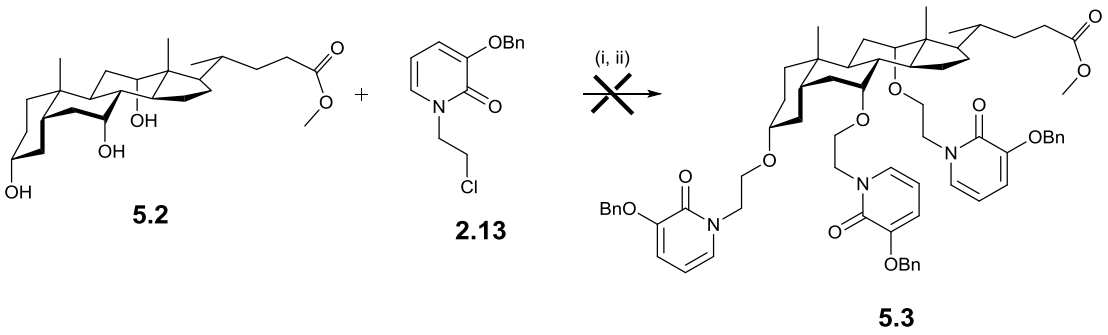

Scheme 5.2 Synthetic conditions attempted for methyl cholate with 3,2-SC-HOPO-chloride. Reagents and conditions: (i) K_2CO_3, acetone (ii) NaH, dry DCM

Unfortunately none of the conditions used here for this reaction were able to successfully generate the desired product. The ^{1}H NMR of the products showed that there had been no functionalization of the core scaffold. In light of the failings to functionalise the scaffold with this moiety the longer chained 3,2-HOPO moiety (**14**) was used in the attempted formation of the protected ligand, Scheme 5.3.

Several different reaction conditions were used here. Conditions (i) of K_2CO_3 in acetone were those previously utilised in the synthesis of the shorter chained analogue. These again, did not produce the desired product.

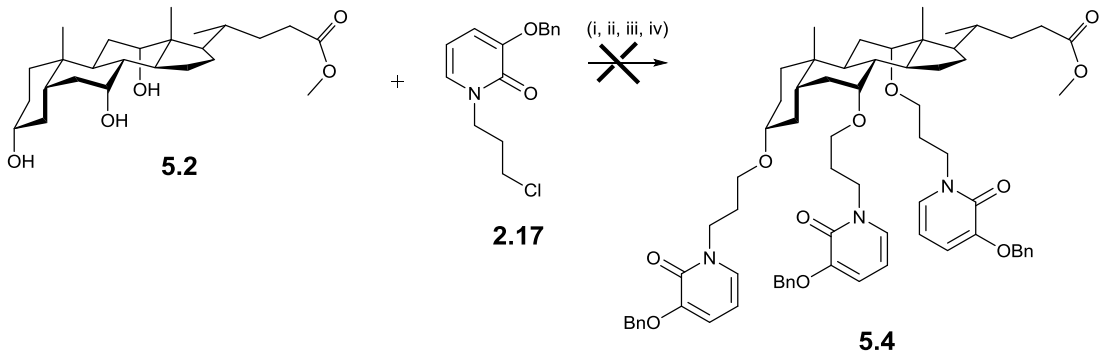

Scheme 5.3 Synthetic conditions attempted for methyl cholate with 3,2-LC-HOPO. Reagents and conditions: (i) K_2CO_3, acetone (ii) NaI, K_2CO_3, acetone (iii) DIPEA, dry DCM (iv) Cs_2CO_3, DMF

Failing this, NaI was added to try and catalyse the reaction; however this was unsuccessful in producing the desired product. DIPEA and Cs_2CO_3 were also tried in dry DCM and DMF however

these conditions were, as previous, unsuccessful. Attempts to functionalise the core scaffold via these methods were therefore abandoned due to the lack of success.

The continued attempted functionisation of methyl cholate was done so by trying to couple 3,2-SC-HOPO-acid **2.11** to the core scaffold via two methods, Scheme 5.4.

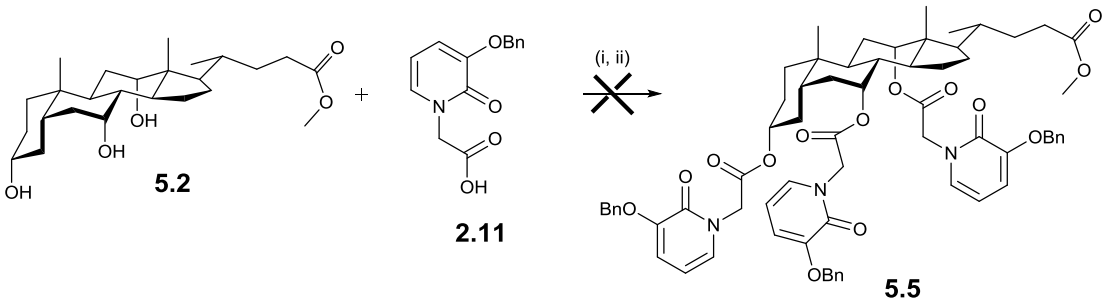

Scheme 5.4 Synthetic conditions attempted for methyl cholate with **2.11**. Reagents and conditions: (i) DCC, DMAP, dry DCM (ii) Ph_3P, DIAD, dry DCM

The coupling reagent combination of DCCI and DMAP was utilised in the attempted coupling of the acid **2.11** to the scaffold. However, this reaction did not proceed as expected and the starting materials were recovered unreacted. As an alternative, a Mitsunobu coupling was attempted using Ph_3P and DIAD. However, this again failed to produce the desired compound and the starting materials were recovered unreacted.

Failing to functionalise methyl cholate via any of the methods discussed, the functionalization of this was attempted with **2.21** of which there had been previous success (Chapter 2). **2.21** has previously been shown to react with hindered alcohols, to produce products with the HOPO moiety attached.[86] In light of this it was thought this could be a viable route to the desired compound, Scheme 5.5

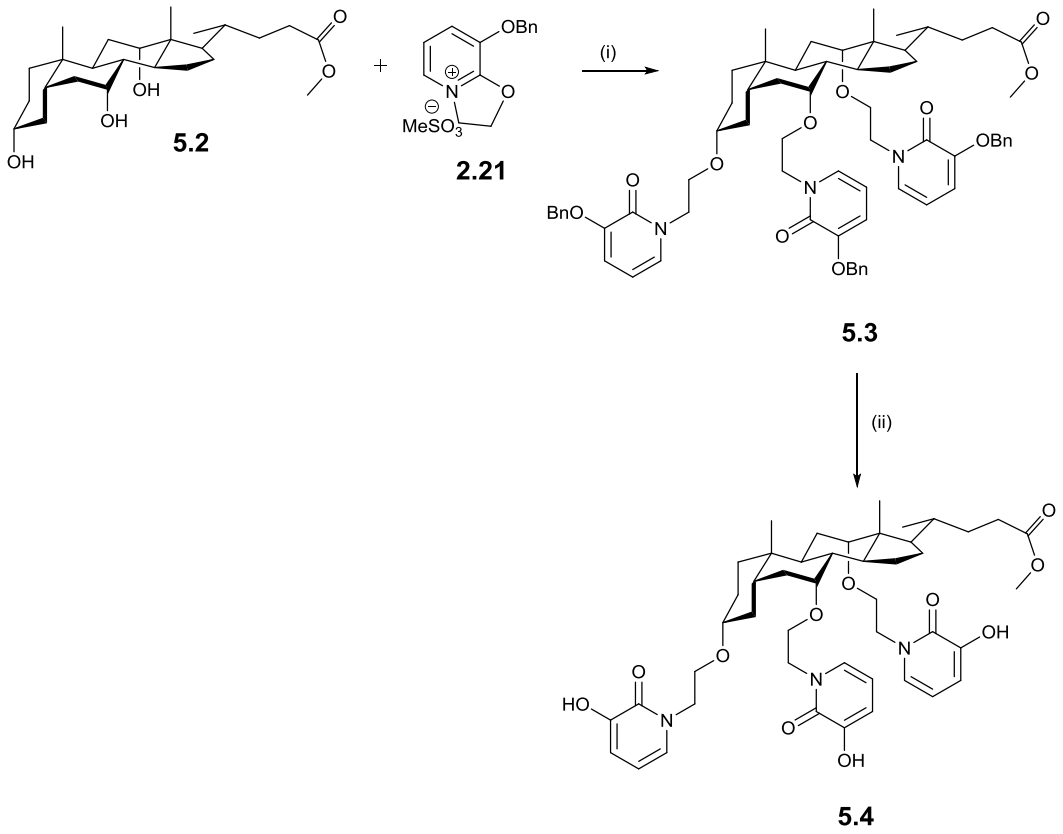

Scheme 5.5 Synthetic conditions attempted for methyl cholate and iminium salt. Reagents and conditions: (i) Toluene, CaH_2, reflux, 48 hours (ii) Pd/C, $H_{2(g)}$

There is literature precedent describing the use of CaH_2 and toluene as the reaction conditions in the formation of functionalised methyl cholate molecules. These conditions were employed here. The core scaffold was dissolved in toluene, to which CaH_2 was added along with the iminium salt under an inert $N_{2(g)}$ atmosphere. The reaction was held for 2 days at reflux after which time the residue was subject to purification via flash column chromatography to give the desire methyl cholate-3,2-HOPO-Bn protected ligand.

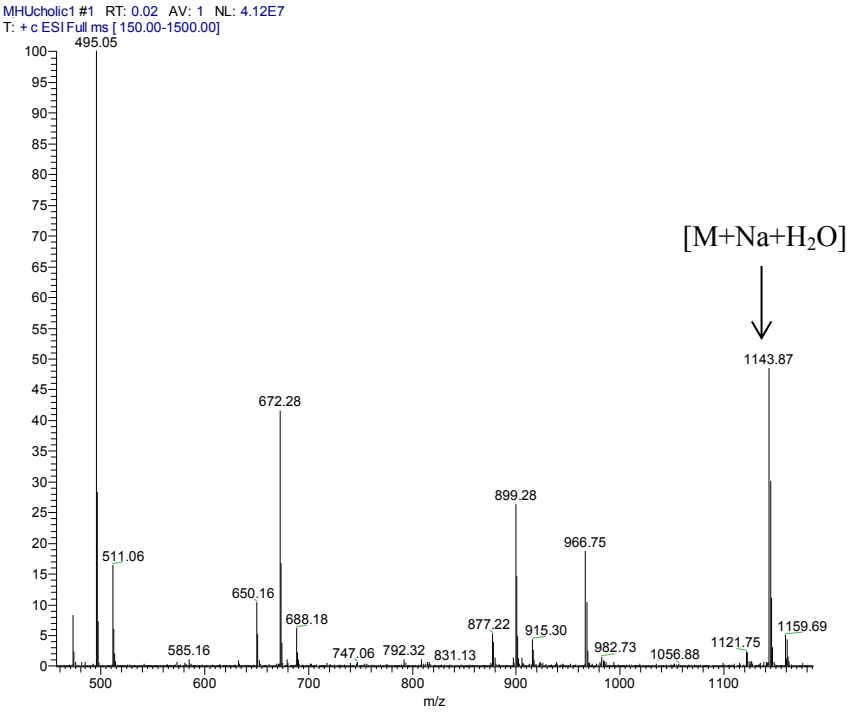

Figure 5.2 (+)-ESI low resolution mass spectrum of the purified methyl cholate-3,2-HOPO (**5.3**) for the reaction depicted in Scheme 5.5.

The mass spectrum of the purified product from Scheme 5.5 showed peaks at m/z values which could be attributed to the di- and mono-functionalised core species by mass spec; m/z = 899.23 [M^++Na] for the di-functionalised molecule and the peak at m/z = 672.22 [M^++Na] for the mono-functionalised. High resolution mass spectrometry has determined the possibility that the peak at m/z = 1143.87 could be attributed to the [M+Na+H_2O] adduct.

The product was hydrogenated using a H-Cube® Continuous-flow Hydrogenation Reactor (ThalesNano) in methanol, using a Pd/C cartridge (full $H_{2(g)}$ mode) to attempt removal of the O-benzyl protection. The low resolution (+)-ESI mass spectrum of the product isolated from the hydrogenation via this method displays in the region 872-878 m/z a peak corresponding to 873.86 m/z. Previously, the high resolution mass spectrum from the compound **5.3** displayed the [M+Na+H_2O] adduct for this compound and in the same way it is believed the compound **5.4** is displaying the same adduct as indicated in Figure 5.3.

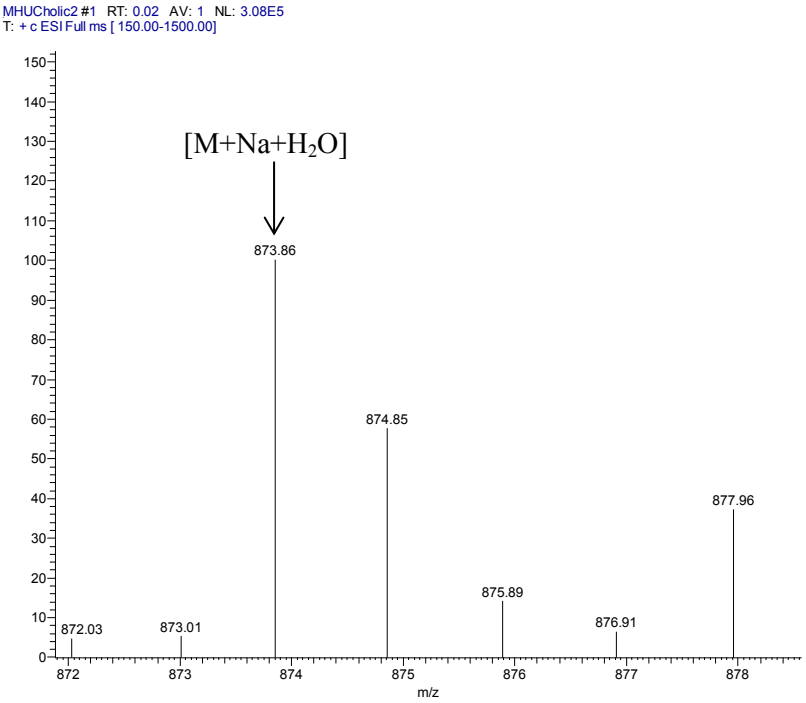

Figure 5.3 (+)-ESI low resolution mass spectrum of the hydrogenated product **5.4**

The Synthesis of Novel and Previously Described TREN-based Fe^{3+} Selective Ligands Bearing hydroxypyridinone Binding Moieties

6 Chapter Aims

This chapter aims to report the synthesis of two novel TREN-based ligands and two TREN based ligands which were synthesised based upon literature procedures for comparison; the molecules CP130 and TRENCAM.

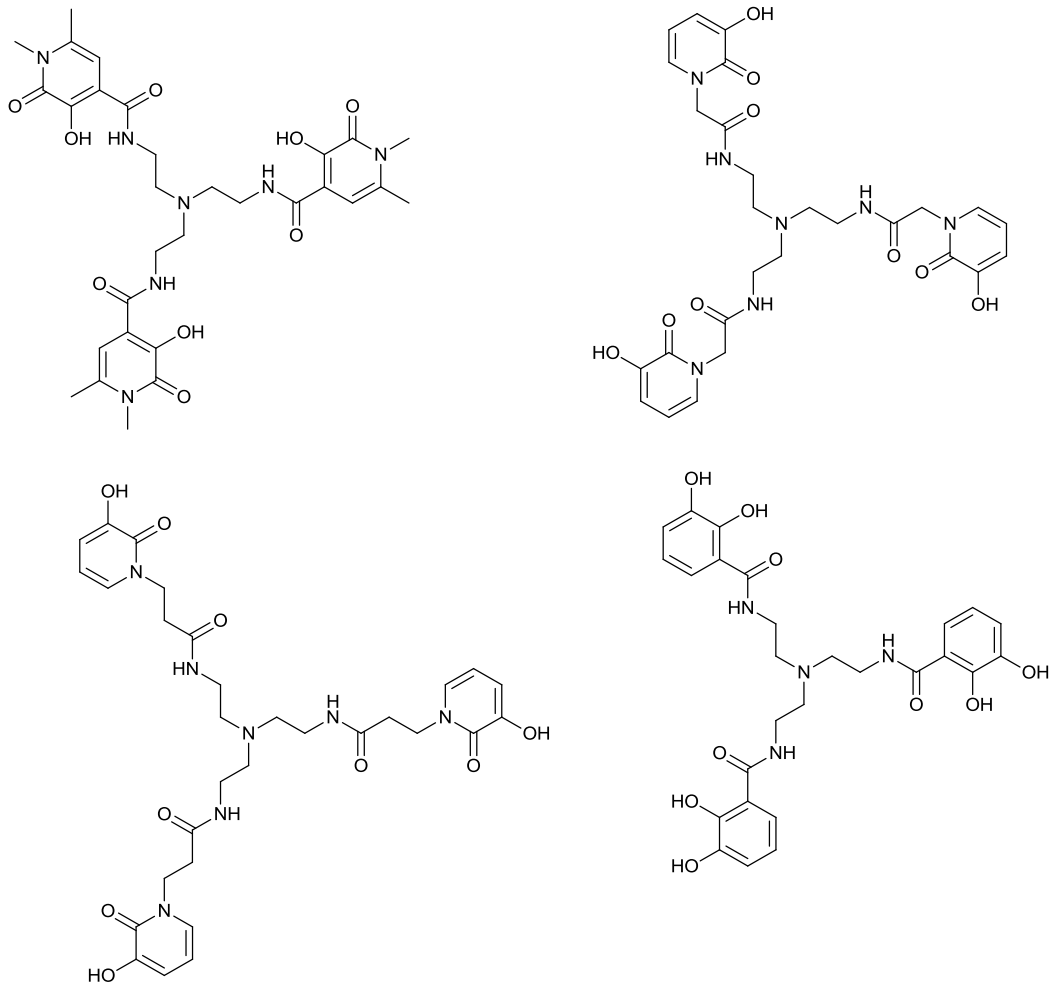

Figure 6.1 Structure of ligands to be reported herein: Novel ligands: TREN-R-3,2-HOPO (top left) and LC-CP130 (bottom left) and literature examples CP130 (top right) TRENCAM (bottom right)

The synthetic methodology will be provided for the bidentate HOPO units which have not been previously discussed. The methods of coupling to the core scaffold will be provided and the subsequent deprotection methods.

6.1 Introduction

The TREN scaffold has been widely used in the design of chelators for various applications as a core tripodal molecule; the core itself has been shown to provide some preorganisation of binding groups towards Fe^{3+} chelation. A network of intramolecular hydrogen bonds stemming from the secondary amide linkages has been shown to increase the stability of ligands based on this core in certain cases, Figure 6.2.[25]

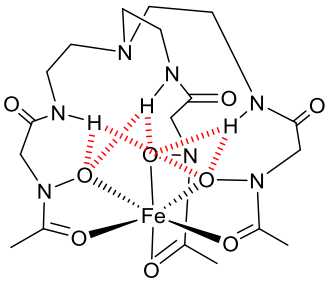

6.1

Figure 6.2 Figure displaying the intramolecular H-bonding which occurs within the TREN core scaffold within TAGE. Replicated from **Inorganic Chemistry,** *2004,* **43**, 26, 8538

This H-bond network has been shown by X-ray crystallography to help to organise the core scaffold towards binding a metal centre.[106] The Fe^{3+} affinities for the compounds displayed in Figure 6.3 are displayed in Table 6.1.

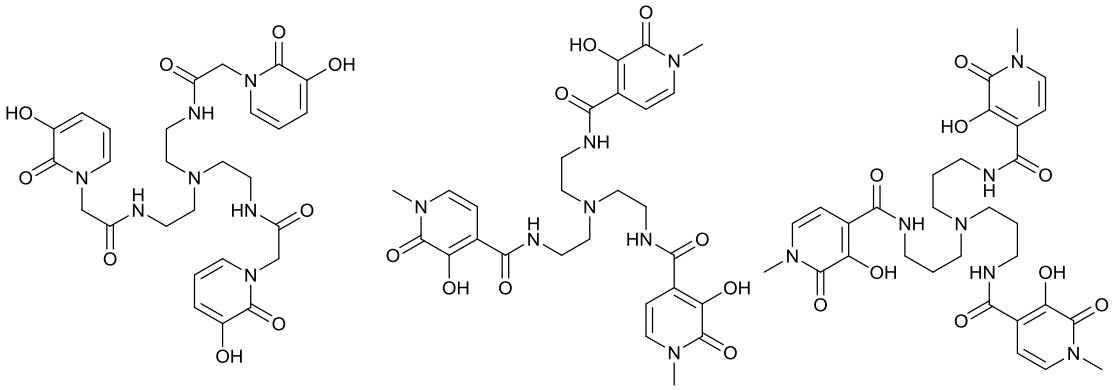

1.6 **6.3** **6.4**

Figure 6.3 Structures of CP130 (**1.6)** TREN-Me-3,2-HOPO (**6.3**) and TRPN-Me-3,2-HOPO (**6.4**)

Table 6.1 Table displaying pFe^{3+} values for CP130, TREN-Me-3,2-HOPO and TRPN-Me-3,2-HOPO

Compound	pFe^{3+}
TRENCAM	27.8
CP130	27.6
TREN-Me-3,2-HOPO	26.8
TRPN-Me-3,2-HOPO	23.8

When looking at the H-bonding in the molecules in Figure 6.3 it can be noted that from the crystal data CP130 does not have the arrangement to produce H-bonds, as this arrangement would form a thermodynamically disfavoured 7 membered ring. This can be seen in Figure 6.4 which is reproduced from Xu *et al*.[106]

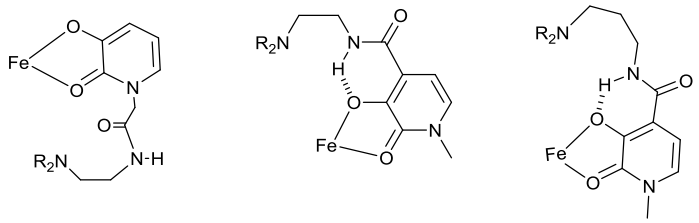

Figure 6.4 Representative diagrams to show H-bonding in CP130, TREN-Me,3,2-HOPO and TRPN-Me-3,2-HOPO.

The pFe^{3+} for CP130 is higher than that of the other two ligands, which would indicate a H-bonding network is not necessary for the strong and selective binding of Fe^{3+} by TREN based ligands. However, when we compare molecules TREN-Me-3,2-HOPO and the closely related TRPN-Me-3,2-HOPO molecule we can see a decrease in the pFe^{3+} when the core scaffold chain length is increased. The extra methylene link introduces some strain to the complex and lowers the thermodynamic stability.

The corresponding catecholate molecule TRENCAM which closely resembles the structure of TREN-Me-3,2-HOPO has been shown under different pH conditions to switch the organisation of its binding groups, Figure 6.5.[107] Under more acidic conditions the two phenolic protons are

present and this facilitates the groups to point outwards and conversely point inwards when one of the catechol groups is deprotonated.

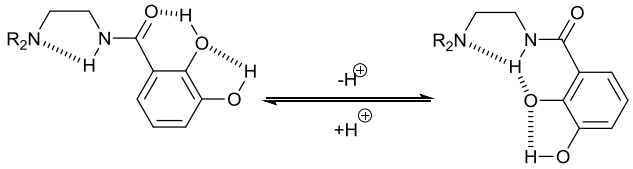

Figure 6.5 Hydrogen bonding scheme for TRENCAM under different protonation conditions.

TRENCAM has a pFe^{3+} value which is higher than any of the other analogues discussed (Table 6.1). This could be due to the extra stability gained from the secondary amide proton being linked with three basic positions on the right of the equilibrium, Figure 6.5, which has the effect of preorganising the ligand towards metal chelation.

The molecules TRENCAM and CP130 will serve as useful comparisons for novel chelators which are based upon more sophisticated scaffolds (Chapters 2-5). In addition to these two new TREN based ligands will be synthesised to see if modification will have an effect on their ability to induce growth inhibition.

The longer chained CP130 (LC-CP130) is a novel compound and will be synthesised to allow access to a derivative where the core scaffold size (TREN) remains the same but the linking chain differs by an increase of one methylene per arm. CP130 is a strong Fe^{3+} ligand however; some residual strain in the molecule must still exist as other TREN derivatives have shown higher pFe^{3+} values, such as TRENCAM. The increase in the length of the linkage arm to the binding unit may serve to alleviate some strain and allow for a stronger chelator.

In addition, the TREN-Me-3,2-HOPO derivative TREN-R-3,2-HOPO will be synthesised to try and increase the binding affinity of the original ligand with the inductive effect of the Me- group in the *para*-position relative to the hydroxyl functionality. In this position the Me group should induct electron density towards the hydroxyl functionality, potentially increasing the electron donating character of the site and as a result increasing the basicity creating a stronger ligand. The methyl group may also serve to make the ligand less likely to be recognised or to induce kinetic stability.

6.2 Results and Discussion

6.3 Ligand Synthesis

6.3.1 Preparation of CP130

The preparation of the literature molecule CP130 was performed as per the literature precedent, Scheme 6.1. **2.11**was firstly subjected to activation by NHS in DMF using DCCI to form the succinate ester. The reaction proceeds to give the pure product after recrytallisation from ethyl acetate in 43% yield (lit. 82%).[21]

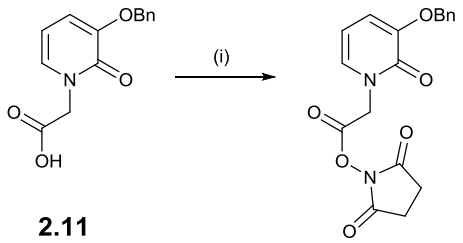

2.11 **6.6**

Scheme 6.1 Synthetic route to compound (**6.6**). Reagents and conditions: (i) NHS, DCCI, DMF, room temperature, 4 days.

Following the successful formation of the activated ester **6.6**, the reaction of the TREN core with this product allows for the formation of the protected CP130 ligand **6.7**, Scheme 6.2. The reaction proceeds via the addition of the triamine scaffold in DMF to a solution containing the activated compound. After 24 hours the reaction provides the pure benzyl-protected ligand in 49% yield after work up and recrystallisation from EtOH and H_2O. The literature procedure does not include the isolation of this compound. However, the ^1H NMR clearly displays the expected peaks for amide protons in the correct integral ratio for the triamide to have been produced.

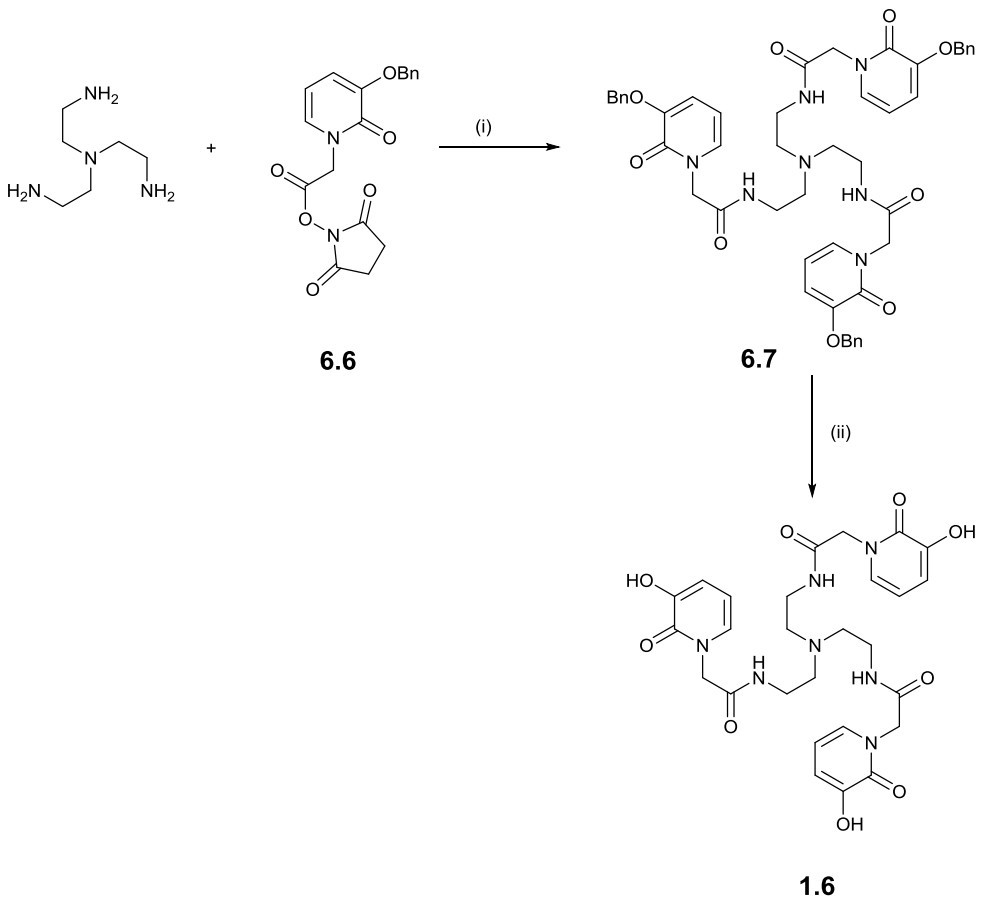

Scheme 6.2 Synthetic route to CP130 (**1.6**). Reagents and conditions: (i) DMF, room temperature, 24 hours. (ii) H_2, Pd/C in EtOH:H_2O (10:1), 24 hours room temperature.

The deprotection of **6.7** proceeds as per the literature, Scheme 6.2, catalytic hydrogenation of **6.7** affords the pure CP130 as a purple solid after recrystallisation from EtOH in 25% yield (lit. 72%).

6.3.2 Preparation of LC-CP130 (6.9)

The preparation of LC-CP130 (**6.9**) follows the methodology described for the molecules based upon the 1,3,5-trisaminomethyl-2,4,6-triethylbezene scaffold (Chapter 3). Interestingly, after a thorough review of the literature it can be noted that the LC-HOPO-acid (**2.15**) has not previously been incorporated into a scaffold via an amide linkage, except reported herein (**6.8**).

The synthesis of this molecule was firstly attempted via the same methodology to produce the shorter chained CP130. The activation of the free acid (**2.15**) was successful forming the succinate activated molecule in with N-hydroxysuccinimide and DCCI, however the pure product could not be accessed in high yield and amounts were insufficient to allow the coupling reaction to follow to produce sufficient ligand for testing. To try and combat this yield issue, the N-hydroxyphthalimide activating group was tried however this failed to produce the desired activated ester.

Following the failures to synthesise the ligand via the activated ester, the synthetic methodology used for other amide formations reported previously (Chapter 3) was used. Utilising the same experimental procedure, **2.15** is coupled with the TREN core via use of the TBTU coupling reagent, Scheme 6.3. This provided the novel protected LC-CP130 (**6.8)** in 23% yield after workup. The lack of an activation step here provides a shorter route for the successful synthesis of the amide linked ligands; though the yields are not fully optimised the shorter synthetic preparation is favoured.

The deprotection of the benzyl-protected LC-CP130 was attempted with concentrated acids as had been previously successful (Chapter 3) however; this failed to yield the desired product. In light of this, the deprotection was performed as for CP130 and the catalytic hydrogenation afforded the free ligand **6.9** in 68% yield, requiring no purification.

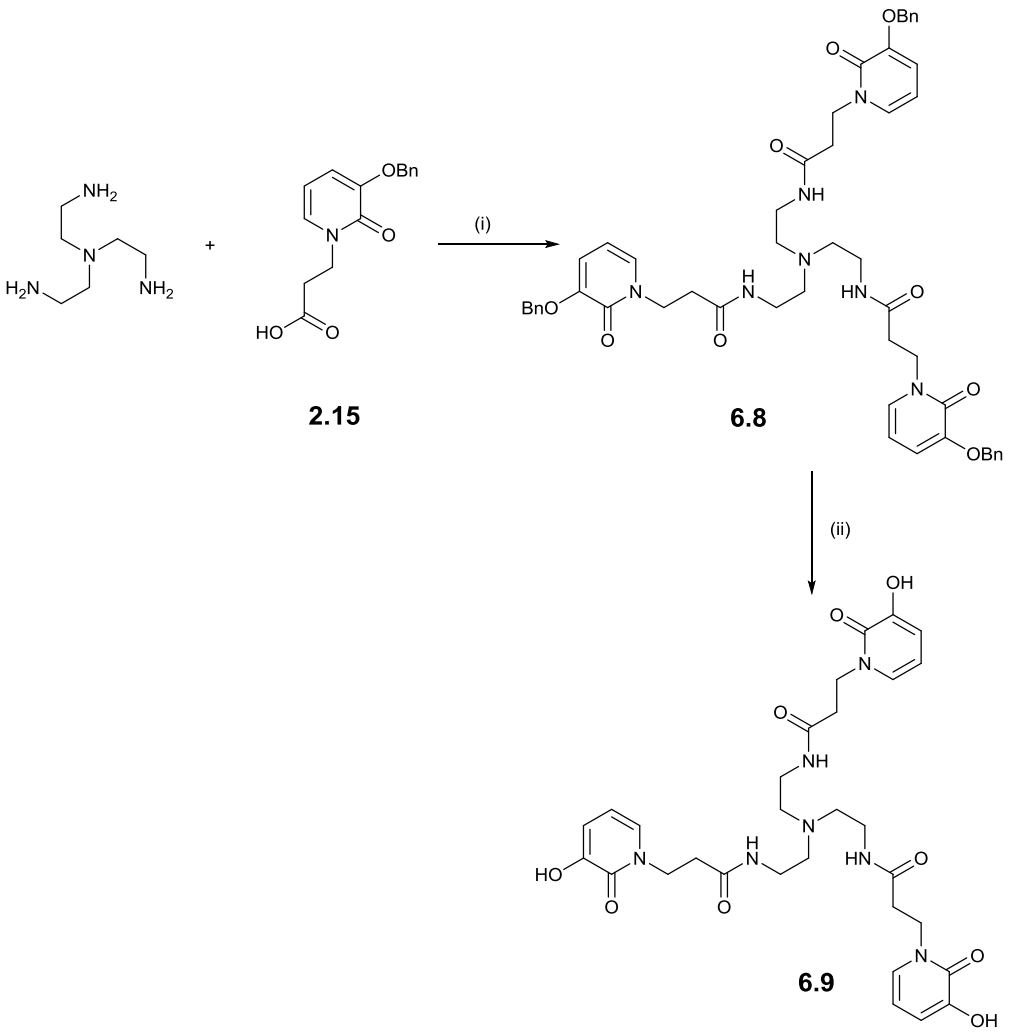

Scheme 6.3 Synthetic route for molecule **6.9**. Reagents and conditions (i) TBTU, N-Me-morpholine, dry DMF, 60°C (ii) H_2, Pd/C in EtOH:H_2O (10:1), 8 hours at room temperature**.**

The novel LC-CP130 ligand may serve to be a valued intermediary molecule between the TRPN-based ligand which contains a larger core scaffold and CP130 which carries some inherent strain. The LC-CP130 molecule has the same capping ligand size as the CP130 ligand, which has been determined to be almost perfect for binding Fe^{3+}, but would allow an increased flexibility in the chain connecting to the HOPO group, which may serve to alleviate any strain and increase the binding affinity for Fe^{3+}.

6.3.3 Preparation of TREN-R-3,2-HOPO (64)

The preparation of the novel TREN-R-3,2-HOPO ligand which has a further methyl group attached in the 6-position of the HOPO ring system begins with the preparation of compound **6.10** from the previously reported compound (**35**) (Chapter 3). The activation of this molecule to the succinate ester is performed in dry DCM with EDCI as the coupling reagent, yielding the pure compound **6.10** as yellow-orange solid in 88% yield (lit. 98%).

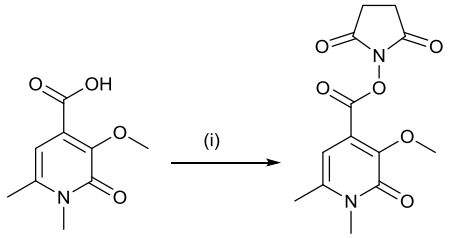

3.14 **6.10**

Scheme 6.4 Synthetic route for molecule (**6.10**). Reagents and conditions: (i) NHS, EDCI, dry DCM, room temperature for 3 days.

The subsequent triamide formation to yield novel intermediate **6.11** occurs simply with addition of the TREN core scaffold to the activated ester in dry DCM. The amide formed can be accessed as the pure compound after evaporation of the solvent and solidifies on standing. The compound is accessed as an orange solid in 92% yield.

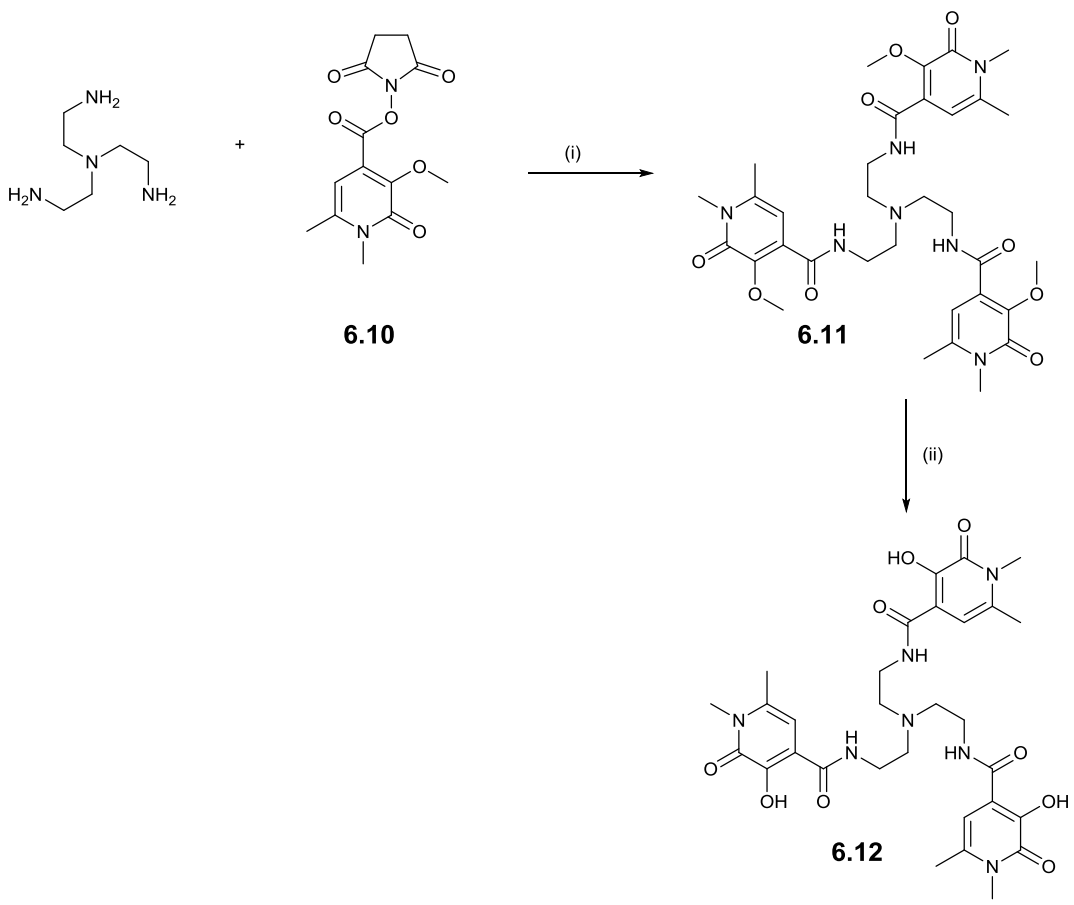

Scheme 6.5 Synthetic route for molecule **6.12**. Reagents and conditions: (i) dry DCM, room temperature, 2 days. (ii) dry DCM, BCl_3 (1M in heptane), $N_{2(g)}$ atmosphere, room temperature 2 days.

The deprotection of **6.11** occurs via demethylation with BCl_3 (1M in heptane) over two days. The pure deprotected ligand **6.12** can be accessed in 23% yield via precipitation from MeOH.

The previous molecules containing the retro-3,2-HOPO moiety as the binding group did not have in place the secondary methylated position as has been produced here **6.12**. This extra methyl, in the *para*-position with repect to the hydroxyl functionality may serve to induct electron density to this position and increase the binding affinity of the ligand with respect to TREN-Me-3,2-HOPO ($pFe^{3+} = 23.8$).

6.3.4 Preparation of TRENCAM

Literature preparation of TRENCAM occurs via the following synthetic methodology. Firstly, the 2,3-dimethoxybenzoic acid is activated to produce the acyl chloride with $SOCl_2$. The activated compound allows the formation of the triamide when reacted with the TREN core scaffold, Scheme 6.6 and Scheme 6.7.

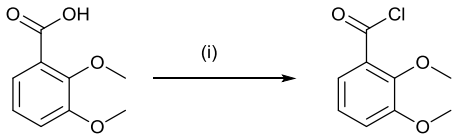

6.13 **6.14**

Scheme 6.6 Literature synthetic methodology for 2,3-dimethoxybenzoyl chloride. Reagents and conditions: (i) $SOCl_2$, benzene, reflux.

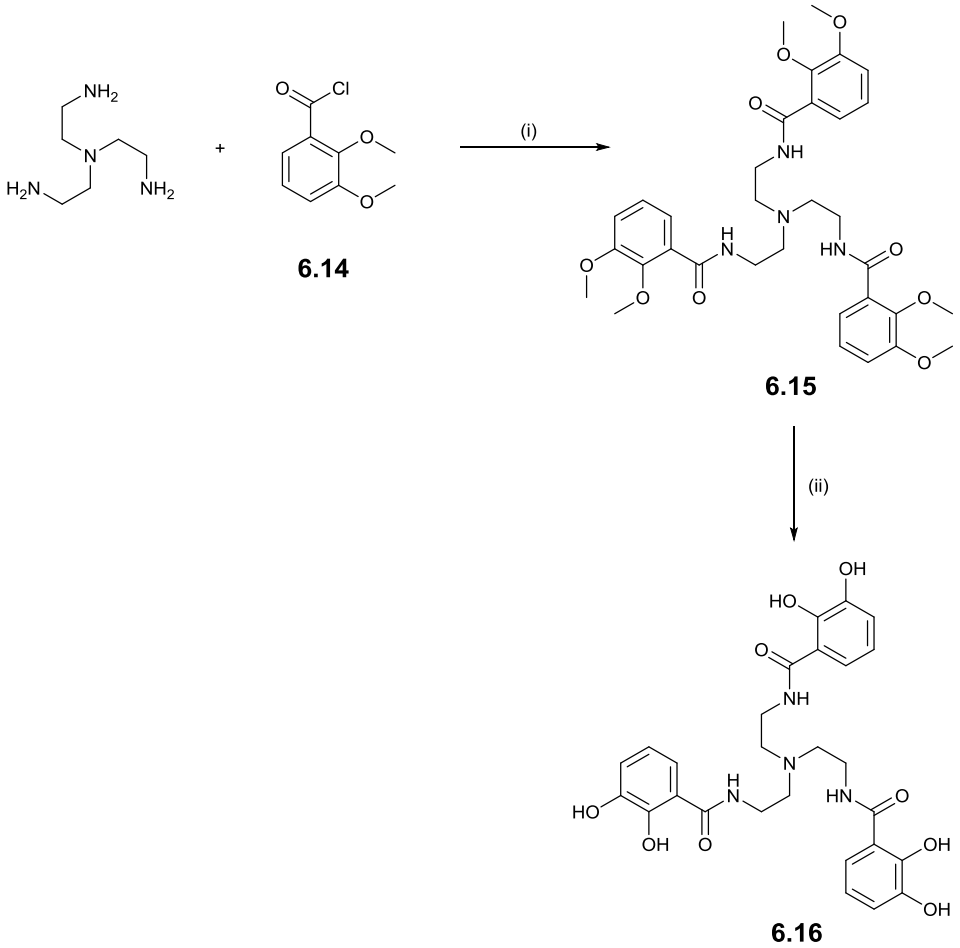

6.14 **6.15** **6.16**

Scheme 6.7 Literature synthetic methodology for TRENCAM. Reagents and conditions: (i) DCM, NaOH (0.5M), simultaneous drop-wise addition. **(ii)** (i) BBr_3, DCM, overnight, $N_{2(g)}$ atmosphere

The deprotection of the methoxy groups occurs via reaction of the protected compound with BBr_3 to produce the TRENCAM ligand.

In an attempt to exploit the chemistry previously explored herein (Chapter 2) and shorten the synthetic route to TRENCAM an alternative synthetic methodology was sought. The free acid **3.32** whose synthesis was previously reported (Chapter 3) is subject to direct coupling with the TREN core, activated *in situ* with the TBTU reagent as has been previously discussed, Scheme 6.8. This methodology provides a shortened sequence to the previous synthetic route, avoiding the need for isolation of the protected acyl chloride intermediate. The coupling takes place with a yield of 41% after purification.

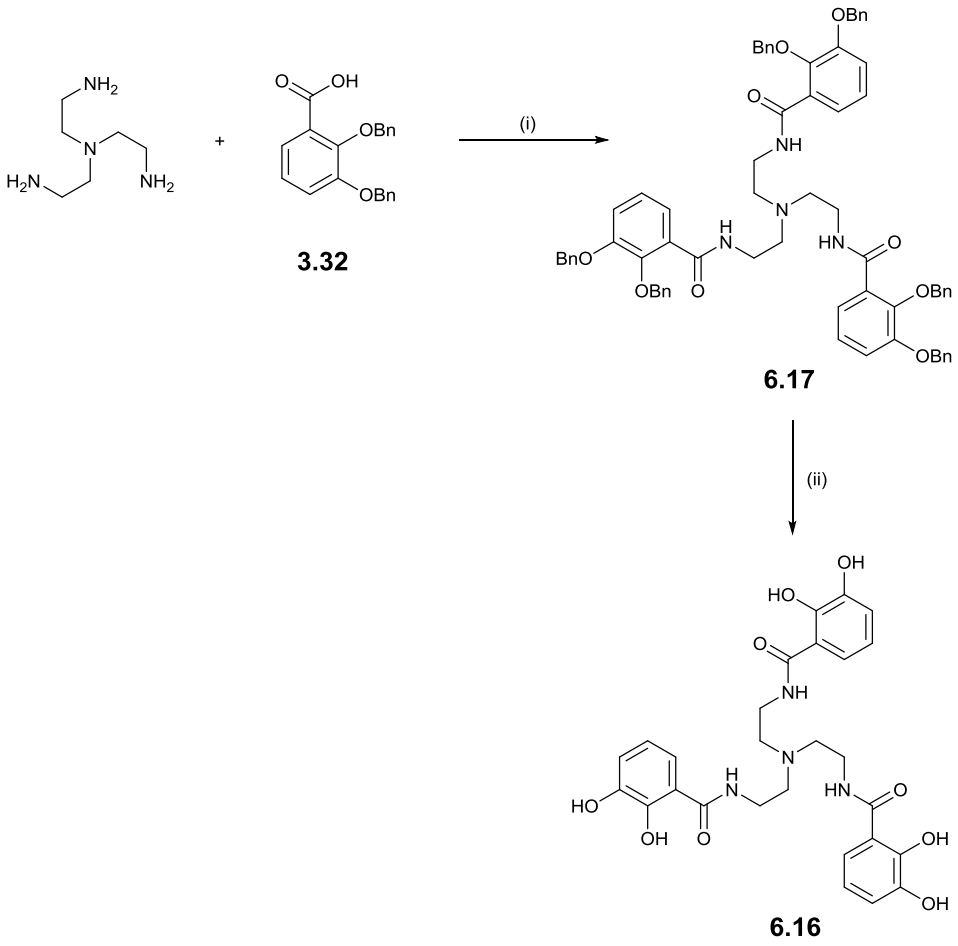

Scheme 6.8 Synthetic route for molecule **6.16**. Reagents and conditions (i) TBTU, N-Me-morpholine, dry DMF, 60°C (ii) 37%HCl:glacial acetic acid 1:1, 60°C 5-7 days

The final deprotection step to produce the free TRENCAM ligand **6.16**, Scheme 6.9 occurs via reaction with concentrated acids. The free ligand can be isolated by precipitation from MeOH with diethyl ether in yield of 77%, requiring no purification.

6.4 Conclusions

This chapter has reported the synthesis of two novel TREN-based ligands which display modification to the electronic structure (TREN-R-3,2-HOPO) and the chain length (LC-3,2-HOPO) of two previously accessed HOPO ligands TREN-Me-3,2-HOPO and CP130.

The synthesis of the literature ligands CP130 and TRENCAM are reported with modification to the synthetic methodology for TRENCAM with respect to the literature procedure. The synthesis of TRENCAM has been shortened compared to the literature which reports requiring activation of the protected 2,3-dihydroxybenzoic acid moiety, which the reported procedure here avoids.

All of the ligands presented herein can be obtained in high purity following minimal purification.

The Determination and Analysis of the Effect of Novel Fe^{3+} Chelators Bearing hydroxypyridinone Moieties on the Growth of Clinically Relevant Microbes

7 Chapter Aims

This chapter aims to present the microbes used in this study and highlight their significance as being of clinical relevance. In addition, the results of MIC assays conducted for the ligands which have been previously presented in Chapters 2-6 will be reported. An analysis of the MIC values will describe any important features which contribute towards inhibition of the organisms used.

The study of the growth profiles of the organisms presented herein will be included in the form of kinetic studies, with respect to the optical density change over time. This will help to provide an insight into the action of inhibition and to the distortion of the growth of microbes with and without the novel iron chelators and the previously accessed ligands from the literature.

7.1 Introduction

7.1.1 Microorganisms

In order to effectively assess the efficacy of the novel ligands presented herein to induce a distortion to the normal growth patterns of microorganisms; a panel of organisms which display differences in their cell structure and iron acquisition and regulatory systems were chosen. In addition, these organisms displayed in Table 7.1 are all implicated in infections that are associated with hospital environments i.e. nosocomial, and so will provide an insight into the likelihood of these compounds being competent at reducing the ability of these pathogens to proliferate and spread disease.

Table 7.1 Characteristics of the panel of microbes used in this study, some information on their cell structure and additional information regarding their clinical relevance.[108-114]

Microorganism Panel	Information	Additional Info
***Escherichia coli* 18039**	Gram-negative, rod shaped.	Found in lower intestine of warm mammalian hosts. Causative agent in food poisoning though most strains harmless.
***Klebsiella pneumoniae* 30104**	Gram-negative, encapsulated, rod shaped,	Able to infect tissues when the skin or mucosal barriers have been breached. Klebsiellae have become important pathogens in nosocomial infections for impaired respiratory host defenses. Klebsiella pneumonia is a form of bacterial pneumonia.
***Pseudomonas aeroginosa* 19880**	Gram-negative, aerobic.	Opportunistic human pathogen. Colonises most man-made and natural environments. An opportunistic, nosocomial pathogen of immunocompromised individuals, *P. aeruginosa* typically infects the pulmonary tract, urinary tract, burns, wounds, and also causes other blood infections. Low antibiotic susceptibility.
***Acinetobacter Baumannii* 30007**	Gram-negative, almost round rod shape.	Opportunistic human pathogen to immunocompromised. Common association as a nosocomial infection causative agent.
***Staphylococcus aureus* 1104**	Gram-positive	Able to infect tissues when the skin or mucosal barriers have been breached, prevalent in atopic dermatitis patients.
***Bacillus subtilis* 23778**	Gram-positive, spore former	Causes disease in severely immunocompromised patients. Otherwise non-infectious.
***Candida albicans* 1386**	Diploid fungus that grows both as yeast and filamentous cells	Causal agent of opportunistic oral and genital infections

As discussed in Chapter 1, there are known structural biological differences between Gram-positive and Gram-negative bacterial cells which impact upon their iron uptake mechanisms.[57] The Gram-positive organisms have cytoplasmic membrane-anchored high affinity receptors which allow transport of ferri-siderophore complexes via an ATP binding cassette. Conversely, the Gram-negative cells possess an outer membrane and it is here that the high affinity ferri-siderophore receptors are located. On binding, ferrisiderophore complexes are translocated to the periplasm where they then interact with lower affinity and more generic siderophore binding proteins that interact with an ATP binding cassette to initiate transport of the complex to the cytoplasm. These differences are such that it is thought that the novel compounds presented in Chapters 2-6 will interact differently depending on the membrane structure. In addition, the siderophores produced by different bacteria will be of particular importance when looking at the binding of extracellular iron.

As previously discussed *E. coli* produces enterobactin, the most powerful natural siderophore yet discovered, therefore to see how this organism interacts with these novel compounds will be of particular interest. *E. coli* is a diverse species that is a normal inhabitant of the healthy human gut. However, various strains have been implicated as the primary causative agent in outbreaks of food poisoning. Other strains are diarrhoeagenic causing many thousands of deaths per year worldwide.[113] In terms of nosocomial infections, *E. coli* is responsible for uncomplicated urinary tract infections in patients which cause severe discomfort and are often the result of interaction of the body with medical implements, such as catheters.[115]

B. subtilis produces the siderophore bacillibactin which itself is a very powerful sideophore (Logβ = 48), and is thought of as the Gram-positive analogue of enterobactin due to their structural similarities. Coupled with data from *E. coli* these two organisms will provide a good insight as to how the novel chelators perform in relation to powerful natural siderophores, assuming any inhibition mode is due to iron restriction and not due to the differences in the membrane architecture. *B. subtilis* is generally considered to be non-pathogenic and infections are very rare, however there have been cases where infections have taken hold in severely immunocompromised patients such as those with leukaemia.[111]

K. pneumoniae, a Gram-negative rod-shaped organism is an important pathogen when considering nosocomial infection; *K. pneumonia* infections are the primary cause of many deaths every year especially to the immunocomprised.[110] In terms of the siderophores associated with this organism, it has been shown that under iron limitation *K. pneumoniae* is able to produce enterobactin.[116] This was determined by the comparison of R_f values associated with the known phenolate compounds produced by enterobactin in 1979. Chromatographic identification of enterobactin, linear-enterobactin, (2,3-dihydroxybenzyoylserine)$_2$, 2,3-dihydroxybenzyoylserine and 2,3-dihydroxybenzoic acid was confirmed. These products are the resulting fragments from the hydrolysis of enterobactin and thus confirm its presence. The quantities of each isolate produced by *K. pneumoniae* were approximately equivalent to that of *E. coli* K12 under similar conditions, which could indicate the siderophore enterobactin is utilised in the same manner for both of these organisms.

As shown in Table 7.1 *P. aeruginosa* is a Gram-negative opportunistic human pathogen,[117] for which the primary siderophores associated with this organism are those of the pyoverdines (pFe^{3+} = ~27) and pyochelin (pFe^{3+} = 16).[117-119] Of the pyoverdines (PVDs) there are three group types shown in Figure 7.1 which were found from several different strains of the bacteria in a large study.[118]

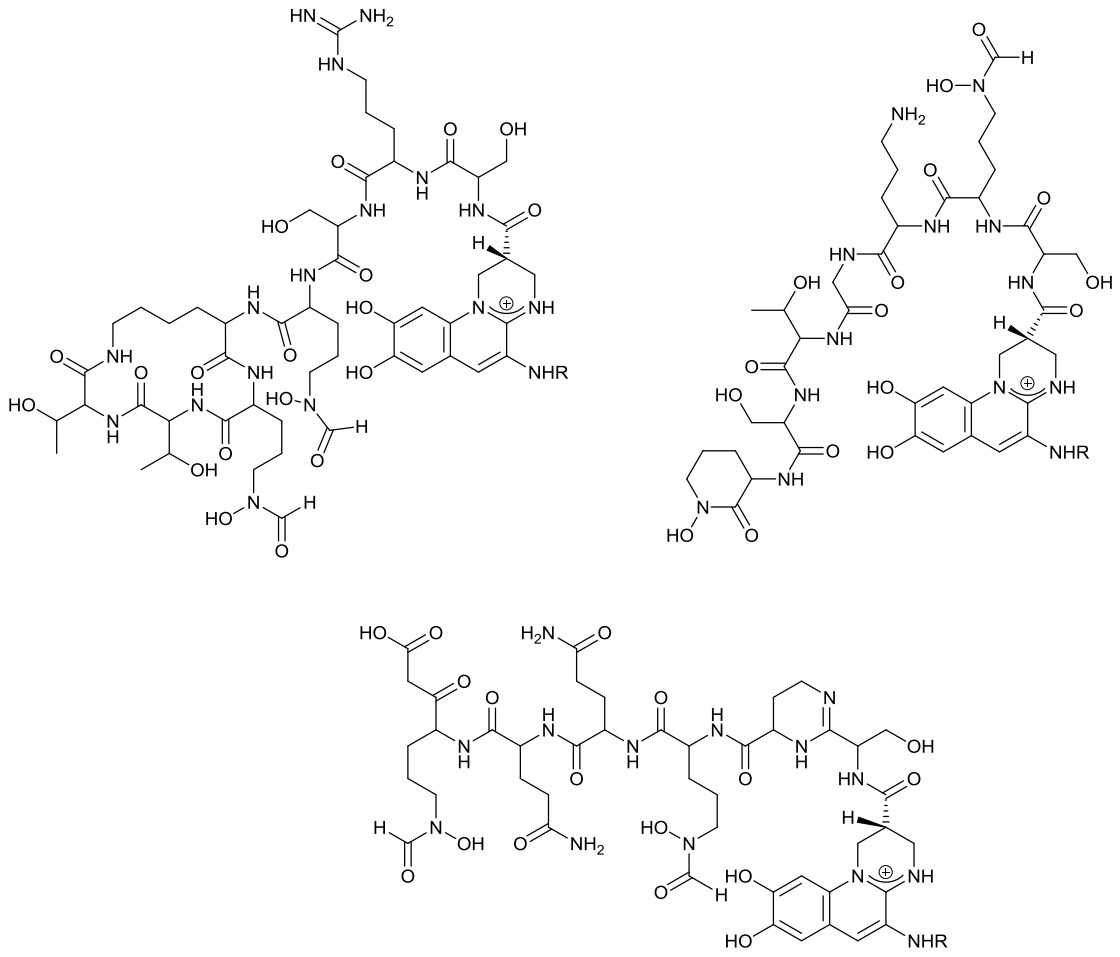

Figure 7.1 Structures of the three group types for PVDs; siderophores secreted by *P. aeruginosa*. Structures reproduced from; **Microbiology**, *1997*, **143**, 35-43

The specificity for Fe^{3+} by PVDs would suggest that this is the primary siderophore used for iron sequestration. Conversely, the pyochelin molecule, Figure 7.2 , has a pFe^{3+} = 16 which is a significantly lower affinity for Fe^{3+}. However, other pseudomonad species, such as *P. cepacia* have been shown to produce pyochelin, which acts alongside cepabactin (a 1,2-HOPO based siderophore, Chapter 1) to form a ternary complex to bind Fe^{3+}.[66]

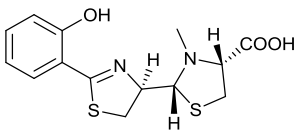

Figure 7.2 Structure of pyochelin; a siderophore secreted by *P. aeruginosa*.

It has been suggested that within the crystal structure of FptA (the ferri-pyochelin receptor) that the ternary complex is involved in iron release to the cell. However, it is yet unreported as to whether *P. aeruginosa* is capable of producing cepabactin and hence utilising the complex in its iron uptake and regulatory systems.

S. aureus infections have become a major concern. In 2008 the volume of infections associated with the bacterium in hospitals led to this organism being the most isolated human bacterial pathogen that year.[120] The organism itself is a Gram-positive bacterium whose iron regulatory systems are quite well established. [115] *S. aureus* has an added disadvantage with respect to human infections; certain pathogenic strains are showing antibiotic resistance to the point of being of global concern. MRSA (methicillin resistant *Staphylococcus aureus*) is resistant to all β-lactam based antibiotics.[120] The spread pattern for an MRSA infection has been linked with, in some opinions, the same pattern which is noted from methicillin-susceptible *S. aureus* (MSSA).[112] The organism is able to survive on nearly all surfaces and has been found currently populating: the air, tools of medicine, bed frames and linen, stationery, furniture, food, flooring, clothing and toilets.[112] The strain used in this study is not antibiotic resistant organism, however it should be able to provide a good level of insight as to how all *S. aureus* would react to the ligands. Staphylococci have been primarily shown to utilise trihydroxamate based siderophores. There are two siderophores associated with staphylococci in particular which are staphyloferrin A and staphyloferrin B, Figure 7.3.

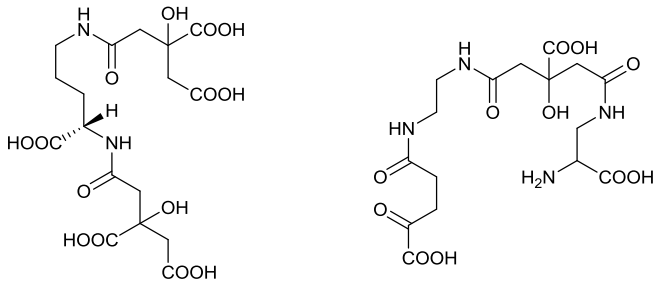

Figure 7.3 Structures of staphyloferrin A (left) and staphyloferrin B (right); siderophores secreted by *S. aureus*

A. baumannii is a Gram-negative bacterium which is an opportunistic human pathogen and is commonly associated with infections following traumatic war wounds.[108] This bacterium has the added danger of being capable of quickly adapting antibiotic resistance, creating MDR (multi-drug resistant) and PDR (pan-drug resistant) mutants.[108,121] In 2012 Zurawski *et al*. showed that the addition of a chelating agent (2,2-bipyridyl, Figure 7.4), which is non-specific to iron but is capable of binding iron, can significantly reduce the surface mobility of the organism with comparison to a growth media lacking the ligand.

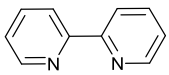

Figure 7.4 Structure of 2,2-bipyridyl

Certain strains of *A. baumannii* have been shown to secrete the siderophore acinetobactin (Figure 7.5), this siderophore is associated with those species that secrete histamine as this is a precursor to acinetobactin.

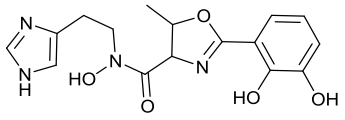

Figure 7.5 Structure of acinetobactin; a siderophore produced by *A. baumannii*

Also, those strains showing histamine secretion were in general found to express a FatA like protein receptor within their membrane architecture.[122] Those strains lacking the FatA-like protein have been proposed to utilise a catecholate iron acquisition system as they also do not secrete the histamine precursor and so most likely do not utilise acinetobactin in iron acquisition.[122] The strain *A. baumannii* 30007 used in this study does produce acinetobactin as a siderophore as per the providers information and so may be able to utilise ligands with a catecholate binding mode.

Candida species are known to be common opportunistic pathogens in humans and are the agents responsible for most fungal infections per year globally.[109] *C. albicans* of all of the species is the dominant causative agent in human infections; however other species such as *C. glabrata, C.*

tropicalis and C. parapsilosis are also involved in the causation of infection.[109] Iron is necessary for *C. albicans* to proliferate as a pathogen and the ability of this organism to acquire iron from the host is linked to virulence, as has been seen for bacterial species.[6,61,123] *C. albicans* has three main high-affinity pathways to acquire iron from a host; (i) a reductive system allowing host transferrin and ferritin to be utilised (ii) a siderophore uptake system (iii) a haem-iron uptake system.[123] Though *C. albicans* has been shown to secrete siderophore compounds in biological assays, the siderophore systems within *C. albicans* are thought to be typically xenosiderophoric in nature as no genes have been found which encode for the biosynthesis of siderophores from *C. albicans*.[123] The Sit1/Arn1 receptor is present as a transport receptor and has been shown to allow for a range of ferri-siderophore complexes to be taken up which were derived from a range of other organisms.[123] In addition, the uptake system for the iron-ferrichrome complex has been discovered for *C. albicans*,[124] this siderophore group has been shown to be an important growth factor for many organisms, including bacterial species.[125]

7.1.2 MIC assessment methods

For the purpose of this study a broth serial dilution technique was employed to determine the MIC levels for the ligands tested on all microorganisms. In this way, the liquid media may give a better insight into the sorts of levels which would be required to be employed when in a cleaning solution. The general layout of the 96-well plates used in this study is given, Figure 7.6.

	1 →	2 →	3 →	4 →	5 →	6 →	7 →	8 →	9 →	10 →	11	12
A											-	+
B											-	+
C											-	+
D											-	+
E											-	+
F											-	+
G											-	+
H											-	+

Figure 7.6 Figure denoting the general layout of the 96-well plates used in MIC assays. + indicates positive control well, - indicates negative control. Arrow denotes serial dilution to next column for all rows which had compound in A-H. No cross plating of bacteria occurred to minimise contamination.

However, there are variations on this method which have been previously used to determine the MIC level for other compounds, including ligands assumed to work via iron restriction. For example, recently in 2011 Hider *et al*. employed an agar dilution technique. This method involves preloading the agar media with the agent and then using this to create agar plates on which the inoculated culture of the organism desired is added.[46] The technique is standardised with respect to a text on the subject of antimicrobial susceptibility.[126] However, this agar dilution method is dependent on the ability of the ligands to solubilise and diffuse through the media and since the solubility and diffusion properties of the compounds presented herein in an agar media are unknown, in order to maximise the likelihood of obtaining results at sort of levels which are needed for testing the broth dilution technique was deemed to be more suitable.

7.2 Materials and Methods

7.2.1 Preparation of bacteriostatic agents

The solutions of these compounds were prepared by dissolving the chelators in deionized water. Volumetric flasks were rinsed with an EDTA solution (10mM in deionised water) before each use and then several times with deionised water. The solutions of the chelators were obtained after the addition of NaOH (3 mol eq) to produce the expected trisodium salt which in all cases was then soluble after heating in deionised water. The solvated ligands were then filtered through 0.2µm sterile filters to remove any contaminant bacteria or particulate matter and stored at 4°C in sterile plastic universal vials. TREN-1,2-HOPO* results were provided by David Workman, with consent, the compound was prepared by dissolving in deionised water and required no sonication or heating.

7.2.2 Bacterial strains

All microbes were purchased from DSMZ and cultured in the media and conditions recommended by the provider. Subcultures of all bacteria were produced on BHI agar purchased from Sigma-Aldrich except *C. albicans* 1386 was grown on a yeast selective media. For MIC assays, all microbes were inoculated in sterilised glass universal tubes containing 10mL BHI broth media. *C. albicans* 1386 was incubated for 48 hours at 28°C, *A. baumannii* 30007 and *B. subtilis* 23778 were incubated at 30°C for 48 hours. The remaining bacteria: *E. coli* 18039, *K. pneumoniae* 30104, *S. aureus* 1104 and *P. aeruginosa* 19880 were incubated at 37°C for 24 hours prior to performing the MIC assay.

7.2.3 MIC Assay

All compounds were tested in duplicate in MIC assays at several appropriate concentrations so as to determine their efficacy. All assays were cultured at 37°C for 24 hours before being assessed by eye and were conducted in 96 well U-bottomed sterile microtitre plates. For *C. albicans, A. baumannii* and *B. subtilis* an additional 24 hours was given after the initial assessment to determine any change. OD kinetic studies were repeated with F-bottomed microtitre plates (*E. coli, K. pneumoniae*) or U-bottomed microtitre plates (*P .aeruginosa, A .baumannii, B .subtilis, S .aureus* and *C .albicans*), runs were carried out at 37°C for 24 hours with agitation for 30s before each

reading. The incubation media was BHI broth and the experiment performed once for the compounds which showed inhibition in MIC assays. All wells contained 100µL of inoculum and 100µL of compound to be assessed following 2x serial dilutions for the MIC assays and the volume of each was halved for the OD studies. Positive and negative control wells were included for each plate and in all cases were cleared.

7.2.4 Recap of ligand structures used in this study

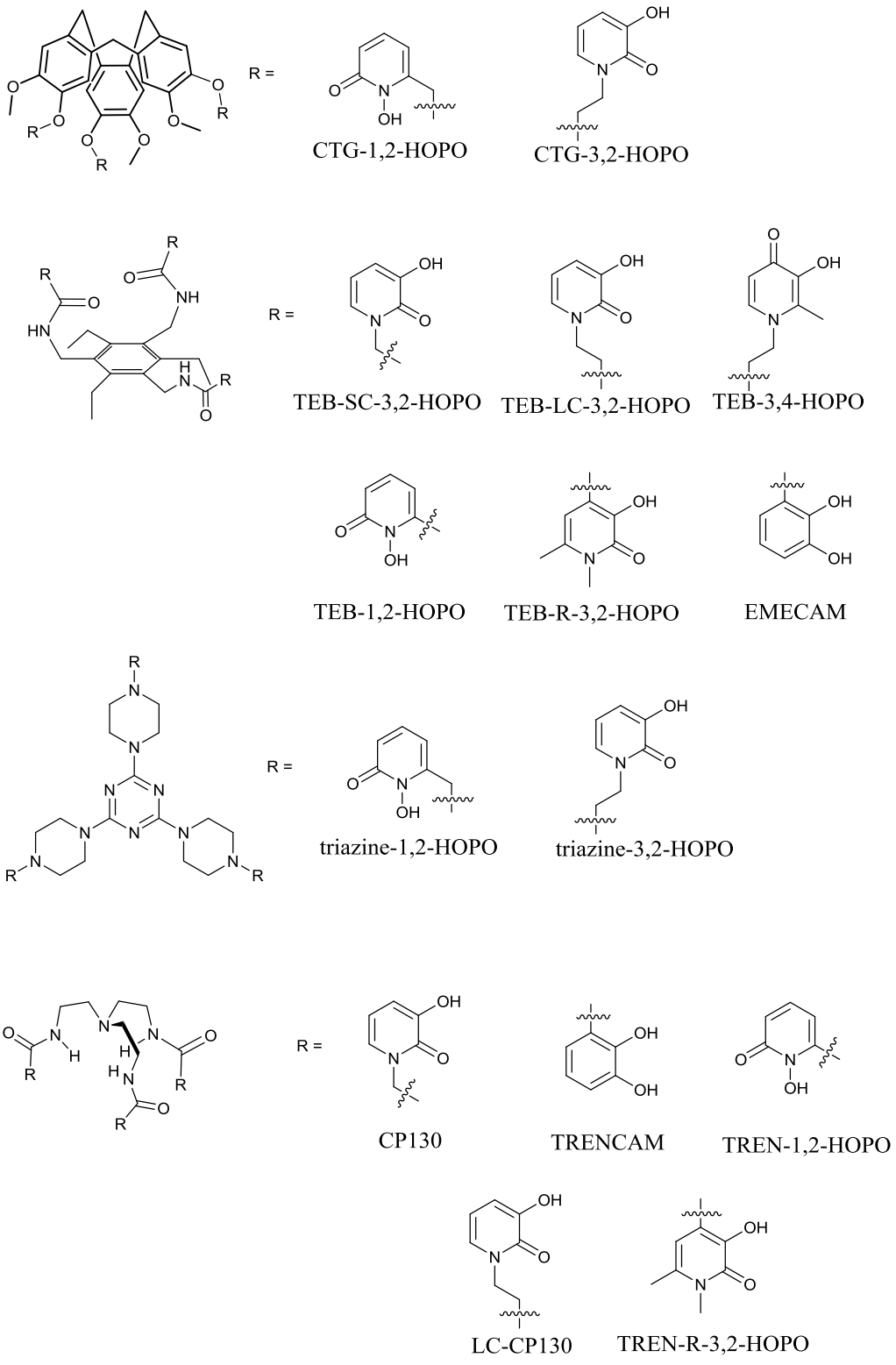

Figure 7.7 Structures of the bacteriostatic agents for which the MIC values were determined in this study. SC denotes short-chained and LC denotes long-chained, CTG = cyclotriguaiacylene, TEB = triethylbenzene, triazine = tris(piperazin-1-yl)-1,3,5-triazine, and TREN = tris(2-aminoethyl)amine. CP130 is designated as per literature precedent. TREN-1,2-HOPO was provided by an external source (see 7.2.1 Preparation of bacteriostatic agents)

7.3 Results and Discussion

7.4 MIC Assay Results

The MIC assays for the compounds presented previously (Chapters 2-6, Figure 7.7) yielded some interesting results with regard to the structural features of the compounds and their relative effects on the panel of microbes, the results of which are displayed in Table 7.2.

The data shows that there are three principal candidates that display an inhibitory effect across the panel of microbes. The CTG-1,2-HOPO molecule, the TEB-1,2-HOPO molecule, TEB-R-3,2-HOPO and TREN-1,2-HOPO molecule all inhibit growth at relatively low concentrations i.e. <500μM, with the exception of TEB-R-3,2-HOPO on *K. pneumoniae* which showed an MIC of 964μM. These compounds inhibited growth with no differential between Gram-positive/Gram-negative/fungus, . Conversely, the TEB-SC-3,2-HOPO molecule displayed no inhibitory effect across the whole panel of microbes. This was unexpected because in the previous UV-Vis studies (Chapter 3) this molecule was shown to bind Fe^{3+} in a 1:1 stoichiometry. This may suggest the molecule is being utilised by the microbes' own siderophore uptake systems and is therefore 'feeding' the organisms. However, further work is required to confirm this hypothesis. The same observations for TEB-LC-3,2-HOPO, CP130 and LC-CP130, with the exception of TEB-LC-3,2-HOPO molecule on *C. albicans* which showed inhibition only at high concentration 3855μM. Though the UV-Vis binding study for CP130 and the LC-CP130 were not performed in this work CP130 has been shown to bind Fe^{3+} in a 1:1 stoichiometry;[127] the extra carbon for the LC-CP130 is not expected to alter the binding stoichiometry drastically and so both should bind Fe^{3+} in a 1:1 stoichiometry, but are seen to be non-inhibitory. In addition, as in the TEB-SC-3,2-HOPO the TEB-LC-3,2-HOPO molecule showed a 1:1 stoichiometry binding Fe^{3+} in UV-Vis studies but shows no inhibitory effect again lending to the hypothesis of growth promotion.

TRENCAM and EMECAM show relatively mediocre inhibition across the panel, both having no inhibition against *C. albicans.* With the exception of TRENCAM on *K. pneumoniae* (MIC = 535μM) and both molecules on *S. aureus* (MIC = 482μM) for which the inhibition is fairly promising.

Table 7.2 MIC for the hexadentate ligands tested on the clinically relevant panel of microbes. Assays were performed in BHI broth over 24 hours. (-) denotes no inhibition was noted. (*) Results obtained from external source (see 7.2.1 Preparation of Antimicrobial Agents)

	E. coli		*K. pneumoniae*		*P. aeruginosa*		*A. baumannii*		*S. aureus*		*B. subtilis*		*C. albicans*	
Compound	MIC/μM	ppm	MIC/μM	ppm	MIC/μM	ppm	MIC/μM	ppm	MIC/μM	ppm	MIC/μM	ppm	MIC/μM	ppm
CTG-3,2-HOPO	-	-	3855	3162	3855	3162	3855	3162	241	198	1928	1581	482	395
CTG-1,2-HOPO	241	188	482	375	482	375	241	188	241	187	482	375	120	94
triazine-3.2-HOPO	3855	2873	-	-	-	-	2855	2873	964	718	3855	2873	482	359
triazine-1,2-HOPO	482	339	964	678	482	339	-	-	-	-	-	-	120	85
TEB-SC-3,2-HOPO	-	-	-	-	-	-	-	-	-	-	-	-	-	-
TEB-LC-3,2-HOPO	-	-	-	-	-	-	-	-	-	-	-	-	3855	2873
TEB-1,2-HOPO	241	159	482	319	482	319	241	159	241	159	241	159	241	159
TEB-R-3,2-HOPO	241	180	964	718	482	359	60	45	241	180	241	180	241	180
TEB-3,4-HOPO	-	-	-	-	-	-	-	-	-	-	-	-	964	718
CP130	-	-	-	-	-	-	-	-	-	-	-	-	-	-
LC-CP130	-	-	-	-	-	-	-	-	-	-	-	-	-	-
TREN-R-3,2-HOPO	2944	1889	-	-	2944	1889	368	236	368	236	1472	944	1472	944
TREN-1,2-HOPO*	625	371	313	186	313	186	313	186	5	3	313	186	313	186
TRENCAM	1928	1069	964	535	1928	1069	1928	1069	482	267	1928	1069	-	-
EMECAM	3855	2537	1928	1268	1928	1268	1928	1268	482	317	1928	1268	-	-

CTG-3,2-HOPO appears to be ineffective at inhibiting the growth of *E. coli* up to the highest concentration of the ligand which corresponds to 7710μM (6324ppm). This could indicate that the bacteria in this case have the capability to utilise any Fe^{3+} complexed by this molecule or, alternatively that the Fe^{3+} is not successfully bound by the ligand. Though this would contrast with the UV-Vis binding studies previously discussed (Chapter 2) where the ligand was shown to bind iron in a 1:1 stoichiometry. Alternatively, the result could indicate a kinetic issue of the speed at which the ligand binds Fe^{3+}. If the ligand binding is a slow process there may not be any inhibition to be seen within the timeframe. In contrast, this molecule appears to be reasonably inhibitory against Gram-positive *S. aureus*, reaching levels of 241μM (197ppm). The difference between these results could be due to the structural differences in the membrane architecture between Gram-negative and Gram-positive or even the ferri-siderophore shuttling mechanisms. Alternatively, it could be the differences in competing siderophores produced by the two bacteria and how they interact with the ligand i.e. *E. coli* can produce the very powerful enterobactin.

The CTG-1,2-HOPO ligand bearing CTG scaffold was as effective at inhibiting the growth of *E. coli* as *S. aureus*. This could indicate that this molecule is not interacting with the uptake of Fe^{3+} in terms of the receptor proteins involved but more likely is just binding extracellular Fe^{3+}. It may be expected to see a difference in the levels of inhibition obtained if the inhibition was due to an interaction with the siderophore receptors, as these are different for the different organisms. In addition, as can be seen for the CTG-1,2-HOPO analogue, if the inhibition were a case of competing siderophore interaction we might expect to see a difference between Gram-positive and Gram-negative such as for CTG-3,2-HOPO. It may be, as per the UV-study, that we have seen this molecule able to hold possibly 2 equivalents of Fe^{3+} per ligand that this has shown its effectiveness in both cases. The Fe^{3+} cation maybe held too strong/close into the ligand; cavity facilitated by the shorter linkage, to allow competing siderophores to sequester the Fe^{3+} away from the complex, in this way inducing growth inhibition. Alternatively, another mechanism of inhibition may be in effect for the 1,2-HOPO bearing ligand.

The triazine-1,2-HOPO molecule was shown to inhibit effectively at relatively low concentration (<500μM) for the organisms *E. coli, P. aeruginosa* and *C. albicans*. The ligands also showed

inhibition for *K. pneumoniae* at slightly higher levels (678μM). However, the molecule displayed no inhibitory effect against the Gram-positive organisms or *A. baumannii.* These results could indicate certain selectivity for the inhibition of Gram-negative organisms; however a larger panel of microbes must be explored to test this selectivity as *A. baumannii* was uninhibited. Conversely, the triazine-3,2-HOPO molecule showed inhibition against the Gram-positive organisms however, not to below 500μM. Both of the triazine-based ligands showed good inhibition towards *C. albicans*, this may be in part due to the limited siderophore transport systems the organism has available. UV-Vis analysis showed that the triazine-1,2-HOPO molecule does not quickly bind Fe^{3+} in a 1:1 stoichiometry but the 3,2-HOPO analogue does after 14 days, under the experimental conditions described. The activity of the triazine-1,2-HOPO could be due to kinetically favourable binding of Fe^{3+}, which, once bound is unable to be used by the microbes. Alternatively, the exchange reaction rates between the ferrated ligand complex and the siderophore molecules may be too slow to allow the organisms own systems to successfully overcome the nutrient deficiency. The triazine-3,2-HOPO molecule can form a 1:1 complex with Fe^{3+} which is undoubtedly thermodynamically favoured however this is achieved at a slow rate. It could be the case that the siderophore systems form the ferric complexes at a faster rate and although the triazine-3,2-HOPO ligand may form a stable complex thermodynamically, under the experimental conditions, the rate of Fe^{3+} binding is too slow to be effective.

The results for the molecules which are built upon the triethylbenzene (TEB) scaffold raise some interesting observations. The TEB-1,2-HOPO and TEB-R-3,2-HOPO molecules show inhibition at low concentrations (<500μM) across the panel, with the exception of the TEB-R-3,2-HOPO on *K. pneumoniae* which was inhibitory at 718μM. Whereas, the other compounds built upon this core: TEB-SC-3,2-HOPO, TEB-LC-3,2-HOPO and TEB-3,4-HOPO showed no or poor inhibition across the panel. The TEB-LC-3,2-HOPO on *C. albicans* which inhibited at high concentration <1000μM and the TEB-3,4-HOPO on *C. albicans* which inhibited at 964μM. This may suggest that these molecules are being utilised by the microbes' own siderophore transport systems and are therefore 'feeding' the organisms. However, further work which involves a colony number determination portion is required to confirm this hypothesis.

The selectivity for inhibition which is seen for the 1,2- and R-3,2 HOPO moieties could be attributed to a number of contributing factors. Firstly, it may be that the selection of either the 1,2-HOPO or the R-3,2-HOPO moiety to induce non-species dependent inhibition is important for this core scaffold, as these are the only full panel inhibitors. The presence of a carbon chain spacer between the HOPO moiety and core scaffold appears to be detrimental to the ability of the ligand to inhibit growth. For example the TEB-SC-3,2-HOPO and the TEB-LC-3,2-HOPO molecules show no inhibition, whereas the 1,2- and R-3,2-HOPO analogues display strong inhibition across the panel. Possibly, the closer the binding moieties are to the core scaffold the more effective the microbial growth inhibition. A carbon chain spacer between HOPO and core may facilitate recognition by the microbial systems or it could lower the binding affinity of the ligand for the metal centre and allow competing siderophore molecules to sequester the metal from the ferrated ligand complex. The poor inhibition in the 3,4-HOPO containing ligand could be due to the orientation of the binding atoms with respect to the attachment which has been show previously to be important. Although in UV-Vis studies the molecule was shown to bind Fe^{3+} in a 1:1 stoichiometry. The binding affinities for the compounds would need to be determined in order to explore this reasoning.

The results for the TEB core mirror those displayed for the CTG core scaffold in that the 1,2-HOPO which includes a shorter chain attachment of HOPO to the core than the 3,2-HOPO analogue is a more effective inhibitor of growth across the panel of organisms, with the exception of *S. aureus* which showed an MIC of 241μM for both molecules. The triazine results show that although the 3,2-HOPO containing analogue inhibited more organisms than the 1,2-HOPO the concentration levels were lower in the cases for the 1,2-HOPO for the same organism. These results could indicate that chain length is important for inhibition and that the inclusion of the 1,2-HOPO is significant. However, without further work to dissect these two contributing factors the significance of either with respect to the other cannot be distinguished.

The TREN-based ligand results show that CP130 and the novel LC-CP130 were ineffective at inhibiting across the panel. Conversely, the TREN-R-3,2-HOPO molecule showed inhibition at low concentration against *A. baumannii* and *S. aureus* (>500μM) and inhibition at medium

concentrations (>1000μM) for *B. subtilis* and *C. albicans*. These results might indicate that the 3,2-HOPO moiety is again possibly being recognised on this core scaffold in both the short and long chained analogues, as was possibly seen for the TEB based ligands. Whereas, the R-3,2-HOPO is again proving more effective than those ligands where the HOPO moiety is attached via the N-atom of the ring system and which contain a carbon chain spacer between the attachment at the ligand core and HOPO group. In addition, results obtained for the TREN-1,2-HOPO* indicate inhibition across the panel <500μM with all microbes except *E. coli* which showed inhibition at 625μM. Again, these results corroborate the hypothesis that the 1,2-HOPO and R-3,2-HOPO are important moieties for inhibition of the microbes in this panel as they once again stand out on the same core as being effective with respect to the 3,2-HOPO both long and short chained derivatives. Whether this is due to the lack of a carbon spacer these ligands possess or that they are unable to be recognised and therefore prevent iron uptake requires more in depth study.

C. albicans was shown to be more susceptible to growth inhibition by more of the ligands than the other species; this could in part be due to the organism having been found to so far to have no known genes for the biosynthesis of its own siderophores. This may mean it has no high affinity iron sequestants with which to compete for the extracellular iron. Though *C. albicans* has been noted to utilise siderophores from other organisms, the ligands presented here may be too alien for the organism to utilise for its own means of iron acquisition, with the exception of those which showed no inhibition.

S. aureus was shown to be susceptible to inhibition by the compounds to concentrations below 500μM in all cases except for the triazine-3,2-HOPO where inhibition was noted at 964μM. The other organisms showed some resistance to one or more ligands to above 1000μM. This could signify that *S. aureus* is more susceptible to inhibition through the induction of an Fe^{3+} nutrient deficiency than the other organisms, or that once inhibited *S. aureus* is not able to recover or compete for the Fe^{3+} effectively via its own siderophore uptake mechanisms.

7.5 Determination of the Inhibitory Effect of Novel Chelators on the Growth of Clinically Relevant Microbes

The ligands presented herein were assessed on their ability to inhibit the growth of the panel of microbes through measurement of the optical density (OD) of a solution containing: growth media, ligand and microbe with respect to the same solution containing no ligand, over an appropriate time period at 630nm. The kinetic assays were performed for those compounds which showed an inhibitory effect in MIC assays as previously discussed. These assays were performed at concentrations to two dilutions below the MIC value for comparison, graphs have been normalised for clarity. The results of the assays are to be discussed in terms of an apparent 'lag time' which for these purposes refers to the time required to observe bacterial growth via the development of turbidity. In addition the differences in final cellular yield of each culture (indicated by a simple ratio $OD_{630\ (treated)}$:$OD_{630\ (untreated)}$) will also be discussed. All kinetic assay graphical analyses are available in the Appendix. The assays performed on *S. aureus* for TEB-R-3,2-HOPO, TREN-R-3,2-HOPO, TRENCAM and EMECAM were unsuitable to extract any data from and so have been omitted from discussion, however these are available in the Appendix .

In general, most of the MIC values were found to be valid in this system also. In a number of cases however, some growth was noted at the MIC concentrations. In most cases it is clear that an appropriate MIC for this assay system (with periodic agitation and presumed media reoxygenation) is the concentration represented by the next highest concentration in the series.

7.5.1 Assessment of the effect of the CTG-3,2-HOPO ligand (2.22) on the growth of microbes: *K. pneumoniae, P. aeruginosa, A. baumannii, S. aureus, B. subtilis* and *C. albicans*

The results of the kinetic assays performed on the *K. pneumoniae* bacterium for the CTG-3,2-HOPO molecule show that at the MIC level (3855μM) there is no discernible growth of bacteria

over the 24 hour period, Figure 7.8. However, at those concentrations below that of that MIC (1928 and 964μM) the growth of bacteria is normal,, although at approximately the 12 hour time point the data shows slightly erratic OD readings, the growth of bacteria is still visible. The bacterial growth at lower concentration occurs with no significant 'lag-time' with respect to the control but the final OD_{630} values are lower than those of the control indicating lower bacterial concentration over the same time period.

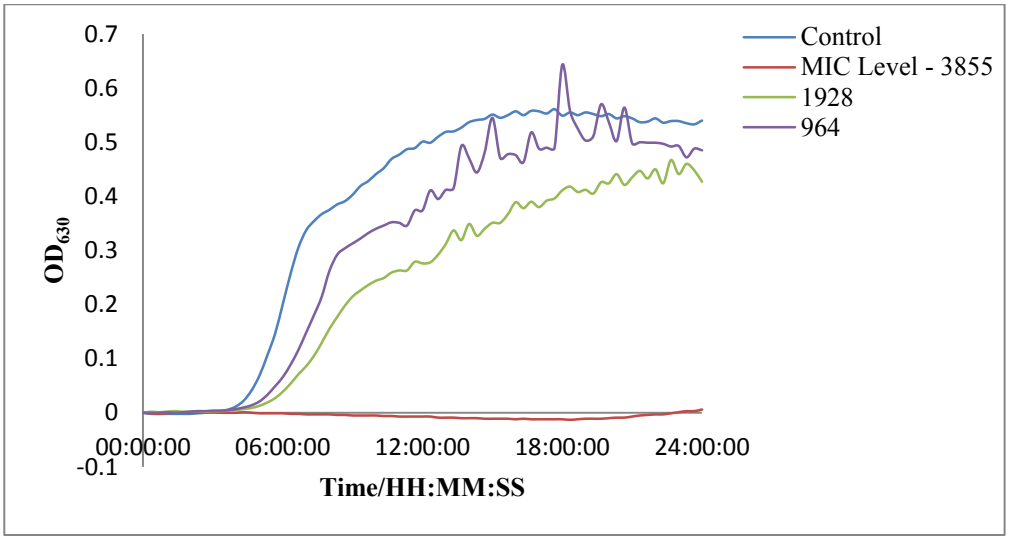

Figure 7.8 OD_{630} development over 24 hours for CTG-3,2-HOPO (**2.22**) on *K. pneumoniae* (MIC = 3855μM). Values displayed in legend are given as micromolar (μM) concentrations.

This assay confirms that at the MIC level the CTG-3,2-HOPO molecule is bacteriostatic in this adjusted format. At this stage assessment of the bacteriocidal activity has not been carried out. Growth is apparent early in all sub-MIC cultures but the growth rate is reduced with respect to increasing inhibitor concentration. This could be a due to the thermodynamic stability of the Fe^{3+}-CTG-3,2-HOPO complex being too high for competing natural siderphores to sequester the metal away or, that the complex to 'too alien' for the organisms regulatory systems to utilise the complex.

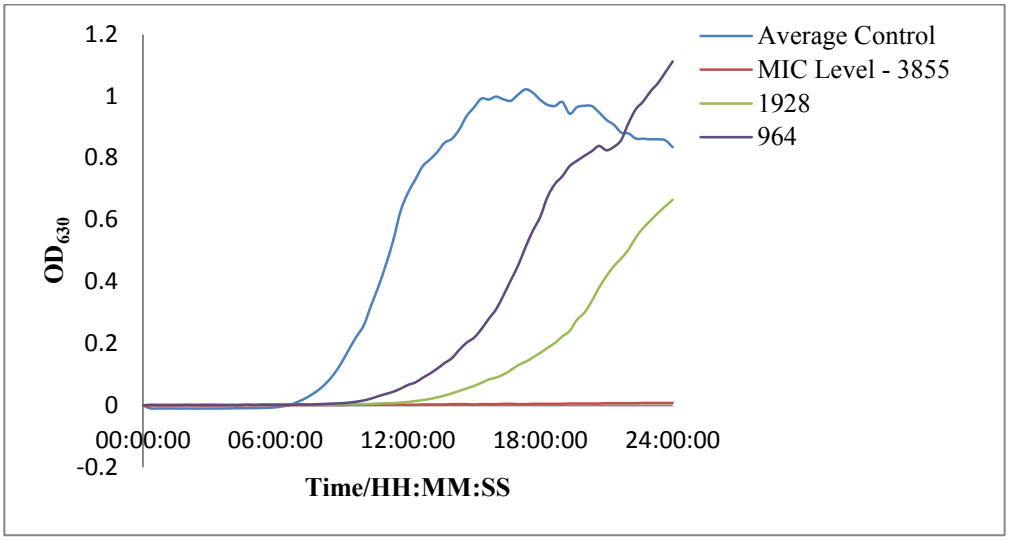

Figure 7.9 OD_{630} development over 24 hours for CTG-3,2-HOPO (**2.22**) on *P. aeruginosa* (MIC = 3855μM). Values displayed in legend are given as micromolar (μM) concentrations.

The CTG-3,2-HOPO molecule shows similar results for the assays performed on *P. aeruginosa* and *A. baumannii,* Figure 7.9 and Figure 7.10, though some differences are apparent. Both *P. aeruginosa* and *A. baumannii* show no discernible growth at the predetermined ligand MIC (3855μM) and, both organisms show an apparently extended lag period for those concentrations below the MIC value, summarised in Table 7.3. *A. baumannii* in particular displays a reduced growth rate with increasing chelator concentration, Figure 7.10.

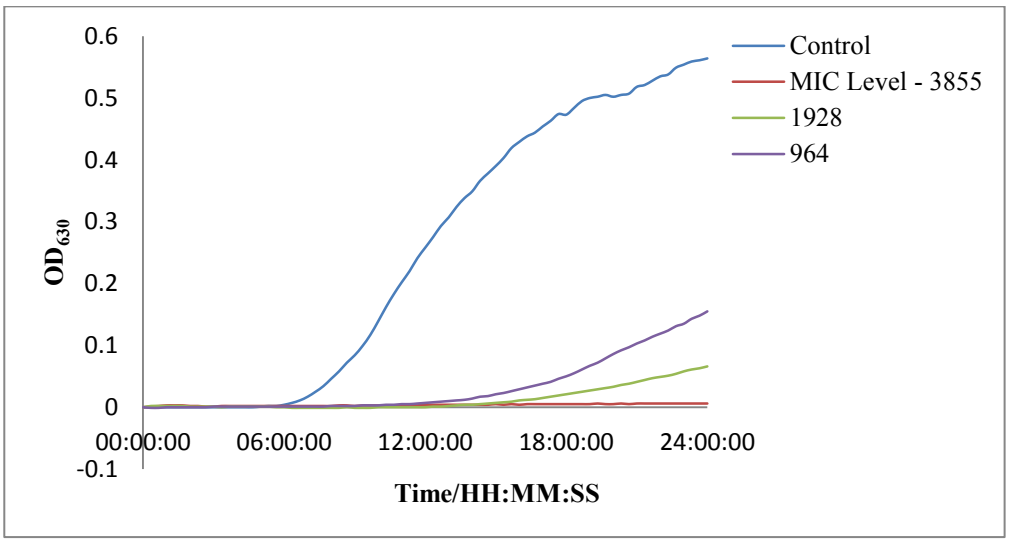

Figure 7.10 OD_{630} development over 24 hours for CTG-3,2-HOPO (**2.22**) on *A. baumannii* (MIC = 3855μM). Values displayed in legend are given as micromolar (μM) concentrations.

The organism *S. aureus* shows no growth at the MIC level (241µM). However, significant growth is illustrated at those concentrations below the MIC after a lag period, results displayed in Table 7.3.

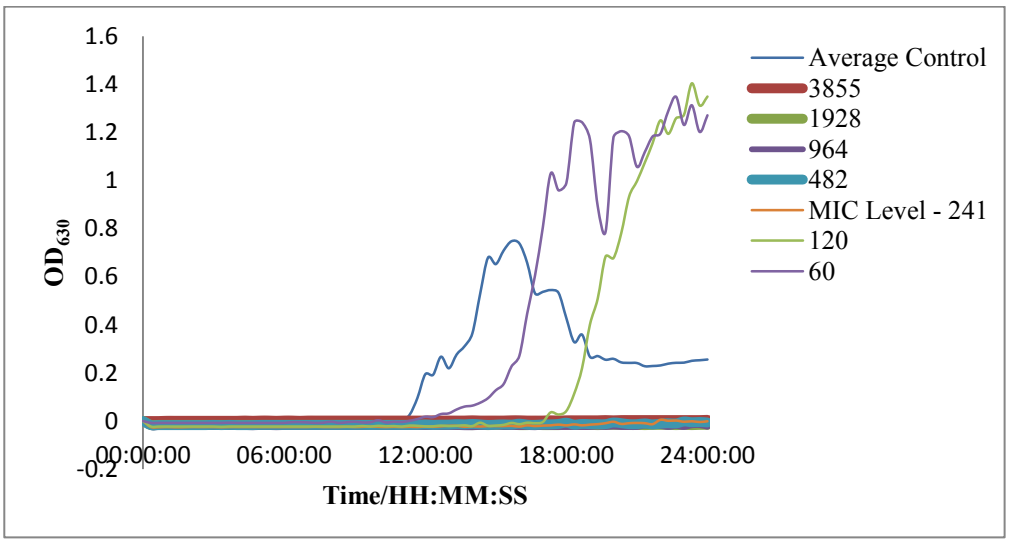

Figure 7.11 OD_{630} development over 24 hours for CTG-3,2-HOPO (**2.22**) on *S. aureus* (MIC = 3855µM). Values displayed in legend are given as micromolar (µM) concentrations.

However, these curves are complex and poorly reproducible; the characteristic incomplete cell division of this organism may be important here. *S. aureus* daughter cells infrequently dissociate from the parent cell on division and consequently these form multicellular clumps which could influence their rate of settling and the overall growth kinetics in the culture plates. Nevertheless, marked extension of the apparent lag period with increasing sub-MIC concentrations is evident.

In contrast, the organism *B. subtilis* displays no significant difference in the lag time and final OD_{630} at the concentrations 1928, 964 and 482µM, of which 1928µM is the determined MIC value. The rate of growth of the MIC value with respect to the lower concentrations appears to be reduced, however, overall the same levels are reached, Figure 7.12. The resulting growth at the MIC value could be a result of the stimulation to growth that may occur when organisms are subject to agitation, as per the conditions of the assay. In addition, it may be the case that the organism has reached a different growth phase with respect to other organisms and requires an acclimatisation period which may produce the synchronised lag time periods for the three concentrations.

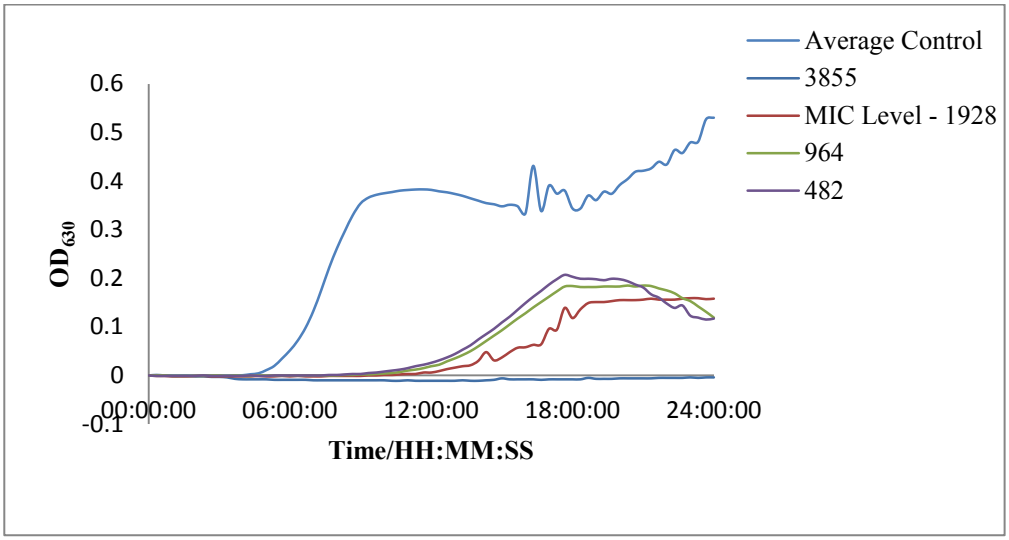

Figure 7.12 OD_{630} development over 24 hours for CTG-3,2-HOPO (**2.22**) on *B. subtilis* (MIC = 1928μM). Values displayed in legend are given as micromolar (μM) concentrations.

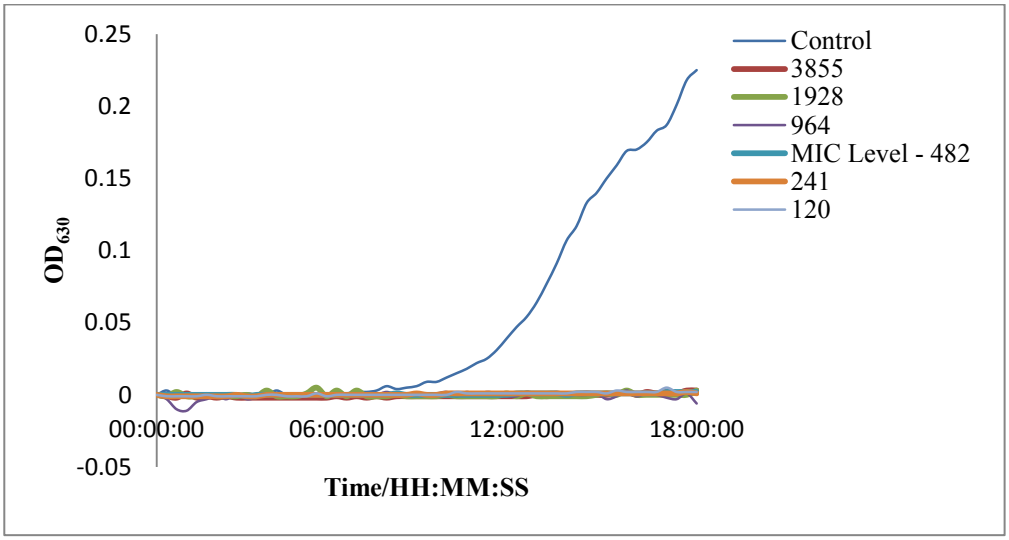

Figure 7.13 OD_{630} development over 18 hours for CTG-3,2-HOPO (**2.22**) on *C. albicans* (MIC = 482μM). Values displayed in legend are given as micromolar (μM) concentrations.

C. albicans displays no discernible growth as determined by turbidity detection at the MIC value previously determined or at those concentrations below the MIC value, displayed in Figure 7.13.

Table 7.3 summarises the data for those organisms which displayed growth, the lag time for these organisms at the various concentration and the difference in OD_{630} between the control and ligand containing samples is given. The OD_L/OD_C value is a measure of how successful an organism is at growing to the same OD as the control sample; in this representation a value close to 1 denotes strong growth relative to the control.

Table 7.3 Summary of the lag time at concentrations of ligand which showed growth and the observed difference in OD_{630} for those organisms that displayed growth for the CTG-3,2-HOPO (**2.22**) ligand. [a]OD_L/OD_C = OD_{630} with the ligand at the corresponding concentration/OD_{630} of the control sample.

Organism	Concentration /μM	MIC/μM	Extended Lag time/ approximate hours	Final Control OD_{630}	Final Ligand OD_{630}	Ratio [a]OD_L/OD_C
K. pneumoniae	1928	3855	0	0.54	0.47	0.87
	964		0		0.49	0.90
P. aeruginosa	1928	3855	5	0.86	0.62	0.72
	964		3		1.08	1.26
A. baumannii	1928	3855	6	0.55	0.06	0.11
	964		6		0.14	0.25
S. aureus	120	241	6	0.25	1.35	5.40
	60		0		1.27	5.08
B. subtilis	1928	1928	4	0.53	0.13	0.25
	964		4		0.12	0.25
	482		4		0.12	0.25

The data (Table 7.3) indicates that in terms of lag time, *K. pneumoniae* does not show any measureable difference in the starting points of organism growth with or without chelator. Also, at those values below the MIC, the growth of the samples containing CTG-3,2-HOPO (**2.22**) is fairly uninhibited, reaching a similar OD_{630} as the control. In contrast *P. aeruginosa* displays lag times of 3 and 5 hours at concentrations 1928 and 964μM respectively. The OD_{630} measurements here show that at 1928μM the OD_{630} with the ligand reaches levels around 72% of that of the control. However, the OD_L/OD_C value for 964μM shows over 100% OD_{630} is reached which could indicate some growth promotion properties at this concentration. *A. baumannii* showed favourable lag periods at both concentrations of approximately 6 hours and in both case the levels of growth reached were significantly reduced with respect to the control measurement. *S. aureus* displayed what may be considered significant organism growth with respect the control the OD_L/OD_C for the values 120 and 60μM being 5.40 and 5.08 respectively. This could signify utilisation of the ligand complex by the organism, producing a growth promotion effect. However, these values should not be over interpreted due to the relatively poor data from which they were derived. *B. subtilis* showed a similar lag period of 4 hours for all three measured concentrations and the OD_L/OD_C value indicates that all of the samples reached the same final OD_{630} with respect to the control. The

growth at the MIC level could be attributed to some stimulation to growth cause by the agitation as per the conditions of the kinetic assays which was not the case for the MIC assays.

7.5.2 Assessment of the effect of the CTG-1,2-HOPO (2.30) ligand on the growth of microbes: *E. coli, K. pneumoniae, P. aeruginosa, A. baumannii, S. aureus, B. subtilis* and *C. albicans*

The kinetic OD_{630} assays performed for the CTG-1,2-HOPO (**2.30**) showed that for *E. coli* and *K. pneumoniae* no significant lag period could be detected in their growth profiles in the assay time period. In addition, for both organisms, the MIC showed no growth with respect to the control. However, at the concentrations tested below the MIC value growth could be seen but reaching OD_{630} values below that of the control, summary in Table 7.4.

P. aeruginosa displayed no growth at the MIC level (482µM) but displayed growth at two dilutions below this level (120µM) to a lower OD_{630} than the control and with a lag period as displayed in Figure 7.14. The data for 3855µM showed significant precipitation and has been removed for clarity, full data available in the Appendix. Both of the organisms *A. baumannii* and *B. subtilis* displayed no growth at the MIC level or at the dilution below this; growth was only seen at two dilutions below and to significantly reduced level of OD_{630} with respect to the control. In both cases a lag time of approximately18 hours was noted. The organisms *S. aureus* and *C. albicans* showed no growth over the assay time period with the lowest concentration of inhibitor applied, suggesting that both are more sensitive to this type of inhibition.

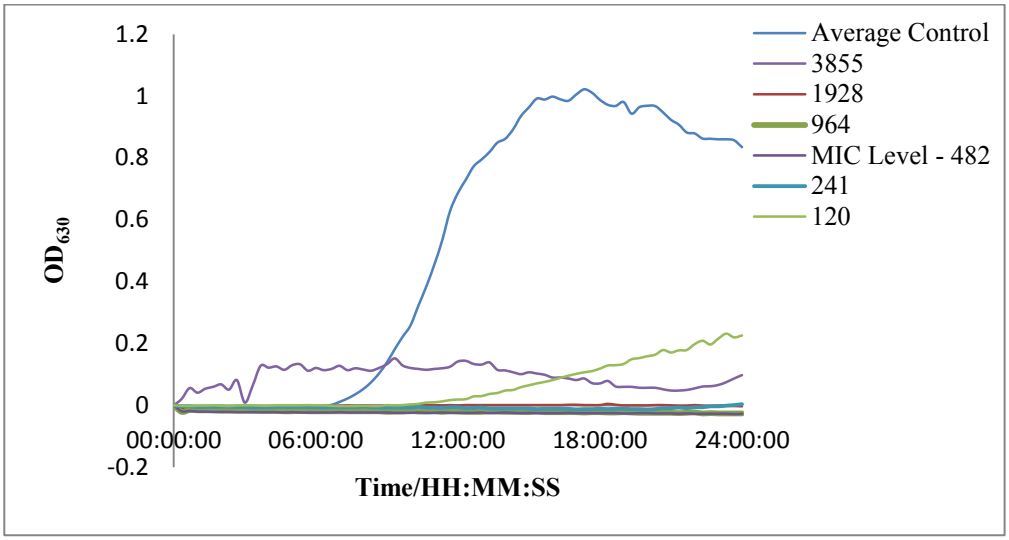

Figure 7.14 OD_{630} development over 24 hours for CTG-1,2-HOPO (**2.30**) on *P. aeruginosa* (MIC = 482µM). Values displayed in legend are given as micromolar (µM) concentrations.

Table 7.4 Summary of the lag time at concentrations of ligand which showed growth and the observed difference in OD_{630} for those organisms that displayed growth for the CTG-1,2-HOPO (**2.30**) ligand. [a]OD_L/OD_C = OD_{630} with the ligand at the corresponding concentration/OD_{630} of the control sample.

Organism	Concentration /µM	MIC/µM	Extended Lag time/ approximate hours	Final Control OD_{630}	Final Ligand OD_{630}	Ratio [a]OD_L/OD_C
E. coli	120	241	0	0.41	0.12	0.29
	60		0		0.21	0.51
K. pneumoniae	241	482	0	0.54	0.20	0.37
	120		0		0.29	0.54
P. aeruginosa	120	482	4	0.86	0.22	0.26
A. baumannii	60	241	12	0.55	0.02	0.04
B. subtilis	120	482	15	0.53	0.12	0.23

The data displayed in Table 7.4 shows that in most cases the levels to which the organisms grow to as determined by the OD_L/OD_C ratio are reduced in the CTG-1,2-HOPO (**2.30**) ligand with respect to the CTG-3,2-HOPO (**2.22**). This can be interpreted as the 1,2-HOPO containing ligand being more effective at creating an inhibitory effect.

7.5.3 Assessment of the effect of the triazine-1,2-HOPO (4.9) ligand on the growth of microbes: *E. coli, K. pneumoniae, P. aeruginosa,* and *C. albicans*

The results from the assays containing the triazine-1,2-HOPO ligand (**4.9**) show that on the organism *E. coli* there is no growth seen at the MIC level. However, at both dilutions below this concentration growth is noted. There is no appreciable lag time between the growth control and the growth at 241 and 120µM however there is a definite difference in the OD_{630} reached, Table 7.5. It can be noted that the cellular yields appear to decrease with increasing chelator concentration.

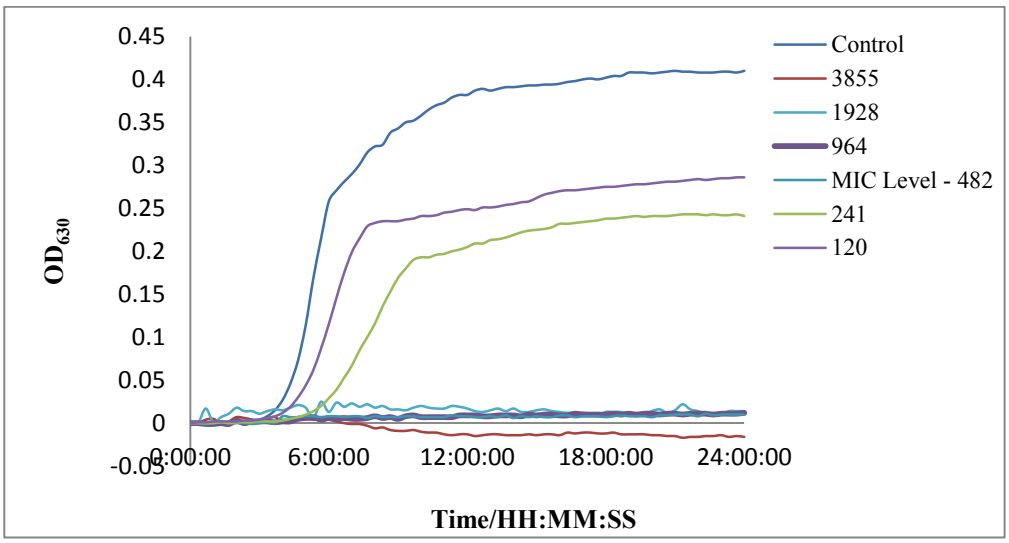

Figure 7.15 OD_{630} development over 24 hours for triazine-1,2-HOPO (**4.9**) on *E. coli* (MIC = 482µM). Values displayed in legend are given as micromolar (µM) concentrations.

Treatment of *K. pneumoniae* generated similar results in the assay, in that no growth over the 24 hour period was noted at the MIC concentration (964µM) however, at the two dilutions below this some growth was noted, summarised in Table 7.5.

For *P. aeruginosa* the same trend was displayed, however the growth at the second dilution (120µM) below the MIC (482µM) occurred at a rapid rate and to reach an OD_{630} at 94% that of the control. This contrasts with the other organisms where this level of growth was not reached. However, the rate of growth for this organism was markedly diminished with respect to the control. This may be due to the growth speed difference between the organisms or that at this concentration,

once the initial inhibition is overcome *P. aeruginosa* may be able to utilise the ligand for its own nutrient sequestration systems. Alternatively, the profiles may be explained by a low inoculum concentration eventually generating a high concentration of siderophore which then supports the rapid growth of the culture.

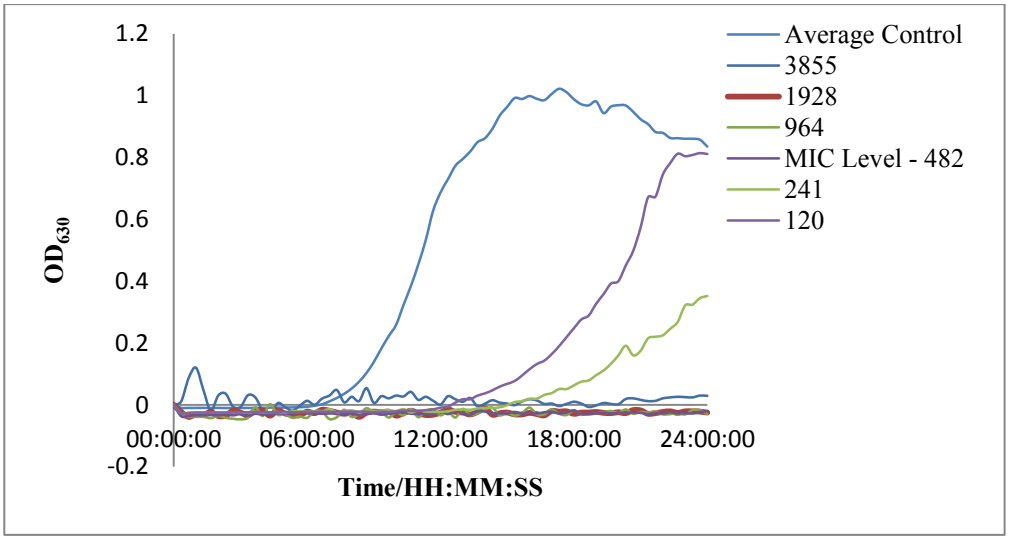

Figure 7.16 OD_{630} development over 24 hours for triazine-1,2-HOPO (**4.9**) on *P. aeruginosa* (MIC = 482μM). Values displayed in legend are given as micromolar (μM) concentrations.

C. albicans showed no growth in the periodically agitated assay format at any concentration at or below the predetermined MIC (120μM). This organism can adopt yeast and filamentous growth modes. It is possible that the agitation necessary for this technique may have induced a different growth mode than the static MIC determinations, reducing the MIC in this assay format.

Table 7.5 Summary of the lag time at concentrations of ligand which showed growth and the observed difference in OD_{630} for those organisms that displayed growth for the triazine-1,2-HOPO (**4.9**) ligand. $^{a}OD_L/OD_C = OD_{630}$ with the ligand at the corresponding concentration/OD_{630} of the control sample.

Organism	Concentration /μM	MIC/μM	Extended Lag time/ approximate hours	Final Control OD_{630}	Final Ligand OD_{630}	Ratio $^{a}OD_L/OD_C$
E. coli	241	482	0	0.41	0.24	0.59
	120		0		0.29	0.70
K. pneumoniae	482	964	2	0.54	0.27	0.50
	241		0		0.34	0.63
P. aeruginosa	241	482	7	0.86	0.32	0.37
	120		5		0.81	0.94

7.5.4 Assessment of the effect of the triazine-3,2-HOPO (4.11) ligand on the growth of microbes: *E. coli, A. baumannii, S. aureus, B. subtilis* and *C. albicans*

The kinetic assays for this particular ligand were compromised by the precipitation of the compound and as a result some of the higher concentrations gave unusable data, all data shown in Appendix. However, some assays did show useful data sets such as the *E. coli* bacterium at two levels below the MIC (964μM) which showed no appreciable lag time in the growth and reached an OD_{630} close to that of the control.

A. baumannii, S. aureus and *B. subtilis* showed no growth at any of concentrations tested which in both cases were 3855, 1928 and 964μM where 3855μM was the predetermined MIC for this ligand on those bacteria.

C. albicans was found to show no growth at the MIC level (482μM), Figure 7.17. However, several dilutions below this level showed no growth. Growth was recorded at 30μM ligand concentration but no extension to the lag period was observed and culture turbidity almost reached the same levels as the control assay.

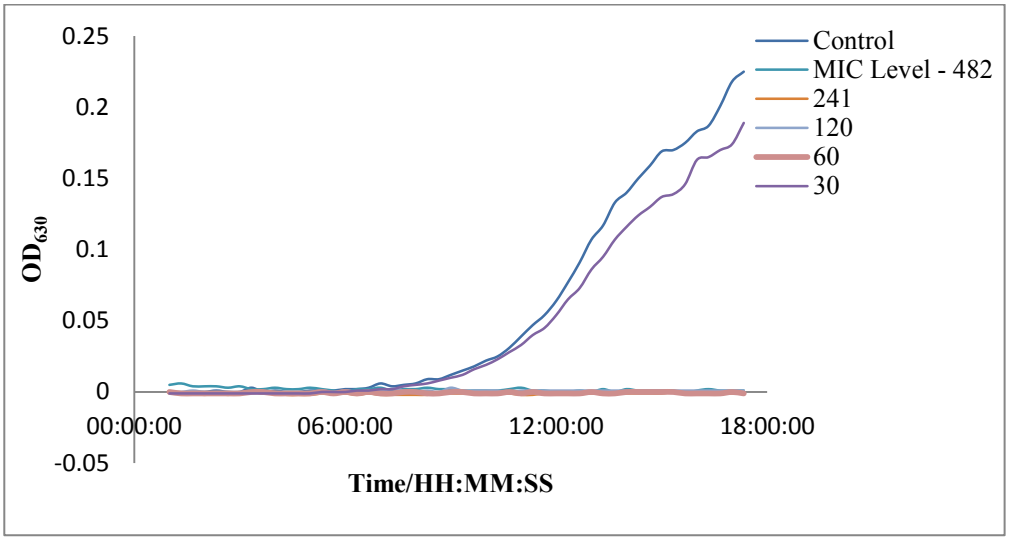

Figure 7.17 OD_{630} development over 18 hours for triazine-3,2-HOPO (**4.11**) on *C. albicans* (MIC = 482µM). Values displayed in legend are given as micromolar (µM) concentrations

.

7.5.5 Assessment of the effect of the TEB-LC-3,2-HOPO (3.25) ligand on the growth of *C. albicans*

The TEB-LC-3,2-HOPO (**3.25**) only displayed inhibition on the growth of the organism *C. albicans*. There was no growth noted at the MIC level (3855µM) however, at the second dilution below this level (964µM) growth was noted. An extension to the lag time of approximately 3 hours could be noted and an OD_L/OD_L of 0.50 (Figure 7.18).

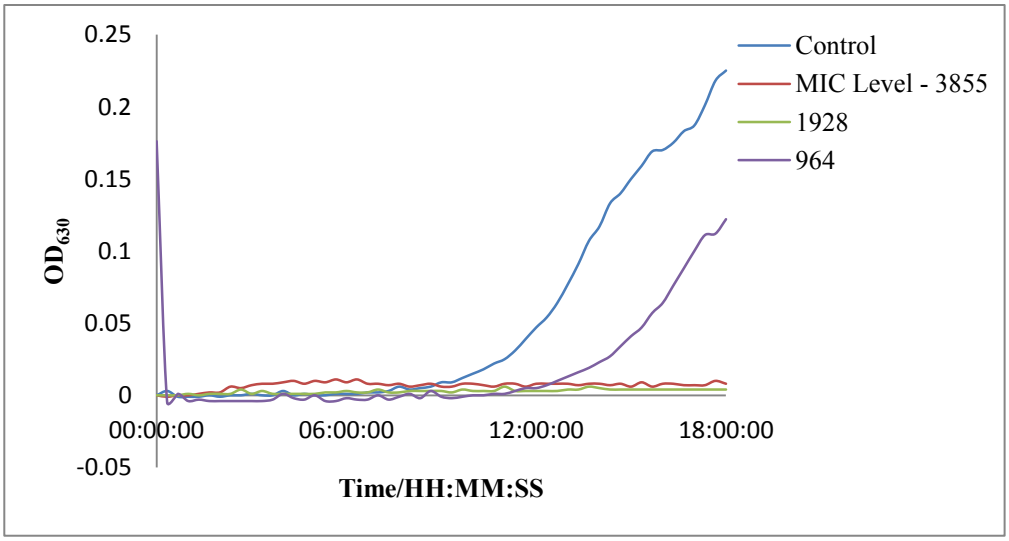

Figure 7.18 OD_{630} development over 18 hours for TEB-LC-3,2-HOPO (**3.25**) on *C. albicans* (MIC = 3855µM). Values displayed in legend are given as micromolar (µM) concentrations.

7.5.6 Assessment of the effect of the TEB-1,2-HOPO (3.27) ligand on the growth of microbes: *E. coli, K. pneumoniae, P. aeruginosa, A. baumannii, B. subtilis* and *C. albicans*

In the kinetic assay for the TEB-1,2-HOPO (**3.27**) *E. coli* displayed no growth at the MIC level, but as previously seen for other samples showed growth at the two dilutions below this. There was no extension to the apparent lag time noted in the growth with respect to the control; however, the OD_{630} was diminished with respect to the control, Table 7.6.

The organism *K. pneumoniae* showed similar trends to that of *E. coli,* the two levels below the MIC value showed growth with respect to the control. In contrast *P. aeruginosa* only displayed growth at the second dilution (120µM) below the MIC, only reaching an OD_{630} around 30% of that of the control samples. Both *K. pneumoniae* and *P. aeruginosa* showed no masureable lag time with respect to the growth control, Table 7.6.

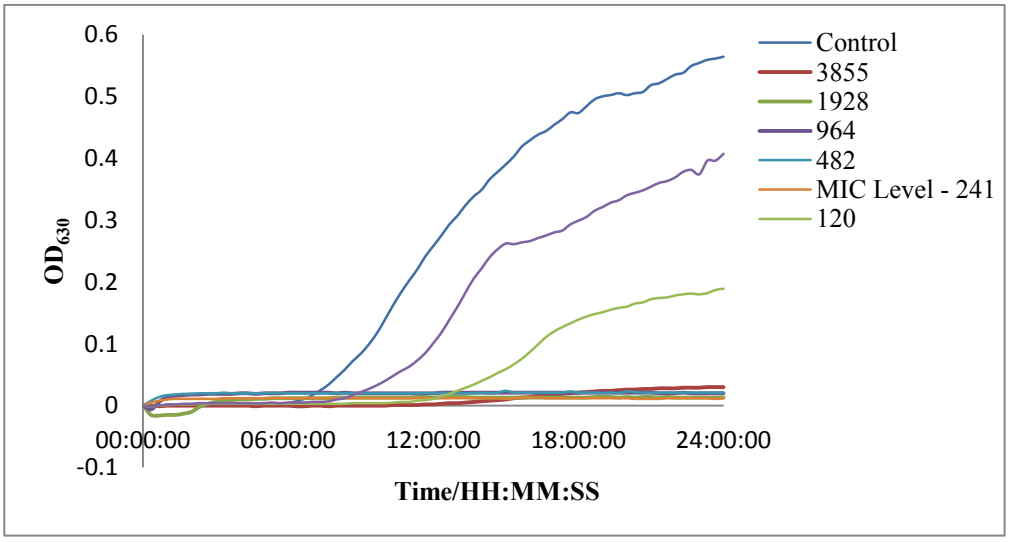

Figure 7.19 OD_{630} development over 24 hours for TEB-1,2-HOPO (**3.27**) on *A. baumannii* (MIC = 241µM). Values displayed in legend are given as micromolar (µM) concentrations.

The organism *A. baumannii* displayed both growth inhibition and a lag time period with respect to the control at the two dilutions below the MIC, no growth was shown at the MIC level (241µM). At a fairly low concentration of 120µM a lag time of approximately 6 hours is noted on *A.*

baumannii; similar or longer lag periods have been noted previously for the CTG based ligands **2.22** and **2.30**. Neither *S. aureus* nor *C. albicans* showed no growth with respect to the control over the assay time periods at or below the MIC value.

Table 7.6 Summary of the lag time at concentrations of ligand which showed growth and the observed difference in OD_{630} for those organisms that displayed growth for the TEB-1,2-HOPO (**3.27**) ligand. $^{a}OD_L/OD_C = OD_{630}$ with the ligand at the corresponding concentration/OD_{630} of the control sample.

Organism	Concentration /µM	MIC/µM	Extended Lag time/ approximate hours	Final Control OD_{630}	Final Ligand OD_{630}	Ratio $^{a}OD_L/OD_C$
E. coli	120	241	0	0.41	0.21	0.51
	60		0		0.37	0.90
K. pneumoniae	241	482	0	0.54	0.10	0.19
	120		0		0.32	0.59
P. aeruginosa	120	482	0	0.86	0.27	0.31
A. baumannii	120	241	6	0.55	0.19	0.35
	60		2		0.40	0.73
B. subtilis	60	241	4	0.53	0.14	0.26

7.5.7 Assessment of the effect of the TEB-R-3,2-HOPO (3.28) ligand on the growth of microbes*: E. coli, K. pneumoniae, P. aeruginosa, A. baumannii, B. subtilis* and *C. albicans*

Kinetic assays for the compound TEB-R-3,2-HOPO (**3.28**) showed that for *E. coli* there was no lag time in the growth of the organism at those concentrations which displayed growth which were the MIC level (241µM) and the two dilutions below this level (120 and 60µM), Figure 7.20. That there was growth detected at the MIC level could be due to stimulation of growth by the agitation set in the conditions of the assays. It is worthy to note that the MIC level did not reach the same OD_{630} and therefore, it may be the case that this is not detectable by eye as per the MIC assays. The dilution two below the MIC level did show recovery to the same level as the control sample which could be indicative of the organism overcoming the bacteriostasis through production of its own siderophores in response to application of the ligand.

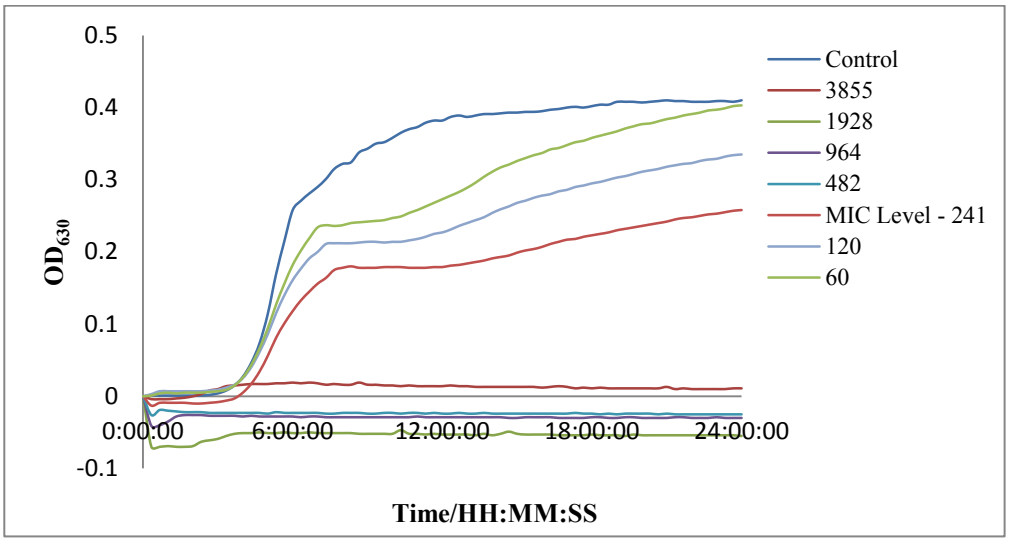

Figure 7.20 OD_{630} development over 24 hours for TEB-R-3,2-HOPO (**3.28**) on *E. coli* (MIC = 241µM). Values displayed in legend are given as micromolar (µM) concentrations.

The organisms *K. pneumoniae*, *P. aeruginosa* and *A. baumannii* displayed similar trends in that the MIC level for each displayed no growth but as has been previously shown, the two dilutions below this displayed measurable growth to an OD_{630} below the control value, Table 7.7. *P. aeruginosa* at 184µM showed a lag time in the growth of the organism of 2 hours and *A. baumannii* displayed a lag time of 5 hours for the concentration 23µM.

The organism *B. subtilis* displayed no growth at the MIC level (241µM), however as previously noted the two levels below this displayed growth. The concentration 120µM showed a lag time of approximately 3 hours with respect to the control, however, the result at 60µM showed almost uninhibited growth reaching the same level as the control sample, Table 7.7. *C. albicans* showed no growth with respect to the control at any concentration tested on TEB-R-3,2-HOPO (**3.28**).

Table 7.7 Summary of the lag time at concentrations of ligand which showed growth and the observed difference in OD_{630} for those organisms that displayed growth for the TEB-R-3,2-HOPO (**3.28**) ligand. [a]$OD_L/OD_C = OD_{630}$ with the ligand at the corresponding concentration/OD_{630} of the control sample.

Organism	Concentration /µM	MIC/µM	Extended Lag time/ approximate hours	Final Control OD_{630}	Final Ligand OD_{630}	Ratio [a]OD_L/OD_C
E. coli	241	241	0	0.41	0.26	0.63
	120		0		0.33	0.80
	60		0		0.41	1.0
K. pneumoniae	482	964	0	0.54	0.21	0.39
	241		0		0.37	0.69
P. aeruginosa	241	482	2	0.86	0.29	0.34
	120		0		0.30	0.35
A. baumannii	30	60	5	0.55	0.26	0.47
	15		0		0.49	0.89
B. subtilis	120	241	3	0.53	0.36	0.70
	60		0		0.53	1.0

7.5.8 Assessment of the effect of the TREN-R-3,2-HOPO (6.12) ligand on the growth of microbes: *E. coli, P. aeruginosa, A. baumannii, B. subtilis* and *C. albicans*

The results from the assay containing the TREN-R-3,2-HOPO (**6.12**) performed on *E. coli* after 15 hours were difficult to analyse as they displayed large and unusual fluctuations in optical density below the MIC value, however both of these concentrations of ligand did display growth until this time point and the results are summarised in Table 7.8. After 15 hours the MIC concentration (2944μM) displayed growth reaching a level somewhat diminished with respect to the control (OD_L/OD_C = 0.34) the compound therefore at the MIC level seems to create a profound bacteriostatic effect, which only after 15 hours is overcome by the organism, Figure 7.21.

For the organisms *P. aeruginosa* and *A. baumannii* a similar trend can be noted; both show growth at the MIC level and to two dilutions below the MIC level, however the *A. baumannii* is seen to grow to a higher OD_L/OD_C compared to *P. aeruginosa* indicating the organism is able to recover more effectively from the bacteriostasis, Table 7.8.

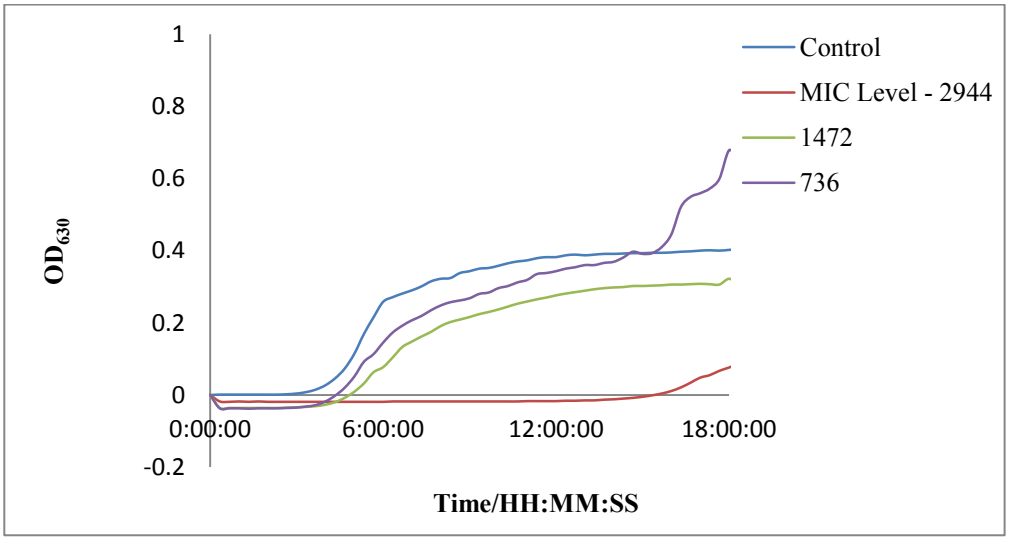

Figure 7.21 OD_{630} development over 18 hours for TREN-R-3,2-HOPO (**6.12**) on *E. coli* (MIC = 2944μM). Values displayed in legend are given as micromolar (μM) concentrations.

B. subtilis displayed issues similar to that of *E. coli* and after around 15 hours the data was no longer viable to extract useful information (see Appendix). However, some information regarding the lag time and OD_{630} levels reached for the dilutions below the MIC value (1472μM) can be obtained and is therefore displayed in Table 7.8. *C. albicans* showed no growth at the MIC or at dilutions below this level over the assay time period.

Table 7.8 Summary of the lag time at concentrations of ligand which showed growth and the observed difference in OD_{630} for those organisms that displayed growth for the TREN-R-3,2-HOPO (**6.12**) ligand. $^{a}OD_L/OD_C = OD_{630}$ with the ligand at the corresponding concentration/OD_{630} of the control sample.

Organism	Concentration /μM	MIC/μM	Extended Lag time/ approximate hours	Final Control OD_{630}	Final Ligand OD_{630}	Ratio $^{a}OD_L/OD_C$
E. coli	2944	2944	12	0.41	0.14	0.34
	1472		1		0.30	0.73
	736		0		0.39	0.95
P. aeruginosa	2944	2944	7	0.86	0.19	0.22
	1472		3		0.38	0.44
	736		0		0.57	0.66
A. baumannii	368	368	6	0.55	0.28	0.51
	184		2		0.39	0.71
	92		2		0.47	0.85
B. subtilis	736	1472	6	0.53	0.12	0.23
	368		0		0.26	0.49

7.5.9 Assessment of the effect of the TRENCAM (6.16) Ligand on the growth of microbes: *E. coli, K. pneumoniae, P. aeruginosa, A. baumannii* and *B. subtilis*

The TRENCAM ligand when applied to *E. coli* in the kinetic assay showed a different result for the MIC concentrations with respect to the MIC assays performed previously. At the predetermined MIC level (964μM) we can see in Figure 7.22 that growth is apparent at the MIC level, and at the two concentrations below this. At these lower concentrations the OD_{630} exceeds that of the control, indicating a possible growth promoting mode of action of the compound. This for *E. coli* is not surprising as the organism has the capability to interact and utilise catecholate based ligands i.e.

enterobactin and this may be the cause of the lack of inhibition. The concentrations above the determined MIC show some inhibition for this organism with a lag time of ~9 hours for the highest concentration of ligand before growth is noted. The lack of inhibition and the observed difference in the MIC value could be a result of the stimulation to growth which occurs when the solutions are agitated however, further work is required to confirm this wherever this phenomenon has been noted.

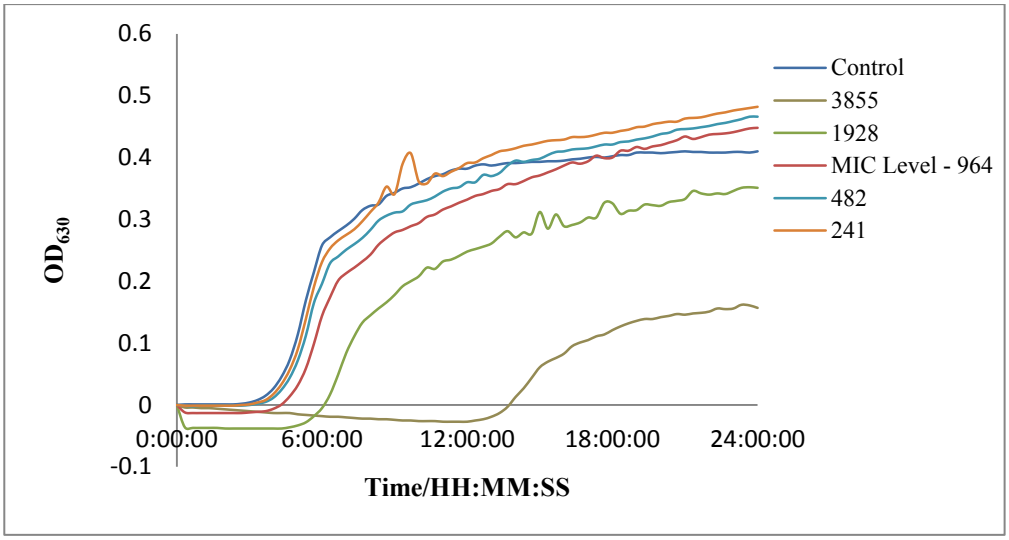

Figure 7.22 OD_{630} development over 24 hours for TRENCAM (**6.16**) on *E. coli* (MIC = 964μM). Values displayed in legend are given as micromolar (μM) concentrations.

The organism *K. pneumoniae* displayed similar results as those for *E. coli* in that growth was noted at the MIC level to the same OD_{630} as the control sample, though the same observed levels of the control OD_{630} were noted only in the case of the lowest concentration (241μM).

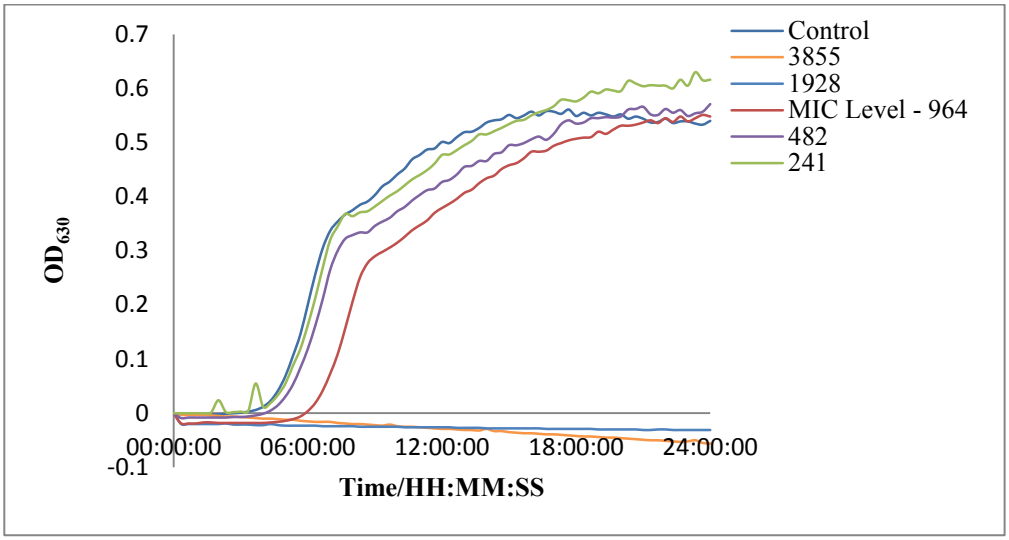

Figure 7.23 OD_{630} development over 24 hours for TRENCAM (**6.16**) on *K. pneumoniae* (MIC = 964µM). Values displayed in legend are given as micromolar (µM) concentrations.

P. aeruginosa displayed growth to a concentration one dilution above the predetermined MIC level (1928µM) however; the growth was diminished with respect to the control OD_{630} reached, Table 7.9. *B. subtilis* displayed growth at the MIC level but remained totally inhibited above this concentration; the levels of growth in this case did not exceed that of the control as have been discussed previously for *E. coli* and *K. pneumoniae* with TRENCAM. This may indicate the inability of *B. subtilis* to utilise the synthetic chelator as a siderophore. A lag time of around 7 hours could be noted at the MIC level for *A. baumannii*, Table 7.9.

At an assay time point above ~18 hours the results of the *B. subtilis* OD_{630} reading were deemed unsuitable to extract viable data from. However, up until this time point it can be noted that *B. subtilis* showed growth at the MIC level with a lag time of around 7 hours with respect to the growth of the control. The other concentrations below this level also showed lag times, but not to this extent and in addition the final level of OD_{630} reached in all cases where growth was noted was nearing that of the control. This indicates that any inhibition is being overcome by the organism within the timeframe of the experiment, Table 7.9.

Table 7.9 Summary of the apparent lag time at concentrations of ligand which showed growth and the observed difference in OD_{630} for those organisms that displayed growth for the TRENCAM (**6.16**) ligand. [a]$OD_L/OD_C = OD_{630}$ with the ligand at the corresponding concentration/OD_{630} of the control sample.

Organism	Concentration /µM	MIC/µM	Extended Lag time/ approximate hours	Final Control OD_{630}	Final Ligand OD_{630}	Ratio [a]OD_L/OD_C
E. coli	3855	1928	7	0.41	0.16	0.39
	1928		2		0.35	0.85
	964		0		0.46	1.12
	482		0		0.48	1.17
	241		0		0.48	1.17
K. pneumoniae	964	964	2	0.54	0.55	1.01
	482		0		0.55	1.01
	241		0		0.62	1.15
P. aeruginosa	1928	1928	0	0.86	0.34	0.40
	964		0		0.62	0.72
	482		0		0.48	0.56
	241		0		0.58	0.67
A. baumannii	1928	1928	7	0.55	0.23	0.42
	964		0		0.36	0.65
	482		0		0.43	0.78
B. subtilis	1928	1928	7	0.31	0.30	0.97
	964		3		0.31	1.0
	482		3		0.31	1.0

7.5.10 Assessment of the effect of the EMECAM (1.32) Ligand on the Growth of Microbes: *E. coli, K. pneumoniae, P. aeruginosa, A. baumannii* and *B. subtilis*

At the MIC concentration (3855µM) for the organism *E. coli* the ligand EMECAM appeared inhibitory with a growth lag time of approximately 7 hours. At this level the final OD_L/OD_C was 0.46 indicating the culture reached only around half of the OD_{630} as the growth control. At the concentrations below the MIC (1928 and 964µM) the growth of the culture reach the same levels as the control, however did display some lag in the initial growth start time. Data shown in Figure 7.24

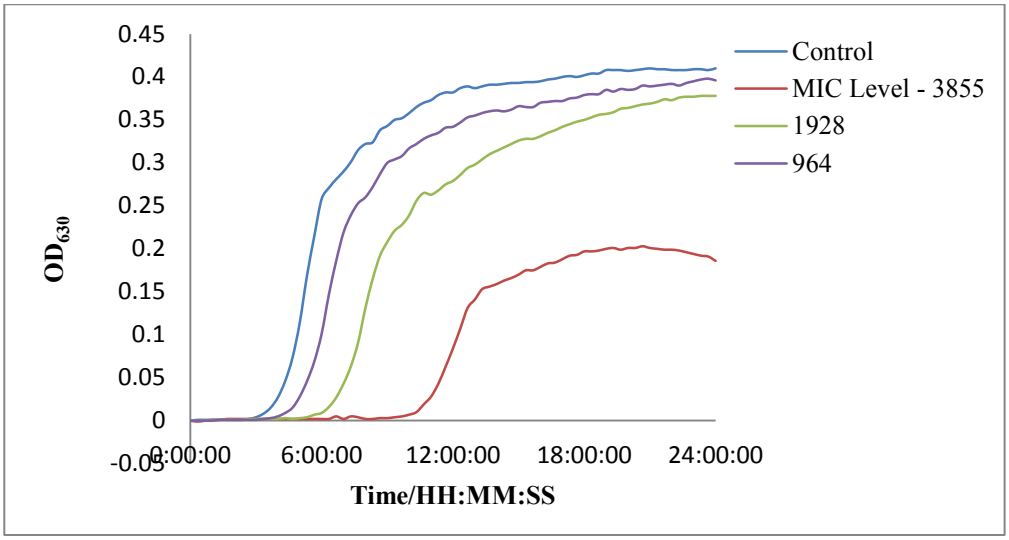

Figure 7.24 OD_{630} development over 24 hours for EMECAM (**1.32**) on *E. coli* (MIC = 3855µM). Values displayed in legend are given as micromolar (µM) concentrations.

The *E. coli* organism has been shown to utilise catecholate based siderophores within its natural iron regulatory systems i.e. enterobactin and so it is not surprising that the EMECAM compound may not produce a profound inhibitory effect on this organism at low concentration. At the MIC it may be that the compound is toxic and below this level it is able to be utilised or is not a strong enough ligand to disturb the growth cycle significantly of *E. coli*.

As displayed in Table 7.10, the organism *K. pneumoniae* displayed full inhibition by the EMECAM ligand at the MIC concentration (1928µM) however below this level the organism displayed virtually no distortion with respect to the growth control. No lag time was observed and the OD_{630} was shown to equal that of the control, with possible evidence of growth of a promoted effect at 964µM. *P. aeruginosa* showed a similar trend to *K. pneumoniae* however; at even at the MIC level an OD_L/OD_C value of 0.66 was calculated for this organism. Both *P. aeruginosa* and *K. pneumoniae* have been shown to able to utilise catecholate siderophores (see 7.1.1) which may be the cause of their lack of lag time and ability to show measureable growth at the MIC concentration in the case of *P. aeruginosa* and to show virtually no inhibition below the MIC for *K. pneumoniae*.

The organism *A. baumannii* displays a relatively prolonged lag time in its growth at the MIC level with respect to the control of 15 hours for EMECAM (1928µM) and only reaches an OD_{630} of around 13% of that of the control. However, below this level no lag time is noted and the growth of the organism is relatively uninhibited with respect to the control, Figure 7.25.

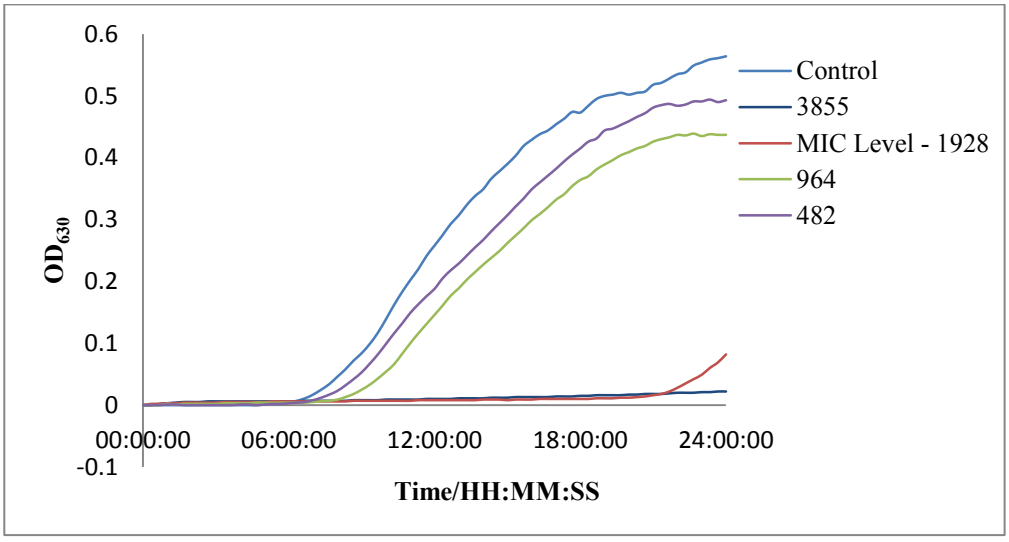

Figure 7.25 OD_{630} development over 24 hours for EMECAM (**1.32**) on *A. baumannii* (MIC = 1928µM). Values displayed in legend are given as micromolar (µM) concentrations.

More promisingly, the organism *B. subtilis* displayed measureable lag times at the MIC (1928µM) and at the two concentrations below this level of around 2 hours. Though at the two concentrations

below the MIC the growth of the organism was more pronounced (OD_L/OD_C = 0.62) the control OD_{630} was never reached, Table 7.10. Though some growth was detected at the concentration above the MIC (3855μM) the level of OD_{630} reached was significantly reduced with respect to the control and so may have been undetectable by eye. Measurements for *B. subtilis* were taken after 14 hours as above this the data was deemed unusable, full data set is available in the Appendix.

Table 7.10 Summary of the apparent lag time at concentrations of ligand which showed growth and the observed difference in OD_{630} for those organisms that displayed growth for the EMECAM (**1.32**) ligand. [a]$OD_L/OD_C = OD_{630}$ with the ligand at the corresponding concentration/OD_{630} of the control sample.

Organism	Concentration /μM	MIC/μM	Extended Lag time/ approximate hours	Final Control OD_{630}	Final Ligand OD_{630}	Ratio [a]OD_L/OD_C
E. coli	3855	3855	7	0.41	0.19	0.46
	1928		3		0.40	0.98
	964		1		0.41	1.0
K. pneumoniae	964	964	0	0.54	0.58	1.07
	482		0		0.5	0.93
P. aeruginosa	964	1928	0	0.86	0.57	0.66
	482		0		0.57	0.66
	241		0		0.57	0.66
A. baumannii	1928	1928	15	0.55	0.07	0.13
	964		0		0.44	0.8
	482		0		0.49	0.83
B. subtilis	3855	1928	7	0.53	0.08	0.15
	1928		4		0.24	0.45
	964		2		0.33	0.62
	482		2		0.33	0.62

7.6 Chapter Conclusions

The work presented herein has demonstrated the ability of a series of novel compounds to inhibit the growth of microorganisms. The compounds were designed to be strong Fe^{3+} ligands and this is the proposed mode of action for the inhibition, though further study is required to fully assess the mode of inhibition.

The ligands CTG-1,2-HOPO, TEB-1,2-HOPO and TEB-R-3,2-HOPO consistently inhibit across a diverse panel of microbes tested. This broad spectrum inhibition defines these three compounds as the most promising candidates for application in the reduction of nosocomial infections. Further study of their efficacy in authentic surface colonisation assays is required. Likewise, bactericidal rate determination is required to confirm their mode of action.

A. baumannii appears to be particularly susceptible to the inhibition of growth with respect to the induction of an extended lag time from the normal growth. This is particularly pronounced at the MIC level but does in some cases extend to below this level (CTG-3,2-HOPO and TREN-R-3,2-HOPO).

Some ligands show signs of growth promotion in the kinetic assays such as the CTG-3,2-HOPO ligand on the organisms *P. aeruginosa* and *S. aureus* at concentrations 964μM and <120μM respectively. Further work is required to assess whether this is the case and to what extent the growth promotion effect can be induced to determine an iron transport route.

7.7 Future Work

Future work in this area would be to confirm the mode of action of the compound which showed inhibition. This could be achieved through radiolabelled uptake studies determining what portion of the available iron remained bound to the ligands in the extracellular matrix. This technique would also be useful in confirming the possible growth promotion which has been noted in some assays.

In addition, any ligands showing promotion and recovery of the culture OD_{630} to that of the control could be used in purified receptor-ligand assays to determine by what system they are being utilised if this is the mode of action. Alternatively, utilising a panel of modified microbes with various siderophore receptor systems modified may aid in the elucidation of any inhibition and promotion modes of action.

7.8 Project Summary

The project was carried out to discover whether core molecular scaffolds, that have both previously been associated and new scaffolds that have not been associated with Fe^{3+} binding, could be synthesised to have incorporated hydroxypyridinone binding groups onto them. The purpose of this being to produce powerful Fe^{3+} ligands. There are many applications for ligands of this type which include; potential antimalarial drugs, anti-Alzheimer's drugs and MRI contrast agents. However, for the purposes of this study the bacteriostatic properties of the ligands has been assessed. The ligands when applied to a microbial system should restrict the available nutrient Fe^{3+} available to the organisms and induce a distortion to growth. This distortion should be in the form of bacteriostasis, where the organisms, unable to feed are therefore unable to multiply to levels which may cause potential harm in the environment.

To test this hypothesis, ligands have been designed based upon cyclotriguiaicylene (CTG), tris(piperazin-1-yl)-1,3,5-triazine, 1,3,5-tris(aminomethyl)-2,4,6-triethyl benzene (TEB) and the tris(2-aminoethyl)amine (TREN) core molecular scaffolds, with attempted functionalization of the methyl cholate molecule. These core scaffolds were chosen for their unique properties (i) potentially preorganise the HOPO binding moieties towards Fe^{3+} chelation (ii) to be potentially 'alien' enough to avoid recognition in microorganism Fe^{3+} uptake (iii) be able to support three HOPO groups to allow for hexadentate ligands to be accessed.

HOPO groups have previously never been associated with the CTG or triazine cores. Functionalization of these cores has been achieved utilising a previously accessed 3,2-HOPO derivative and a novel 1,2-HOPO-chloride which has been developed in house. This functionalization has produced ligands which have variation in: chain length, HOPO group, core size and attachment mode (ether and tertiary amine).

These property variations have impacted upon the outcomes of the ligands abilities to bind Fe^{3+}, as determined via UV-Vis spectroscopy. The triazine-based ligands have shown that where in the first instance if allowed to equilibrate for only two days, the stoichiometry for the 1,2-HOPO and the 3,2-HOPO based ligands was approximately the same. However, after fourteen days the

triazine-3,2-HOPO ligand showed that it was able to accommodate a 1:1 L:M stoichiometry, which was the preferred outcome. However, this was not the case for the triazine-1,2-HOPO ligand and this was attributed primarily to the shorter connecting chain between core scaffold and binding group. Whereas for the CTG based ligands it was discovered through the same technique that in the first instance the 3,2-HOPO containing ligand showed a clear 1:1 L:M stoichiometry after two days which was retained for the fourteen day test period. Conversely, the CTG-1,2-HOPO ligand in the first instance showed signs, such as was shown for the triazine-1,2-HOPO, the stoichiometry favoured more ligands per metal centre, which could be indicative that the shorter chain linker was effecting the ability of the ligand to bind Fe^{3+} in the preferred 1:1 ratio. However, after the test period it was discovered that the CTG-1,2-HOPO ligand appeared to be able to accommodate more than one metal into the most stable complex formula, as determined via modified Job's plot analysis. This phenomenon has been attributed to the previous literature surrounding the ability of the CTG scaffold to accommodate small cationic guests into the molecular cavity.

The library of TEB-based ligands, of which five have been produced all displayed similar characteristics in terms of Fe^{3+} binding as determined by UV-Vis spectroscopy. With the exception of the 3,4-HOPO bearing ligand whose stoichiometry after the test period was 0.6:0.4 L:M, which may be attributed to previous literature precedent surrounding the position of attachment of the scaffold to the binding moiety, all the ligand showed their preference for a 1:1 L:M stoichiometry. Previously, only one example of a HOPO has been shown for a TEB core scaffold, which includes the retro-3,2-HOPO binding moiety. In light of this, this work has extended the range of ligands for Fe^{3+} binding available for this core significantly. The novel ligands include variations in chain length and HOPO isomer.

Furthermore, the ligands produced herein have added to the range of TREN-based technology currently available. Previous to this study, the CP130 ligand had been shown to bind Fe^{3+} in a 1:1 ratio, however, the pFe^{3+} indicates that this binding is not perfect and so the LC-CP130 produced herein may help to alleviate some of the strain and increase the potential to bind Fe^{3+} with greater affinity. The previous TREN-Me-3,2-HOPO containing ligand has also been modified to include an extra methyl group on the binding moiety in the *para*-position to the binding hydroxyl

functionality. It is hoped that this may increase the binding affinity through induction of electron density through the hydroxyl functionality.

The novel ligands and some literature examples were assessed for their bacteriostatic activities in two ways; firstly, MIC values have been deduced from dilution assays to gather an overview of the chelators' performance with respect to each other and the literature examples. Secondly, kinetic assays have been performed to attempt to further asses the properties of these ligands and to discover any preliminary evidence for their use as bacteriostatic agents.

Of the fourteen synthesised ligands only three showed no measurable activity on any of the microbes tested. The other all showed some activity on at least one organism. The inhibition to growth doesn't seem to be biased towards a particular core scaffold, which may mean the ligands are working as designed, by binding extracellular Fe^{3+}. Those of particular significance are the CTG-1,2-HOPO, TEB-1,2-HOPO and TEB-R-3,2-HOPO which inhibited growth at relatively low concentrations across the panel of microbes. In addition the TREN-1,2-HOPO* literature ligand has shown strong activity.[128] Implicating that there may be an activity-HOPO relationship in which the R-3,2-HOPO and the 1,2-HOPO are important functionalities for ligands for strong growth inhibition.

Since the conditions provided to the microorganisms in the assays here were suited for growth i.e. nutrient rich media, the concentrations required here to inhibit the growth of organisms do not reflect those which may be necessary for inhibition on a surface. Surfaces do not have a rich nutrient supply and so it may be the case that far less of the compounds are needed to inhibit growth in a 'real life' situation. That being so, the ligands' which showed inhibition >500μM and were not flagged as being particularly good in MIC assays may still prove to be successful at inhibiting growth on a surface. The CTG-3,2-HOPO and TREN-R-3,2-HOPO showed appreciable inhibition of many of the panel members and so, they could provide targets along with the three previously highlighted to take through to a real testing situation.

Kinetic assays have provided a positive insight into the ligands ability to perturb the growth of organisms with respect to their normal growth profile. Many of the ligands could be seen to elongate the time period before detectable growth could be measured by OD. This property of the

molecules is of particular interest due to the implications for prolonging a disinfection timeframe. This apparent elongation of the growth lag time could be indicative of the mode of action of these ligands being bacteriostatic in nature.

The next stage in the development of these molecules is to confirm their mode of action of growth inhibition as bacteriostasis. This could be achieved through viable colony count analysis; this information, coupled with the acquired kinetic data should provide a good insight into the inhibition mechanism of these compounds. In addition, the realistic testing of the ligands to give similar results in terms of the inhibition of growth on surfaces should be analysed. This can be achieved through applying the ligands onto surfaces and to see how they are able to affect the growth of organisms in a situation more akin to that which you would find in a hospital environment.

The Fe^{3+} binding affinities for these compounds are still yet to be assessed in as far as the determination of their logβ or pFe^{3+} values is concerned. This information would help to provide an insight into whether the inhibitory efficacy of the compounds is linked to their respective binding affinities or whether it is purely a matter of ligand architecture which is the cause of the inhibitory effect i.e. are the 1,2-HOPO and R-3,2-HOPO binding moieties required for strong inhibition for these ligands? Despite this evidence, the library of chelators produced here have provided lead ligand candidates to take through to further testing whose action of growth inhibition on the microorganisms discussed herein is believed to be bacteriostasis induced by Fe^{3+} nutrient restriction.

8 Experimental

8.1 Materials and Methods

All solvents and reagents were purchased from Sigma-Aldrich, Acros Organics or Alfa-Aeser and used without further purification, unless otherwise specified. Reactions were followed by TLC using silica gel with UV_{254} fluorescent indicator. Column chromatography was conducted using 0.060 - 0.20 mm silica gel (70 - 230 mesh), automated flash column chromatography was conducted using a Biotage Isolera One ISO-1SV.

8.2 General physical measurements

NMR spectra were recorded using a Jeol JNM Ex270 instrument at 270 MHz and 68 MHz or a Jeol JNM-ECS400 instrument at 400 MHz and 100 MHz, as specified, for ^{1}H- and ^{13}C- NMR respectively. ^{1}H NMR data are reported as follows: chemical shift (δ, ppm), multiplicity (s = singlet, d = doublet, t =triplet, q = quartet, m = multiplet, br = broad), integration, coupling constants reported in Hz. Data for ^{13}C NMR are reported in terms of chemical shift (δ, ppm). UV/Visible spectra were run on a Varian Cary 50 UV-Visible spectrophotometer (range 600-200nm), using a 10mm quartz cell at room temperature (20°C). Infrared spectra were obtained using a Durascope diamond ATR system on a Perkin Elmer RX1 FTIR spectrometer. Positive and negative electrospray ionisation mass spectrometry (ESI-MS) was conducted using a Thermo LCQ Advantage spectrometer by direct injection and high resolution mass spectrometry (HRMS) was performed by the EPSRC National Mass Spectrometry Service (Swansea, Wales). Melting points were taken on a SRS DigiMelt MPA161 digital melting point apparatus (200 to 250 VAC 1/2AMP 50-60Hz). Samples were read in SAMCO soda glass capillary tubes 100mm and are reported uncorrected. Optical density measurements were performed on a Synergy^{TM}HT Multi-Detection Automated Microplate Reader from Bio-TEK® using greiner bio-one CELLSTAR® 96 well sterile culture plates. Compound names were generated via the Reaxys programme online as the preferred IUPAC name unless simplified as designated in the text.

8.3 Determination of L:M Stoichiometry

The UV-Vis spectra were measured for the L:M ratios displayed in Table (Table 8.1) over the range 600-200nm. The overall volume of solutions was kept constant as was the total molar concentration of species in solution.

Table 8.1 Table displaying ratios of ligand and metal recorded in UV-Vis experiments. Solutions made in distilled H_2O using the minimum volume DMSO to solvate ligand. $FeCl_3.6H_2O$ used as iron source. Spectra were recorded over the range 200-600nm at room temperature.

Solution	[Ligand]/μM	[Metal]/μM	[Ligand]/[Ligand]+[Metal]
1	200	0	1
2	180	20	0.9
3	160	40	0.8
4	140	60	0.7
5	120	80	0.6
6	100	100	0.5
7	80	120	0.4
8	60	140	0.3
9	40	160	0.2
10	20	180	0.1
11	0	200	0

The obtained UV-Vis spectra were then subject to analysis following literature procedure. The absorbance of the resulting complex obtained at the λ_{max} in the visible region (~430nm) was corrected by taking the observed absorbance and removing the percentage contributions for the free ligand and free metal in solution to leave the absorbance of the complex ($A-A_M-A_L$). This was plotted against [Ligand]/[Ligand]+[Metal] to give a modified Job's plot of which the highest point of absorbance is then taken to be the stoichiometric ratio for the species.

8.3.1 Experimental CTG Molecules

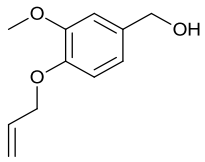

[3-methoxy-4-(prop-2-en-1-yloxy)phenyl]methanol

(2.7): Vanillyl alcohol (5.00g, 32.4mmol) and K_2CO_3 (4.50g, 32.5mmol) were stirred in acetone (30mL). Allyl bromide (4.50g, 37.19mmol) was added dropwise to the stirring suspension, after addition the reaction was allowed to reflux at 70°C for 18 hours. The solution was cooled to room temperature and the solvent and excess allyl bromide removed under high vacuum. Distilled H_2O (100mL) was added and the aqueous solution extracted with DCM (5 x 50mL). The organic extracts were combined and dried ($MgSO_4$), evaporated to dryness and left to dry in air. Upon cooling a yellow-green solid crystallised from the yellow oil. This yielded the pure product in 93% yield (5.83g). ^{1}H NMR ($CDCl_3$) δ (ppm) = 6.91 (s, 1H) 6.83 (s,2H) 6.12-5.99 (m, 1H) 5.38 (dd, $^3J_1$ = 17.4Hz $^3J_2$ = 1.4Hz) 5.28 (dd, $^3J_1$ = 10.5Hz $^3J_2$ = 1.4Hz) 4.60 (s, 2H) 4.59 (s, 2H) 3.86 (s, 3H) 1.70 (t, ^{3}J = 6Hz, 1H); ^{13}C NMR ($CDCl_3$) δ (ppm) = 149.59, 147.53, 134.04, 133.35, 119.34, 118.10, 69.99, 65.31, 55.95.

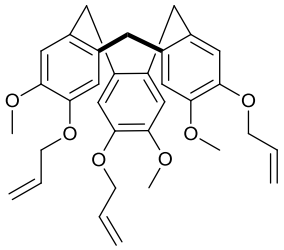

Tris-allyl-CTG

(2.8): (2.7) (5.95g, 0.03mol) was dissolved in MeOH (38mL) and stirred at 0°C. 70% $HClO_4$ solution (18.5mL) was added dropwise to the stirring solution which was allowed to stir at room temperature for 48 hours. (After 3 hours a white solid precipitated out of the pink solution). DCM (100mL) was added and the product extracted into DCM (2 x 100mL). The organic extracts were washed with distilled H_2O (~ 1L) to ensure no residual was $HClO_4$ present. The DCM extract was

dried ($MgSO_4$) and evaporated to dryness. Ether (50mL) was added and the product allowed to precipitate fully overnight. The precipitate was collected by suction filtration to yield a light pink solid in 38% yield (2.05g). ^1H NMR ($CDCl_3$) δ (ppm) = 6.84 (s, 3H) 6.78 (s, 3H) 6.04 (m, 3H) 5.36 (dd, $^3J_1$ = 17.4Hz, $^3J_2$ = 1.4Hz, 3H) 5.23 (dd, $^3J_1$ = 10.5Hz, $^3J_2$ = 1.4Hz, 3H) 4.72 (d, ^3J = 13.7Hz, 3H) 4.58 (m, 6H) 3.82 (s, 9H) 3.52 (d, ^3J = 13.7Hz, 3H); ^{13}C NMR ($CDCl_3$) δ (ppm) = 148.23, 146.78, 133.79, 132.37, 131.78117.62, 115.54, 70.24, 56.16, 36.61

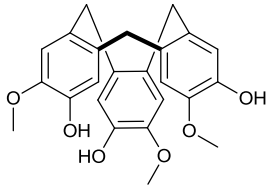

CTG

Cyclotriguaiacylene (2.2): (2.7) (1.00g, 1.89mmol) was dissolved in dry dioxane (8mL) at 50°C under a nitrogen atmosphere. EtOH (18mL), Pd/C (0.20g) and 70% $HClO_4$ (0.20mL) were added under a nitrogen atmosphere and the reaction stirred at 57-60°C for 24 hours. The reaction was allowed to cool to room temperature and the catalyst removed by filtration and washed with DCM (40mL). The organic solution was washed with distilled H_2O (5 x 100mL), dried ($MgSO_4$) and evaporated to dryness yielding a white solid in 37% yield (0.29g). Mp = >260°C ^1H NMR (DMSO-d_6) δ (ppm) = 6.80 (s, 3H) 6.78 (s, 3H) 4.54 (d, ^3J = 13.2Hz, 3H) 3.67 (s, 9H) 3.31 (d, ^3J = 13.7Hz, 3H); ^{13}C NMR (DMSO-d_6) δ (ppm) = 146.5, 145.4, 133.1, 131.0, 117.3, 114.4, 56.5, 36.6

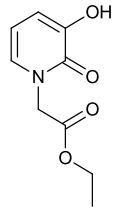

ethyl 2-(3-hydroxy-2-oxo-1,2-dihydropyridin-1-yl)acetate

(**2.10**) 2,3-dihydroxy pyridine (20.35g, 0.1832mol) and ethyl bromoacetate (101.6mL, 0.9159mol) were refluxed at 155-160°C for 48 hours. The solution was left to cool in a water-ice bath, until a grey-brown solid precipitated. The solid was collected by suction filtration, the filtrate evaporated and cooled again and any further precipitate collected. The solid was washed with ice-cold acetone

(50mL) and ice-cold distilled water (50mL). Recrystallisation from hot ethanol:H_2O 95:5 yielded product in 50% yield (18.29g). Mp = 151-153°C. ^{1}H NMR (DMSO-d_6) δ (ppm) = 6.84 (dd, $^3J_1$ = 7.17Hz, $^3J_2$ = 1.73Hz, 1H) 6.77 (dd, $^3J_1$ = 6.93Hz, $^3J_2$ = 1.73Hz, 1H) 6.20 (t, ^3J = 7.17Hz, 1H) 4.26 (q, ^3J = 7.17Hz, 2H) 1.30 (t, ^3J = 7.17Hz, 3H) ^{13}C NMR (DMSO-d_6) δ (ppm) = 168.20, 158.06, 146.84, 129.03, 115.51, 105.37, 61.12, 50.48, 14.22

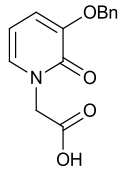

2-[3-(benzyloxy)-2-oxo-1,2-dihydropyridin-1-yl]acetic acid

(2.11): (2.10) (3.88g, 0.01967mol) was dissolved in $MeOH_{aq}$ (120mL, 90%) at 50°C with stirring. The solution was adjusted to ~ pH 12 with $NaOH_{aq}$ (4M). Benzyl bromide (10mL, 0.08407mol) was added drop wise to the stirring solution and the solution refluxed for 8 hours at 90-100°C. The solution was allowed to cool to room temperature, and MeOH was removed by rotary evaporation. The aqueous solution was washed with DCM (3 x 50mL) and the aqueous phase diluted with distilled H_2O (30mL). The solution was acidified to pH 1 with HCl_{aq} (37% w/v) whereupon a solid precipitated. The solid was collected via suction filtration and recrystallised from hot EtOH:H_2O 95:5 to yield fluffy white crytals, 4.02g (78%). Mp = 182-187°C. ^{1}H NMR (DMSO-d_6) δ (ppm) = 7.38 (m, 5H) 7.24 (dd, , $^3J_1$ = 6.9 Hz, $^3J_2$ = 1.2 Hz, 1H) 6.92 (dd, , $^3J_1$ = 7.6 Hz, $^3J_2$ = 1.5 Hz, 1H) 5.00 (s, 2H) 4.6 (s, 2H); ^{13}C NMR (DMSO-d_6) δ (ppm) = 169.94, 157.60, 148.41, 137.01, 131.25, 128.95, 128.53, 128.48, 116.22, 104.35, 70.27, 50.74

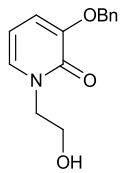

3-(benzyloxy)-1-(2-hydroxyethyl)-1,2-dihydropyridin-2-one

(2.12): (2.11) (1.96g, 7.56mmol) was suspended in dry THF (25mL) under $N_{2(g)}$ and cooled in an ice-water bath for 30mins. $BH_{3(THF)}$ (1M in THF, 30mL) was added to the cooled suspension under

$N_{2(g)}$ over 10 minutes and the solution allowed to stir at room temperature for 24 hours. After 24 hours a further addition of $BH_{3(THF)}$ (1M in THF, 12mL) was made and stirring continued for 4 days. The reaction was cooled to 0°C and quenched with ice. The aqueous solution was extracted with DCM(3 x 100mL), dried ($MgSO_4$) filtered and the DCM removed by rotary evaporation to yield pure product in 78% yield (1.46g). ^{1}H NMR ($CDCl_3$) δ (ppm) = 7.33 (m, 5H) 6.93 (dd, , $^3J_1$ = 6.8 Hz, $^3J_2$ = 1.3 Hz, 1H) 6.64 (dd, , $^3J_1$ = 7.3 Hz, $^3J_2$ = 1.4 Hz, 1H) 5.03 (s, 2H) 4.00 (t, ^3J = 5.0 Hz, 2H) 3.69 (m, 2H). ^{13}C NMR ($CDCl_3$) δ (ppm) = 158.9, 148.7, 136.1, 130.2, 128.7, 127.4, 115.9, 105.0, 70.8, 61.3, 53.2

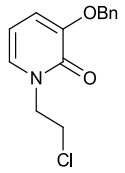

3-(benzyloxy)-1-(2-chloroethyl)-1,2-dihydropyridin-2-one

(2.13): (2.12) (0.77g, 3.13mmol) was dissolved in dry DCM(50mL), to this solution tosyl chloride (0.77g, 4.02mmol) and triethyl amine (1.20mL 9.16mmol) were added, the solution was allowed to stir at room temperature for 36 hours. DCM (100mL) was added and the resulting solution was washed with saturated sodium carbonate solution (3 x 50mL) and brine (50mL), dried ($MgSO_4$) and evaporated to dryness to yield a yellow oil 0.92g which solidified on standing. The crude oil was purified by column chromatography over silica gel, eluting with ethyl acetate:DCM 1:1 increasing polarity to 5% MeOH after elution of first impurity. The purified product was isolated after column fractions were dried ($MgSO_4$) and evaporated to dryness to yield a yellow oil of mass 0.67g (81%) which solidified on standing. R_f = 0.54. ^{1}H NMR ($CDCl_3$) δ (ppm) 7.38 (m, 5H) 6.94 (dd, , $^3J_1$ = 6.8 Hz, $^3J_2$ = 1.8 Hz, 1H) 6.67 (dd, , $^3J_1$ = 7.3 Hz, $^3J_2$ = 1.8 Hz, 1H) 6.02 (t, ^3J = 6.8 Hz, 1H) 5.1 (s, 2H) 4.23 (t, ^3J = 5.5 Hz, 2H) 3.89 (t, ^3J = 5.9 Hz, 2H). ^{13}C NMR ($CDCl_3$) δ (ppm) = 158.1, 148.7, 136.2, 130.3, 128.7, 128.1, 127.4, 115.8, 104.5, 71.2, 53.5, 52.4, 46.4, 42.0

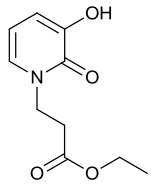

ethyl 3-(3-hydroxy-2-oxo-1,2-dihydropyridin-1-yl)propanoate

(**2.14**): 2,3-dihydroxy pyridine (5.00g, 0.045mol) was added along with CsF (10mol %) to acetonitrile (40mL). Ethyl acrylate (4.51g, 0.045mol) was added and the mixture allowed to reflux for 48 hours at 90°C. The solution was cooled to room temperature and acidified to pH 1 with HCl_{aq} (37% w/v) and distilled H_2O (200mL) added. The product was extracted into DCM (200mL), the DCM extracts washed with distilled H_2O (4 x 100mL), brine (1 x 20mL), dried ($MgSO_4$) and evaporated to dryness. The product was isolated pure as a brown solid, 6.44g (72%). Mp = 92-98°C. ^{1}H NMR ($CDCl_3$) δ (ppm) = 6.9 (dd, , $^3J_1$ = 6.9 Hz, $^3J_2$ = 1.7 Hz, 1H) 6.74 (dd, , $^3J_1$ = 7.1 Hz, $^3J_2$ = 1.7 Hz, 1H) 6.06 (t, ^3J = 6.8 Hz, 1H) 4.18 (t, ^3J = 6.4 Hz, 2H) 4.06 (q, ^3J = 7.1 Hz, 2H) 2.78 (t, ^3J = 6.4 Hz, 2H) 1.16 (t, ^3J = 7.0 Hz, 3H); ^{13}C NMR ($CDCl_3$) δ (ppm) = 169.94, 157.60, 148.41, 137.01, 131.25, 128.95, 128.53, 128.48, 116.22, 104.35, 70.27, 50.76

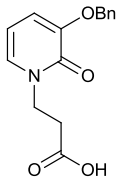

3-[3-(benzyloxy)-2-oxo-1,2-dihydropyridin-1-yl]propanoic acid

(2.15): (2.14) (5.00g, 0.0236mol) was dissolved in $MeOH_{aq}$ (90%, 130mL) and adjusted to pH 12 with $NaOH_{aq}$ (4M). Benzyl bromide (12.41g, 0.071mol) was added dropwise and the solution allowed to reflux for 48 hours at 75-80°C, the pH being kept above pH 10 with $NaOH_{aq}$ (4M). The solution was cooled to room temperature and the methanol and excess benzyl bromide removed by rotary evaporation. The aqueous solution was extracted with DCM (4 x 100mL) and diluted with distilled H_2O (30mL). Acidification with HCl_{aq} (37% w/v) yielded a yellow precipitate which was collected by suction filtration to yield the product in 75% yield (6.14g). Mp = 182-187°C. ^{1}H NMR (DMSO-d_6) δ (ppm) = 7.39 (m, 5H) 7.26 (dd, $^3J_1$ = 6.9 Hz, $^3J_2$ = 1.5 Hz, 1H) 6.89 (dd, $^3J_1$ =

7.4 Hz, $^3J_2$ = 1.5 Hz, 1H) 6.10 Hz (t, ^3J = 6.9 Hz, 1H) 4.99 (s, 2H) 4.06 (t, ^3J = 6.9 Hz, 2H) 2.64 (t, ^3J = 6.9 Hz, 2H); ^{13}C NMR (DMSO-d_6) δ (ppm) = 172.94, 157.32, 148.54, 137.17, 130.99, 128.97, 128.51, 120.74, 111.56, 104.50, 70.32, 45.90, 33.47

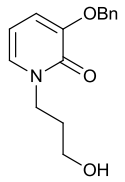

3-(benzyloxy)-1-(3-hydroxypropyl)-1,2-dihydropyridin-2-one

(2.16): (2.15) (4.97g, 0.0181mol) was suspended in dry THF (100mL) under an atmosphere of nitrogen, stirred and cooled to 0°C. To this, $BH_{3(THF)}$ (1M in THF, 90mL) was added under nitrogen and the solution was allowed to stir at room temperature for 48 hours. The solution was cooled to 0°C and quenched with ice. The product was extracted into DCM (5 x 100mL), the extracts washed with distilled H2O (4 x 250mL), brine (250mL), dried ($MgSO_4$), filtered and evaporated to dryness to yield a viscous purple liquid of mass 3.07g. Crude product purified by column chromatography over silica gel eluent DCM:ethyl acetate 1:1 increasing polarity to 10% MeOH after R_f >0.2 eluted. Yielding pure product in 31% yield (1.49g) R_f = 0.10. ^1H NMR ($CDCl_3$) δ (ppm) = 7.30 (m, 5H) 6.84 (dd, $^3J_1$ = 6.9 Hz, $^3J_2$ = 1.7 Hz, 1H) 6.62 (dd, $^3J_1$ = 7.6 Hz, $^3J_2$ = 1.5 Hz, 1H) 6.00 (t, ^3J = 6.9 Hz, 1H) 5.04 (s, 2H) 4.08 (t, ^3J = 5.9 Hz, 1H) 3.42 (q, ^3J = 5.7Hz, 2H) 1.83 (p, ^3J = 5.7 Hz, 2H); ^{13}C NMR ($CDCl_3$) δ (ppm) = 158.99, 148.64, 136.12, 128.96, 128.67, 128.15, 127.44, 116.07, 106.02, 70.87, 57.69, 45.93, 32.38

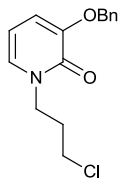

3-(benzyloxy)-1-(3-chloropropyl)-1,2-dihydropyridin-2-one

(i) **(2.17): (2.16)** (1.49g, 5.768mmol) was dissolved in dry DCM (50mL) to this triethyl amine (2.41mL, 0.0173mol) and tosyl chloride (1.43g, 7.498mmol) were added and the

solution allowed stirring at room temperature for 4 days. Solution was diluted with DCM (50mL) washed with saturated sodium carbonate solution (2 x 100mL) and brine (50mL). Organic extracts were dried ($MgSO_4$) and evaporated to give a red-brown oil. Crude product purified by column chromatography eluted with DCM:ethyl acetate 1:1 over silica gel to yield pure product as a red-brown solid 0.84g (52%), R_f = 0.634. mp = 72-74°C

(ii) **(2.17): (2.16)** (0.2717g, 1.01mmol) was dissolved in dry DCM (15mL) and the solution stirred at 0°C. $SOCl_2$ (0.74g, 6.88mmol) was added and the solution allowed to reflux at 50°C overnight. The reaction was quenched with ice water, extracted into DCM (150mL), washed with saturated sodium carbonate solution (100mL), dried ($MgSO_4$) and evaporated to dryness to yield the product in near quantitative yield. ^1H NMR ($CDCl_3$) δ (ppm) = 7.30 (m, 5H) 6.89 (dd, $^3J_1$ = 6.9 Hz, $^3J_2$ = 1.7 Hz, 1H) 6.59 (dd, $^3J_1$ = 7.4 Hz, $^3J_2$ = 1.7 Hz, 1H) 5.97 (t, ^3J = 6.9 Hz, 1H) 5.03 (s, 2H) 4.06 (t, ^3J = 6.4 Hz, 2H) 3.47 (t, ^3J = 5.9 Hz, 2H) 2.20 (p, (t, ^3J = 6.4 Hz, 2H). ^{13}C NMR ($CDCl_3$) δ (ppm) = 158.22, 149.01, 136.29, 129.48, 128.64, 128.07, 127.39, 115.62, 104.66, 70.84, 47.67, 41.99, 30.91

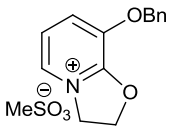

Iminium salt

(2.21): (2.12) (1.38g, 5.62 x 10^{-3}mol) was dissolved in dry DCM (30mL) and added under $N_{2(g)}$ to a flame dried 3n-round bottomed flask under $N_{2(g)}$. Et_3N (1.14g,11.25mmol) was added and the solution brought to 0°C in an ice-water bath and stirred for 10 mins. Mesyl anhydride (1.47g,835mmol) was added as a solution in dry DCM (10mL) dropwise to the stirring solution. Stirring was maintained at 0°C for 1 hour and then at room temperature for 1.5 hours. The DCM was removed by rotary evaporation, $CHCl_3$ (50mL) was added and the reaction stirred for 17 hours at room temperature. The chloroform was evaporated and the residue was triturated with EtOAc (6 x 80mL) which was decanted from the solid formed. The product was obtained as a yellow powder

mass = 1.54g (85%). ^{1}H NMR ($CDCl_3$) δ (ppm) = 8.50 (d, ^{3}J = 6.41Hz, 1H), 7.67 (d, ^{3}J = 8.24Hz, 1H), 7.35 (m, 6H) 5.40 (t, ^{3}J = 9.16, 2H) 5.25 (s, 2H) 5.22 (t, ^{3}J = 9.16Hz, 2H) 2.67 (s, 3H). ^{13}C NMR ($CDCl_3$) δ (ppm) = 153.88, 142.93, 133.92, 130.18, 129.20, 129.10, 127.92, 127.77, 119.77, 77.32, 72.62, 72.11, 39.54.

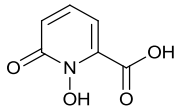

1-hydroxy-6-oxo-1,6-dihydropyridine-2-carboxylic acid

(**2.24**): 6-hydroxypyridine-2-carboxylic acid (20.0g, 0.1437mol) was suspended in glacial acetic acid (240mL). 36-40% wt% peracetic acid (70mL) was added dropwise to the suspension over 15 minutes with stirring. Once addition was complete the reaction was heated from 22°C to 80°C in 10°C increments. Stirring was maintained at 80°C for 12 hours. The reaction was allowed to cool to room temperature, forming a fine yellow precipitate. The precipitate was collected via suction filtration and washed with ether to give 16.28g of the product (73%). ^{1}H NMR (DMSO-d_6) δ (ppm) = 7.39 (dd, $^{3}J_1$ = 6.9 Hz $^{3}J_2$ = 8.7 Hz, 1H) 6.66 (dd, $^{3}J_1$ = 1.8 Hz $^{3}J_2$ = 9.2 Hz, 1H) 6.60 (dd, $^{3}J_1$ = 1.8 Hz $^{3}J_2$ = 6.9 Hz, 1H); ^{13}C NMR (DMSO-d_6) δ (ppm) = 162.5, 157.7, 139.4, 137.2, 120.9, 106.7

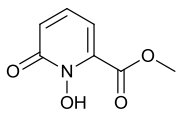

methyl 1-hydroxy-6-oxo-1,6-dihydropyridine-2-carboxylate

(**2.25**): **2.24** (16.28g, 0.1049mol) was suspended in MeOH (600mL) and allowed to stir at 0°C. To this $SOCl_2$ (20mL, 0.274mol) was added dropwise over 15 minutes, after addition the reaction was allowed to stir for 4 days at room temperature. The reaction was evaporated to dryness and co-evaporated twice with toluene to yield the product as a brown solid mass = 17.13g (96%). Mp = 102-111°C^{1}H NMR (DMSO-d_6) δ (ppm) = 7.39 (dd, $^{3}J_1$ = 6.9 Hz $^{3}J_2$ = 9.1 Hz, 1H) 6.64 (dd, $^{3}J_1$ =

1.4 Hz $^3J_2$ = 9.1 Hz, 1H) 6.48 (dd, $^3J_1$ = 1.8 Hz $^3J_2$ = 6.9 Hz, 1H) 3.82 (s, 3H); ^{13}C NMR (DMSO-d_6) δ (ppm) = 161.4, 158.1, 138.8, 137.8, 122.6, 105.8, 53.8

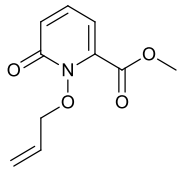

6-oxo-1-(prop-2-en-1-yloxy)-1,6-dihydropyridine-2-carboxylic acid

(**2.26**): To a suspension of methyl **2.25** (17.03g, 0.1007mol) in MeCN (250mL) was added K_2CO_3 (30.61g, 0.2215mol). To this, allyl bromide (20mL, 0.2215mol) was added and the reaction stirred at room temperature for 4 days. The reaction was filtered and the filtrate evaporated under reduced pressure. Co-evaporation with toluene (2 x 100mL) yielded the pure product mass = 20.84g (98%).^{1}H NMR (DMSO-d_6) δ (ppm) = 7.26 (m, 1H) 6.75 (dt, $^3J_1$ = 1.8 Hz $^3J_2$ = 9.1 Hz, 1H) 6.47 (dt, $^3J_1$ = 1.4 Hz $^3J_2$ = 6.9 Hz, 1H) 6.03 (m, 1H) 5.41 (dt, $^3J_1$ = 1.4 Hz $^3J_2$ = 17.4 Hz, 1H) 5.32 (d, ^3J = 10.1 Hz, 1H) 4.85 (d, ^3J = 6.4 Hz, 2H) 3.89 (s, 3H) ^{13}C NMR (DMSO-d_6) δ (ppm) = 160.4, 158.8, 138.7, 137.2, 130.6, 125.9, 121.9, 107.9, 78.0, 53.3

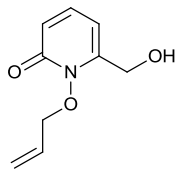

6-(hydroxymethyl)-1-(prop-2-en-1-yloxy)-1,2-dihydropyridin-2-one

(**2.27**): **2.26** (18.8g, 0.0898mol) was suspended in THF (500mL), to which, $NaBH_4$ (25.5g, 0.674mol) was added and the mixture brought to reflux for 15 minutes. At reflux MeOH (150mL) was added portionwise (CAUTION! VIOLENT BUBBLING) over six hours. The reaction was allowed to stir at reflux for a further hour and after was allowed to cool to room temperature before being placed in an ice-water bath and cooled to 0°C. Slow addition of saturated ammonium acetate solution was used to quench the reaction and the THF was mostly removed by rotary evaporation. The aqueous solution was extracted with DCM (5 x 200mL), the extracts dried ($MgSO_4$) and evaporated to dryness to yield the crude product. The pure product was obtained after purification

via silica gel column chromatography DCM:MeOH (0-4%) to give a white solid of mass = 7.49g (41%). Mp = 100-103°C ^{1}H NMR ($CDCl_3$) δ (ppm) = 7.28 (dd, $^{3}J_1$ = 6.9 Hz $^{3}J_2$ = 9.2 Hz, 1H) 6.56 (dd, $^{3}J_1$ = 1.8 Hz $^{3}J_2$ = 9.2 Hz, 1H) 6.24 (dd, $^{3}J_1$ = 0.9 Hz $^{3}J_2$ = 6.9 Hz, 1H) 6.03 (m, 1H) 5.42 (dd, $^{3}J_1$ = 0.9 Hz $^{3}J_2$ = 16.9 Hz, 1H) 5.36 (dd, $^{3}J_1$ = 1.4 Hz $^{3}J_2$ = 10.1 Hz, 1H) 4.8 (d, ^{3}J = 6.4, 2H) 4.66 (d, ^{3}J = 6.4, 2H) 2.99 (t, ^{3}J = 6.9 Hz, 1H); ^{13}C NMR ($CDCl_3$) δ (ppm) = 159.4, 148.4, 138.4, 130.2, 122.3, 120.8, 103.3, 59.7

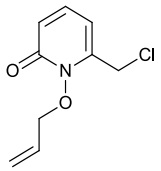

6-(chloromethyl)-1-(prop-2-en-1-yloxy)-1,2-dihydropyridin-2-one

(**2.28**): **2.27** (5.00g, 0.02759mol) was dissolved in DCM (150mL) and cooled to 0°C in an ice-water bath. $SOCl_2$ (12mL, 0.16557mol) was added dropwise to the solution and the reaction allowed to reflux for 18 hours. After which time a further addition of $SOCl_2$ (1mL, 0.0138mol) was made and reflux continued for a further three hours. The reaction was quenched with ice water at 0°C and then partitioned between DCM (100mL) and H_2O (100mL). The aqueous phase was extracted with DCM (2 x 100mL) and the DCM washed with H_2O (50mL) and brine (50mL), dried ($MgSO_4$) and evaporated to dryness. The product was dissolved in boiling DCM with activated charcoal and filtered hot. The DCM dried ($MgSO_4$) and evaporated to dryness to yield the pure product as an orange solid mass = 4.49g (81%). Mp = 61-65°C. ^{1}H NMR ($CDCl_3$) δ (ppm) = 7.25 (dd, $^{3}J_1$ = 6.9 Hz $^{3}J_2$ = 9.2 Hz, 1H) 6.65 (dd, $^{3}J_1$ = 1.8 Hz $^{3}J_2$ = 9.6 Hz, 1H) 6.23 (dd, $^{3}J_1$ = 1.4 Hz $^{3}J_2$ = 6.9 Hz, 1H) 6.09 (m, 1H) 5.48 (dd, $^{3}J_1$ = 1.4 Hz $^{3}J_2$ = 17.4 Hz, 1H) 5.39 (d, ^{3}J = 10.1 Hz, 1H) 4.90 (d, ^{3}J = 6.9 Hz, 2H) 4.55 (s, 2H); ^{13}C NMR ($CDCl_3$) δ (ppm) = 159.3, 144.3, 137.8, 130.3, 123.1, 122.5, 106.3, 77.5, 39.5

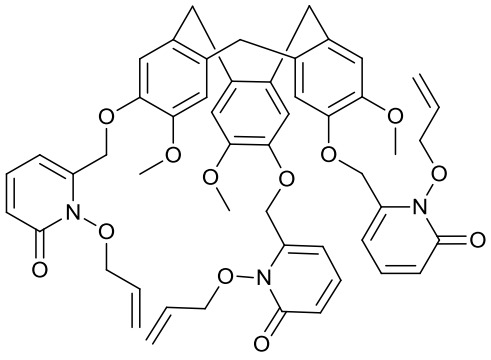

Tris-allyl-CTG-1,2-HOPO

(**2.29**): CTG (0.20g, 4.896 x 10^{-4}mol) was suspended in MeCN (20mL) under $N_{2(g)}$ atmosphere at room temperature. To this Cs_2CO_3 (0.16g, 4.91 x 10^{-4}mol) was added and the two stirred at room temperature for 15 minutes. After which time, 6-(chloromethyl)-1-(prop-2-en-1-yloxy)-1,2-dihydropyridin-2-one (0.29, 1.469 x 10^{-3}mol) was dissolved in MeCN (10mL) and added under $N_{2(g)}$ to the stirring solution. The reaction was stirred at reflux for 72 hours and then allowed to cool to room temperature, filtered and the filtrate evaporated to dryness. The residue was taken up in DCM (25mL) and then washed with distilled H_2O (4 x 25mL), dried $MgSO_4$ and the organic phase evaporated to dryness. Purification completed on a Isolera automated column, Biotage SNAP 50g silica cartridge DCM:MeOH (0-5%). To yield a light brown solid mass = 0.35g (79%) after purification (R_f = 0.6 DCM:MeOH 10%). Mp = 95-102° C; ^{1}H NMR ($CDCl_3$) δ (ppm) = 7.22 (m, 3H) 6.81 (s, 3H) 6.73 (s, 3H) 6.58 (d, ^{3}J = 9.1Hz, 3H) 6.22 (d, ^{3}J = 6.87Hz, 3H) 5.98 (m, 3H) 5.33 (m, 6H) 5.05 (dd, $^3J_1$ = 40.3Hz $^3J_2$ = 10.9Hz, 6H) 4.83 (m, 6H) 4.17 (d, ^{3}J = 13.7Hz, 3H) 3.73 (s, 9H) 3.49 (d, ^{3}J = 13.7 Hz, 3H); ^{13}C NMR ($CDCl_3$) δ (ppm) = 159.3, 148.8, 146.1, 144.8, 138.2, 133.9, 131.7, 130.4, 122.6, 121.5, 116.8, 113.8, 104.2, 77.2, 66.1, 56.1, 36.5; HRMS (ESI) *m/z* $[M+H]^+$: calcd for $C_{51}H_{52}N_3O_{12}^+$, 898.3551; found, 898.3543.

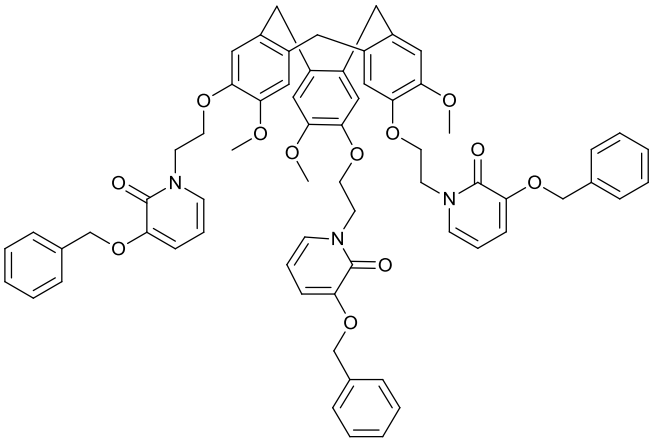

CTG-Bn_3-3,2-HOPO

(**2.18**): CTG (0.25g, 6.12 x 10^{-4} mol) and iminium salt (0.61g, 323.3613mol) along with Cs_2CO_3 (1.0g, 3.06mmol) were added to dry MeCN (40mL) under $N_{2(g)}$ and the reaction allowed to reflux for 24 hours. After which time a further addition of iminium salt (80mg, 2.45 x 10^{-4}mol) was made under $N_{2(g)}$ and the reaction stirred again for 24 hours. The reaction was filtered and the

filtrate evaporated to dryness. Purification was performed on an Isolera automated column 100g SNAP silica cartridge DCM:MeOH (0-10%). To yield a yellow solid mass = 0.62g (93%) after purification. Mp = 82-94°C. ^{1}H NMR ($CDCl_3$) δ (ppm) = 7.35-7.26 (m, 15H) 7.02 (dd, $^{3}J_1$ = 1.8Hz, $^{3}J_2$ = 6.9Hz, 3H) 6.98 (s, 3H) 6.92 (s, 3H) 6.63 (dd, $^{3}J_1$ = 1.8Hz, $^{3}J_2$ = 7.8Hz, 3H) 5.97 (t, ^{3}J = 6.9Hz, 3H) 5.09 (s, 6H) 4.68 (d, ^{3}J = 13.7Hz, 3H) 4.30 (m, 12H) 3.75 (s, 9H) 3.52 (d, ^{3}J = 13.7Hz, 3H)^{13}C NMR ($CDCl_3$) δ (ppm) = 158.2, 148.8, 148.2, 146.3, 136.5, 132.9, 131.9, 130.4, 128.7, 128.1, 127.6, 115.6, 115.3, 113.9, 104.3, 70.8, 66.7, 56.4, 49.3, 36.4; HRMS (ESI) *m/z* $[M+H]^+$: calcd for $C_{66}H_{64}N_3O_{12}^+$, 1090.4490; found, 1090.4486.

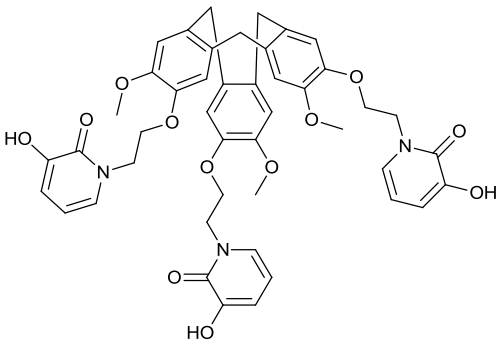

CTG-3,2-HOPO

(**2.22**): **2.18** (120mg, 1.1x10^{-4}mol) was hydrogenated over Pd/C (15% wt) with HCl (cat.) in dioxane:H_2O (4:1, 5mL) for 18 hours at 40°C. After filtration of the catalyst and evaporation of the solvent the residue was stirred in HCl:AcOH (1:1, 10mL) for 4 days at room temperature. The reaction was evaporated to dryness to yield the product in 12% yield (11mg). ^{1}H NMR (DMSO) δ (ppm) = 7.12 (m, 6H) 7.06 (s, 3H) 6.67 (dd, $^{3}J_1$ = 1.37Hz, $^{3}J_2$ = 7.33Hz, 3H) 6.04 (t, ^{3}J = 6.87Hz, 3H) 4.62 (d, ^{3}J = 13.28Hz, 3H) 3.59 (s, 9H) 3.42 (d, ^{3}J = 13.28Hz, 3H) ^{13}C NMR (DMSO) δ (ppm) = 158.37, 148.05, 147.19, 146.51, 133.26, 132.59, 129.47, 115.69, 115.47, 114.72, 105.56, 66.72, 56.53, 49.10, 48.59, 35.51; HRMS (ESI) *m/z* $[M+Na]^+$: calcd for $C_{45}H_{45}N_3NaO_{12}^+$, 842.2901; found, 842.2899.

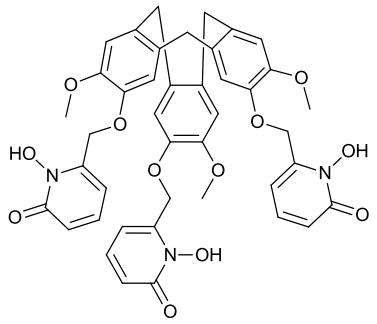

CTG-1,2-HOPO

(**2.30**): **2.29** (105mg, 1.169 x10^{-4}mol) was stirred in dioxane:H_2O (4:1, 8mL) with TFA (0.15M) in solution. Pd/C (15% wt) was added and the reaction allowed to stir at reflux for 18 hours. After which time the catalyst was filtered and washed with dioxane. The filtrate was evaporated to dryness to yield a solid mass = 80mg (87%). ^{1}H NMR (DMSO) δ (ppm) = 7.29 (dd,$^{3}J_1$ = 6.87Hz, $^{3}J_2$ = 8.7Hz, 3H) 7.16 (s, 3H) 7.03 (s, 3H) 6.13 (d, ^{3}J = 7.79, 3H) 6.21 (d, ^{3}J = 6.41Hz, 3H) 5.06 (m, 6H) ^{13}C NMR (DMSO) δ (ppm) = 161.31, 146.28, 137.66, 117.57, 116.01, 114.46, 103.04, 64.99, 64.45, 56.44, 35.49; HRMS (ESI) *m/z* $[M+Na]^+$: calcd for $C_{42}H_{39}N_3NaO_{12}^+$, 800.2431; found, 800.2391

8.3.2 Experimental 1,3,5-tris(aminomethyl)-2,4,6-triethylbenzene molecules

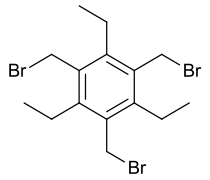

1,3,5-tris(bromomethyl)-2,4,6-triethylbenzene

(**3.8**): To a mixture of paraformaldehyde (8.40g, 0.279mol) and 1,3,5-triethylbenzene (5mL, 26.55mmol) in HBr:Acetic acid (~33% w/v), $ZnBr_2$ (10.0g, 0.044mol) was added portionwise at room temperature. The mixture was heated to 90°C for 18 hours, during which time a white crystalline precipitate formed. The reaction was allowed to cool to room temperature before the precipitate was collected via suction filtration and washed with distilled H_2O. The solid was dried in a desiccator to yield a pink solid mass = 8.78g (74%). Mp = 169-173°C ^{1}H NMR ($CDCl_3$) δ (ppm) = 4.57 (s, 6H) 2.95 (q, ^{3}J = 7.79 Hz, 6H) 1.34 (t, ^{3}J = 7.79 Hz, 9H) ^{13}C NMR ($CDCl_3$) δ (ppm) = 145.28, 132.73, 28.66, 22.84, 15.72

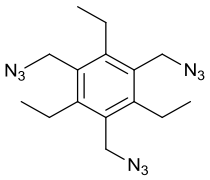

1,3,5-tris(azidomethyl)-2,4,6-triethylbenzene

(**3.10**): 1,3,5-tris(bromomethyl)-2,4,6-triethylbenzene (6.0g, 0.0136mol) was dissolved in DMF (100mL)under an atmosphere of $N_{2(g)}$, to which NaN_3 (4.0g, 0.0612mol) was added and the reaction portion-wise over 10 minutes. The reaction was allowed to stir at room temperature for three days after which time DCM (500mL) was added and the resultant solution washed with distilled H_2O (5 x 500mL). The DCM portion was dried ($MgSO_4$), filtered and evaporated to dryness to yield a viscous oil of mass = 2.06g (45%). ^{1}H NMR ($CDCl_3$) δ (ppm) = 4.48 (s, 6H) 2.86 (q, ^{3}J = 7.79 Hz, 6H) 1.24 (t, ^{3}J = 7.79 Hz, 9H) ^{13}C NMR ($CDCl_3$) δ (ppm) =145.05,130.07, 48.01, 23.26, 15.85

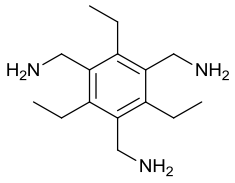

1,3,5-tris(aminomethyl)-2,4,6-triethylbenzene

(**3.11**): To 1,3,5-tris(azidomethyl)-2,4,6-triethylbenzene (2.06g, 6.292mmol) and Ph_3P (11.08g, 0.0422mol) in THF (50mL) was added distilled H_2O (2mL). Stirring was continued overnight at room temperature. The THF was removed by rotary evaporation and the aqueous solution partitioned between DCM (100mL) and $HCl_{(aq)}$ (6m, 100mL). The organic portion was extracted with $HCl_{(aq)}$ (3 x 100mL). The aqueous extracts were combined and brought to pH 14 with $NaOH_{(s)}$ pellets. The basic solution was then extracted with DCM (3 x 200mL), the DCM dried ($MgSO_4$) and then evaporated by rotary evaporation giving a brown solid. Mp = 131-136°C.^{1}H NMR ($CDCl_3$) δ (ppm) = 3.86 (s, 6H) 2.82 (q, ^{3}J = 7.79 Hz, 6H) 1.23 (t, ^{3}J = 7.33 Hz, 9H) ^{13}C NMR ($CDCl_3$) δ (ppm) = 141.45, 135.94, 38.54, 22.62, 16.29

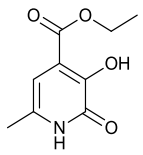

ethyl 3-hydroxy-6-methyl-2-oxo-1,2-dihydropyridine-4-carboxylate (15)

(**3.12**): Sodium diethyloxy acetate (10.0g, 0.0475mol) was dissolved in THF (170mL). Chloroacetone (4.4g, 0.0475mol) was added at room temperature and the reaction stirred for 15 mins. Ammonium acetate (10.0, 0.129mol) was added and $AlCl_3$ (0.64g) was added in portions to the stirring solution. Stirring was maintained at room temperature for 12 days, after which time a brown-yellow precipitate was collected via suction filtration. The precipitate was then stirred in HCl_{aq} (1M) pH ~2 for 1.5 hours and the solid collected via suction filtration. The product was isolated as a bright yellow solid in 43% yield (4.10g). Mp = 230-233°C. ^{1}H NMR (DMSO-d_6) δ

(ppm) = 6.05 (s, 1H) 4.21 (q, ^{3}J = 7.3 Hz, 2H) 2.05 (s, 3H) 1.24 (t, ^{3}J = 7.3 Hz, 3H). ^{13}C NMR (DMSO-d_6) δ (ppm) = 166.54, 159.16, 147.75, 132.70, 116.29, 102.10, 61.49, 18.56, 14.52

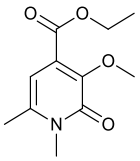

ethyl 3-methoxy-1,6-dimethyl-2-oxo-1,2-dihydropyridine-4-carboxylate (16)

(**3.13**): To **3.12** (0.157g, 0.792mmol) in DMF (10mL) was added K_2CO_3 (0.274g, 1.98mmol) and iodomethane (1.12g, 7.89mmol), the mixture was stirred at room temperature for 24 hours, after which time the reaction was concentrated under vacuum and partitioned between DCM (20mL) and H_2O (20mL). The aqueous phase was extracted with DCM (5 x 20mL), the organic extracts were combined, dried ($MgSO_4$) and evaporated to dryness to give the crude product. ^{1}H NMR ($CDCl_3$) δ (ppm) = 6.14 (s, 1H) 4.29 (q, ^{3}J = 6.9 Hz, 2H) 3.90 (s, 3H) 3.49 (s, 3H) 2.28 (s, 3H) 1.32 (t, ^{3}J = 6.8 Hz, 2H)

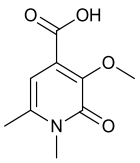

3-methoxy-1,6-dimethyl-2-oxo-1,2-dihydropyridine-4-carboxylic acid (17)

(**3.14**): Crude **3.13** was dissolved in MeOH (120mL), $NaOH_{aq}$ (4M, 120mL) was added and the reaction was allowed to stir at reflux for 48 hours. The MeOH was reduced under reduced pressure and HCl_{aq} (3M) was used to adjust the pH to 1. The solution was extracted with EtOAc (2 x 100mL), dried ($MgSO_4$) and the solvent removed under reduced pressure to give a crude product which was recrystallised from EtOAc to yield a tan solid (1.68g, 50%) mp = 206-211°C. ^{1}H NMR (DMSO-d_6) δ (ppm) = 6.32 (s, 1H) 3.83 (s, 3H) 3.54 (s, 3H) 2.37 (s, 3H)

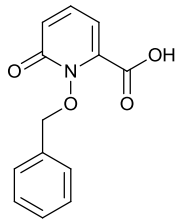

1-(benzyloxy)-6-oxo-1,6-dihydropyridine-2-carboxylic acid

(**3.15**): **2.24** (2.45g, 0.0158mol) and K_2CO_3 (4.36g, 0.0315mol) were added with benzyl bromide (3.24g, 0.01895mol) into MeOH (100mL). The reagents were refluxed for three days (colour change from white-green-brown). The reaction was allowed to cool to room temperature and evaporated to dryness. The residue was taken into H_2O (100mL), the aqueous solution brought to pH 2 with 37% $HCl_{(aq)}$. Upon acidification a white precipitate formed which was collected via suction filtration and washed with distilled H_2O. The wet product was dried overnight in a desiccator to yield a beige solid of mass = 3.42g (88%). Mp = 180-183°C ^{1}H NMR (DMSO-d_6) δ (ppm) = 7.41 (m, 6H) 6.70 (dd, $^3J_1$ = 0.9 Hz $^3J_2$ = 9.2 Hz, 1H) 6.52 (dd, $^3J_1$ = 1.4 Hz $^3J_2$ = 6.9 Hz, 1H) 5.24 (s, 2H). ^{13}C NMR (DMSO-d_6) δ (ppm) = 162.3, 158.2, 141.0, 139.2, 134.3, 130.1, 129.6, 129.0, 124.6, 106.6, 78.3

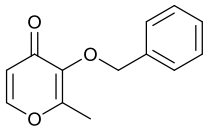

3-(benzyloxy)-2-methyl-4H-pyran-4-one

(**3.17**): Maltol (40g, 0.317mol) was added to MeOH (400mL) with stirring, to which $NaOH_{aq}$ (16g in 50mL H_2O) was added whereupon addition the maltol dissolved. The solution was brought to reflux before BnBr (54.25g, 0.317mol) was added drop wise over 15 mins. Reflux was continued overnight before the solution was cooled, the MeOH removed by rotary evaporation and H_2O (200mL) added. The aqueous solution was extracted with DCM (3 x 200mL) and the extracts washed with 5% $NaOH_{aq}$ (2 x 250mL), H_2O (2 x 300mL) and brine (200mL). The organic phase was dried ($MgSO_4$) and the solvent evaporated to leave an orange oil mass = 59.30g (86.5%). ^{1}H NMR ($CDCl_3$) δ (ppm) = 7.57 (d, ^3J = 5.5Hz, 1H) 7.33 (m, 5H) 6.34 (d, ^3J = 5.5Hz, 1H) 5.14 (s,

2H) 2.06 (s, 3H). ^{13}C NMR ($CDCl_3$) δ (ppm) = 175.16, 159.80, 153.53, 143.85, 136.95, 129.11, 128.51, 128.40, 117.25, 73.62, 14.88.

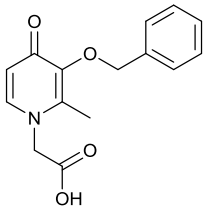

2-[3-(benzyloxy)-2-methyl-4-oxo-1,4-dihydropyridin-1-yl]acetic acid

(**3.18**) **3.17** (4.10g, 0.01896mol) was suspended in EtOH:H_2O 1:1 (34mL) to which sodium glycinate (4.15g, 0.03602mol) was added and the solution brought to reflux for 18hours. The reaction was acidified with 37% HCl_{aq} to pH~1 and stored at 0°C overnight. The solid formed was filtered and stirred in boiling H_2O to which MeOH was added until cloudy. The solution was cooled to 0°C and the precipitate filtered to yield a solid mass = 3.21g, 65%. ^{1}H NMR (MeOD-d_4) δ (ppm) = 7.88 (d, ^{3}J = 7.33Hz, 1H) 7.49 (m, 5H) 6.47 (d, ^{3}J = 7.33Hz, 1H) 5.20 (s, 2H) 4.95 (s, 2H) 2.27 (s, 3H). ^{13}C NMR (MeOD-d_4) δ (ppm) = 172.23, 169.30, 145.83, 145.26, 141.49, 137.02, 128.97, 115.21, 73.85, 55.49, 11.82

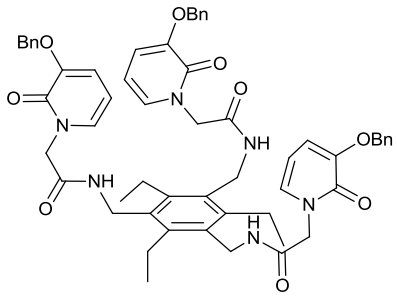

Tris-benzyl-TEB-SC-3,2-HOPO

(**3.19**): **2.11** (0.31g, 1.20mmol) and TBTU (0.39g, 1.20mmol) were dissolved under $N_{2(g)}$ in dry DMF (10mL). N-methyl morpholine (0.20g, 1.97mmol) was added to the solution under $N_{2(g)}$ and the reaction stirred at room temperature for 30 minutes. After which time, [3,5-bis(aminomethyl)-2,4,6-triethylphenyl]methanamine (100mg, 0.38mmol) was added under $N_{2(g)}$, the reaction was stirred at room temperature for 2 hours and then at 60°C for 24 hours. The DMF was mostly removed under vacuum and the residue taken into DCM (50mL). The organic solution was washed

~5% HCl_{aq} (2 x 50mL), $NaOH_{aq}$ (5% w/v, 2 x 50mL), distilled H_2O (50mL) and brine (50mL). The organic portion was dried ($MgSO_4$), filtered and evaporated to dryness. The crude product was purified using Isolera automated column 100g SNAP silica cartridge DCM:MeOH (3-12%) to yield a light yellow solid mass =144mg, R_f = 0.53 DCM:MeOH (10%); ^{1}H NMR ($CDCl_3$) δ (ppm) = 7.30 (m, 15H) 6.94 (br d ^{3}J = 6.41Hz, 3H) 6.67 (br d, ^{3}J = 7.33Hz, 3H) 6.08 (^{3}J = 6.87Hz, 3H) 5.04 (s, 6H) 4.42 (br s, 6H) 4.37 (br s, 6H) 2.59 (br q, ^{3}J = 6.87Hz, 6H) 1.07 (br t, ^{3}J = 6.87Hz, 9H); ^{13}C NMR ($CDCl_3$) δ (ppm) = 166.75, 158.30, 148.68, 144.21, 136.11, 131.60, 129.83, 128.70, 128.22, 127.55, 116.22, 105.48, 77.32, 70.89, 38.14, 23.09, 16.35; HRMS (ESI) *m/z* $[M+H]^+$: calcd for $C_{57}H_{61}N_6O_9^+$, 973.4500; found, 973.4491

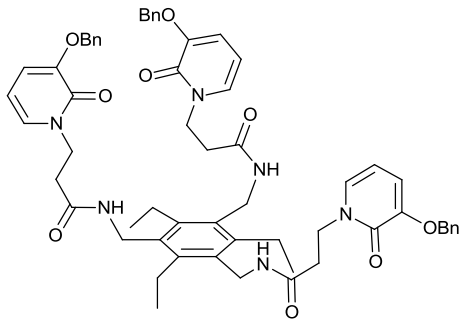

Tris-benzyl-TEB-LC-3,2-HOPO

(**3.20**): **2.15** (0.32g, 1.20mmol) and TBTU (0.39g, 1.20mmol) were dissolved under $N_{2(g)}$ in dry DMF (10mL). N-methyl morpholine (0.20g, 1.97mmol) was added to the solution under $N_{2(g)}$ and the reaction stirred at room temperature for 30 minutes. After which time, 1,3,5-tris(aminomethyl)-2,4,6-triethyl benzene (100mg, 0.38mmol) was added under $N_{2(g)}$, the reaction was stirred at room temperature for 2 hours and then at 60°C for 24 hours. The DMF was mostly removed under vacuum and the residue taken into DCM (50mL). The organic solution was washed ~5% HCl_{aq} (2 x 50mL), $NaOH_{aq}$ (5% w/v, 2 x 50mL), distilled H_2O (50mL) and brine (50mL). The organic portion was dried ($MgSO_4$), filtered and evaporated to dryness. The crude product was purified using Isolera automated column 100g SNAP silica cartridge DCM:MeOH (2-20%), to yield a yellow solid mass = 169mg. ^{1}H NMR ($CDCl_3$) δ (ppm) = 7.31 (m, 15H) 7.01 (br d, ^{3}J = 5.95Hz, 3H) 6.63 (d, ^{3}J = 6.41Hz, 6H) 6.00 (t, ^{3}J = 7.33Hz, 3H) 4.99 (s, 6H) 4.26 (d, ^{3}J = 3.21Hz, 6H) 4.04 (t, ^{3}J = 5.95Hz, 6H) 2.57 (t, ^{3}J = 5.95Hz, 6H) 2.45 (br q, ^{3}J = 7.33Hz, 6H) 1.00 (t, ^{3}J = 7.33Hz, 9H); ^{13}C NMR ($CDCl_3$) δ (ppm) = 169.73, 158.13, 148.64, 143.74, 136.12, 131.74, 130.08, 128.67,

128.20, 127.49, 115.98, 105.03, 70.85, 46.36, 37.90, 35.08, 23.08, 16.39; HRMS (ESI) *m/z* $[M+H]^+$: calcd for $C_{60}H_{67}N_6O_9^+$, 1015.4969; found, 1015.4958.

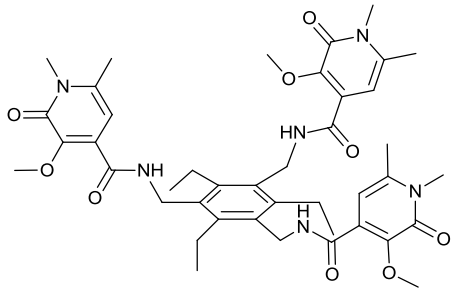

Tris-methoxy-TEB-R-3,2-HOPO

(**3.21**): **3.14** (0.23g, 1.155mmol) was added with TBTU (0.40g, 1.245mmol) and N-methylmorpholine (0.23g, 1.245mmol) to dry DMF (10mL) under $N_{2(g)}$. The reaction was stirred at room temperature for 20 minutes before 1,3,5-tris(aminomethyl)-2,4,6-triethyl benzene (0.10g, 3.85 x 10^{-4}mol) was added under $N_{2(g)}$ and the reaction allowed to stir at 60°C for 18 hours. The DMF was mostly removed via rotary evaporation and the residue was taken up into DCM (50mL). The organic solution was washed ~5% HCl_{aq} (2 x 50mL), $NaOH_{aq}$ (5% w/v, 2 x 50mL), distilled H_2O (50mL) and brine (50mL). The organic portion was dried ($MgSO_4$), filtered and evaporated to dryness. The crude product was purified using Isolera automated column 100g SNAP silica cartridge DCM:MeOH (2-20%), to yield a beige solid mass = 187mg (61%). ^{1}H NMR ($CDCl_3$) δ (ppm) = 7.87 (br t, ^{3}J = 3.66Hz, 3H) 6.61 (s, 3H) 4.64 (d, ^{3}J = 4.12Hz, 6H) 3.80 (s, 9H) 3.48 (s, 9H) 2.76 (p, ^{3}J = 4.12Hz, 6H) 2.32 (s, 9H) 1.20 (t, ^{3}J = 7.33Hz, 9H); ^{13}C NMR ($CDCl_3$) δ (ppm) = 163.28, 160.01, 144.91, 144.04, 140.46, 132.10, 129.20, 104.26, 59.95, 38.40, 31.86, 23.02, 20.70, 16.46; HRMS (ESI) *m/z* $[M+H]^+$: calcd for $C_{42}H_{55}N_6O_9^+$, 987.3031; found, 987.4020

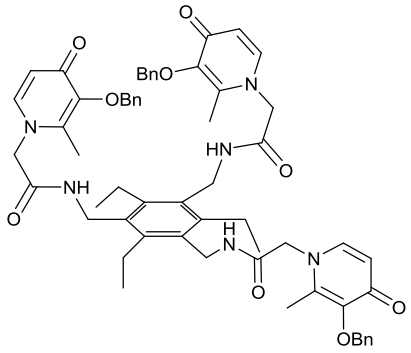

Tris-benzyl-TEB-3,4-HOPO

(**3.22**): **3.18** (0.66g, 2.41mmol) and TBTU (0.78g, 2.41mmol) were dissolved under $N_{2(g)}$ in dry DMF (20mL). N-methyl morpholine (0.41g, 4.01mmol) was added to the solution under $N_{2(g)}$ and the reaction stirred at room temperature for 30 minutes. After which time, 1,3,5-tris(aminomethyl)-2,4,6-triethyl benzene (200mg, 8.02mmol) was added under $N_{2(g)}$, the reaction was stirred at room temperature for 2 hours and then at 60°C for 24 hours. The DMF was mostly removed under vacuum and the residue taken into DCM (50mL). A solid was recovered which precipitated from DCM to yield the pure product in 82% yield (0.82g). ^{1}H NMR (DMSO-d_6) δ (ppm) = 8.50 (br s, 3H) 7.92 (d, ^{3}J = 6.87Hz, 3H) 7.40 (m, 15H) 6.69 (d, ^{3}J = 7.33Hz, 3H) 5.06 (s, 6H) 4.84 (s, 6H) 4.37 (s, 6H) 2.68 (br s, 6H) 2.17 (s, 9H) 1.11 (t, ^{3}J = 7.33Hz, 9H); ^{13}C NMR (DMSO-d_6) δ (ppm) = 165.71, 145.44, 144.11, 144.02, 142.60, 137.42, 131.92, 128.85, 128.70, 128.45, 114.44, 73.42, 56.48, 37.81, 22.83, 16.50, 12.94

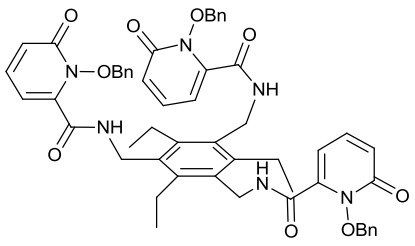

Tris-benzyl-TEB-1,2-HOPO

(**3.23**): **3.15** (0.29g, 1.20mmol) and TBTU (0.39g, 1.20mmol) were dissolved under $N_{2(g)}$ in dry DMF (10mL). N-methyl morpholine (0.20g, 1.97mmol) was added to the solution under $N_{2(g)}$ and the reaction stirred at room temperature for 30 minutes. After which time, 1,3,5-tris(aminomethyl)-2,4,6-triethyl benzene (100mg, 0.38mmol) was added under $N_{2(g)}$, the reaction was stirred at room temperature for 2 hours and then at 60°C for 24 hours. The DMF was mostly removed under

vacuum and the residue taken into DCM (50mL). The organic solution was washed ~5% HCl_{aq} (2 x 50mL), $NaOH_{aq}$ (5% w/v, 2 x 50mL), distilled H_2O (50mL) and brine (50mL). The organic portion was dried ($MgSO_4$), filtered and evaporated to dryness. The crude product was purified using Isolera automated column 100g SNAP silica cartridge DCM:MeOH (2-20%), to yield a solid mass = 222mg, R_f = 0.5 DCM:MeOH (10%). ^{1}H NMR ($CDCl_3$) δ (ppm) = 7.30 (m, 15H) 7.16 (dd, $^3J_1$ = 9.16Hz $^3J_2$ = 6.41Hz, 3H) 6.53 (d, ^3J = 1.83Hz, 3H) 6.50 (d, ^3J = 1.37Hz, 3H) 6.28 (dd, $^3J_1$ = 6.87Hz $^3J_2$ = 1.83Hz, 3H) 5.16 (s, 6H) 4.49 (d, ^3J = 4.12Hz, 6H) 2.45 (q, ^3J = 7.79Hz, 6H) 1.06 (t, ^3J = 7.33Hz, 9H); ^{13}C NMR ($CDCl_3$) δ (ppm) = 159.69, 158.34, 144.43, 141.90, 138.04, 133.10, 131.32, 130.30, 129.65, 128.61, 124.37, 106.33, 79.54, 38.35, 23.12, 16.38; HRMS (ESI) *m/z* $[M+H]^+$: calcd for $C_{54}H_{55}N_6O_9^+$, 931.4031; found, 931.4023

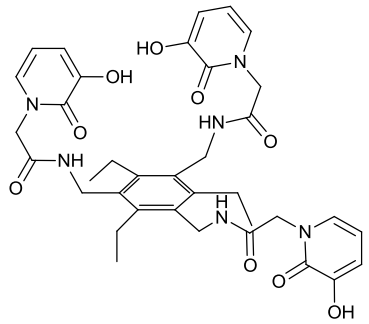

TEB-SC-3,2-HOPO

(**3.24**): **3.19** (144mg, 0.148mmol) was stirred at room temperature for 4 days and then 60°C for 4 days in 37% HCl:glacial acetic acid (1:1). The acids were removed by rotary evaporation and the product was precipitated from MeOH with diethyl ether to yield a hygroscopic solid mass = 65mg (35%). mp = >260°C ^{1}H NMR (DMSO-d_6) δ (ppm) = 8.36 (s, 3H)7.13 (td, $^3J_1$ = 6.87Hz, $^3J_2$ = 1.83Hz, 3H) 6.72 (td, $^3J_1$ = 7.33Hz, $^3J_2$ = 1.83Hz, 3H) (dt, $^3J_1$ = 10.53Hz, $^3J_2$ = 6.87Hz, 3H) 4.04 (d, ^3J = 5.04Hz, 6H) 3.68 (s, 6H) 2.78 (q, ^3J = 7.19Hz, 6H) 1.12 (t, ^3J = 7.33Hz, 9H); ^{13}C NMR (DMSO-d_6) δ (ppm) = 169.83, 169.12, 158.56, 147.27, 146.17, 129.53, 129.48, 129.37, 115.93, 115.67, 105.76, 105.49, 52.63, 50.73, 36.44, 23.85, 16.33; HRMS (ESI) *m/z* $[M+H]^+$: calcd for $C_{36}H_{43}N_6O_9^+$, 703.3092; found, 703.3086

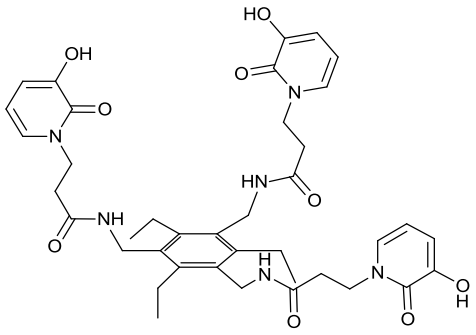

TEB-LC-3,2-HOPO

(**3.25**): **3.20** (169mg, 0.166mmol) was stirred at room temperature for 4 days and then 60°C for 4 days in 37% HCl:glacial acetic acid (1:1). The acids were removed by rotary evaporation and the product was precipitated from MeOH with diethyl ether to yield a hygroscopic solid mass = 124mg (40%). mp = 220-227°C ^{1}H NMR (DMSO-d_6) δ (ppm) = 7.88 (t, ^{3}J = 4.58Hz, 3H) 7.04 (dd, $^{3}J_1$ = 7.33Hz, $^{3}J_2$ = 1.83Hz, 3H) 6.63 (dd, $^{3}J_1$ = 7.33Hz, $^{3}J_2$ = 1.83Hz, 3H) 6.02 (t, ^{3}J = 6.87Hz, 3H) 4.26 (d, ^{3}J = 4.12Hz, 6H) 4.11 (t, ^{3}J = 6.87Hz, 6H) 1.01 (m, ^{3}J = 7.10Hz, 9H) ^{13}C NMR (DMSO-d_6) δ (ppm) = 169.91, 157.35, 147.19, 146.23, 129.53, 115.77, 105.59, 50.99, 36.58, 23.83, 21.55, 16.31; HRMS (ESI) *m/z* $[M+H]^+$: calcd for $C_{39}H_{49}N_6O_9^+$, 745.3561; found, 745.3554

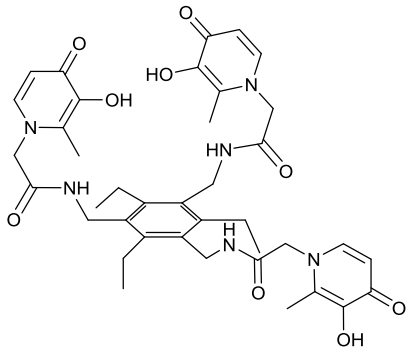

TEB-3,4-HOPO

(**3.26**): **3.22** (384mg, 0.378mmol) was stirred at room temperature for 4 days and then 60°C for 4 days in 37% HCl:glacial acetic acid (1:1). The acids were removed by rotary evaporation and the product was precipitated from MeOH with diethyl ether to yield a hygroscopic solid mass = 248mg (88%). ^{1}H NMR (DMSO) δ (ppm) = 7.96 (br d, ^{3}J = 6.87Hz, 3H) 6.95 (d, ^{3}J = 6.87Hz, 3H) 5.11-5.05 (s, br m, 6H) 4.41 (s, 3H) 4.12 (s, 3H) 6.69 (br m, 6H) 2.39 (s, 9H) 1.07 (br m, 9H) ^{13}C NMR

(DMSO) δ (ppm) = 140.17, 139.79, 110.97, 110.86, 58.21, 57.19, 23.58, 16.00, 15.83, 12.40, 12.11; HRMS (ESI) *m/z* $[M+H]^+$: calcd for $C_{39}H_{49}N_6O_9^+$, 745.3561; found, 745.3551

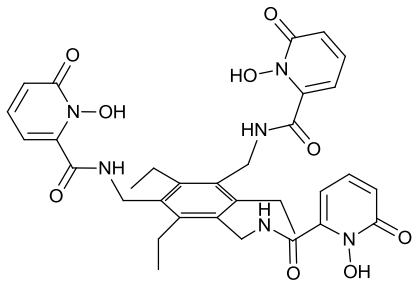

TEB-1,2-HOPO

(**3.27**): **3.23** (304mg, $3.27x10^{-4}$mol) was stirred at 60°C for 4 days in 37% Hcl:glacial acetic acid (1:1). The acids were removed by rotary evaporation and the product was precipitated from MeOH with diethyl ether to yield a hygroscopic solid mass = 201mg (93%). mp = 255-260°C. ^{1}H NMR (DMSO) δ (ppm) = 9.02 (t, ^{3}J = 4.02, 3H) 7.38 (m, 3H) 6.60 (dd, $^3J_1$ = 8.70Hz, $^3J_2$ = 1.37Hz, 3H) 6.35 (dd, $^3J_1$ = 6.87, $^3J_2$ = 1.83Hz, 3H) 4.50 (t, ^{3}J = 4.58, 6H) 2.77 (br m, 6H) 1.16 (t, ^{3}J = 7.79Hz, 9H) ^{13}C NMR (DMSO) δ (ppm) = 160.49, 157.83, 144.38, 142.18, 137.25, 131.81, 119.37, 105.31, 38.02, 23.02, 16.61; HRMS (ESI) *m/z* $[M+H]^+$: calcd for $C_{33}H_{37}N_6O_9^+$, 661.2622; found, 661.2616

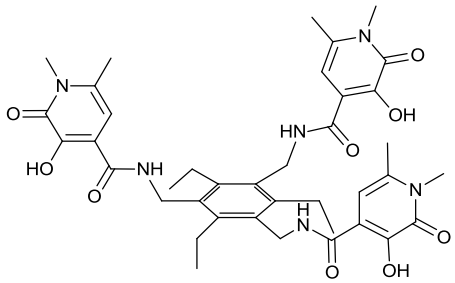

TEB-R-3,2-HOPO

(**3.28**): **3.21** (110mg, 0.139mmol) was dissolvd in dry DCM (10mL) and cooled under $N_{2(g)}$ in a ice-water bath. Once cool, BCl_3(1M in heptane, 1mL) was added and the reaction allowed to stir at room temperature for 4 days. The reaction was quenched with drop wise addition of MeOH, the solvent evaporated and the re-evaporation of additions of MeOH (6 x 20mL) yielded the pure product in 60% yield (63mg). ^{1}H NMR (DMSO-d_6) δ (ppm) = 8.26 (t, ^{3}J = 3.66Hz, 3H) 6.54 (s, 3H) 4.56 (d, ^{3}J = 3.81Hz, 6H) 3.42 (s, 9H) 2.72 (q, ^{3}J = 7.33Hz, 6H) 2.29 (s, 9H) 1.13 (t, ^{3}J = 7.33Hz, 9H) ^{13}C NMR (DMSO-d_6) δ (ppm) = 167.21, 164.77, 157.75, 142.09, 133.43, 123.15,

111.54, 105.20, 36.74, 31.27, 22.76, 19.57, 16.30; HRMS (ESI) *m/z* $[M+H]^+$: calcd for $C_{39}H_{49}N_6O_9^+$, 745.3561; found, 745.3560

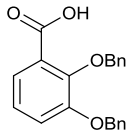

2,3-bis(benzyloxy)benzoic acid

(**3.32**): To a solution of 2,3-dihydroxybenzoic acid (2g, 12.98mmol), BnBr (13.32g, 77.85mmol) in acetone (100mL)was added K_2CO_3 (10.76g, 77.85mmol) and the reaction allowed to stir at 100°C overnight. The solution was cooled, filtered and the residue taken into MeOH (120mL) and $NaOH_{aq}$ (5M, 30mL) added. The mixture was refluxed for 4 hours, cooled, the MeOH evaporated and diluted with H_2O until homogenous. The aqueous solution was extracted with hexane (2 x 50mL) and the aqueous portion acidified with 37% HCl_{aq} upon which a precipitate could be isolated by filtration and was used without further purification mass = 5.35g ^{1}H NMR ($CDCl_3$) δ (ppm) = 7.48-7.15 (m, 13H) 5.18 (s, 2H) 5.25 (s, 2H) ^{13}C NMR ($CDCl_3$) δ (ppm) = 165.20, 151.37, 147.14, 135.92, 134.68, 129.41, 128.96, 128.92, 128.65, 127.88, 125.15, 124.55, 123.06, 119.06, 77.24, 71.63

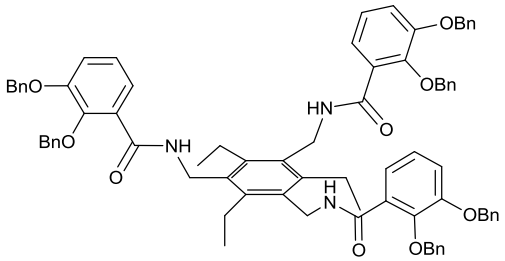

Bn_6EMECAM

(**3.33**): 2,3-dibenzyloxybenzoic acid (49) (0.38g, 1.16mmol) and TBTU (0.39g, 1.20mmol) were dissolved under $N_{2(g)}$ in dry DMF (10mL). N-methyl morpholine (0.23g, 1.97mmol) was added to the solution under $N_{2(g)}$ and the reaction stirred at room temperature for 30 minutes. After which time, 1,3,5-tris(aminomethyl)-2,4,6-triethyl benzene (100mg, 0.38mmol) was added under $N_{2(g)}$, the reaction was stirred at room temperature for 2 hours and then at 60°C for 24 hours. The DMF was mostly removed under vacuum and the residue taken into DCM (50mL). The organic solution was

washed ~5% HCl_{aq} (2 x 50mL), $NaOH_{aq}$ (5% w/v, 2 x 50mL), distilled H_2O (50mL) and brine (50mL). The organic portion was dried ($MgSO_4$), filtered and evaporated to dryness. The crude product was purified using Isolera automated column 100g SNAP silica cartridge DCM:MeOH (3-12%) to yield a solid mass = 462mg (52%). 35g ^{1}H NMR ($CDCl_3$) δ (ppm) = 7.69 (dd, $^3J_1$ = 7.79Hz, $^3J_2$ = 1.83Hz, 3H) 7.63 (br t, ^{3}J = 4.58Hz, 3H) 7.40-7.30 (m, 18H) 7.16-6.82 (m, 21H) 5.04 (s, 6H) 4.80 (s, 6H) 4.54 (d, ^{3}J = 4.58Hz, 6H) 2.47 (q, ^{3}J = 7.79Hz, 6H) 1.03 (t, ^{3}J = 7.33Hz, 9H)

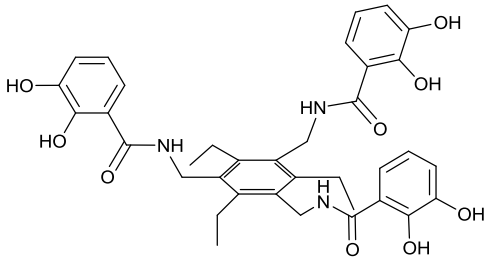

EMECAM

(**1.32**): **3.33** (522mg, 0.432mmol) was hydrogenated over Pd/C in EtOH:H_2O with an acid catalyst for 8 hours at room temperature. The reaction TLC showed incomplete. The catalyst was filtered, solvents evaporated and the solid taken into dry DCM. To which BCl_3 (1M in heptane, 2.6mL) was added under $N_{2(g)}$ and the reaction stirred for 18 hours before quenching with drop wise addition of MeOH. Evaporation to dryness and repeated MeOH evaporations (5 x 20mL) yielded the pure product mass = 243mg (85%) as a solid. Mp = 119-127°C. ^{1}H NMR (DMSO-d_6) δ (ppm) = 8.68 (br s, 3H) 7.40 (dd, $^3J_1$ = 8.24Hz, $^3J_2$ = 1.37Hz, 3H) 6.90 (dd, $^3J_1$ = 7.79Hz, $^3J_2$ = 1.37Hz, 3H) 4.60 (d, ^{3}J = 3.66Hz, 6H) 2.82 (br q, ^{3}J = 7.33Hz, 6H) 1.13 (t, ^{3}J = 7.33Hz, 9H) ^{13}C NMR (DMSO-d_6) δ (ppm) = 168.32, 148.44, 145.95, 144.05, 131.67, 118.61, 118.38, 118.05, 115.85, 37.53, 22.72, 16.07

8.3.3 Experimental tris(piperazin-1-yl)-1,3,5-triazine molecules

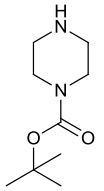

tert-butyl piperazine-1-carboxylate (49)

(**4.6**): To a solution of pipirazine (15.0g, 0.174mol) in DCM (300mL) was added di-tert-butyl carbonate (19.2g, 0.0871mol) as a solution in DCM (70mL) at 0°C. The resulting solution was stirred at 0°C for 2 hours, during which time a white precipitate formed. The reaction was filtered and the filtrate evaporated to dryness. H_2O (30mL) was added and the reaction was filtered again. The filtrate was saturated with K_2CO_3 and then extracted with ether (3 x 100mL), the ether dried (MgSO4) and evaporated to dryness to yield 10.0g of the product (61%). ^{1}H NMR (CDCl3) δ/ppm = 3.36 (t, 3J = 4.1Hz, 4H) 2.78 (t, 3J = 4.6Hz, 4H) 1.44 (d, 3J = 1.4Hz, 9H). ^{13}C NMR ($CDCl_3$) δ (ppm) = 154.92, 79.60, 46.00, 28.50

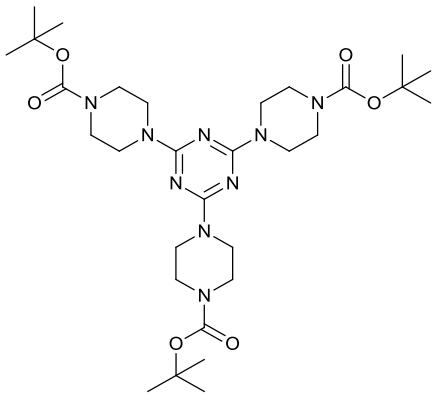

tert-butyl-4-[bis({4-[(tert-butoxy)carbonyl]piperazin-1-yl})-1,3,5-triazin-2-yl]piperazine-1-carboxylate (50)

(**4.7**): Cyanuric chloride (3.10g, 16.8mmol), **4.6** (10g, 50.4mmol) and K_2CO_3 (20g, 144mmol) were suspended in THF (50mL) and refluxed at 80°C overnight. The solution was cooled and the solvent evaporated to leave a residue which was taken into DCM and washed with H_2O and brine.

Evaporation of the DCM gave the product in 58% yield (6.22g). ^{1}H NMR ($CDCl_3$) δ (ppm) = 3.73 (br t, ^{3}J = 5.04Hz, 12H) 3.44 (br t,^{3}J = 5.50Hz,) 1.48 (s, 27H) ^{13}C NMR ($CDCl_3$) δ (ppm) = 165.39, 164.54, 80.32, 43.36, 43.06, 28.49

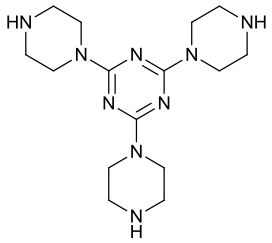

tris(piperazin-1-yl)-1,3,5-triazine

(**4.2**): **4.7** (1.48g, 2.33mmol) was dissolved in DCM:TFA 1:1 (25mL) and allowed to stir at room temperature for 6 hours. After which time the solution was evaporated to give a viscous residue which was brought to pH 14 with $NaOH_{aq}$ (6M). The basic solution was extracted with DCM (3 x 50mL), dried ($MgSO_4$) and the solvent evaporated to yield the product in 58% yield (450mg). mp = >260°C. ^{1}H NMR (MeOD-d_4) δ (ppm) = 3.75-3.60 (br m, 12H) 3.24-3.21 (m, 3H) 2.76-2.64 (m, 9H) ^{13}C NMR (MeOD-d_4) δ (ppm) = 165.30, 45.05, 43.53

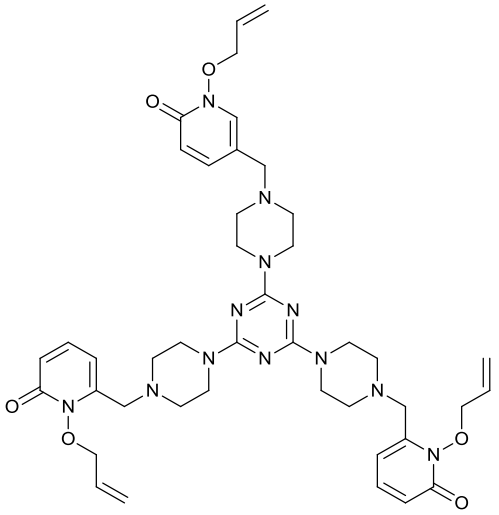

Tris-allyl-triazine-1,2-HOPO

(**4.8**): **4.2** (0.25g, 7.497 x 10^{-4} mol) and Et_3N (0.47g, 4.648 x 10^{-3}mol) were added under $N_{2(g)}$ to MeCN (10mL). To this **2.28** (0.46g, 2.342 x 10^{-3} mol) was added under $N_{2(g)}$ and the reaction

allowed to stir at room temperature for 72 hours and a further 48 hours at reflux. The reaction was evaporated to dryness, taken into DCM (100mL) washed $NaHCO_{3(sat)}$ (3 x 100mL) and purified using Isolera automated column 100g SNAP silica cartridge DCM:MeOH (3-12%). To yield a viscous oil mass = 105mg (17%). ^{1}H NMR ($CDCl_3$) δ (ppm) = 7.25 (dd, $^{3}J_1$ = 6.4Hz, $^{3}J_2$ = 9.2Hz, 3H) 6.57 (dd, $^{3}J_1$ = 1.8Hz, $^{3}J_2$ = 9.2Hz, 3H) 6.14 (dd, $^{3}J_1$ = 1.4Hz, $^{3}J_2$ = 6.9Hz, 3H) 6.04 (m, 3H) 5.42 (dd, $^{3}J_1$ = 1.4Hz, $^{3}J_2$ = 17.4Hz, 3H) 5.32 (dd, $^{3}J_1$ = 0.9Hz, $^{3}J_2$ = 10.1Hz, 3H) 3.74 (br s, 12H) 3.70 (s, 6H) 2.50 (t, ^{3}J = 4.6Hz, 12H)^{13}C NMR ($CDCl_3$) δ (ppm) = 165.3, 160.0, 145.9, 137.9, 130.9, 121.3, 121.1, 105.9, 57.4, 53.2, 50.8, 43.1; HRMS (ESI) *m/z* $[M+H]^+$: calcd for $C_{42}H_{55}N_{12}O_6^+$, 823.4368; found, 823.4358

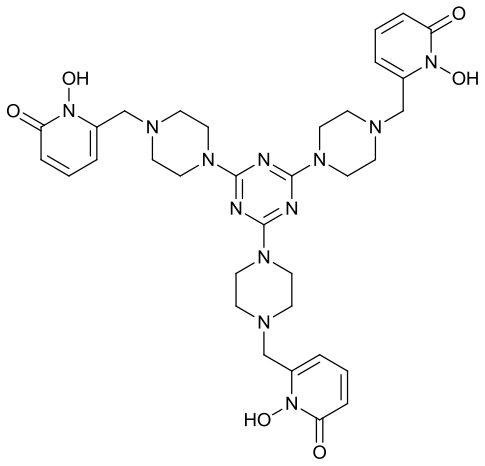

Triazine-1,2-HOPO

(**4.9**): **4.8** (87mg, 0.106mmol) was dissolved in dioxane:H_2O (4:1, 10mL) to which Pd/C (10mg) was added and TFA was added to give a 0.15M solution. The reaction was refluxed overnight, the catalyst filtered and washed with dioxane and water (5mL) and the solvents evaporated. Repeated evaporations from MeOH yielded the pure product in 79% yield (59mg). mp = 122-130°C. ^{1}H NMR (DMSO-d_6) δ (ppm) = 7.45 (dd, $^{3}J_1$ = 9.16Hz, $^{3}J_2$ = 6.87Hz, 3H) 6.64 (dd, $^{3}J_1$ = 9.16Hz, $^{3}J_2$ = 1.37Hz, 3H) 6.47 (dd ($^{3}J_1$ = 6.87Hz, $^{3}J_2$ = 1.37Hz, 3H) 4.31 (s, 6H) 3.92 (br s, 12H) 3.12 (br s, 12H) ^{13}C NMR (DMSO-d_6) δ (ppm) = 165.05, 158.39, 139.78, 137.40, 119.44, 108.40, 54.63, 52.17, 43.22; HRMS (ESI) *m/z* $[M+H]^+$: calcd for $C_{33}H_{43}N_{12}O_6^+$, 703.3429: found, 703.3426

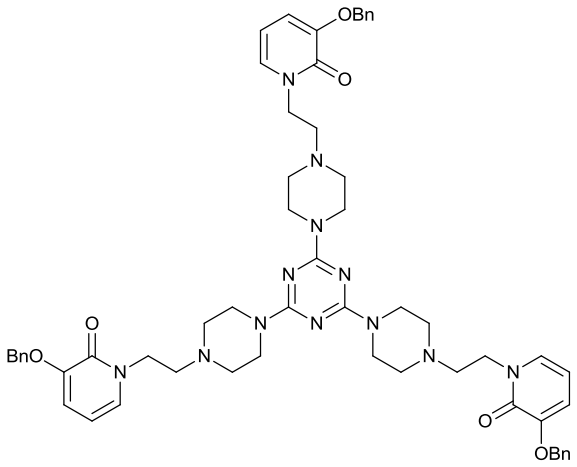

Tris-benzyl-triazine-3,2-HOPO

(**4.10**): To **4.2** (0.23g, 6.897 x 10^{-4}mol) was added dry MeCN (15mL) under $N_{2(g)}$, Et_3N (0.41g, 4.138 x 10^{-3}mol) was added to the reaction. After 10 minutes, **2.21** (0.70g, 2.165 x 10^{-3}mol) was added and the reaction stirred under $N_{2(g)}$ for three days at room temperature. After which time, the reaction was allowed to reflux for 24 hours. The reaction was evaporated to dryness, taken into DCM (50mL), washed $NaHCO_{3(sat)}$ (3 x 50mL), dried ($MgSO_4$) and evaporated to dryness. Purification via silica gel column chromatography DCM:MeOH (1-8%) yielded 203mg (29%). ^{1}H NMR ($CDCl_3$) δ (ppm) = 7.50-7.20 (m, 15H) 6.93 (dd, $^3J_1$ = 1.4Hz, $^3J_2$ = 6.9Hz, 3H) 6.31 (dd, $^3J_1$ = 1.4Hz, $^3J_2$ = 7.3Hz, 3H) 6.00 (t, ^{3}J = 7.3Hz, 3H) 5.08 (s, 6H) 4.08 (t, ^{3}J = 6.5Hz, 6H) 3.7 (br m, 12H) 2.71 (t, ^{3}J = 6.9Hz, 6H) 2.48 (br m, 12H) ^{13}C NMR ($CDCl_3$) δ (ppm) = 165.3, 158.2, 148.8, 136.4, 129.7, 128.6, 128.6, 128.0, 127.4, 115.6, 104.4, 70.8, 56.7, 53.3, 47.2, 43.2, 29.8; HRMS (ESI) *m/z* $[M+H]^+$: calcd for $C_{57}H_{67}N_{12}O_6^+$, 1015.5307; found, 1015.5295

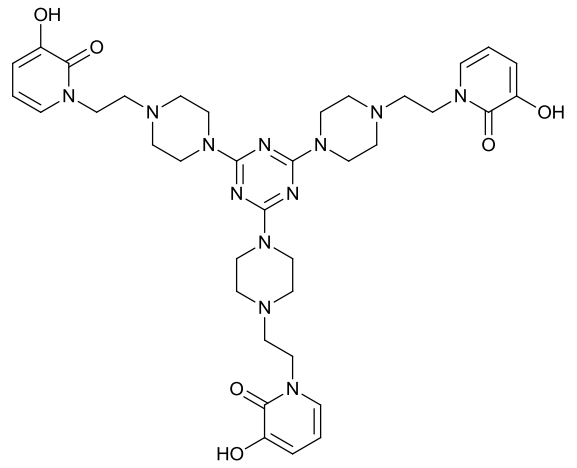

Triazine-3,2-HOPO

(**4.11**): (**4.10**) (201mg, 5.02 x 10^{-5}mol) was dissolved in HCl:AcOH (1:1, 10mL) and allowed to stir at room temperature for 4 days and at 50-70°C for 16 days. The reaction was evaporated to dryness, dissolved in methanol and a solid was collected by precipitation with diethyl ether mass = 43mg. mp = 221-225°C. ^{1}H NMR (DMSO-d_6) δ (ppm) = 7.26 (dd, $^{3}J_1$ = 6.87Hz, $^{3}J_2$ = 1.37Hz, 3H) 6.76 (dd, $^{3}J_1$ = 7.33Hz, $^{3}J_2$ = 1.37Hz, 3H) 6.20 (t, ^{3}J = 6.87Hz, 3H) 4.40 (br t, 6H); HRMS (ESI) *m/z* $[M+H]^+$: calcd for $C_{36}H_{49}N_{12}O_6^+$, 745.3898; found, 745.3891

8.4 Experimental cholic acid

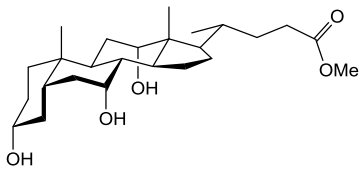

Methyl cholate

(**5.2**): A 50mL 3n-round bottomed flask was charged with cholic acid (2.00g, 4.89mmol) and MeOH (15mL). The flask was equipped with a reflux condenser and the mixture brought to reflux for 1 hour 15 mins. H_2SO_4 (5-6 drops) was added till pH ~ 1-2 determined via indicator paper. The solution was allowed to cool to room temperature and stirred for one day. Saturated $Na_2CO_{3(aq)}$ (20mL) was added to the reaction and upon addition a white precipitate was filtered after 10 mins of stirring. The solid was recrystallized in toluene and stored at 4°C for 24 hours. The solid was filtered to yield a white powder mass = 1.36g (66%). mp = 155-158°C ^{1}H NMR ($CDCl_3$) δ (ppm) = 3.97 (s, 1H) 3.63 (s, 3H) 3.14 (m, 1H) 1.18 (d, ^{3}J = 6.19Hz, 3H) 1.01 (s, 3H) 0.81 (s, 3H)

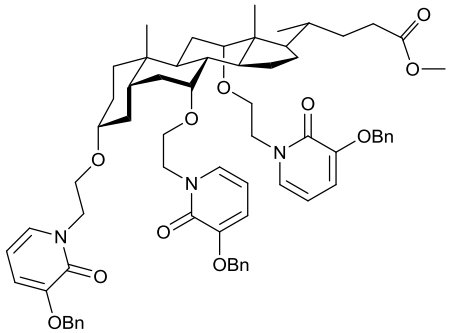

Methyl cholate- Bn_6-3,2-HOPO

(5.3) To methyl cholate (100mg, 2.37 x 10^{-4}mol) was added in dry toluene to a dry 3-necked round bottomed flask under $N_{2(g)}$. Calcium hydride (60mg, 1.43mmol) was added to this before **2.21** was added drop wise as

a solution in dry toluene. The reaction was brought to reflux for 2 days after which time, the reaction was filtered and the solvent evaporated. The crude residue was purified via Isolera automated column 50g SNAP silica cartridge DCM:MeOH (3-12%). ^{13}C NMR ($CDCl_3$) δ (ppm) = 174.8, 158.2, 148.8, 148.6, 136.5, 136.4, 130.3, 128.6, 128.0, 127.4, 116.0, 115.7, 104.0, 103.9, 80.0, 72.9, 70.8, 68.7, 68.3, 65.8, 51.6, 50.4, 49.6, 47.2, 46.6, 42.1, 41.4, 39.6, 36.21, 35.21, 35.12, 35.0, 34.6, 31.1, 30.9, 28.5, 27.5, 27.1, 26.8, 23.2, 22.7, 17.4, 12.6. HRMS (ESI) *m/z* $[M+Na+H_2O]^+$: calcd for $C_{67}H_{83}N_3O_{12}$, 1144.5869; found, 1144.5864.

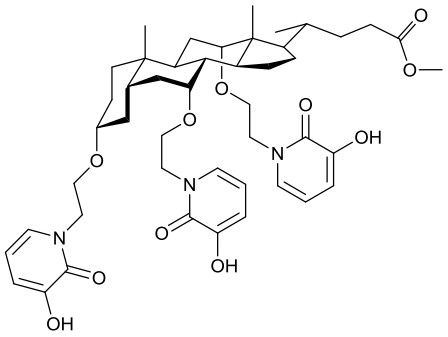

Methyl cholate-3,2-HOPO

(5.4) The isolated residue **5.3** was the subject to hydrogenation with a H-Cube® Continuous-flow Hydrogenation Reactor (ThalesNano) in methanol, using a Pd/C cartridge (full $H_{2(g)}$ mode). The product was isolated via evaporation of the methanol to yield a solid 90mg. ^{13}C NMR (CD_3OD) δ (ppm) = 175.8, 159.3, 147.4, 129.9, 129.5, 116.3, 106.8, 80.8, 73.4, 68.9, 38.4, 65.8, 51.3, 50.8, 50.0, 49.2, 47.3, 46.8, 42.4, 42.3, 40.3, 36.8, 36.1, 35.6, 35.5, 35.2, 31.6, 31.2, 28.9, 28.0, 27.4, 27.2, 23.6, 22.5, 16.9, 12.3. (+) ESI-MS found 873.86 = $[M+Na+H_2O]$

8.4.1 Experimental TREN core scaffold

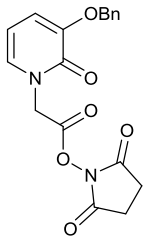

2,5-dioxopyrrolidin-1-yl 2-[3-(benzyloxy)-2-oxo-1,2-dihydropyridin-1-yl]acetate

(**6.6**): **2.11** (0.30g, 1.16mmol) in DMF (20mL) was added NHS (0.14g, 1.12mmol) and DCC (0.25g, 1.21mmol) each as a solution in DMF (5mL). The solution was stirred in the dark for 4 days after which time glacial AcOH (0.5mL) was added and the solution stirred for 1 hour. The precipitate was filtered and the DMF evaporated to give a residue which was recrystallized from EtOAc to yield a pink powder mass = 0.18g (43%).

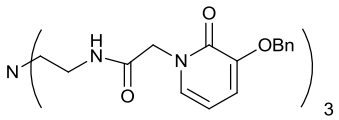

Bn-CP130

(**6.7**): TREN (133mg, 9.12 x 10^{-4} mol) was added with stirring to a solution of 2,5-dioxopyrrolidin-1-yl 2-[3-(benzyloxy)-2-oxo-1,2-dihydropyridin-1-yl]acetate (976mg, 2.73mmol) in DMF (30mL). After 24 hours the solution was evaporated to dryness, the residue dissolved in DCM (50mL). The organic solution was washed Na_2CO_3 (0.05M, 3 x 10mL) and H_2O (2 x 20mL). The organic phase was dried ($MgSO_4$), filtered and evaporated to dryness. The resulting residue was recrystallized in EtOH/H_2O and the precipitate collected after 4 days at 4°C as a white solid mass =0.51g (64%). ^{1}H NMR ($CDCl_3$) δ (ppm) = 8.38 (t, ^3J = 5.50Hz, 3H) 7.41-7.27 (m, 15H) 6.68 (d, $^3J_1$ = 7.79Hz, 3H) 6.67 (d, ^3J = 6.87 Hz, 3H) 6.01 (td, $^3J_1$ = 7.33Hz, $^3J_2$ = 1.37Hz, 3H) 4.97 (s, 6H) 4.48 (s, 6H) 3.20 (br q, ^3J = 4.12Hz, 6H) 2.51 (br t, ^3J = 5.04Hz, 6H)

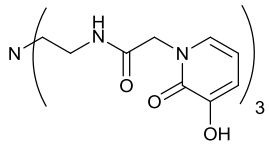

CP130

(**1.6**): **6.7** (454mg, 0.512mmol) was dissolved in EtOH and H_2O (10:1) with glacial AcOH (1mL) and Pd/C (140mg). The mixture was hydrogenated overnight at room temperature and the solution the filtered and evaporated after the catalyst was washed with EtOH. The crude solid was recrystallized from EtOH to yield a powder mass = 80mg (25%). mp = 145-153°C. ^{1}H NMR (DMSO-d_6) δ (ppm) = 8.54 (br s, 3H) 7.09 (d, ^{3}J = 6.41Hz, 3H) 6.74 (d, ^{3}J = 6.87Hz, 3H) 6.10 (t, ^{3}J = 6.87Hz, 3H) 4.59 (s, 6H) 3.51 (s, 6H) 3.31 (s, 6H) . ^{13}C NMR (DMSO-d_6) δ (ppm) = 168.35, 158.45, 147.11, 129.98, 115.86, 105.56, 52.00, 34.13

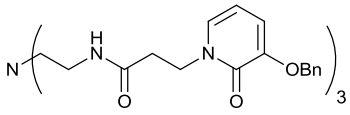

Bn-LC-CP130

(**6.8**): **2.15** (0.56g, 2.0519mmol) and TBTU (0.705g, 2.19mmol) were dissolved under $N_{2(g)}$ in dry DMF (20mL). N-methyl morpholine (0.42g, 4.1mmol) was added to the solution under $N_{2(g)}$ and the reaction stirred at room temperature for 30 minutes. After which time, TREN (0.10g, 6.84 x 10^{-4}mol) was added under $N_{2(g)}$, the reaction was stirred at room temperature for 2 hours and then at 60°C for 24 hours. The DMF was mostly removed under vacuum and the residue taken into DCM (50mL). The organic solution was washed ~5% HCl_{aq} (2 x 50mL), $NaOH_{aq}$ (5% w/v, 2 x 50mL), distilled H_2O (50mL) and brine (50mL). The organic portion was dried ($MgSO_4$), filtered and evaporated to dryness. The crude product was purified using Isolera automated column 100g SNAP silica cartridge DCM:MeOH (2-20%), to yield a brown solid mass = 191mg (30%) ^{1}H NMR ($CDCl_3$) δ (ppm) = 7.83 (t, ^{3}J = 5.04Hz, 3H) 7.33 (m, 15H) 7.03 (dd, $^3J_1$ = 6.92Hz, $^3J_2$ = 1.37Hz, 3H) 6.34 (dd, $^3J_1$ = 7.33Hz, $^3J_2$ = 1.37Hz, 3H) 5.99 (t, ^{3}J = 7.33Hz, 3H) 4.98 (s, 6H) 4.12 (t, ^{3}J = 5.95Hz, 6H) 3.05 (br q, ^{3}J = 3.66Hz, 6H) 2.57 (t, ^{3}J = 5.95Hz, 6H) 2.37 (br t, 6H) ^{13}C NMR

($CDCl_3$) δ (ppm) = 170.57, 158.10, 148.51, 136.20, 130.22, 128.61, 128.15, 127.55, 115.56, 105.10, 70.58, 54.91, 46.50, 37.73, 35.42

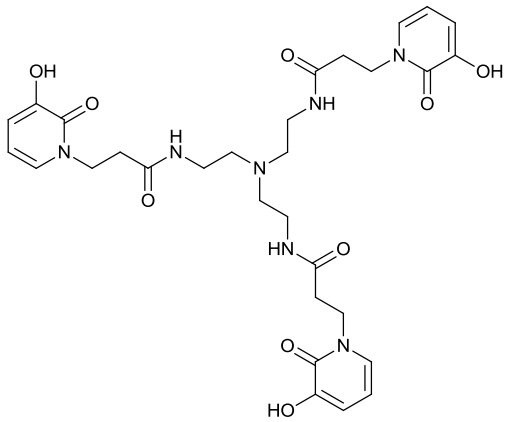

LC-CP130

(**6.9**): **6.8** (283mg) was hydrogenated over Pd/C (30mg) for 8 hours in a solvent mixture of EtOH:H_2O (9:1). The solution was filtered and the catalyst washed. The solvent and washings were combined and were evaporated to dryness to yield the product in 68% yield (135mg). mp = 90-95°C. ^{1}H NMR (MeOD-d_4) δ (ppm) = 6.99 (d, ^{3}J = 6.41Hz, 3H) 6.71 (d, ^{3}J = 7.33Hz, 3H) 6.11 (t, ^{3}J = 6.87Hz, 3H) 4.18 (t, ^{3}J = 6.41Hz, 6H) 3.08 (t, ^{3}J = 5.50Hz, 6H) 2.62 (t, ^{3}J = 5.95, 6H) 2.48 (t, ^{3}J = 5.04Hz, 6H) ^{13}C NMR (MeOD-d_4) δ (ppm) = 173.02, 159.95, 148.39, 129.64, 117.10, 108.11, 54.86, 47.88, 38.22, 36.06; (+)-ESI-MS *m/z* calcd for $C_{30}H_{40}N_7O_9^+$, 642.29; found, 642.20: HRMS (ESI) *m/z* $[M+H]^+$: calcd for $C_{30}H_{40}N_7O_9^+$, 642.2882: found, 642.2878

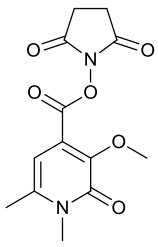

2,5-dioxopyrrolidin-1-yl 3-methoxy-1,6-dimethyl-2-oxo-1,2-dihydropyridine-4-carboxylate

(**6.10**): **3.14** (1.00g, 5.02mmol) in DCM (100mL) was added N-hydroxysuccinimide (0.79g, $6.84x10^{-3}$mol) and EDAC (1.285g, $6.7x10^{-3}$mol) and the resulting mixture stirred at room temperature for three days. The reaction was washed with HCl_{aq} (0.1M (2x100mL), organic phase

was dried ($MgSO_4$) and evaporated to dryness to yield a yellow-orange solid, 1.30g (88%). Mp = 110-113°C. ^{1}H NMR ($CDCl_3$) δ (ppm) = 6.28 (s, 1H) 3.96 (s, 3H) 3.49 (s, 3H) 2.83 (s, 4H) 2.30 (s, 3H). ^{13}C NMR ($CDCl_3$) δ (ppm) = 169.05, 160.27, 159.96, 148.80, 140.65, 122.85, 103.01, 60.77, 32.06, 25.75, 20.66

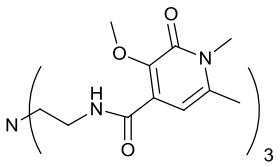

Me_6-TREN-R-3,2-HOPO

(**6.11**): To **6.10** (0.60g, 2.05mmol) in DCM (15mL) was added TREN (0.10g, 0.684mmol) as a solution in DCM (5mL). The reagents were allowed to stir at room temperature for 2 days. The evaporation of the solvent gave a residue which solidified on standing to provide the pure compound in 92% yield (0.43g). ^{1}H NMR ($CDCl_3$) δ (ppm) = 8.30 (t, ^{3}J = 5.5Hz, 3H) 6.57 (s, 3H) 3.98 (s, 9H) 3.62 (q, ^{3}J = 6.41Hz, 6H) 3.54 (s, 9H) 2.36 (s, 9H) 2.97 (t, ^{3}J = 6.41Hz, 6H)

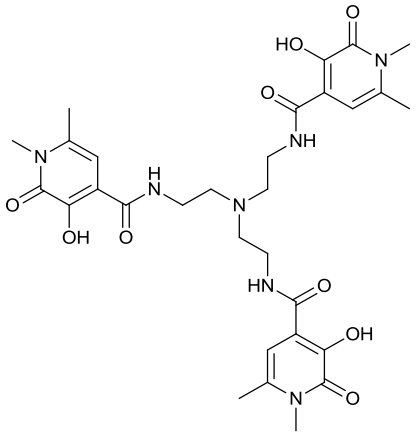

TREN-R-3,2-HOPO

(**6.12**): **6.11** (0.20g, 0.293mmol) was added to a clean, dry, 3n round-bottomed flask under $N_{2(g)}$ as a solution in dry DCM (20mL). The solution was cooled in an ice-water bath for 15 minutes before BCl_3 (1M in heptane, 1.70mL) was added via gas tight syringe under $N_{2(g)}$. The reaction was stirred at room temperature for 2 days before MeOH (50mL) was added drop wise at 0°C. The solvents were evaporated and the residue precipitated from suspension in MeOH. The solid was collected after storage for 2 days at 4°C to give the pure product in 23% yield (43mg). ^{1}H NMR (DMSO) δ (ppm) = 8.57 (br t, 3H) 6.29 (s, 3H) 3.66 (br s, 6H) 2.19 (s, 9H) ^{13}C NMR (DMSO) δ (ppm) =

166.34, 159.26, 144.86, 134.99, 117.02, 102.96, 52.41, 34.70, 32.01, 20.01; HRMS (ESI) *m/z* $[M+H]^+$: calcd for $C_{30}H_{40}N_7O_9^+$, 642.2888; found, 642.2886

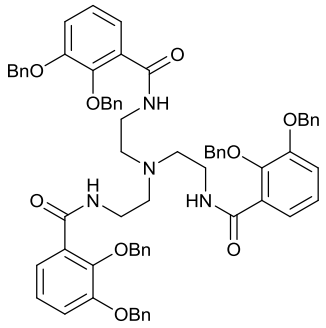

Bn_6-TRENCAM

(**6.17**): **3.32** (686mg, 2.05mmol) and TBTU (702mg, 2.19mmol) were dissolved under $N_{2(g)}$ in dry DMF (20mL). N-methyl morpholine (0.42g, 4.1mmol) was added to the solution under $N_{2(g)}$ and the reaction stirred at room temperature for 30 minutes. After which time, TREN (100mg, 0.684mmol) was added under $N_{2(g)}$, the reaction was stirred at room temperature for 2 hours and then at 60°C for 24 hours. The DMF was mostly removed under vacuum and the residue taken into DCM (50mL). The organic solution was washed ~5% HCl_{aq} (2 x 50mL), $NaOH_{aq}$ (5% w/v, 2 x 50mL), distilled H_2O (50mL) and brine (50mL). The organic portion was dried ($MgSO_4$), filtered and evaporated to dryness. The crude product was purified using Isolera automated column 100g SNAP silica cartridge DCM:MeOH (2-20%), to yield a brown solid mass = 310mg (41%). ^1H NMR ($CDCl_3$) δ (ppm) = 7.46-7.21 (m, 33H) 7.16-7.04 (m, 6H) 5.17-5.06 (m, 12H) 3.56 (br s, 6H) 3.17 (br s, 6H) %); ^{13}C NMR ($CDCl_3$) δ (ppm) = 165.31, 151.75, 146.79, 136.62, 136.56, 128.73, 128.69, 128.26, 127.88, 127.68, 124.38, 123.14, 116.79, 76.33, 71.23, 52.57, 38.70, 37.35

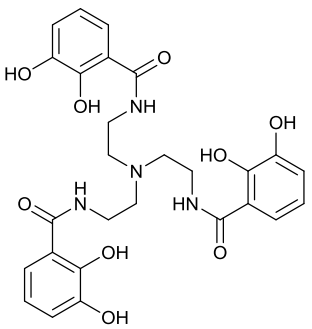

TRENCAM

(**6.16**): **6.17** (310mg, 0.283mmol) was stirred in 37% HCl:glacial AcOH (1:1) at room temperature for 7 days. The acids were evaporated and the residue was repeatedly evaporated from MeOH (6 x 20mL) the pure product was obtained in 77% yield (120mg). ^{1}H NMR (DMSO-d_6) δ (ppm) = 6.77 (dd, $^{3}J_1$ = 7.79Hz, $^{3}J_2$ = 1.37Hz, 3H) 6.57 (dd, $^{3}J_1$ = 7.79Hz, $^{3}J_2$ = 1.37Hz, 3H) 6.31 (t, ^{3}J = 7.79Hz, 3H) 3.52 (br t, ^{3}J = 5.50Hz, 6H) 3.34 (br t, ^{3}J = 5.04Hz, 6H); ^{13}C NMR (DMSO-d_6) δ (ppm) = 170.08, 149.25, 146.15, 119.03, 118.12, 117.66, 115.03, 51.31, 38.22, 33.71

9 Appendix

9.1 OD_{630} Kinetic assay data *E. coli*

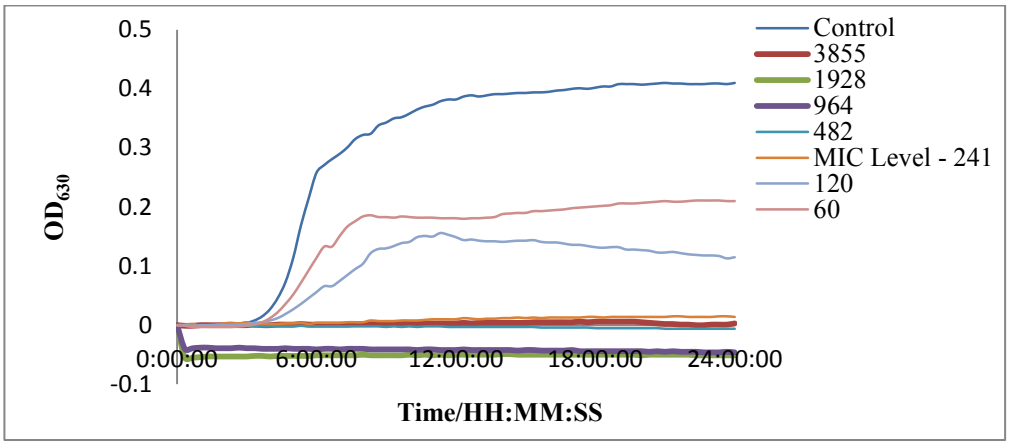

Appendix Figure 9.1 Development of OD_{630} over 24 hours for *E. coli* in BHI broth at 37°C. Containing CTG-3,2-HOPO at concentrations given in legend, reported in micromolar. Control contained no ligand (0μM).

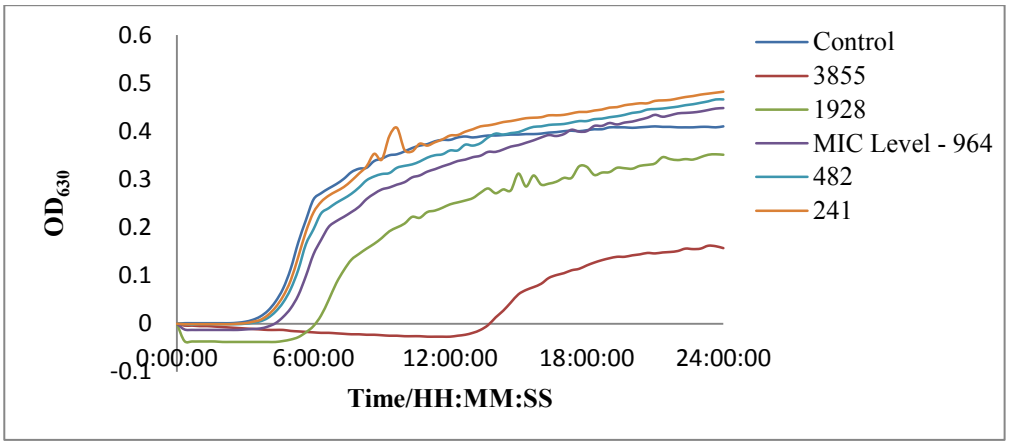

Appendix Figure 9.2 Development of OD_{630} over 24 hours for *E. coli* in BHI broth at 37°C. Containing TRENCAM at concentrations given in legend, reported in micromolar. Control contained no ligand (0μM).

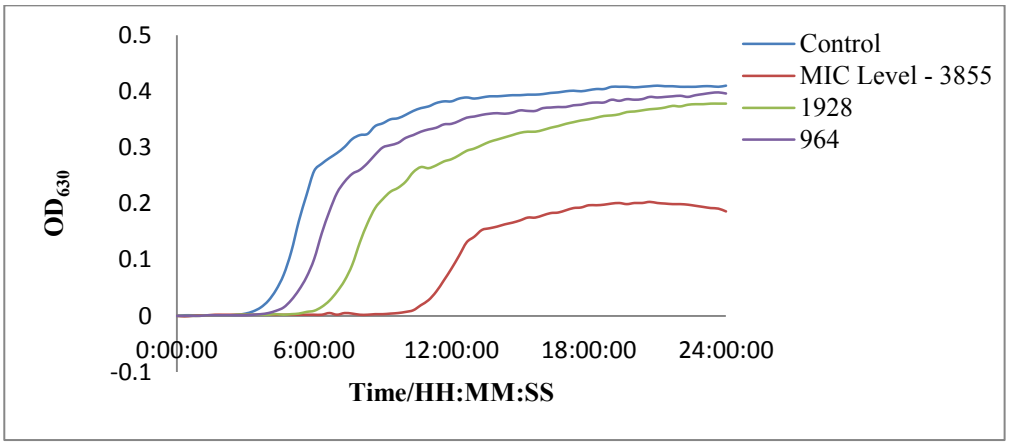

Appendix Figure 9.3 Development of OD_{630} over 24 hours for *E. coli* in BHI broth at 37°C. Containing EMECAM at concentrations given in legend, reported in micromolar. Control contained no ligand (0μM).

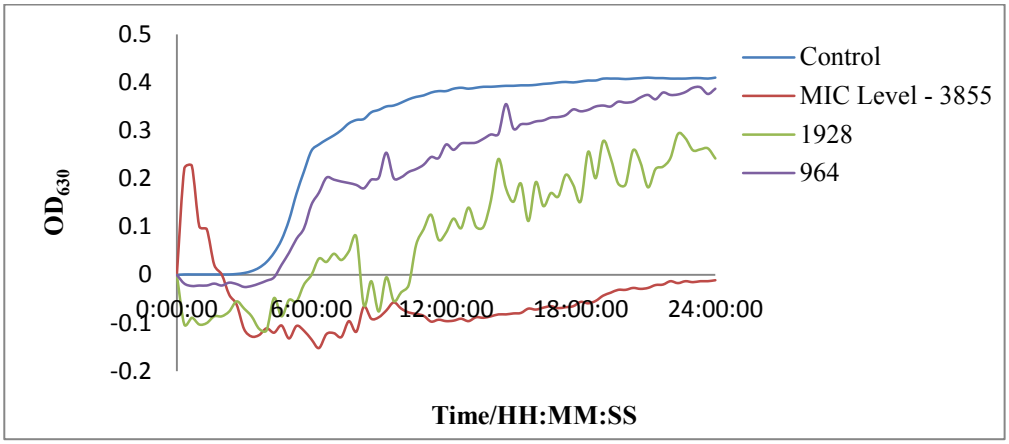

Appendix Figure 9.4 Development of OD_{630} over 24 hours for *E. coli* in BHI broth at 37°C. Containing triazine-3,2-HOPO at concentrations given in legend, reported in micromolar. Control contained no ligand (0μM).

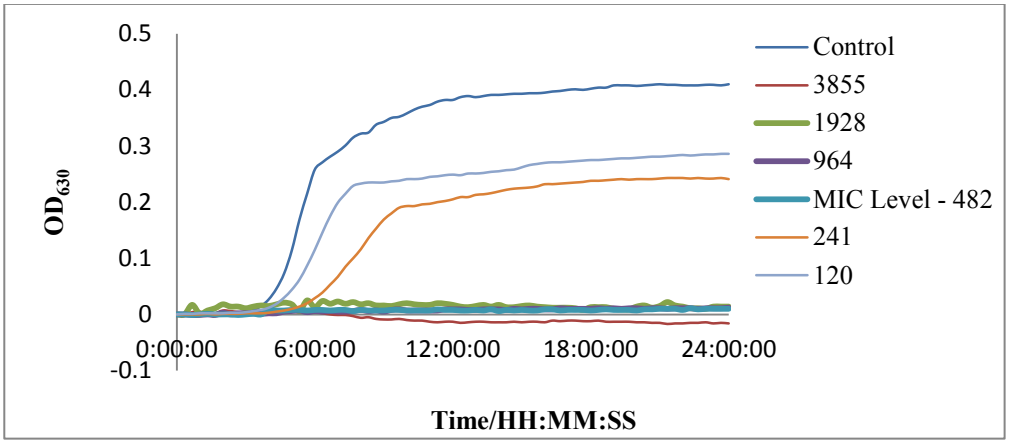

Appendix Figure 9.5 Development of OD_{630} over 24 hours for *E. coli* in BHI broth at 37°C. Containing triazine-1,2-HOPO at concentrations given in legend, reported in micromolar. Control contained no ligand (0μM).

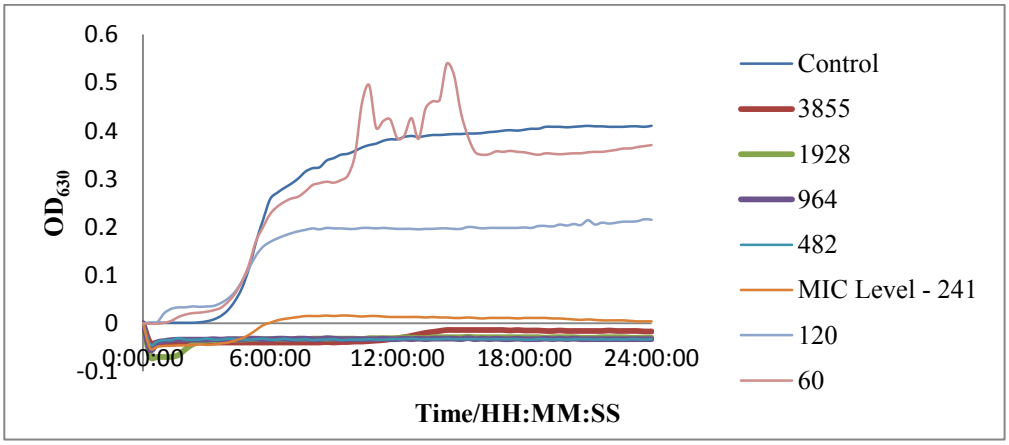

Appendix Figure 9.6 Development of OD_{630} over 24 hours for *E. coli* in BHI broth at 37°C. Containing TEB-1,2-HOPO at concentrations given in legend, reported in micromolar. Control contained no ligand (0μM).

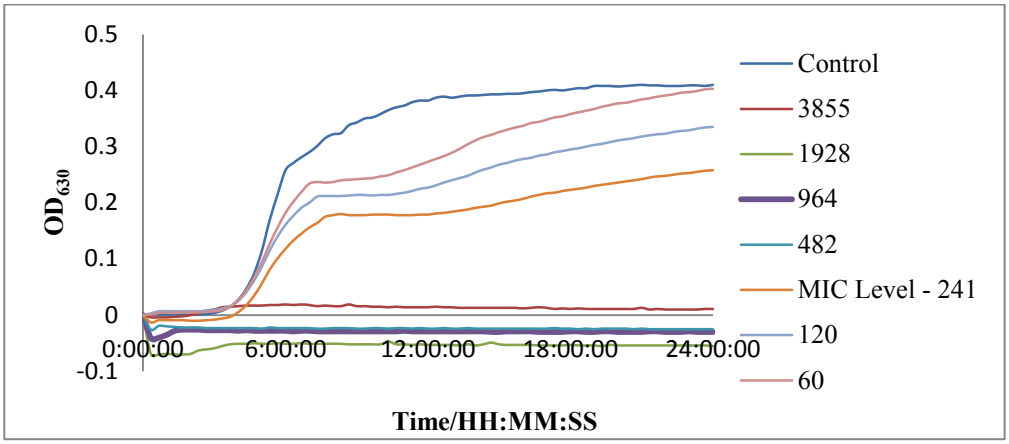

Appendix Figure 9.7 Development of OD_{630} over 24 hours for *E. coli* in BHI broth at 37°C. Containing TEB-R-3,2-HOPO at concentrations given in legend, reported in micromolar. Control contained no ligand (0μM).

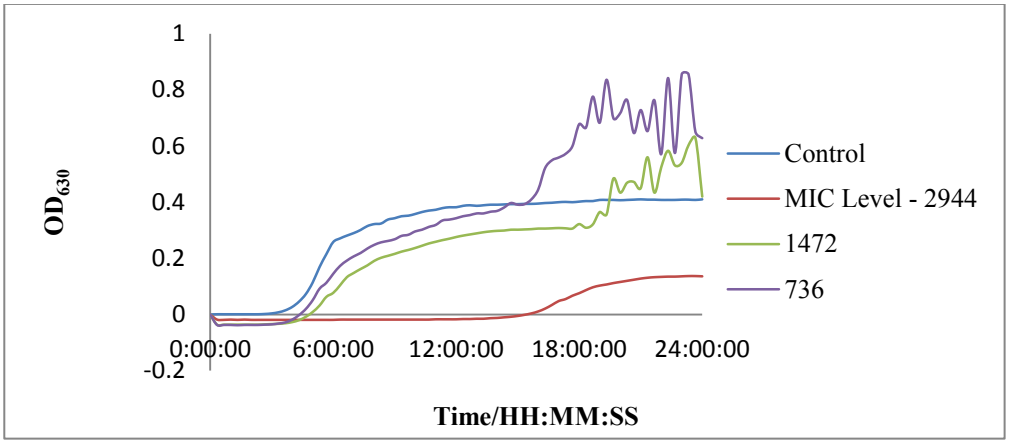

Appendix Figure 9.8 Development of OD_{630} over 24 hours for *E. coli* in BHI broth at 37°C. Containing TREN-R-3,2-HOPO at concentrations given in legend, reported in micromolar. Control contained no ligand (0μM).

9.2 OD_{630} Kinetic assay data *K. pneumoniae*

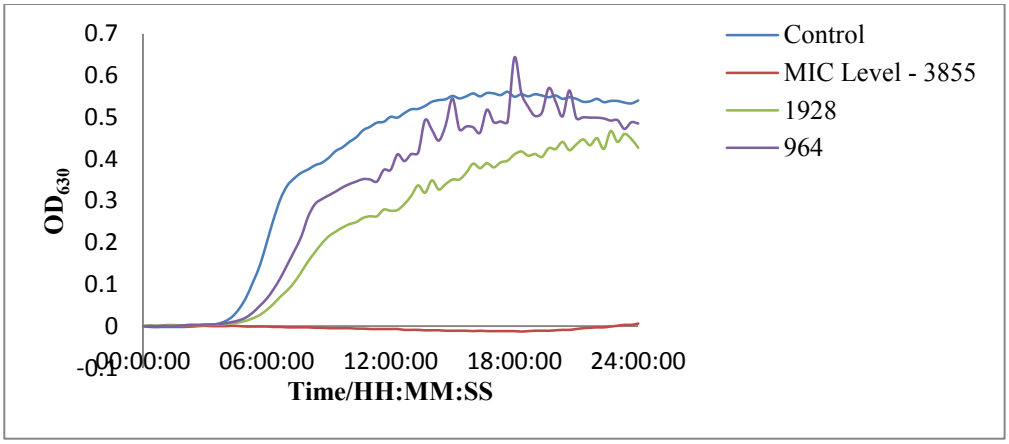

Appendix Figure 9.9 Development of OD_{630} over 24 hours for *K. pneumoniae* in BHI broth at 37°C. Containing CTG-3,2-HOPO at concentrations given in legend, reported in micromolar. Control contained no ligand (0μM).

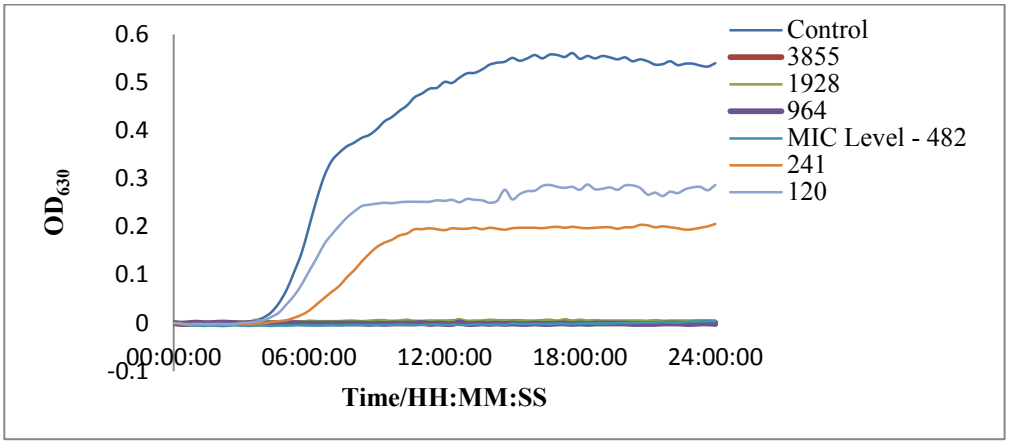

Appendix Figure 9.10 Development of OD_{630} over 24 hours for *K. pneumoniae* in BHI broth at 37°C. Containing CTG-1,2-HOPO at concentrations given in legend, reported in micromolar. Control contained no ligand (0µM).

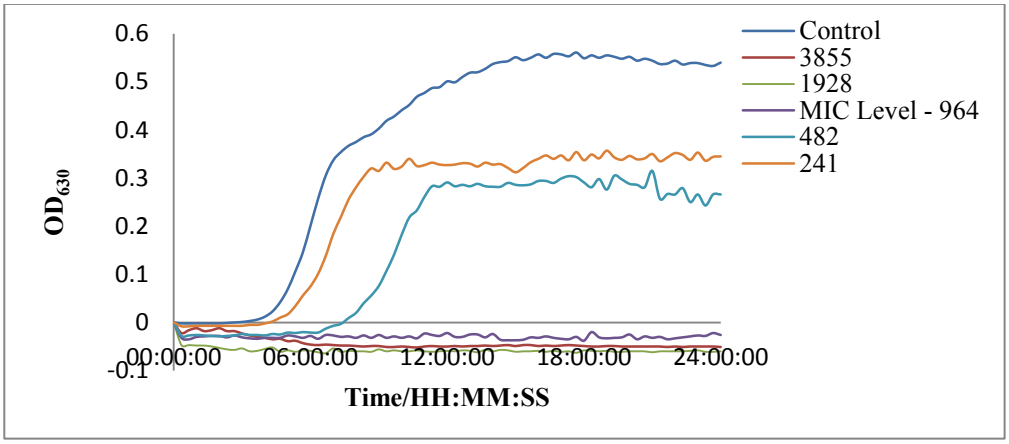

Appendix Figure 9.11 Development of OD_{630} over 24 hours for *K. pneumoniae* in BHI broth at 37°C. Containing triazine-1,2-HOPO at concentrations given in legend, reported in micromolar. Control contained no ligand (0µM).

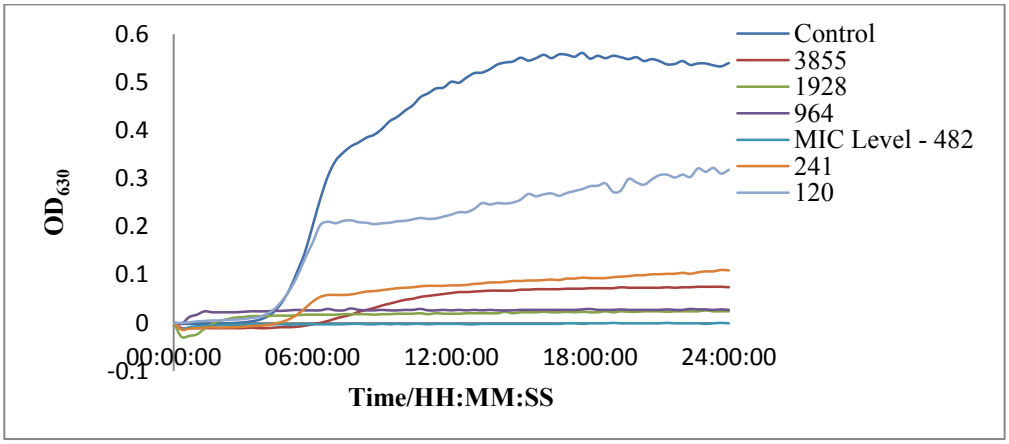

Appendix Figure 9.12 Development of OD_{630} over 24 hours for *K. pneumoniae* in BHI broth at 37°C. Containing TEB-1,2-HOPO at concentrations given in legend, reported in micromolar. Control contained no ligand (0µM).

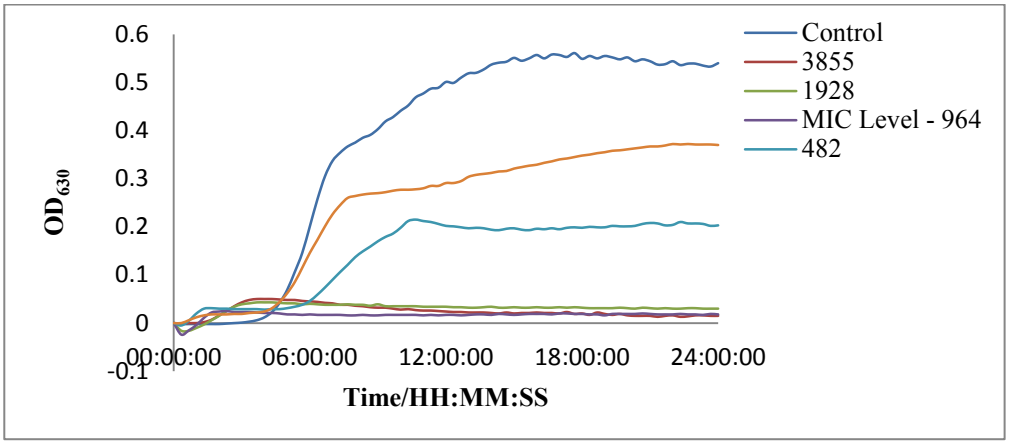

Appendix Figure 9.13 Development of OD_{630} over 24 hours for *K. pneumoniae* in BHI broth at 37°C. Containing TEB-R-3,2-HOPO at concentrations given in legend, reported in micromolar. Control contained no ligand (0µM).

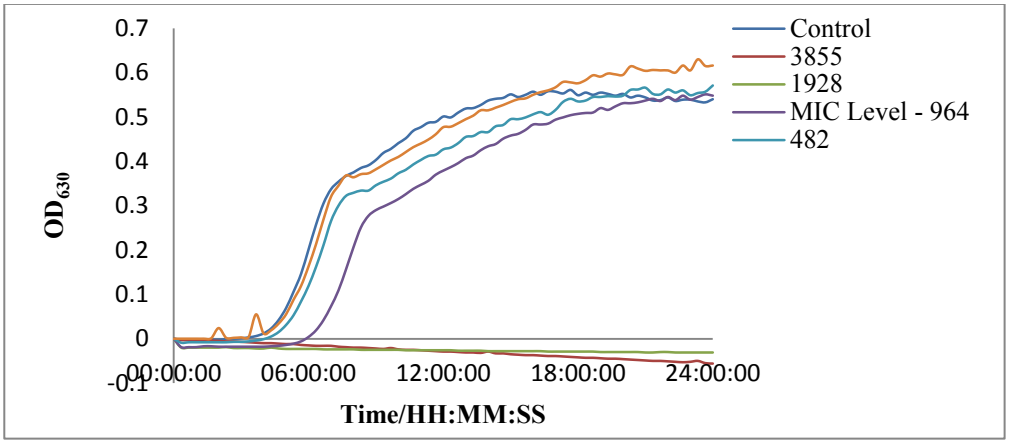

Appendix Figure 9.14 Development of OD_{630} over 24 hours for *K. pneumoniae* in BHI broth at 37°C. Containing TRENCAM at concentrations given in legend, reported in micromolar. Control contained no ligand (0µM).

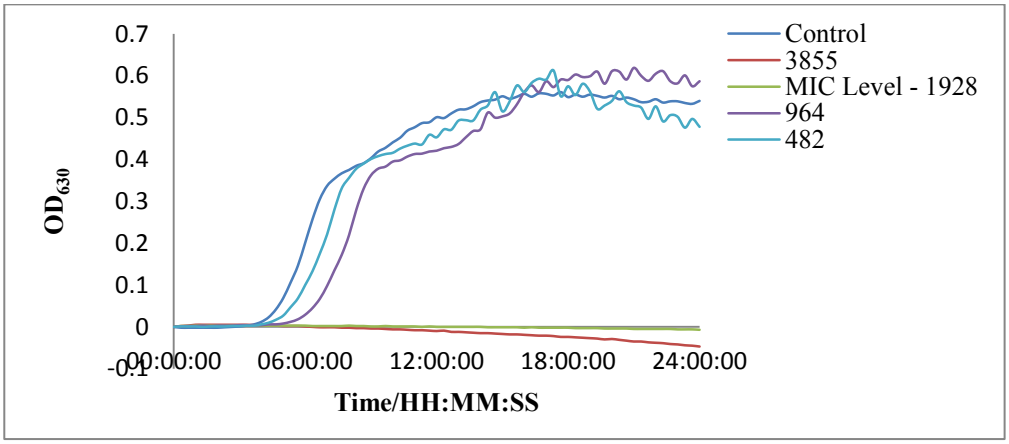

Appendix Figure 9.15 Development of OD_{630} over 24 hours for *K. pneumoniae* in BHI broth at 37°C. Containing EMECAM at concentrations given in legend, reported in micromolar. Control contained no ligand (0µM).

9.3 OD_{630} Kinetic assay data *P. aeruginosa*

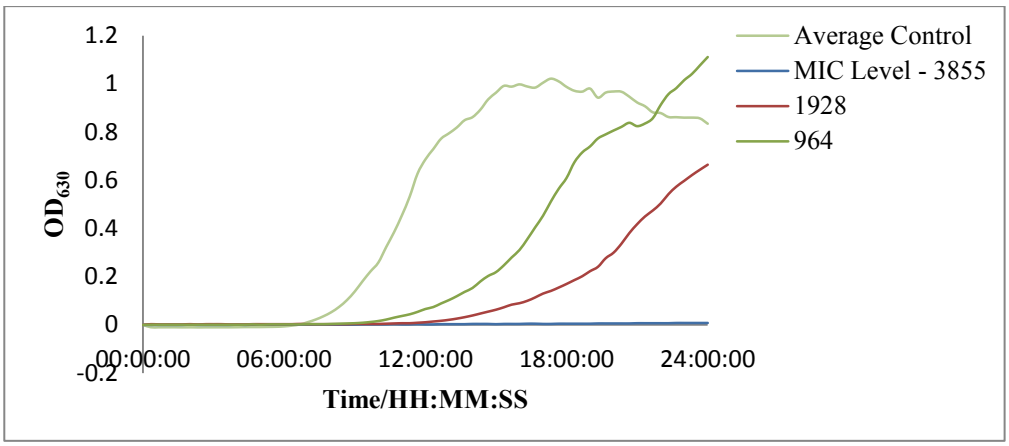

Appendix Figure 9.16 Development of OD_{630} over 24 hours for *P. aeruginosa* in BHI broth at 37°C. Containing CTG-3,2-HOPO at concentrations given in legend, reported in micromolar. Control contained no ligand (0µM).

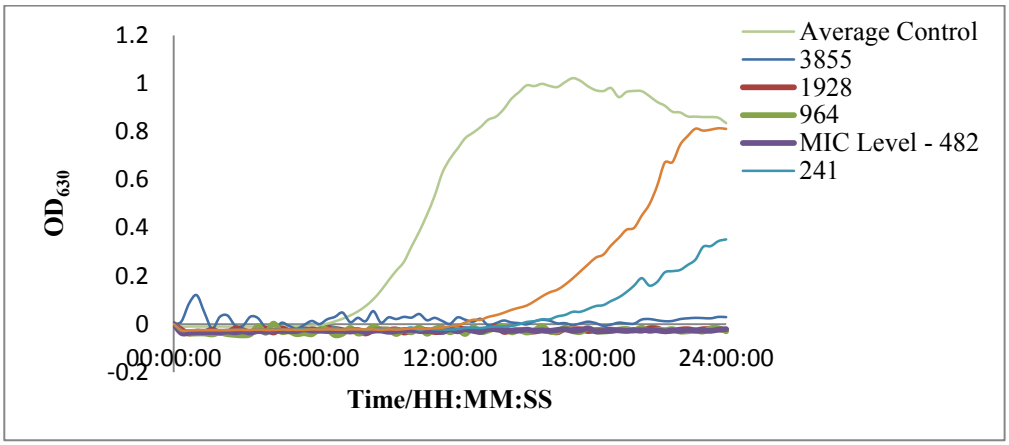

Appendix Figure 9.17 Development of OD_{630} over 24 hours for *P. aeruginosa* in BHI broth at 37°C. Containing triazine-1,2-HOPO at concentrations given in legend, reported in micromolar. Control contained no ligand (0µM).

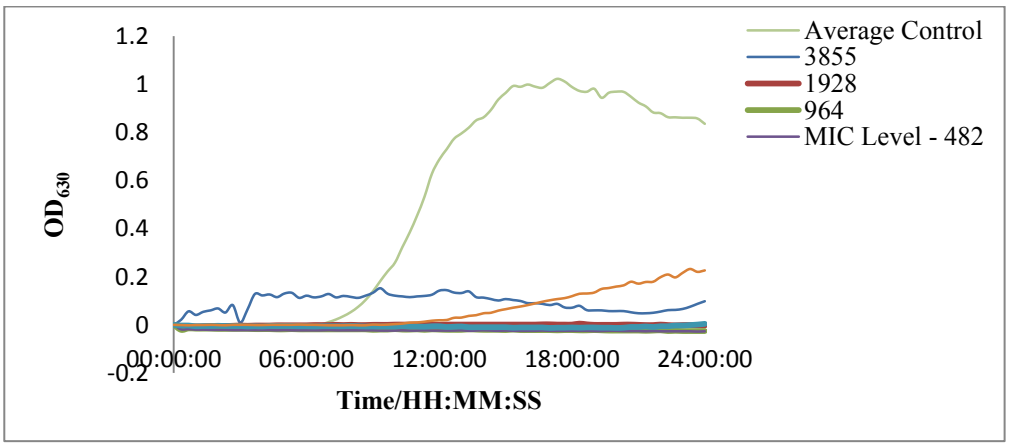

Appendix Figure 9.18 Development of OD_{630} over 24 hours for *P. aeruginosa* in BHI broth at 37°C. Containing CTG-1,2-HOPO at concentrations given in legend, reported in micromolar. Control contained no ligand (0µM).

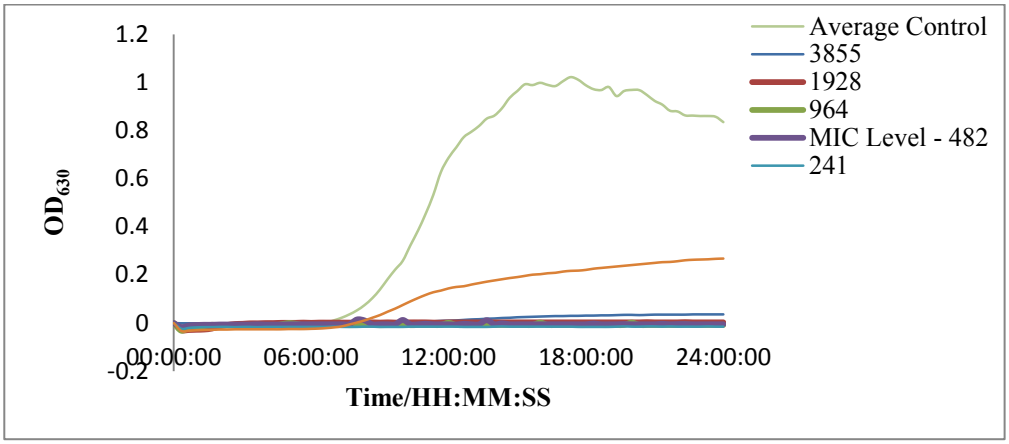

Appendix Figure 9.19 Development of OD_{630} over 24 hours for *P. aeruginosa* in BHI broth at 37°C. Containing TEB-1,2-HOPO at concentrations given in legend, reported in micromolar. Control contained no ligand (0µM).

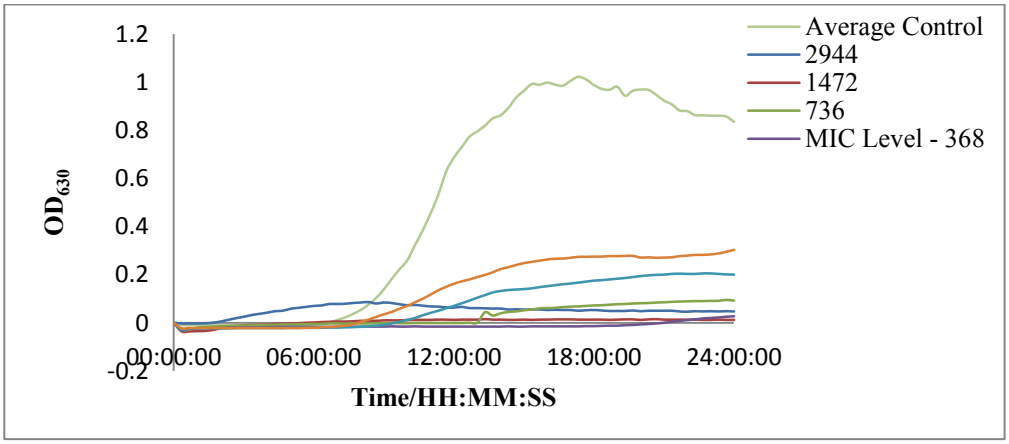

Appendix Figure 9.20 Development of OD_{630} over 24 hours for *P. aeruginosa* in BHI broth at 37°C. Containing TEB-R-3,2-HOPO at concentrations given in legend, reported in micromolar. Control contained no ligand (0µM).

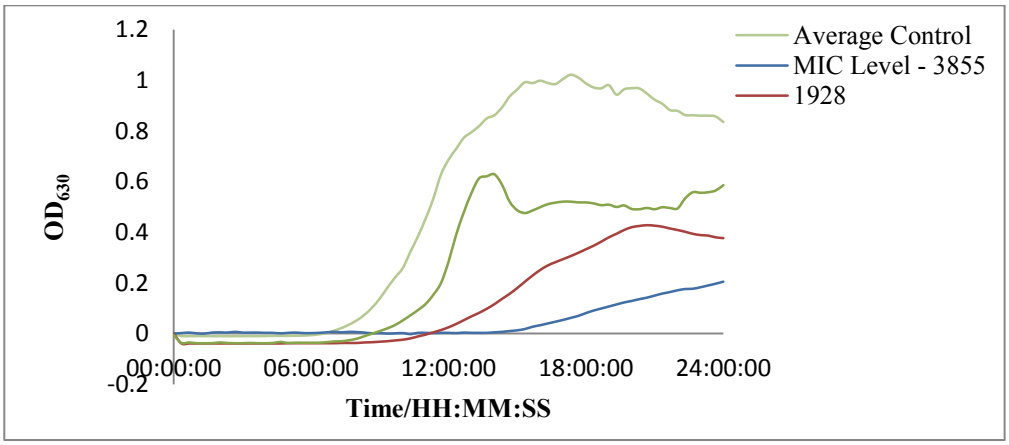

Appendix Figure 9.21 Development of OD_{630} over 24 hours for *P. aeruginosa* in BHI broth at 37°C. Containing TREN-R-3,2-HOPO at concentrations given in legend, reported in micromolar. Control contained no ligand (0µM).

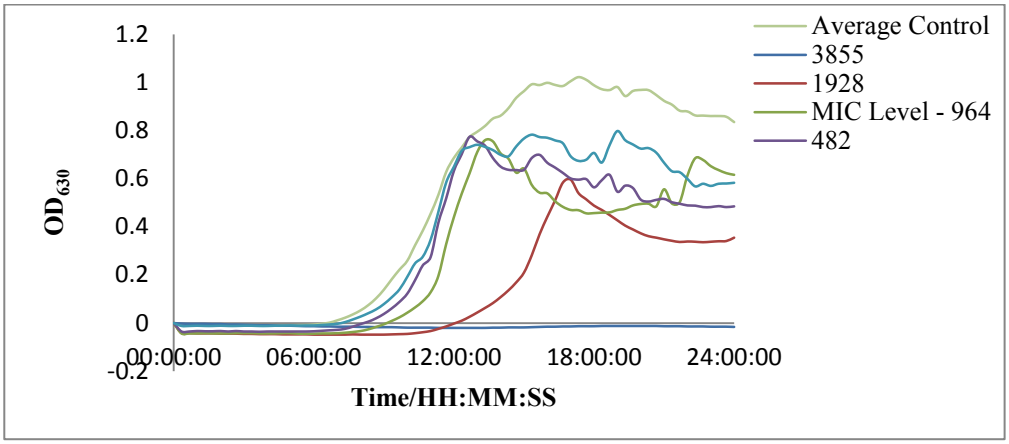

Appendix Figure 9.22 Development of OD_{630} over 24 hours for *P. aeruginosa* in BHI broth at 37°C. Containing TRENCAM at concentrations given in legend, reported in micromolar. Control contained no ligand (0µM).

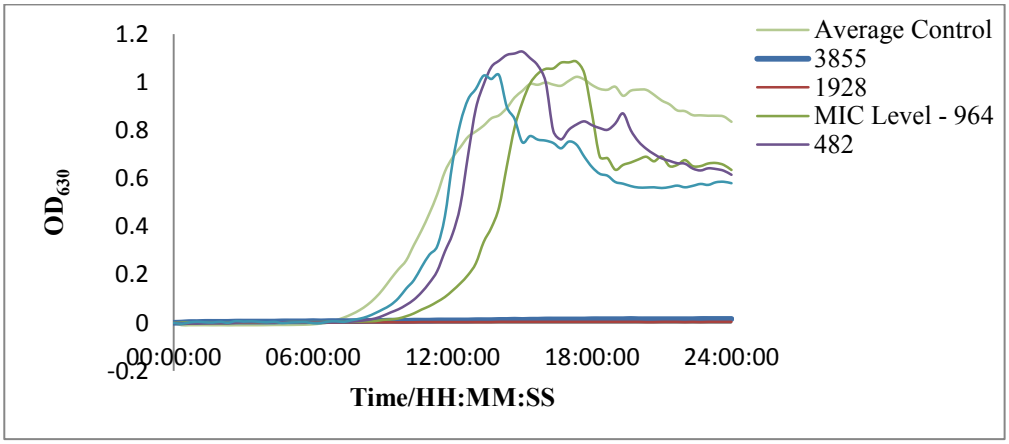

Appendix Figure 9.23 Development of OD_{630} over 24 hours for *P. aeruginosa* in BHI broth at 37°C. Containing EMECAM at concentrations given in legend, reported in micromolar. Control contained no ligand (0µM).

9.4 OD_{630} Kinetic assay data *A. baumannii*

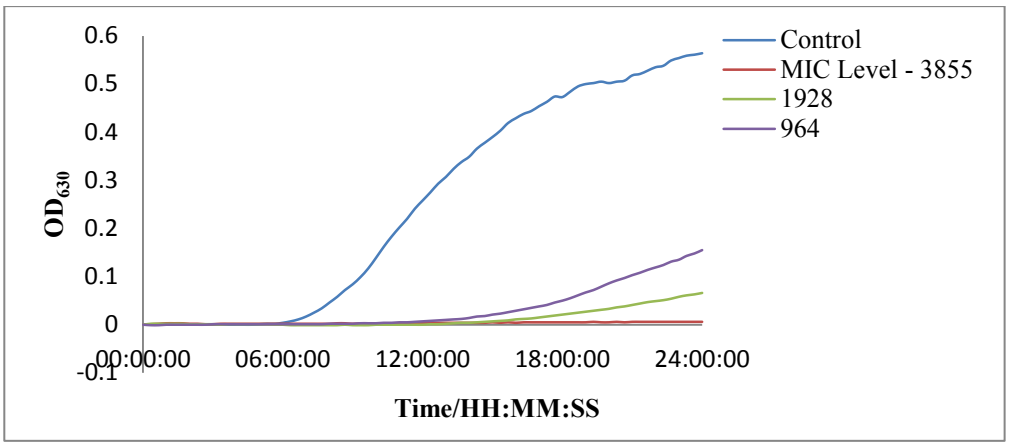

Appendix Figure 9.24 Development of OD_{630} over 24 hours for *A. baumannii* in BHI broth at 37°C. Containing CTG-3,2-HOPO at concentrations given in legend, reported in micromolar. Control contained no ligand (0µM).

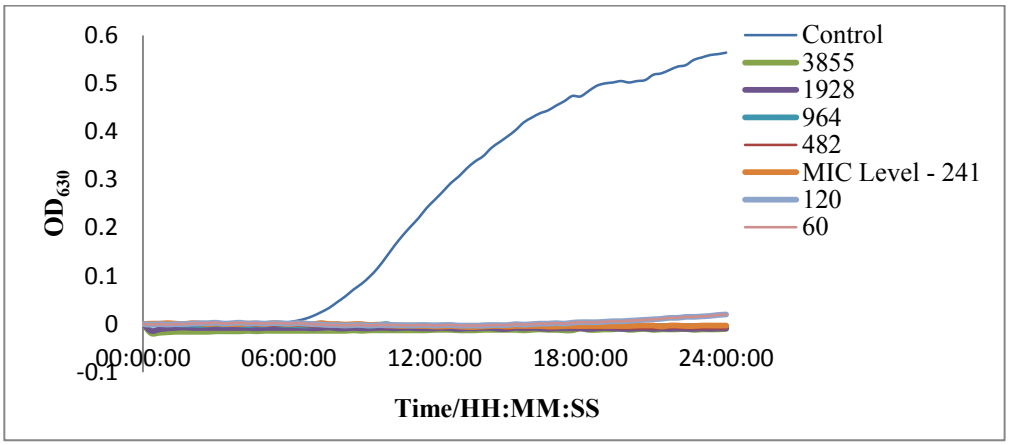

Appendix Figure 9.25 Development of OD_{630} over 24 hours for *A. baumannii* in BHI broth at 37°C. Containing CTG-1,2-HOPO at concentrations given in legend, reported in micromolar. Control contained no ligand (0µM).

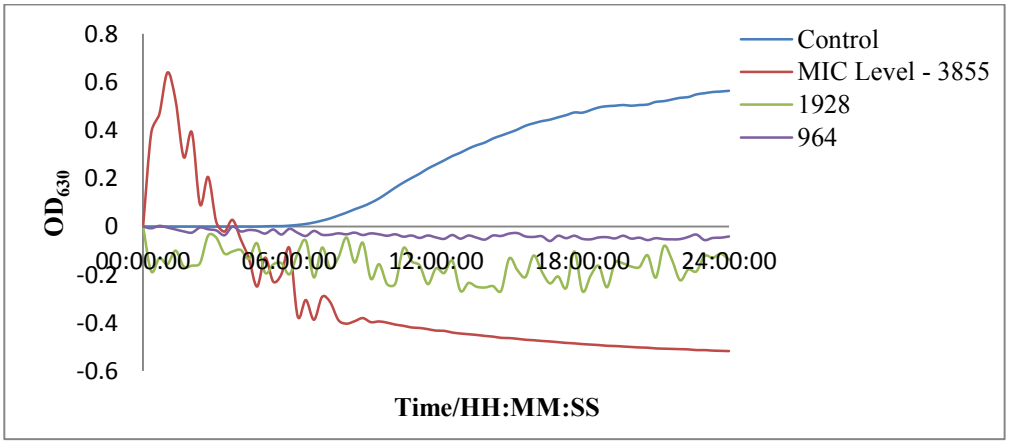

Appendix Figure 9.26 Development of OD_{630} over 24 hours for *A. baumannii* in BHI broth at 37°C. Containing triazine-3,2-HOPO at concentrations given in legend, reported in micromolar. Control contained no ligand (0µM).

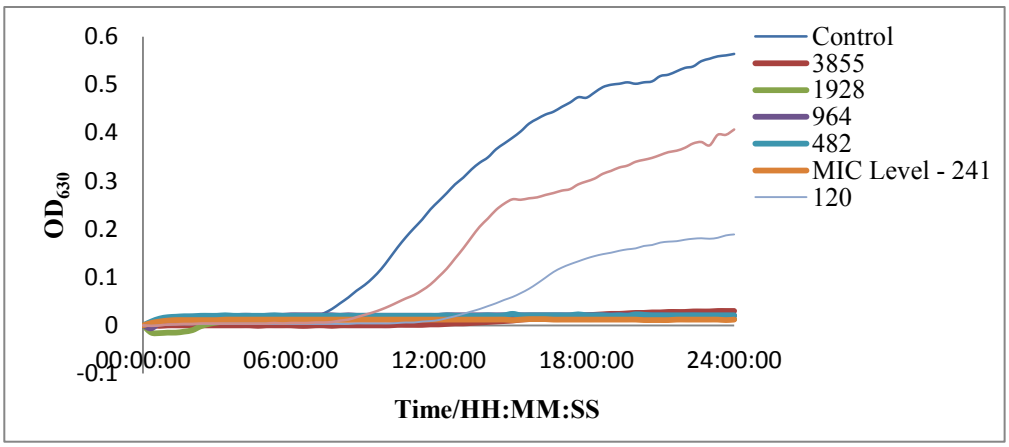

Appendix Figure 9.27 Development of OD_{630} over 24 hours for *A. baumannii* in BHI broth at 37°C. Containing TEB-1,2-HOPO at concentrations given in legend, reported in micromolar. Control contained no ligand (0μM).

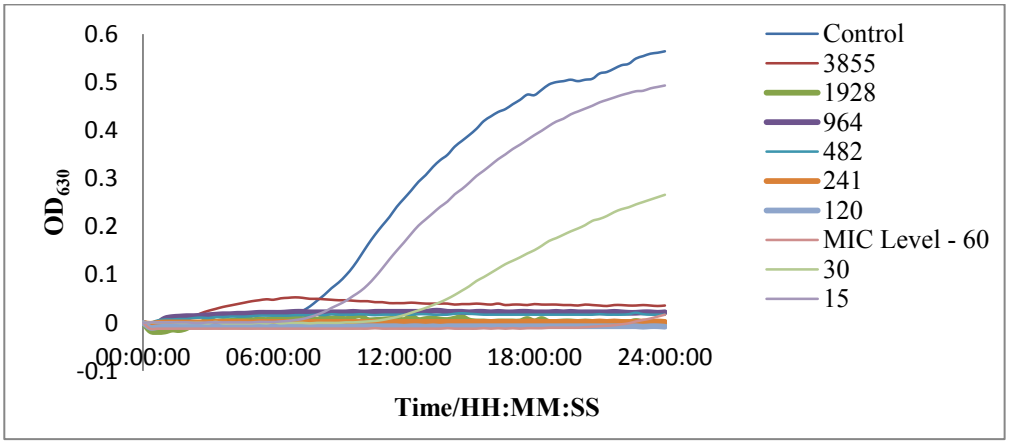

Appendix Figure 9.28 Development of OD_{630} over 24 hours for *A. baumannii* in BHI broth at 37°C. Containing TEB-R-3,2-HOPO at concentrations given in legend, reported in micromolar. Control contained no ligand (0μM).

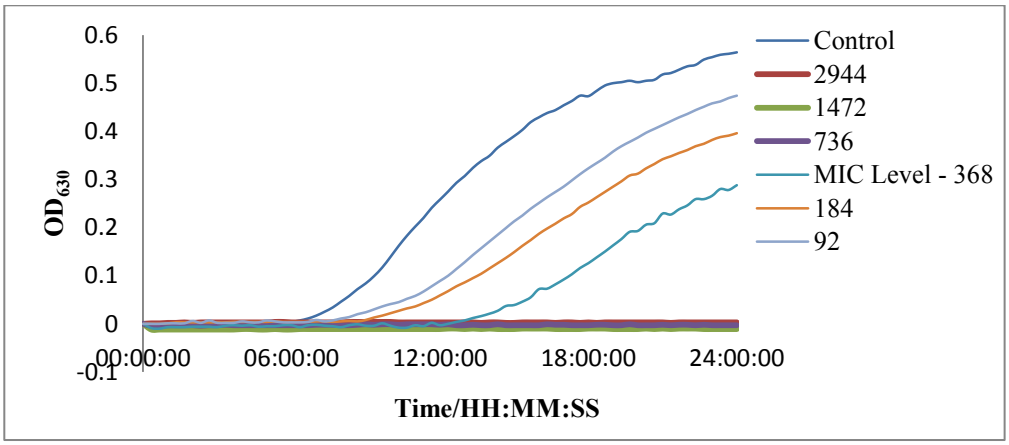

Appendix Figure 9.29 Development of OD_{630} over 24 hours for *A. baumannii* in BHI broth at 37°C. Containing TREN-R-3,2-HOPO at concentrations given in legend, reported in micromolar. Control contained no ligand (0μM).

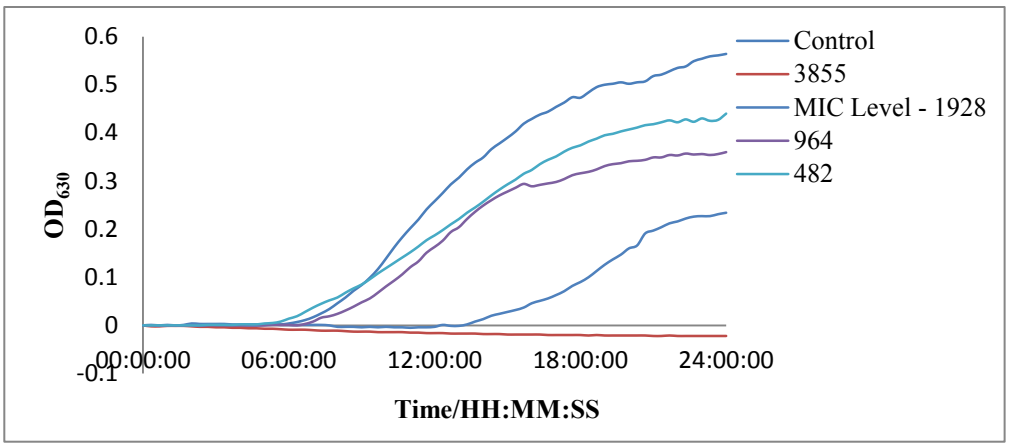

Appendix Figure 9.30 Development of OD_{630} over 24 hours for *A. baumannii* in BHI broth at 37°C. Containing TRENCAM at concentrations given in legend, reported in micromolar. Control contained no ligand (0μM).

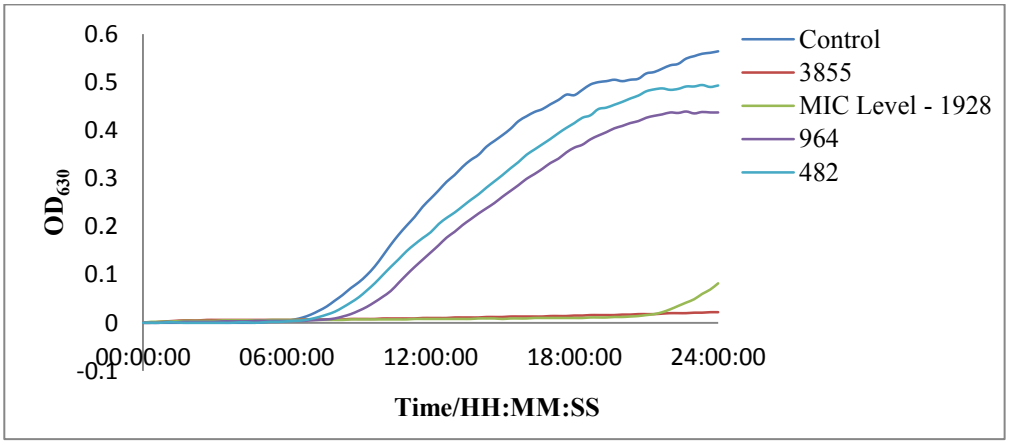

Appendix Figure 9.31 Development of OD_{630} over 24 hours for *A. baumannii* in BHI broth at 37°C. Containing EMECAM at concentrations given in legend, reported in micromolar. Control contained no ligand (0μM).

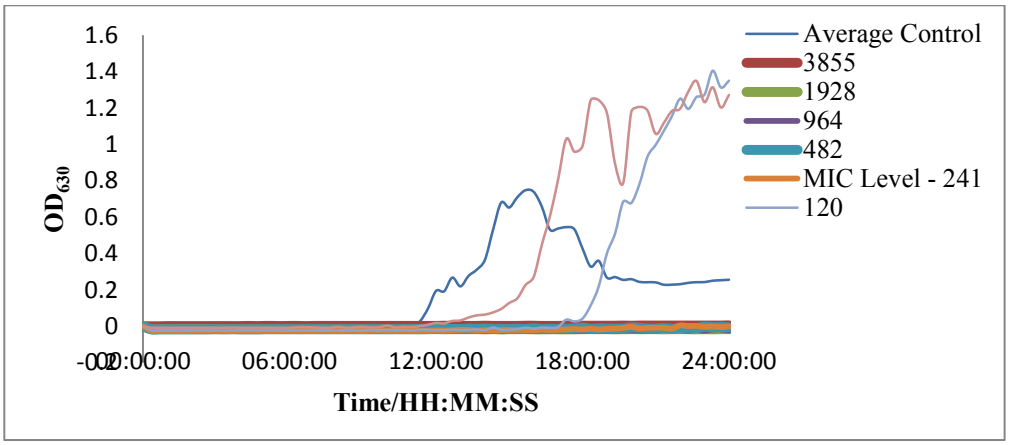

Appendix Figure 9.32 Development of OD_{630} over 24 hours for *S. aureus* in BHI broth at 37°C. Containing CTG-3,2-HOPO at concentrations given in legend, reported in micromolar. Control contained no ligand (0μM).

9.5 OD_{630} Kinetic assay data *S. aureus*

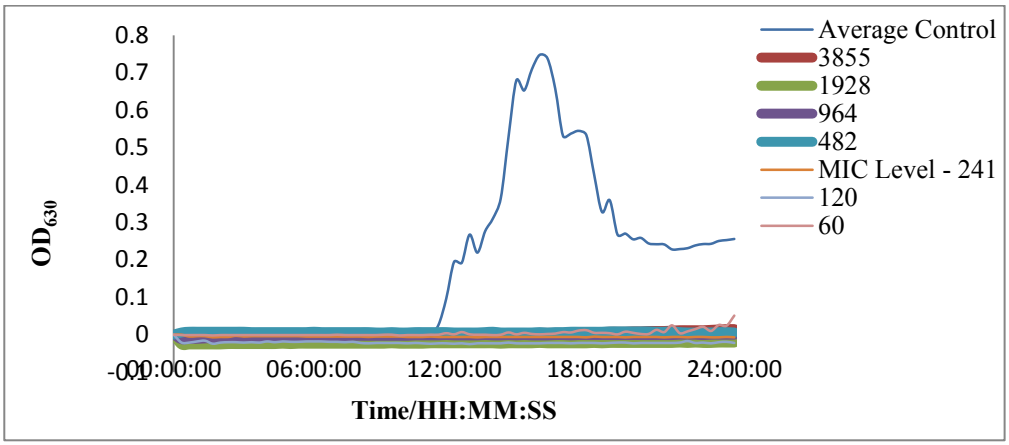

Appendix Figure 9.33 Development of OD_{630} over 24 hours for *S. aureus* in BHI broth at 37°C. Containing CTG-1,2-HOPO at concentrations given in legend, reported in micromolar. Control contained no ligand (0µM).

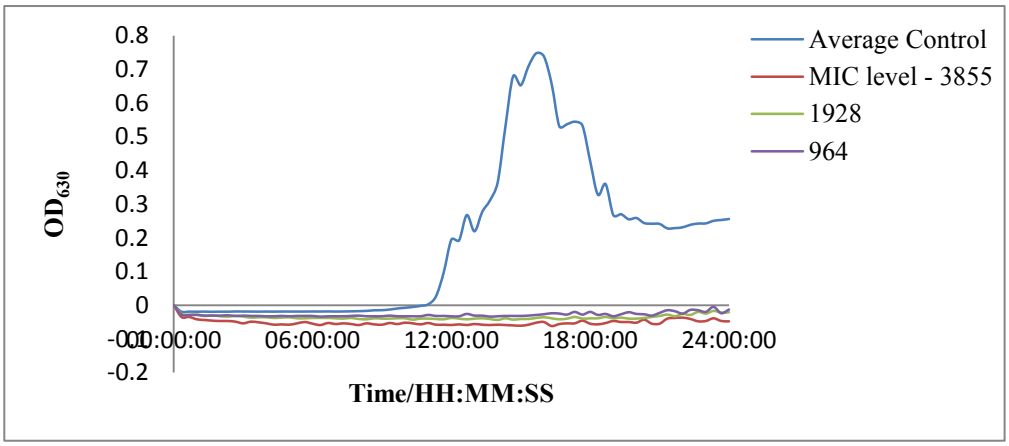

Appendix Figure 9.34 Development of OD_{630} over 24 hours for *S. aureus* in BHI broth at 37°C. Containing triazine-3,2-HOPO at concentrations given in legend, reported in micromolar. Control contained no ligand (0µM).

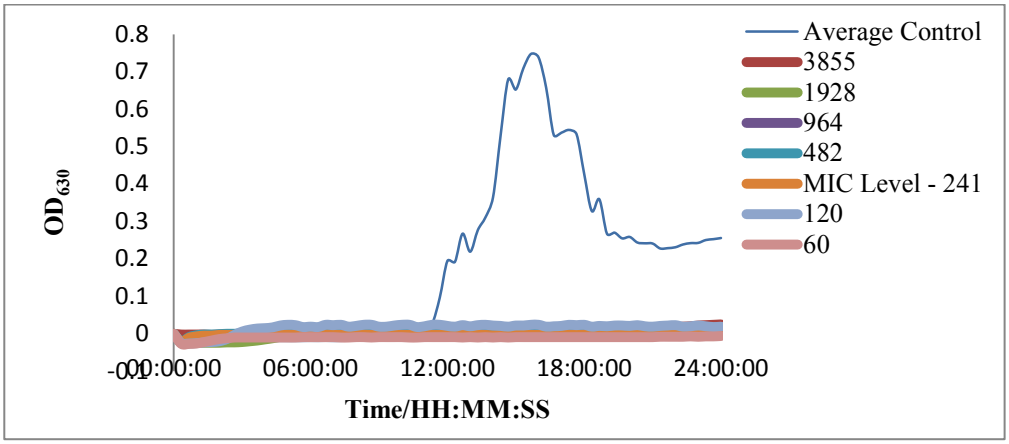

Appendix Figure 9.35 Development of OD_{630} over 24 hours for *S. aureus* in BHI broth at 37°C. Containing TEB-1,2-HOPO at concentrations given in legend, reported in micromolar. Control contained no ligand (0μM).

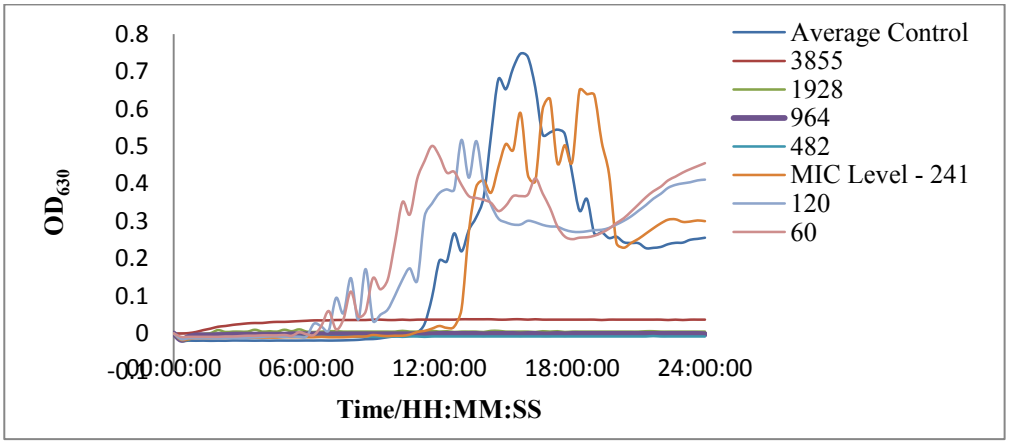

Appendix Figure 9.36 Development of OD_{630} over 24 hours for *S. aureus* in BHI broth at 37°C. Containing TEB-R-3,2-HOPO at concentrations given in legend, reported in micromolar. Control contained no ligand (0μM).

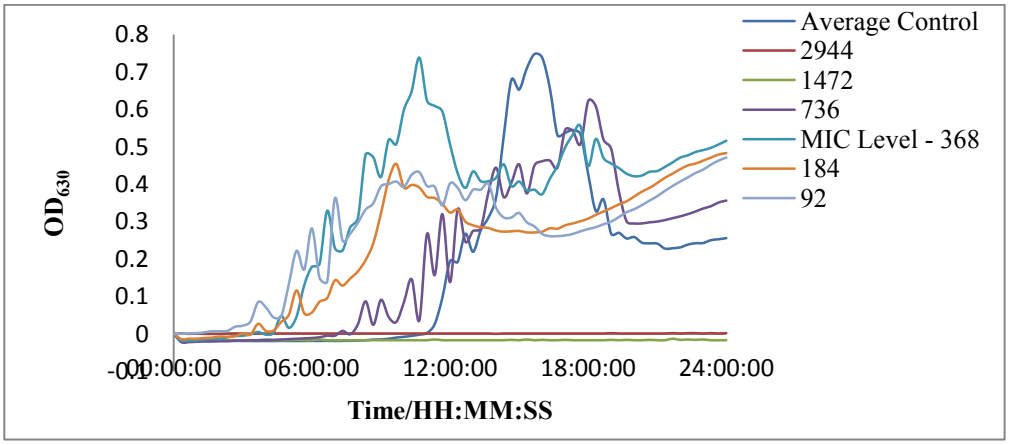

Appendix Figure 9.37 Development of OD_{630} over 24 hours for *S. aureus* in BHI broth at 37°C. Containing TREN-R-3,2-HOPO at concentrations given in legend, reported in micromolar. Control contained no ligand (0μM).

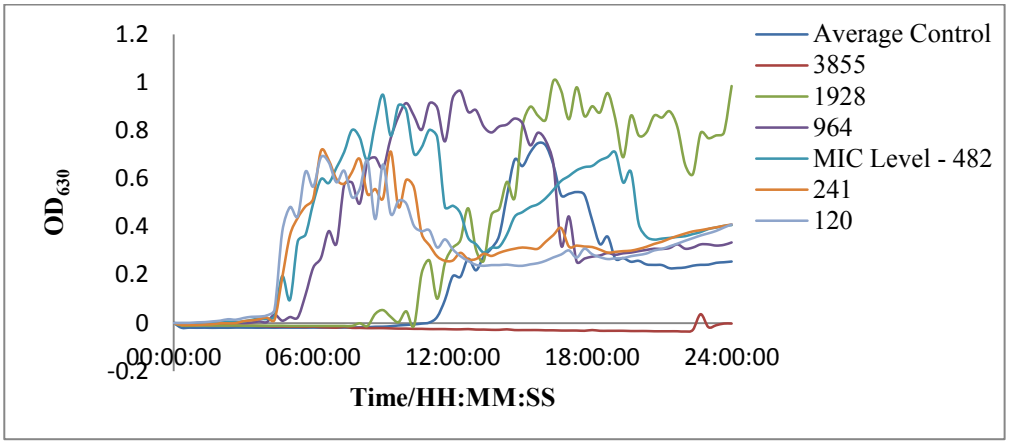

Appendix Figure 9.38 Development of OD_{630} over 24 hours for *S. aureus* in BHI broth at 37°C. Containing TRENCAM at concentrations given in legend, reported in micromolar. Control contained no ligand (0μM).

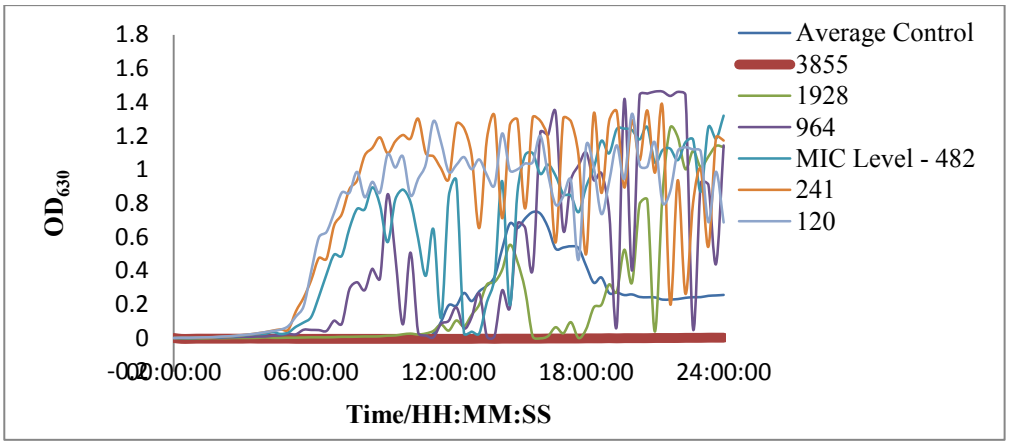

Appendix Figure 9.39 Development of OD_{630} over 24 hours for *S. aureus* in BHI broth at 37°C. Containing EMECAM at concentrations given in legend, reported in micromolar. Control contained no ligand (0μM).

9.6 OD_{630} Kinetic assay data *B. subtilis*

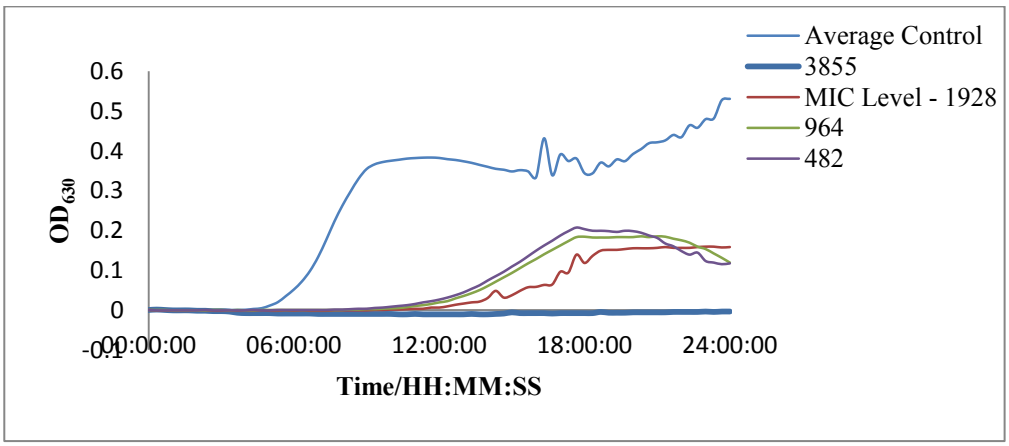

Appendix Figure 9.40 Development of OD_{630} over 24 hours for *B. subtilis* in BHI broth at 37°C. Containing CTG-3,2-HOPO at concentrations given in legend, reported in micromolar. Control contained no ligand (0μM).

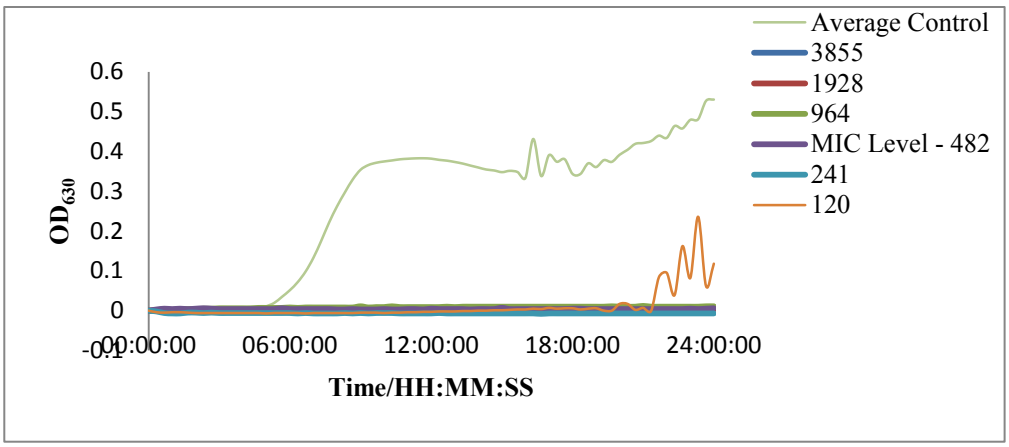

Appendix Figure 9.41 Development of OD_{630} over 24 hours for *B. subtilis* in BHI broth at 37°C. Containing CTG-1,2-HOPO at concentrations given in legend, reported in micromolar. Control contained no ligand (0μM).

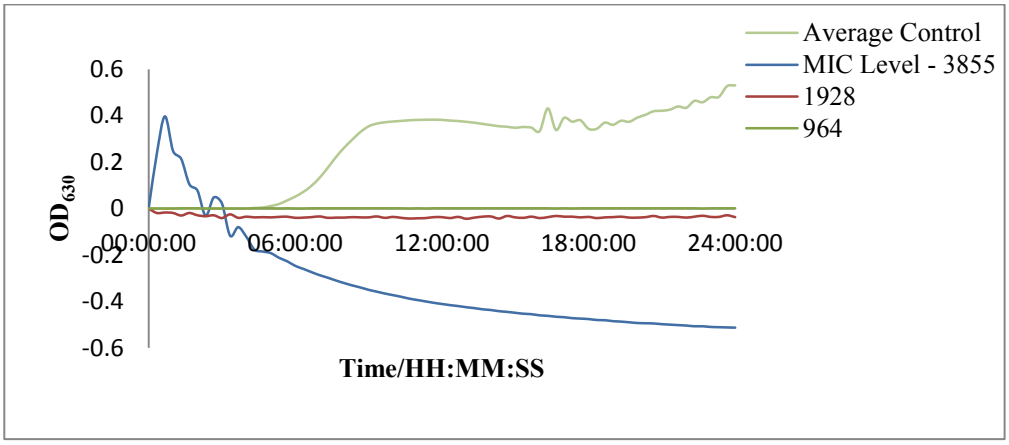

Appendix Figure 9.42 Development of OD_{630} over 24 hours for *B. subtilis* in BHI broth at 37°C. Containing triazine-3,2-HOPO at concentrations given in legend, reported in micromolar. Control contained no ligand (0μM).

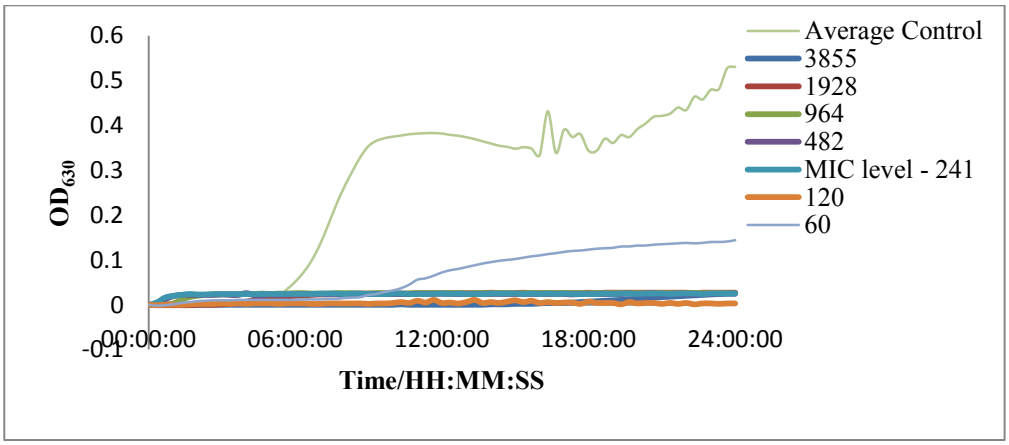

Appendix Figure 9.43 Development of OD_{630} over 24 hours for *B. subtilis* in BHI broth at 37°C. Containing TEB-1,2-HOPO at concentrations given in legend, reported in micromolar. Control contained no ligand (0μM).

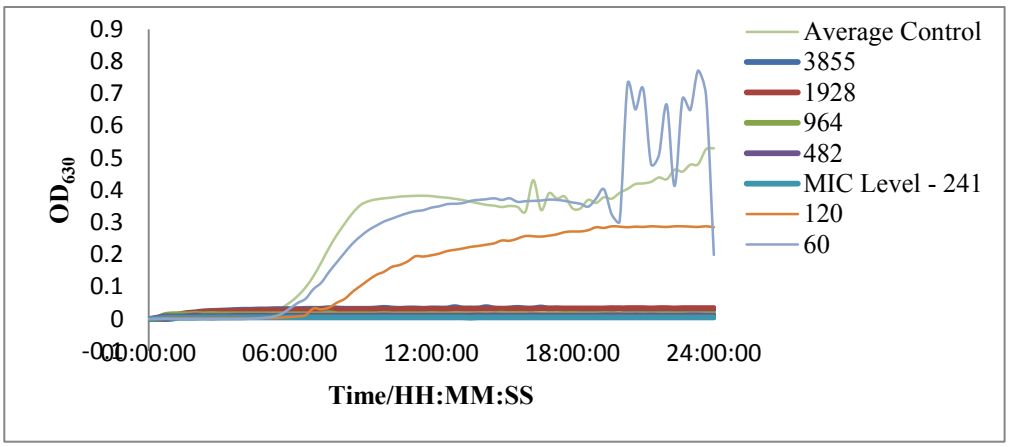

Appendix Figure 9.44 Development of OD_{630} over 24 hours for *B. subtilis* in BHI broth at 37°C. Containing TEB-R-3,2-HOPO at concentrations given in legend, reported in micromolar. Control contained no ligand (0μM).

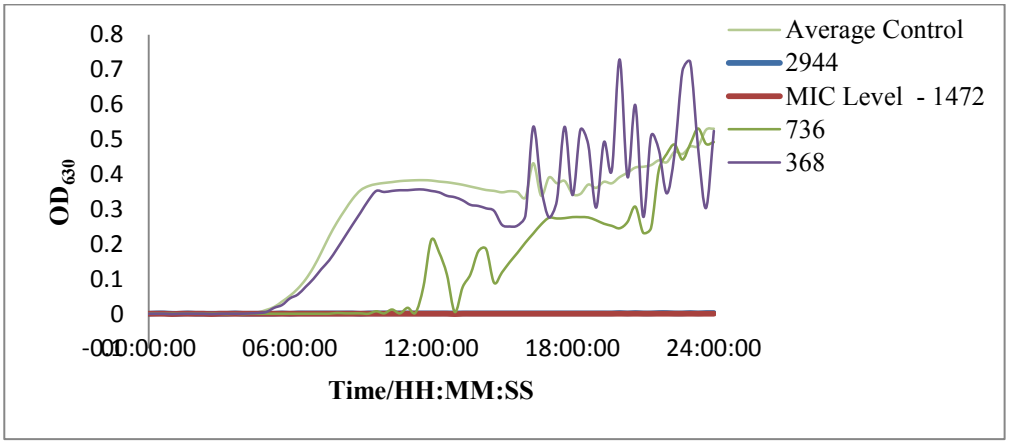

Appendix Figure 9.45 Development of OD_{630} over 24 hours for *B. subtilis* in BHI broth at 37°C. Containing TREN-R-3,2-HOPO at concentrations given in legend, reported in micromolar. Control contained no ligand (0μM).

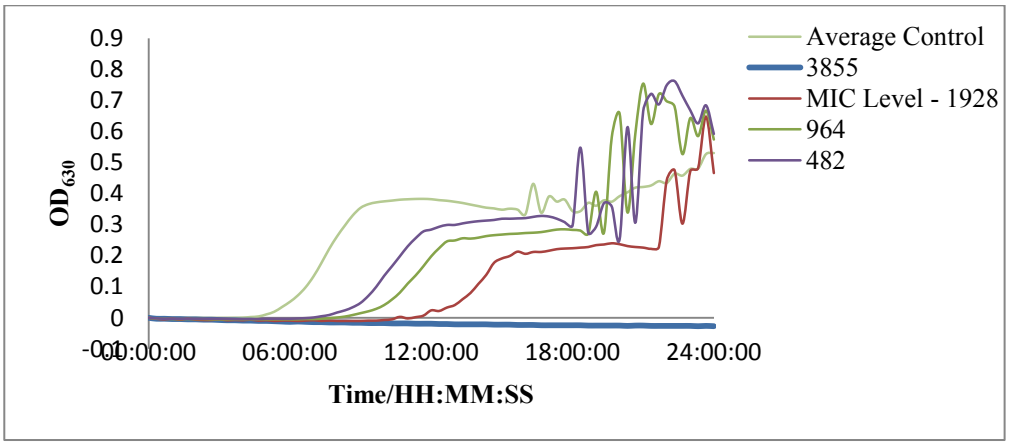

Appendix Figure 9.46 Development of OD_{630} over 24 hours for *B. subtilis* in BHI broth at 37°C. Containing TRENCAM at concentrations given in legend, reported in micromolar. Control contained no ligand (0μM).

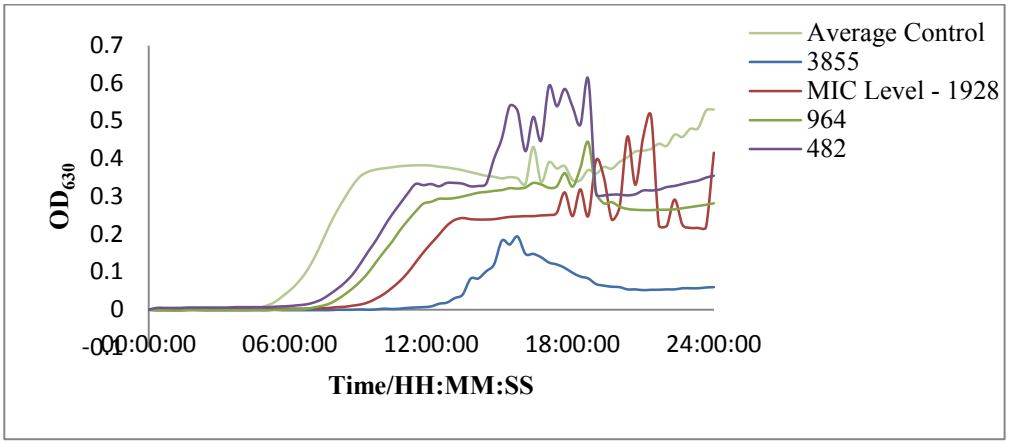

Appendix Figure 9.47 Development of OD_{630} over 24 hours for *B. subtilis* in BHI broth at 37°C. Containing EMECAM at concentrations given in legend, reported in micromolar. Control contained no ligand (0µM).

9.7 OD_{630} Kinetic assay data *C. albicans*

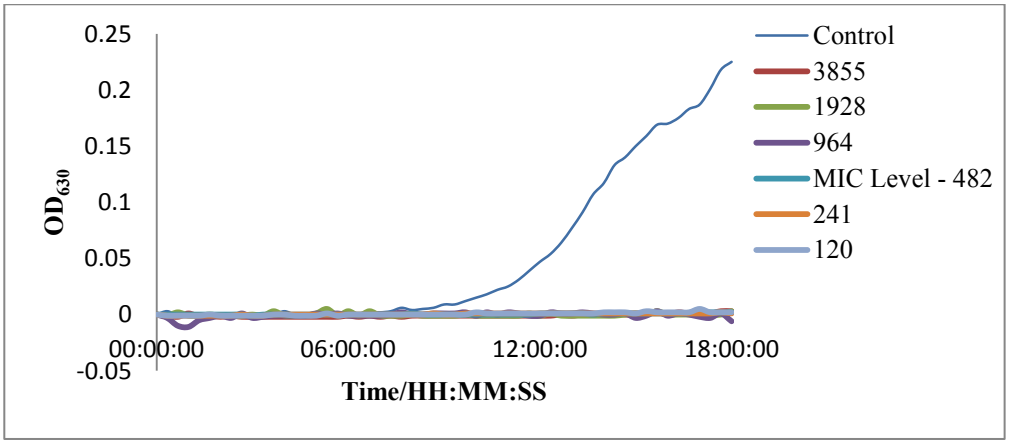

Appendix Figure 9.48 Development of OD_{630} over 18 hours for *C. albicans* in BHI broth at 37°C. Containing CTG-3,2-HOPO at concentrations given in legend, reported in micromolar. Control contained no ligand (0µM).

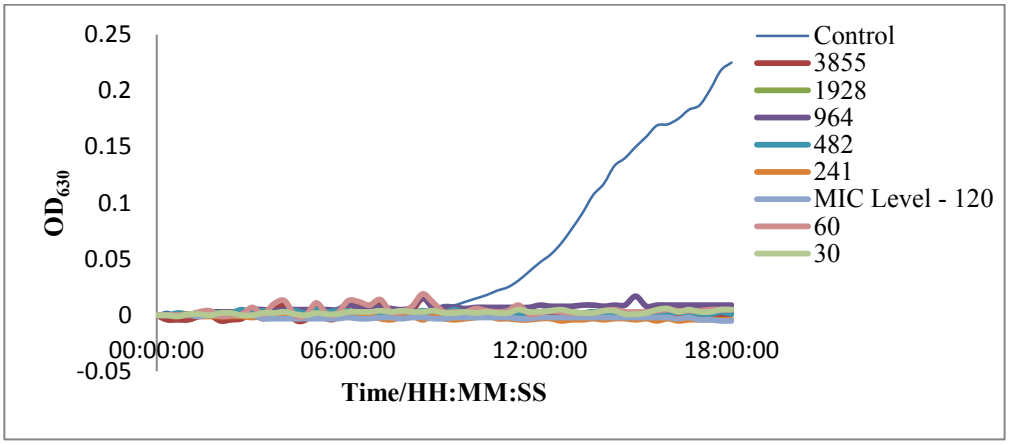

Appendix Figure 9.49 Development of OD_{630} over 18 hours for *C. albicans* in BHI broth at 37°C. Containing CTG-1,2-HOPO at concentrations given in legend, reported in micromolar. Control contained no ligand (0µM).

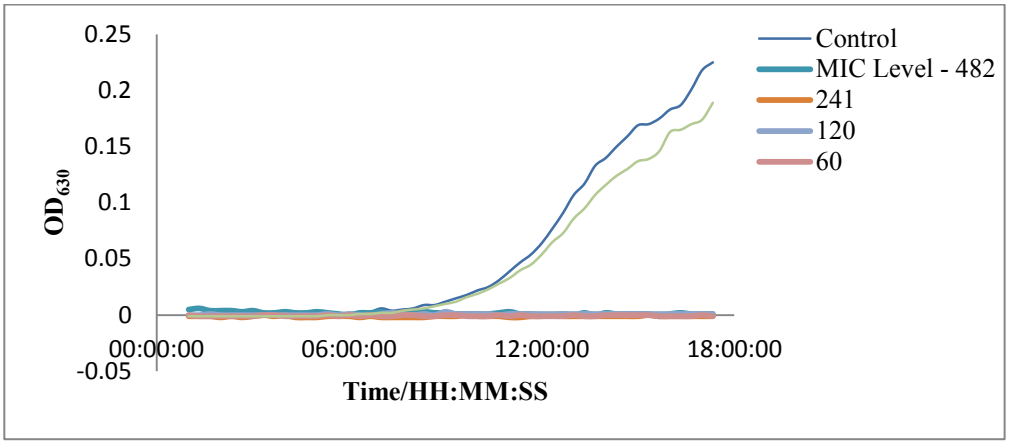

Appendix Figure 9.50 Development of OD_{630} over 18 hours for *C. albicans* in BHI broth at 37°C. Containing triazine-3,2-HOPO at concentrations given in legend, reported in micromolar. Control contained no ligand (0µM).

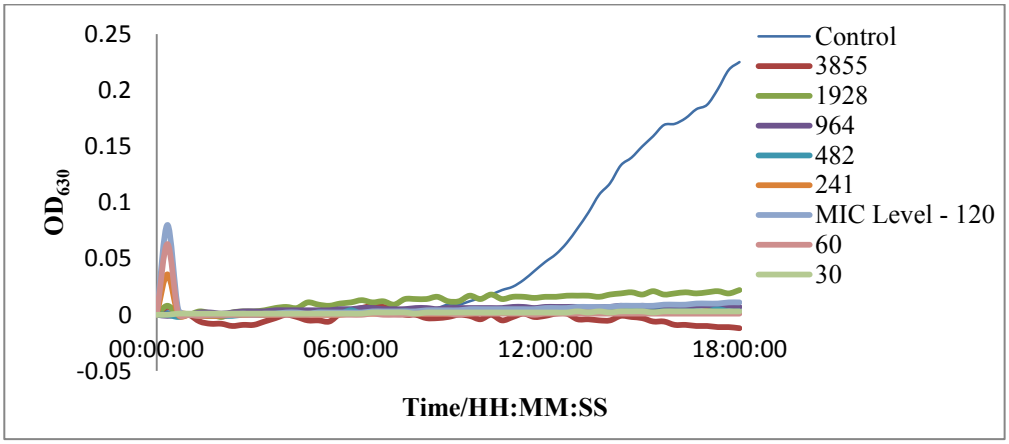

Appendix Figure 9.51 Development of OD_{630} over 18 hours for *C. albicans* in BHI broth at 37°C. Containing triaizne-1,2-HOPO at concentrations given in legend, reported in micromolar. Control contained no ligand (0µM).

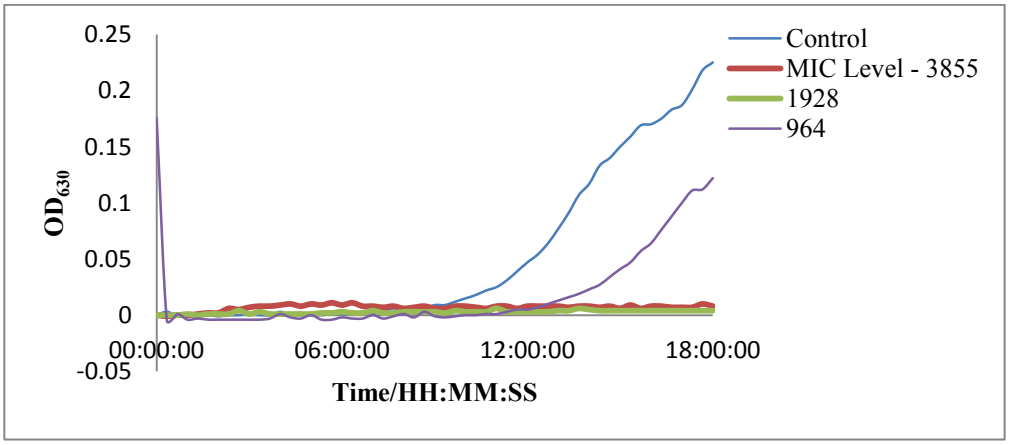

Appendix Figure 9.52 Development of OD_{630} over 18 hours for *C. albicans* in BHI broth at 37°C. Containing TEB-LC-3,2-HOPO at concentrations given in legend, reported in micromolar. Control contained no ligand (0µM).

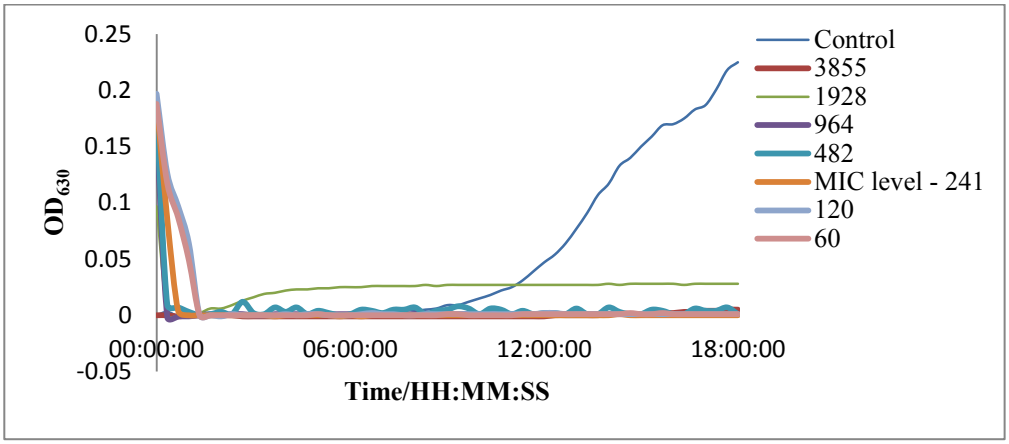

Appendix Figure 9.53 Development of OD_{630} over 18 hours for *C. albicans* in BHI broth at 37°C. Containing TEB-1,2-HOPO at concentrations given in legend, reported in micromolar. Control contained no ligand (0µM).

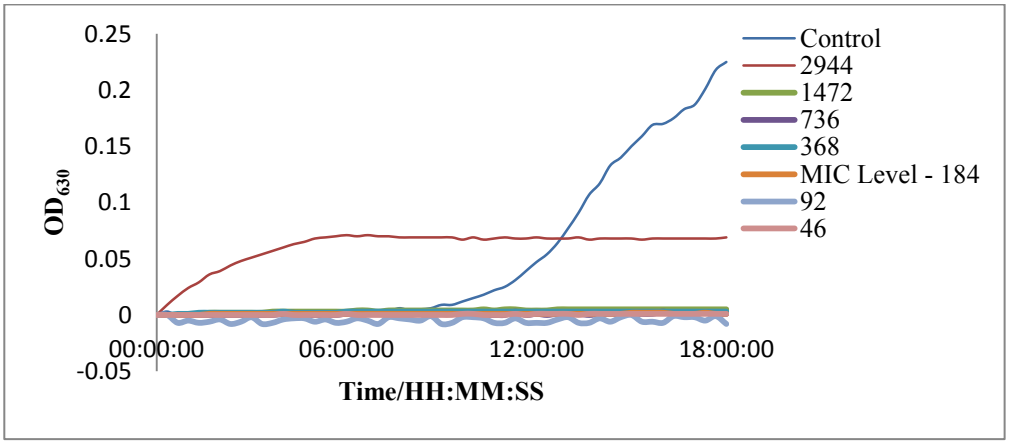

Appendix Figure 9.54 Development of OD_{630} over 18 hours for *C. albicans* in BHI broth at 37°C. Containing TEB-R-3,2-HOPO at concentrations given in legend, reported in micromolar. Control contained no ligand (0µM).

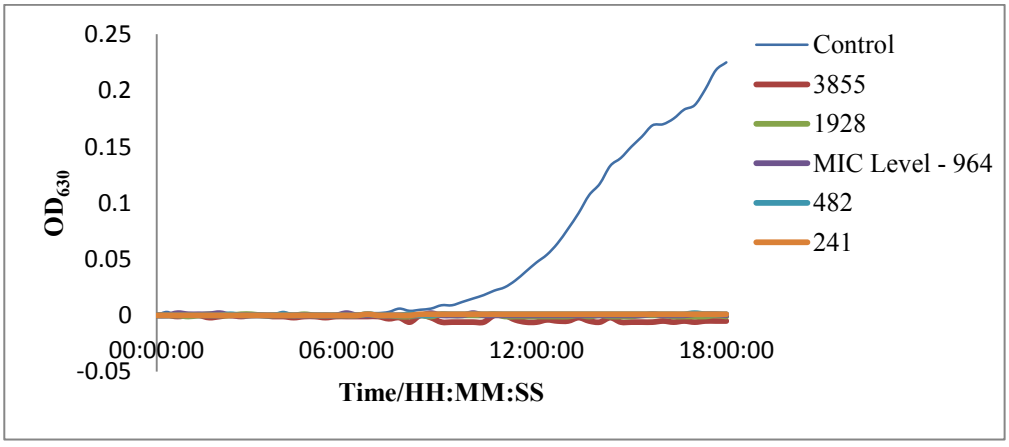

Appendix Figure 9.55 Development of OD_{630} over 18 hours for *C. albicans* in BHI broth at 37°C. Containing TREN-R-3,2-HOPO at concentrations given in legend, reported in micromolar. Control contained no ligand (0µM).

10 References

(1) Bellion, E. *Journal of Chemical Education* **1992**, *69*, A326.
(2) Atreya, S. K. *Eos, Transactions American Geophysical Union* **1999**, *80*, 320.
(3) Williams, R. J. P.; Rickaby, R. *Evolutions Destiny*, 2012.
(4) Boukhalfa, H.; Crumbliss, A. *Biometals* **2002**, *15*, 325.
(5) Buda, F.; Ensing, B.; Gribnau, M. C.; Baerends, E. J. *Chemistry* **2003**, *9*, 3436.
(6) Messenger, A. J. M.; Barclay, R. *Biochemical Education* **1983**, *11*, 54.
(7) Raymond, K. N.; Carrano, C. J. *Accounts of Chemical Research* **1979**, *12*, 183.
(8) Barnes, C. *Journal of Chemical Education* **2003**, *80*, 747.
(9) Harrington, J. M., Duke University, 2010.
(10) Neilands, J. B. *Journal of the American Chemical Society* **1952**, *74*, 4846.
(11) Garibaldi, J. A.; Neilands, J. B. *Journal of the American Chemical Society* **1955**, *77*, 2429.
(12) Emery, T.; Neilands, J. B. *Journal of the American Chemical Society* **1961**, *83*, 1626.
(13) Snow, G. A. *Journal of the Chemical Society (Resumed)* **1954**, *0*, 2588.
(14) Snow, G. A. *Journal of the Chemical Society (Resumed)* **1954**, *0*, 4080.
(15) Ito, T.; Neilands, J. B. *Journal of the American Chemical Society* **1958**, *80*, 4645.
(16) Brot, N.; Goodwin, J.; Fales, H. *Biochem Biophys Res Commun* **1966**, *25*, 454.
(17) O'Brien, I. G.; Cox, G. B.; Gibson, F. *Biochim Biophys Acta* **1970**, *201*, 453.
(18) Pollack, J. R.; Neilands, J. B. *Biochem Biophys Res Commun* **1970**, *38*, 989.
(19) Raymond, K. N.; Dertz, E. A.; Kim, S. S. *Proceedings of the National Academy of Sciences* **2003**, *100*, 3584.
(20) Hider, R. C.; Kong, X. *Natural Product Reports* **2010**, *27*, 637.
(21) Streater, M.; Taylor, P. D.; Hider, R. C.; Porter, J. *Journal of Medicinal Chemistry* **1990**, *33*, 1749.
(22) Sun, Y.; Motekaitis, R. J.; Martell, A. E. *Inorganica Chimica Acta* **1998**, *281*, 60.
(23) d'Hardemare, A.; Torelli, S.; Serratrice, G.; Pierre, J.-L. *Biometals* **2006**, *19*, 349.
(24) Imbert, D.; Thomas, F.; Baret, P.; Serratrice, G.; Gaude, D.; Pierre, J.-L.; Laulhere, J.-P. *New Journal of Chemistry* **2000**, *24*, 281.
(25) Matsumoto, K.; Ozawa, T.; Jitsukawa, K.; Masuda, H. *Inorganic Chemistry* **2004**, *43*, 8538.
(26) Raymond, K. N. *Pure and Applied Chemistry* **1994**, *66*, 773.
(27) Clarke, T. E.; Ku, S.-Y.; Dougan, D. R.; Vogel, H. J.; Tari, L. W. *Nat Struct Mol Biol* **2000**, *7*, 287.
(28) Scarrow, R. C.; Riley, P. E.; Abu-Dari, K.; White, D. L.; Raymond, K. N. *Inorganic Chemistry* **1985**, *24*, 954.
(29) Miethke, M.; Klotz, O.; Linne, U.; May, J. J.; Beckering, C. L.; Marahiel, M. A. *Molecular Microbiology* **2006**, *61*, 1413.
(30) Spasojević, I.; Armstrong, S. K.; Brickman, T. J.; Crumbliss, A. L. *Inorganic Chemistry* **1999**, *38*, 449.
(31) Butler, A.; Theisen, R. M. *Coordination Chemistry Reviews* **2010**, *254*, 288.
(32) Meyer, J.-M.; Hohnadel, D.; Hallé, F. *Journal of General Microbiology* **1989**, *135*, 1479.
(33) White, D. L.; Durbin, P. W.; Jeung, N.; Raymond, K. N. *Journal of Medicinal Chemistry* **1988**, *31*, 11.
(34) Liu, Z. D.; Hider, R. C. *Medicinal Research Reviews* **2002**, *22*, 26.
(35) Liu, Z. D.; Piyamongkol, S.; Hider, R. C. *Transfusion Science* **2000**, *23*, 269.
(36) Xu, J.; Kullgren, B.; Durbin, P. W.; Raymond, K. N. *Journal of Medicinal Chemistry* **1995**, *38*, 2606.
(37) Sheldon W. May; Charlie D. Oldham; Patricia W. Mueller; Stephen R. Padgette; Sowell, A. L. *The Journal of Biological Chemistry* **1982**, *257*, 12746.
(38) Roy, S.; Preston, J. E.; Hider, R. C.; Ma, Y. M. *Journal of Medicinal Chemistry* **2010**, *53*, 5886.
(39) Harrington, J. M.; Chittamuru, S.; Dhungana, S.; Jacobs, H. K.; Gopalan, A. S.; Crumbliss, A. L. *Inorganic Chemistry* **2010**, *49*, 8208.

(40) Scarrow, R. C.; White, D. L.; Raymond, K. N. *Journal of the American Chemical Society* **1985**, *107*, 6540.
(41) Hou, Z.; Raymond, K. N.; O'Sulliva, B.; Esker, T. W.; Nishio, T. *Inorganic Chemistry* **1998**, *37*, 6630.
(42) Jocher, C. J.; Botta, M.; Avedano, S.; Moore, E. G.; Xu, J.; Aime, S.; Raymond, K. N. *Inorganic Chemistry* **2007**, *46*, 4796.
(43) Pierre, V. C.; Melchior, M.; Doble, D. M. J.; Raymond, K. N. *Inorganic Chemistry* **2004**, *43*, 8520.
(44) Cohen, S. M.; Xu, J.; Radkov, E.; Raymond, K. N.; Botta, M.; Barge, A.; Aime, S. *Inorganic Chemistry* **2000**, *39*, 5747.
(45) Nunes, A.; Podinovskaia, M.; Leite, A.; Gameiro, P.; Zhou, T.; Ma, Y.; Kong, X.; Schaible, U.; Hider, R.; Rangel, M. *J Biol Inorg Chem* **2010**, *15*, 861.
(46) Xu, B.; Kong, X.-L.; Zhou, T.; Qiu, D.-H.; Chen, Y.-L.; Liu, M.-S.; Yang, R.-H.; Hider, R. C. *Bioorganic & Medicinal Chemistry Letters* **2011**, *21*, 6376.
(47) Weizman, H.; Shanzer, A. *Chemical Communications* **2000**, *0*, 2013.
(48) Meyer, M.; Telford, J. R.; Cohen, S. M.; White, D. J.; Xu, J.; Raymond, K. N. *Journal of the American Chemical Society* **1997**, *119*, 10093.
(49) Grazina, R.; Gano, L.; Šebestík, J.; Amelia Santos, M. *Journal of Inorganic Biochemistry* **2009**, *103*, 262.
(50) Crisponi, G.; Remelli, M. *Coordination Chemistry Reviews* **2008**, *252*, 1225.
(51) Liu, Z. D.; Khodr, H. H.; Liu, D. Y.; Lu, S. L.; Hider, R. C. *Journal of Medicinal Chemistry* **1999**, *42*, 4814.
(52) Harris, W. R.; Carrano, C. J.; Cooper, S. R.; Sofen, S. R.; Avdeef, A. E.; McArdle, J. V.; Raymond, K. N. *Journal of the American Chemical Society* **1979**, *101*, 6097.
(53) Hay, B. P.; Dixon, D. A.; Vargas, R.; Garza, J.; Raymond, K. N. *Inorganic Chemistry* **2001**, *40*, 3922.
(54) Boukhalfa, H.; Crumbliss, A. L. *Inorganic Chemistry* **2000**, *39*, 4318.
(55) Tufano, T. P.; Raymond, K. N. *Journal of the American Chemical Society* **1981**, *103*, 6617.
(56) Bergeron, R. J.; Elliott, G. T.; Kline, S. J.; Ramphal, R.; St James, L. *Antimicrobial Agents and Chemotherapy* **1983**, *24*, 725.
(57) Krewulak, K. D.; Vogel, H. J. *Biochimica et biophysica acta* **2008**, *1778*, 1781.
(58) Stintzi, A.; Barnes, C.; Xu, J.; Raymond, K. N. *Proceedings of the National Academy of Sciences* **2000**, *97*, 10691.
(59) Braun, V.; Braun, M. *FEBS Lett* **2002**, *529*, 78.
(60) Braun, V.; Hantke, K. *Curr Opin Chem Biol* **2011**, *15*, 328.
(61) Ratledge, C.; Dover, L. *Annu Rev Microbiol.* **2000**, *54*, 881.
(62) Abergel, R. J.; Zawadzka, A. M.; Hoette, T. M.; Raymond, K. N. *Journal of the American Chemical Society* **2009**, *131*, 12682.
(63) Ecker, D. J.; Loomis, L. D.; Cass, M. E.; Raymond, K. N. *Journal of the American Chemical Society* **1988**, *110*, 2457.
(64) Hider, R. C.; Bickar, D.; Morrison, I. E. G.; Silver, J. *Journal of the American Chemical Society* **1984**, *106*, 6983.
(65) Cooper, S. R.; McArdle, J. V.; Raymond, K. N. *Proceedings of the National Academy of Sciences* **1978**, *75*, 3551.
(66) Harrington, J.; Crumbliss, A. *Biometals* **2009**, *22*, 679.
(67) Hou, Z.; Stack, T. D. P.; Sunderland, C. J.; Raymond, K. N. *Inorganica Chimica Acta* **1997**, *263*, 341.
(68) Tse, B.; Kishi, Y. *The Journal of Organic Chemistry* **1994**, *59*, 7807.
(69) Motekaitis, R. J.; Sun, Y.; Martell, A. E. *Inorganica Chimica Acta* **1992**, *198–200*, 421.
(70) Sun, Y.; Martell, A. E.; Reibenspies, J. H.; Welch, M. J. *Tetrahedron* **1991**, *47*, 357.
(71) Martell, A. E.; Motekaitis, R. J.; Sun, Y.; Ma, R.; Welch, M. J.; Pajeau, T. *Inorganica Chimica Acta* **1999**, *291*, 238.
(72) Jurchen, K. M. C.; Raymond, K. N. *Inorganic Chemistry* **2005**, *45*, 1078.
(73) Chew, B. P.; Tjoelker, L. W.; Tanaka, T. S. *Journal of dairy science* **1985**, *68*, 3037.

(74) Rogers, H. J.; Woods, V. E.; Synge, C. *Journal of General Microbiology* **1982**, *128*, 2389.

(75) Juarez-Hernandez, R. E.; Franzblau, S. G.; Miller, M. J. *Organic & Biomolecular Chemistry* **2012**, *10*, 7584.

(76) Panagopoulos, A. M.; Zeller, M.; Becker, D. P. *The Journal of Organic Chemistry* **2010**, *75*, 7887.

(77) Carruthers, C.; Ronson, T. K.; Sumby, C. J.; Westcott, A.; Harding, L. P.; Prior, T. J.; Rizkallah, P.; Hardie, M. J. *Chem. Eur. J.* **2008**, *14*, 10286.

(78) Lijanova, I. V.; Flores Maturano, J.; Domínguez Chávez, J. G.; Sánchez Montes, K. E.; Hernandez Ortega, S.; Klimova, T.; Martínez-García, M. *Supramolecular Chemistry* **2009**, *21*, 24.

(79) Vériot, G.; Dutasta, J.-P.; Matouzenko, G.; Collet, A. *Tetrahedron* **1995**, *51*, 389.

(80) Wytko, J. A.; Weiss, J. *Tetrahedron Letters* **1991**, *32*, 7261.

(81) Canceill, J.; Gabard, J.; Collet, A. *Journal of the Chemical Society, Chemical Communications* **1983**, *0*, 122.

(82) Canceill, J.; Collet, A.; Gottarelli, G. *Journal of the American Chemical Society* **1984**, *106*, 5997.

(83) Rothenberg, G.; Downie, A. P.; Raston, C. L.; Scott, J. L. *Journal of the American Chemical Society* **2001**, *123*, 8701.

(84) Ambrosi, G.; Dapporto, P.; Formica, M.; Fusi, V.; Giorgi, L.; Guerri, A.; Lucarini, S.; Micheloni, M.; Paoli, P.; Pontellini, R.; Rossi, P.; Zappia, G. *New Journal of Chemistry* **2004**, *28*, 1359.

(85) Lambert, T. N.; Chittamuru, S.; Jacobs, H. K.; Gopalan, A. S. *Tetrahedron Letters* **2002**, *43*, 7379.

(86) Chittamuru, S.; Lambert, T. N.; Martinez, G.; Jacobs, H. K.; Gopalan, A. S. *Tetrahedron Lett* **2007**, *48*, 567.

(87) Xu, J.; Durbin, P. W.; Kullgren, B.; Ebbe, S. N.; Uhlir, L. C.; Raymond, K. N. *J Med Chem* **2002**, *45*, 3963.

(88) Burgada, R.; Bailly, T.; Noël, J. P.; Gomis, J. M.; Valleix, A.; Ansoborlo, E.; Hengé-Napoli, M. H.; Paquet, F.; Gourmelon, P. *Journal of Labelled Compounds and Radiopharmaceuticals* **2001**, *44*, 13.

(89) Mikhail, C.; Nagasree, C.; Jean-Jacques, C.; Jianmin, F.; Rajender, K.; Vishnumurthy, K.; Jonathan, L.; Shifeng, L.; Jianyu, S.; Serguei, S.; Zaihui, Z. 2008; Vol. US20080051741 20080319.

(90) Liu, D.; Chen, R.; Hong, L.; Sofia, M. J. *Tetrahedron Letters* **1998**, *39*, 4951.

(91) Hirose, K. In *Analytical Methods in Supramolecular Chemistry*; Wiley-VCH Verlag GmbH & Co. KGaA: 2007, p 17.

(92) Rai, B. L.; Khodr, H.; Hider, R. C. *Tetrahedron* **1999**, *55*, 1129.

(93) Cabell, L. A.; Best, M. D.; Lavigne, J. J.; Schneider, S. E.; Perreault, D. M.; Monahan, M.-K.; Anslyn, E. V. *Journal of the Chemical Society, Perkin Transactions 2* **2001**, *0*, 315.

(94) Vacca, A.; Nativi, C.; Cacciarini, M.; Pergoli, R.; Roelens, S. *J Am Chem Soc* **2004**, *126*, 16456.

(95) Lutz, A.; Ward, T. R. *Helvetica Chimica Acta* **1998**, *81*, 207.

(96) Heidinger, S.; Braun, V.; Pecoraro, V. L.; Raymond, K. N. *J Bacteriol* **1983**, *153*, 109.

(97) Doble, D. M.; Melchior, M.; O'Sullivan, B.; Siering, C.; Xu, J.; Pierre, V. C.; Raymond, K. N. *Inorg Chem* **2003**, *42*, 4930.

(98) Kiessling Laura L; Raines Ronald T; J., A. M. 2007; Vol. WO2007US68099 20070503

(99) Piyamongkol, S.; Liu, Z. D.; Hider, R. C. *Tetrahedron* **2001**, *57*, 3479.

(100) Green, D. E.; Ferreira, C. L.; Stick, R. V.; Patrick, B. O.; Adam, M. J.; Orvig, C. *Bioconjug Chem* **2005**, *16*, 1597.

(101) Gardner, R. A.; Kinkade, R.; Wang, C.; Phanstiel *The Journal of Organic Chemistry* **2004**, *69*, 3530.

(102) Chen, H.-T.; Neerman, M. F.; Parrish, A. R.; Simanek, E. E. *Journal of the American Chemical Society* **2004**, *126*, 10044.

(103) Sellitto, G.; Faruolo, A.; de Caprariis, P.; Altamura, S.; Paonessa, G.; Ciliberto, G. *Bioorganic & Medicinal Chemistry* **2010**, *18*, 6143.

(104) Umali, A. P.; Crampton, H. L.; Simanek, E. E. *The Journal of Organic Chemistry* **2007**, *72*, 9866.

(105) Aher, N. G.; Pore, V. S.; Patil, S. P. *Tetrahedron* **2007**, *63*, 12927.

(106) Xu, J.; O'Sullivan, B.; Raymond, K. N. *Inorg Chem* **2002**, *41*, 6731.

(107) Dertz, E. A.; Xu, J.; Raymond, K. N. *Inorg Chem* **2006**, *45*, 5465.

(108) McQueary, C.; Kirkup, B.; Si, Y.; Barlow, M.; Actis, L.; Craft, D.; Zurawski, D. *J Microbiol.* **2012**, *50*, 434.

(109) Butler, G.; Rasmussen, M. D.; Lin, M. F.; Santos, M. A. S.; Sakthikumar, S.; Munro, C. A.; Rheinbay, E.; Grabherr, M.; Forche, A.; Reedy, J. L.; Agrafioti, I.; Arnaud, M. B.; Bates, S.; Brown, A. J. P.; Brunke, S.; Costanzo, M. C.; Fitzpatrick, D. A.; de Groot, P. W. J.; Harris, D.; Hoyer, L. L.; Hube, B.; Klis, F. M.; Kodira, C.; Lennard, N.; Logue, M. E.; Martin, R.; Neiman, A. M.; Nikolaou, E.; Quail, M. A.; Quinn, J.; Santos, M. C.; Schmitzberger, F. F.; Sherlock, G.; Shah, P.; Silverstein, K. A. T.; Skrzypek, M. S.; Soll, D.; Staggs, R.; Stansfield, I.; Stumpf, M. P. H.; Sudbery, P. E.; Srikantha, T.; Zeng, Q.; Berman, J.; Berriman, M.; Heitman, J.; Gow, N. A. R.; Lorenz, M. C.; Birren, B. W.; Kellis, M.; Cuomo, C. A. *Nature* **2009**, *459*, 657.

(110) Podschun, R.; Ullmann, U. *Clin Microbiol Rev* **1998**, *11*, 589.

(111) Oggioni, M. R.; Pozzi, G.; Valensin, P. E.; Galieni, P.; Bigazzi, C. *Journal of Clinical Microbiology* **1998**, *36*, 325.

(112) Cimolai, N. *Eur J Clin Microbiol Infect Dis* **2008**, *27*, 481.

(113) Ishii, S.; Sadowsky, M. J. *Microbes and Environments* **2008**, *23*, 101.

(114) Podschun, R.; Ullmann, U. *Clinical Microbiology Reviews* **1998**, *11*, 589.

(115) Beasley, F. C.; Heinrichs, D. E. *J Inorg Biochem* **2010**, *104*, 282.

(116) Perry, R. D.; Clemente, C. L. S. *Journal of Bacteriology* **1979** *140*, 1129.

(117) Visca, P.; Colotti, G.; Serino, L.; Verzili, D.; Orsi, N.; Chiancone, E. *Applied and Environmental Microbiology* **1992**, *58*, 2886.

(118) Meyer, J. M.; Stintzi, A.; De Vos, D.; Cornelis, P.; Tappe, R.; Taraz, K.; Budzikiewicz, H. *Microbiology* **1997**, *143*, 35.

(119) Brandel, J.; Humbert, N.; Elhabiri, M.; Schalk, I. J.; Mislin, G. L. A.; Albrecht-Gary, A.-M. *Dalton Transactions* **2012**, *41*, 2820.

(120) David, M. Z.; Daum, R. S. *Clinical Microbiology Reviews* **2010**, *23*, 616.

(121) Eliopoulos, G. M.; Maragakis, L. L.; Perl, T. M. *Clinical Infectious Diseases* **2008**, *46*, 1254.

(122) Dorsey, C. W.; Beglin, M. S.; Actis, L. A. *Journal of Clinical Microbiology* **2003**, *41*, 4188.

(123) Almeida, R. S.; Wilson, D.; Hube, B. *FEMS Yeast Res* **2009**, *9*, 1000.

(124) Ardon, O.; Bussey, H.; Philpott, C.; Ward, D. M.; Davis-Kaplan, S.; Verroneau, S.; Jiang, B.; Kaplan, J. *J Biol Chem* **2001**, *276*, 43049.

(125) Burnham, B. F.; Neilands, J. B. *Journal of Biological Chemistry* **1961**, *236*, 554.

(126) Barry, A. L. *The Antimicrobic Susceptibility Test: Principles and Practices In Kimpton* Philadelphia, 1976.

(127) Xiao, G.; van der Helm, D.; Hider, R. C.; Rai, B. L. *The Journal of Physical Chemistry* **1996**, *100*, 2345.

(128) Jocher, C. J.; Moore, E. G.; Xu, J.; Avedano, S.; Botta, M.; Aime, S.; Raymond, K. N. *Inorganic Chemistry* **2007**, *46*, 9182.

“Few scientists acquainted with the chemistry of biological systems at the molecular level can avoid being inspired.” – Prof. Donald James Cram